# KINETICS AND MECHANISMS OF CHROMIUM(III) OXIDATION AND PRECIPITATION ON MANGANESE OXIDES, IN REAL-TIME AND AT THE MOLECULAR LEVEL

by

Gautier Landrot

A dissertation submitted to the Faculty of the University of Delaware in partial fulfillment of the requirements for the degree of Doctor of Philosophy in Plant and Soil Sciences

Summer 2010

**KINETICS AND MECHANISMS OF CHROMIUM(III) OXIDATION AND PRECIPITATION ON MANGANESE OXIDES, IN REAL-TIME AND AT THE MOLECULAR LEVEL**

by

Gautier Landrot

Approved: _____
Blake C. Meyers, Ph.D.
Chair of the Department of Plant and Soil Sciences

Approved: _____
Robin W. Morgan, Ph.D.
Dean of the College of Agriculture and Natural Resources

Approved: _____
Debra Hess Norris, M.S.
Vice Provost for Graduate and Professional Education

I certify that I have read this dissertation and that in my opinion it meets the academic and professional standard required by the University as a dissertation for the degree of Doctor of Philosophy.

Signed: _____

Donald L. Sparks, Ph.D.
Professor in charge of dissertation

I certify that I have read this dissertation and that in my opinion it meets the academic and professional standard required by the University as a dissertation for the degree of Doctor of Philosophy.

Signed: _____

Jeffrey Fitts, Ph.D.
Member of dissertation committee

I certify that I have read this dissertation and that in my opinion it meets the academic and professional standard required by the University as a dissertation for the degree of Doctor of Philosophy.

Signed: _____

Kenneth Livi, Ph.D.
Member of dissertation committee

I certify that I have read this dissertation and that in my opinion it meets the academic and professional standard required by the University as a dissertation for the degree of Doctor of Philosophy.

Signed: _____

George W. Luther III, Ph.D.
Member of dissertation committee

## ACKNOWLEDGMENTS

First of all, I could never express my gratitude enough to Dr. Sparks for giving me the opportunity to be one of his students. Everybody in the world who has had this privilege could testify not only about his outstanding mentorship, but also his inspiring personality, notably characterized by a strong work ethic and a jovial character. The way he advises his students, by guiding them throughout their degrees towards their future professional autonomy, and his relationships to them, based on trust, could be compared to the way parents educate their children... That is why one can say Dr. Sparks truly has "academic children" all over the world!

I would like to thank Dr. Fitts, Dr. Livi, and Dr. Luther for serving in my PhD Committee, and for their inputs in my research. I thank Dr. Fitts for his help during several beamtrips, Dr. Livi for his assistance and expertise with the TEM analyses, and Dr. Luther for his vast knowledge of chemistry and his outstanding inorganic chemistry class, which considerably influenced my research.

Coming from France to the States to pursue my PhD degree, I will never forget the wonderful hospitality I experienced during my first days in Delaware. I am thankful to all the postdocs, former, and current students in Dr. Sparks group, and those that helped me starting out with my graduate student life and research: Ryan Tappero, who, after working for 5 days straight at the beamline, only for the sake of Science, deserves his "synchrotron trooper" nickname; Dave McNear, for his free home-delivery of my first bed; Jennifer Seiter, for offering me every Christmas a pack of beers so I won't spend the holidays entirely by myself; Dr. Sanjai Parikh, for his

FTIR expertise and punishing me on the Squash court; Masayuki Shimizu, for giving me many rides to the stores during my first year; Brandon Lafferty, for his helpful research and for being my official furniture supplier and cell-phone carrier; Mengqiang ("Mike") Zhu for his great friendship; and Saengdao Khaokaew, for countess things that helped me in writing this thesis. I'd like to wish to the awesome people that joined Dr. Sparks group after me all the best with their future professional endeavors: Matt, Dalton, Camille, Elizabeth, Chunmei, and Shannon. Lastly, but not the least, this dissertation could not have been done without the help of my “XAFS guru”, Dr. Matthew Ginder-Vogel.

I am also thankful to Jerry Hendricks, who always promptly granted me every laboratory supply desire I had.

Special thanks goes to my family; my grandmother Régine Munière Landrot that I will always remember, my cousin Emmanuel Cormier, my brother Arnaud, and my wonderful parents Jean & Christiane, who considerably contributed to the accomplishment of this work.

## TABLE OF CONTENTS

**LIST OF TABLES** ..... **x**
**LIST OF FIGURES** ..... **xi**
**ABSTRACT** ..... **xvi**

**CHAPTER**
**1 INTRODUCTION** ..... **1**
1.1 Chromium ..... 1
1.1.1 Occurrence, Sources & Toxicity ..... 1
1.1.2 Chemical Properties of Chromium ..... 5
1.1.2.1 Redox Reactions ..... 5
1.1.2.2 Precipitation/Dissolution Reactions ..... 7
1.1.2.3 Sorptions/Desorption Reactions ..... 8
1.2 Manganese oxides ..... 8
1.2.1 Structures ..... 8
1.2.2 Three Poorly Crystalline Manganese Oxides: Random Stacked Birnessite (RSB), Acid Birnessite (AB), and Vernadite/∂$MnO_2$/Hydrous Manganese Oxide (HMO) ..... 10
1.2.3 Mn(II) Oxidation and Mn(IV) Reduction Quantum Mechanisms ..... 12
1.3 Manganese Oxide & Cr(III) Reactions ..... 13
1.3.1 Cr(III) Oxidation by $MnO_2$: Kinetics and Mechanisms ..... 14
1.3.1.1 $MnO_2$ Physical & Chemical Property Dependence ..... 14
1.3.1.2 Cr(III) Oxidation Mechanisms ..... 16
1.3.1.2.1 Cr(III) Sorption Mechanisms ..... 16
1.3.1.2.2 Overall Reaction Mechanism ..... 20
1.3.1.3 Rates Constants Reported in the Literature ..... 26
1.3.1.4 Concentration Effects ..... 28
1.3.1.5 pH Effects 29
1.3.1.5.1 pH Effects on the Total Amount of Cr(III) Oxidized at the End of the Reaction ..... 29
1.3.1.5.2 pH Effects on Initial Rates ..... 30
1.3.1.6 Effect of Oxygen ..... 30
1.3.1.7 Sorption Competition Between Cr and Other Elements on $MnO_2$ Surfaces ..... 31
1.3.2 Kinetics and Structures of Chromium Surface Precipitates ..... 34

1.3.2.1 Kinetics of Chromium Surface Precipitate Formation ..... 34
1.3.2.2 Structure of Chromium Hydroxide Surface Precipitates ..... 36
1.4 Experimental Methods to Measure Rapid Kinetic Mechanisms ..... 37
1.4.1 Relaxation Techniques ..... 38
1.4.2 Rapid Scan Attenuated Total Reflectance (ATR) Fourier Transform Infrared (FTIR) ..... 39
1.4.3 Surface Second Harmonic Generation ..... 39
1.4.4 Quick X-Ray Absorption Spectroscopy ..... 40
1.5 Cr and As Speciation in Contaminated Soils ..... 41
1.6 Framework of This Study ..... 43
1.7 References ..... 44

**2 KINETICS OF CHROMIUM(III) OXIDATION BY MANGANESE(IV) OXIDES USING QUICK SCANNING X-RAY ABSORPTION FINE STRUCTURE SPECTROSCOPY (Q-XAFS) ..... 48**
2.1 Abstract ..... 48
2.2 Introduction ..... 49
2.3 Materials and Methods ..... 51
2.3.1 Chromium Solutions, Concentrations, and pH Range ..... 51
2.3.2 Hydrous Manganese Oxide (HMO) ..... 52
2.3.3 pH Control ..... 53
2.3.4 Reaction Conditions ..... 53
2.3.5 Batch Kinetics Studies ..... 55
2.3.6 Elemental Measurements ..... 55
2.3.7 Q-XAFS Experiments ..... 56
2.3.8 Experimental Setup ..... 57
2.3.9 Calculation of Initials Rates and Rate Constants ..... 59
2.4 Results and Discussion ..... 63
2.4.1 Traditional Batch Kinetic Experiments ..... 63
2.4.2 Q-XAFS Experiments ..... 65
2.5 References ..... 75

**3 KINETICS AND MECHANISMS OF CHROMIUM(III) SORPTION, SURFACE PRECIPITATION, AND OXIDATION ON HEXAGONAL MANGANESE(IV) OXIDE SURFACES ..... 80**
3.1 Abstract ..... 80
3.2 Introduction ..... 81
3.3 Material and Methods ..... 85
3.3.1 Experimental Approach ..... 85
3.3.1.1 Reactant and standard syntheses ..... 85

3.3.1.2 Batch Experiments ..... 86
3.3.1.3 Replenishment experiments ..... 87
3.3.1.4 Stirred Flow Experiments ..... 88
3.3.2 Solid Phase Analysis ..... 89
3.3.2.1 Bulk XAFS Analysis ..... 89
3.3.2.2 TEM Analysis ..... 90
3.3.3 Real time, *In Situ* Experiments ..... 90
3.4 Results and Discussion ..... 92
3.4.1 Identification of Chromium Sorption Products on Hexagonal Birnessites ..... 92
3.4.1.1 Identification at the Molecular Level ..... 92
3.4.1.2 Macroscopic Identification ..... 118
3.4.2 Real-Time Kinetics of Chromium Precipitation and Oxidation ..... 127
3.4.2.1 Chromium Surface Precipitation Kinetics ..... 127
3.4.2.2 Chromium Oxidation Kinetics ..... 134
3.4.2.3 Continuum of Cr(III) Oxidation and Surface Precipitation ..... 139
3.5 Conclusions ..... 141
3.6 References ..... 142

**4 ARSENIC AND CHROMIUM SPECIATION IN AN URBAN CONTAMINATED SOIL ..... 146**
4.1 Abstract ..... 146
4.2 Introduction ..... 147
4.3 Material and Methods ..... 150
4.3.1 Sample Collection and Soil Analysis ..... 150
4.3.2 Bulk X-Ray Absorption Fine Structure (Bulk XAFS) Analyses ..... 150
4.3.3 Micro XAS Analyses ..... 151
4.4 Results and Discussion ..... 152
4.4.1 Soil Composition ..... 152
4.4.2 Elemental Distribution ..... 154
4.4.3 Cr and As Oxidation States ..... 163
4.4.4 Molecular Environment of As: Bulk Soil Analyses ..... 167
4.5 Conclusions ..... 175
4.6 References ..... 177

**APPENDICES**
**A** Quantity of HCl or KOH added at the beginning of the batch experiments, in mL ..... 181

**B** pH and concentrations, in ppm, of several elements in soil samples taken at eight locations in Christiana Park, and at depth 0-8” and 8-16” below the surface..... 182

## LIST OF TABLES

**Table 1.1** Formula and type of RSB, AB, HMO, and the manganese oxides used in two previous studies ..... 11

**Table 1.2** Kinetics of Cr(III) by $MnO_2$: experimental conditions used in two batch studies ..... 15

**Table 2.1** Initial conditions, measured initial rates, and rate parameters The partial rate coefficients $\alpha$, $\beta$ at pH 2.5, pH 3, and pH 3.5 shown in this table are averaged values from $\alpha$ and $\beta$ calculated using Eqs. 2.6 and 2.9 and by combining the initial rates measured at different experimental conditions. The rate constant for each experiment was measured with Eq. 2.10. Since all experiments were duplicated, the initial rates and rate parameters are reported with two values separated with "/". The standard error (95% confidence interval) for each initial rate is italicized. Averages of duplicate values are highlighted in bold..... 68

**Table 3.1** Fitting parameters of Fourier transforms depicted in Figure 3.1 (b) and Figure 3.3 (b) ..... 104

**Table 4.1** Shell-by-shell fitting parameters of Soil 1 (8-16"), and comparison to results from two previous studies (see text). CN= coordination number; $\sigma^2$= Debye-Waller factor; R= radial distance, in Å ..... 173

## LIST OF FIGURES

**Figure 1.1** Eh versus pH diagram for chromium (adapted from Rai *et al.*, 1989)..... 6

**Figure 1.2** XRD spectra (top) and SEM data (bottom) of AB, RSB, & HMO ..... 12

**Figure 1.3** Outer-sphere complex and inner-sphere complex between Cr(III) and Mn(IV), according to MOT (adapted from Fendorf, 1992) ..... 18

**Figure 1.4** Cr(III) sorption rate constant dependence on manganese oxidation states of $MnO_2$ surface: six possible reactions (from A to F) ..... 21

**Figure 1.5** A) Mechanism from Fendorf (1992) (adapted from Fendorf (1992)), and B & C) proposed reactions ..... 23

**Figure 1.6** Possible electron transfer reactions from Cr(III) to Mn(III) and/or Mn(IV) ..... 25

**Figure 2.1** Chromium pre-edge height calibration curve. Height of Cr(VI) pre-edge was measured from XANES spectra of standard solution mixtures of 100mM [chromium]total Cr(III) + Cr(VI). The mixtures are respectively 0 % Cr(III)- 100 % Cr(VI), 25 % Cr(III)- 75 % Cr(VI), 50 % Cr(III)- 50 % Cr(VI), 80 % Cr(III)- 20 % Cr(VI), and 100 %Cr(III)- 0 % Cr(VI) ..... 58

**Figure 2.2** Initial rate measurement for an experiment at pH 2.5, where [Cr(III)]=80 mM, and [HMO]=20 g/L ..... 58

**Figure 2.3** Kinetics of Cr(III) oxidation on HMO at a) pH 2.5, b) pH 3, and c) pH 3.5, using a batch technique and reaction conditions of 100mM Cr(III) and 20g/L HMO ..... 62

**Figure 2.4** Cr(III) oxidation kinetics using a QXAFS technique, at pH 2.5, [Cr(III)]=100mM, [HMO]=20g/L and 0-240 seconds. Each XANES spectrum shown represents 3 seconds of the reaction (average of four 0.75s spectra). ..... 64

**Figure 2.5** Percentage of Cr(VI) produced in 4 minutes. Bold line: spectrum of Cr(III) oxidation kinetics at 240 second reaction time (average of two 0.75s Q-XAFS spectra), at pH 2.5, [Cr(III) ]$_0$=100mM, [HMO]=20g/L. Dashed lines: XANES spectra for standard solution mixtures of 100mM [chromium]total Cr(III) + Cr(VI) : 100 % Cr(VI), 75 % Cr(VI), 50 % Cr(VI), 20 % Cr(VI), and 0 % Cr(VI) ..... 66

**Figure 2.6** Percentage of Cr(VI)/Cr(III) in the HMO pastes based on the pre-edge feature at 5993.5eV, at pH 2.5, 3, and 3.5 ..... 67

**Figure 2.7** A) Effect of pH – [Cr(III)]= 100 mM; 20 g/L HMO; pH 2.5, 3, and 3.5; B) Effect of Cr concentration – pH 2.5; 20 g/L HMO; and C) Effect of Mn concentration –pH 2.5; [Cr(III)]= 100 mM; 20, 15, 10, and 5 g/L..... 72

**Figure 3.1** (a) Quantity of Cr(VI) in % inferred from normalized XANES spectra of AB, HMO, and RSB at different reaction times (b) Fourier transforms of AB, HMO, and RSB at different reaction times and (c) Amount of Cr(III) and Cr(VI) sorbed on HMO and AB over time at pH 3. The quantities were measured from the percentage of Cr(III) and Cr(VI) sorbed on the surface of AB and HMO at 2, 5, 10, and 30 minutes (Figure 3.1 (a)) and the total amount of chromium sorbed on AB and HMO at pH 3 and at 2, 5, 10, and 30 minutes (Figure 3.2). ..... 97

**Figure 3.2** Kinetics of Cr(III) oxidation on HMO and AB at (a) pH 2.5, (b) pH 3, and (c) pH 3.5, using a batch technique and reaction conditions of 50 mM Cr(III) and 20 g/L HMO and AB. The grey area represents the amount of Cr sorbed on $Mn(IV)O_2$, which was measured by subtracting the amount of Cr(III) and Cr(VI) measured in solution at 2, 5, 10, 30, 60, and 360 minutes from the amount of Cr(III) introduced at t=0 in the batch vessel (50 mM)..... 101

**Figure 3.3** (a) Quantity of Cr(VI) in % inferred from normalized XANES spectra of HMO at different reaction times and at pH 2.5, 3, and 3.5 (b) Fourier transforms of HMO at different reaction times and at pH 2.5, 3, and 3.5 and (c) Amount of Cr(III) and Cr(VI) sorbed on HMO over time and at pH 2.5, 3, and 3.5. The quantities were measured from the percentage of Cr(III) and Cr(VI) sorbed on the surface of HMO at 2, 5, 10, and 30 minutes (Figure 3.3 (a)) and the total amount of chromium sorbed on HMO at pH 2.5, 3, 3.5, and at 2, 5, 10, and 30 minutes (Figure 3.2)..... 108

**Figure 3.4** Amount of Cr(III), Cr(VI), and Mn(II) desorbed by replenishments after Cr(III) was reacted with HMO and AB for 2, 5, 10, 30, 60, and 360 minutes, with 50m M of KCl, $Al^{3+}$ , and $PO_4^{3-}$ as the desorption agent, at pH 2.5, 3, and 3.5 ..... 115

**Figure 3.5** Chromium(III) sorption mechanism on $Mn(IV)O_2$: Cr(III) binds in a bidentate binuclear complex on the edge sides and a bidentate mononuclear complex on the edge corners. ..... 118

**Figure 3.6** Images A, B, C: HRTEM of AB reacted for 1 hour with 50 mM of Cr(III) at pH 3.5. Images D and E: HRTEM of unreacted AB. ..... 119

**Figure 3.7** EDS patterns taken in the middle (pattern A) and on the rim (pattern B) of an acid birnessite flake. ..... 121

**Figure 3.8** (a) SAED patterns of unreacted HMO and AB, and 1 hour Cr(III)-reacted AB and HMO, at pH 2.5 and 3.5, and (b) EELS pattern of 1 hour Cr(III)-reacted AB. ..... 122

**Figure 3.9** In black color: amount of chromium sorbed on $Mn(IV)O_2$ measured from Figure 3.2 in mM/g, when 50mM of Cr(III) reacted for 6 hours with 20g/L of HMO or AB at pH 2.5, 3 and 3.5; in grey and white colors: amount of chromium in HMO or AB measured when the $Mn(IV)O_2$ solid phase, after replenishment experiments conducted at pH 2.5, 3, and 3.5, were digested with 8N HCl. ..... 123

**Figure 3.10** Concentrations of Cr(III), Cr(VI), and Mn(II) measured by stirred flow experiments, with a suspension of HMO and AB reacted with 50mM Cr(III) for 6 hours in the stirred flow chamber, and using as the flow solution a 50 mM KCl solution, 50 mM $Al^{3+}$ solution, and 50 mM $PO_4^{3-}$ solution, at pH 2.5, 3, and 3.5 ..... 126

**Figure 3.11** Linear combination of Q-XAFS chi spectra of HMO reacted for 2, 10, 30, and 60 minutes with Cr(III) at 50mM and pH 2.5, 3, and 3.5 and corresponding percentages of Cr(III), Cr(VI), $\alpha$-CrOOH, and $\gamma$-CrOOH precipitate phases. ..... 128

**Figure 3.12** Linear combination of Q-XAFS chi spectra of AB reacted for 2, 10, 30, and 60 minutes with Cr(III) at 50mM and pH 2.5, 3, and 3.5, and corresponding percentages of Cr(III), Cr(VI), and $\alpha$-CrOOH precipitate phase. ..... 130

**Figure 3.13** Structure of $Mn(IV)O_2$ compared to γ-CrOOH structure and α-CrOOH structure (profile and top views). ..... 132

**Figure 3.14** (a) Percentage of Cr(VI) produced from normalized Q-XAFS XANES spectra at the Cr K-edge. (b) Normalized Q-XAFS XANES spectra at the Mn K-edge. The dashed lines represent the position in eV of the white line of a Mn(II) standard ($MnCl_2$) at 6554 eV and a Mn(IV) standard (Vernadite) at 6562 eV. ..... 136

**Figure 3.15** Isosbestic points of normalized Q-XAFS XANES spectra at the Mn K-edge of the experiment conducted with 50mM Cr(III) + 20 g/L HMO at pH 2.5. Arrow 1 and 2 represent the position in eV of the white line of a Mn(II) standard ($MnCl_2$) at 6554 eV and a Mn(IV) standard (vernadite) at 6562 eV, respectively. ..... 138

**Figure 4.1** Concentrations, in ppm, of several elements in Soil 1 and 2 ..... 154

**Figure 4.2** Spatial distribution of Cr, As, Fe, Mn, Zn, and Ni in Soil 1 & 2 at depths of 0-8" and 8-16" below the surface. The colors represent elemental concentrations, with blue< yellow<red..... 155

**Figure 4.3** (A) Cr and Fe correlation plots: Cr-Kα intensities over the Fe-Kα intensities per pixel in μ-XRF maps of Soil 1 & 2 at 0-8" and 8-16"; (B) Cr and Fe μ-XRF maps used to make the correlation plot of soil 2 at 0-8" depicted in (A); and (C) Reconstructed Cr μ-XRF maps after selecting with SMAK three sets of points -labeled (1), (2), and (3)- from the correlation plot of soil 2 at 0-8" depicted in (A) ..... 157

**Figure 4.4** (A) Multichannel analysis of As, Cr, Fe, Ni, S, Zn, and Ti, and (B) and μ-XRD, taken at one hot spot containing As, Cr, and Fe, in one of the μ-XRF maps of Soil 1 at 8-16". ..... 159

**Figure 4.5** Multichannel analyzer pattern of As, Cr, Fe, Ni, S, Zn, and Ti, taken at two Cr hot spots, and three As hot spots ..... 160

**Figure 4.6** (A) Multichannel analysis of As, Cr, Fe, Ni, Cu, and Zn; and (B) μ-XRD, taken at a Cr hot spot (Soil 1, 8-16"), and a As hot spot (Soil 2, 0-8"). Mineral phases in As hot spot: Q= quartz ($SiO_2$), P=periclase (MgO), I=Iron(II, III) arsenate ($As_6$ $Fe_7$ $O_2$); in Cr hot spot: Q= tridymite ($Si_5O_{10}$), F= felsobanyaite ($Al_4SO_{18}H_{18}$), P= periclase (MgO), L= lime (CaO), Fe= iron(III) oxide hydroxide-δ-Feroxyhyte (FeOOH)..... 162

**Figure 4.7** (A) Normalized μ-XANES at the Cr K-edge taken at several Cr hot spot in Soil 1 at 8-16" below the surface and Soil 2 at 0-8"and 8-16" below the surface; and (B) Normalized μ-XANES at the As K-edge taken at several As hot spots in Soil 1 at 8-16" below the surface and Soil 2 at 0-8"and 8-16" below the surface. Grey stripe in A: highlight of the pre-white line region or the spectra; dashed line in A: position of the Cr(VI) pre-edge feature at 5993.5 eV; grey stripe in B: highlight of the post-white line region of the spectra; dashed line: position of the As(V) white line standard at 11874 eV; and circle: highlight of a post-white line feature ..... 165

**Figure 4.8** Positions in energy of the XANES first derivative's inflection points of the two soil samples and the As(V) & As(III) standards. ..... 168

**Figure 4.9** (A) Comparison between the EXAFS spectra of As standards and EXAFS spectra of Soil 1 at 8-16" and Soil 2 at 0-8" (B) linear combination fittings of Soil 1 (8-16") & Soil 2 (0-8") ..... 170

**Figure 4.10** Fourier Transform EXAFS of Soil 1 (8-16") ..... 172

## ABSTRACT

The initial kinetics of Cr(III) oxidation on mineral surfaces is poorly understood, yet a significant portion of the oxidation process occurs during the first seconds of the reaction. In this study, the initial rates of Cr(III) oxidation on hydrous manganese oxide (HMO) were measured at three different pH values (pH 2.5, 3, and 3.5), using a quick X-ray absorption fine structure spectroscopy (Q-XAFS) batch method. The calculated rate constants were 0.201, 0.242, and 0.322 $M^{-1}$ $s^{-1}$ at pH 2.5, 3, and 3.5, respectively. These values were independent of both [Cr(III)] and [Mn(II)] and mixing speed, suggesting that the reaction was "chemically" controlled and not dependent upon diffusion at the time period the rate parameters were measured. A second-order overall rate was found at three pH values. This represents the first study to determine the chemical kinetics of Cr(III) oxidation on Mn-oxides. The results have important implications for the determination of rapid, environmentally important reactions that cannot be measured with traditional batch and flow techniques. An understanding of these reactions is critical to predicting the fate of contaminants in aquatic and terrestrial environments.

Additionally, this study investigated the kinetics and mechanisms of the reactions occurring during chromium(III) sorption on three hexagonal manganese(IV) oxide surfaces. Bulk Extended X-ray Absorption Fine Structure spectroscopy (EXAFS) analyses show that trivalent chromium binds to the mineral surface in an inner-sphere complex on the edges of the manganese oxide layers, and rapidly oxidizes to Cr(VI), which can weakly bind to the surface in an outer sphere complex,

or diffuse to solution. As more Cr(III) sorbs on $Mn(IV)O_2$, Cr(III) nucleation occurs on the mineral and simultaneously Cr(VI) oxidation rates decrease. Chromium(III) may precipitate locally on the mineral surface as a γ-CrOOH phase and extend away from the manganese oxide, if the mineral surface is saturated with ions at high ionic strength. Alternatively, Cr(III) can epitaxially nucleate in a α-CrOOH phase on the top of $Mn(IV)O_2$ layers, due to structural similarities between the surfaces of the Cr(III) precipitate and the manganese oxide. After forming, Cr(III) precipitates can desorb from the mineral surface, since more Cr(III) nucleation products are detected in solution than on the solid phase. Quick X-ray Absorption Fine Structure spectroscopy (Q-XAFS) enables us to measure *in situ* the rates of both surface precipitation formation on manganese oxides and Cr(III) oxidation occurring in the entire batch system. The α-CrOOH phase can quickly form at high pH at the early stage of Cr(III) sorption on manganese oxides, thus competing with the rapid Cr(III) oxidation for free Cr(III) monomers in solution. Additionally, the phase can quickly reach high concentrations in the system, thus acting as a sink for Cr(III) ions. Therefore, since both Cr(III) nucleation and Cr(III) oxidation occur rapidly and potentially have opposite effects on Cr toxicity in the environment, this study, which measures for the first time the rates of Cr surface precipitation on manganese oxide surface using Q-XAFS, demonstrates the need for developing new techniques that can follow the kinetics of rapid reactions occurring in the environment.

Lastly, the speciation of As and Cr in a contaminated soil was studied by micro x-ray fluorescence spectroscopy (μ-XRF), and bulk x-ray absorption spectroscopy (bulk XAFS). The soil was taken from a park in Wilmington, DE, which used to be an important center for the leather tanning industry along the Atlantic

seaboard of the United States, until the early 20th century. The concentrations of As, Cr, and Pb measured at different locations in the park were often far above the background levels of these heavy metals in the State of Delaware. Results from micro x-ray absorption near-edge structure spectroscopy (μ-XANES) and bulk XAFS analyses show that Cr(III) and As(V) are mainly present in the soil, with insignificant amounts of Cr(VI) and As(III). The apparent absence of chromate may be notably due to the association between Cr and Fe in different regions of the soil. Micro x-ray fluorescence spectroscopy (μ-XRF) maps show that these two elements are distributed together in regions where their concentrations are diffuse, and at local spots where their concentrations are high. Iron(II) oxides, which can reduce Cr(VI) to Cr(III), are present at some of these hot spots where Cr and Fe are highly concentrated, based on the results obtained by micro x-ray diffraction spectroscopy (μ-XRD) analyses. Results from bulk extended x-ray absorption fine structure spectroscopy (EXAFS) analyses suggest that As is mainly associated with Al in the soil, and to a minor extent with Fe, which is supported by μ-XRF and μ-XRD results. Arsenate may be sorbed to aluminum oxides, which might have transformed after a long period of time into an As-Al precipitate phase, having a structure and chemical composition similar to mansfieldite. The latter hypothesis is supported by the fact that only a small amount of As present in the soil was desorbed using the characteristic toxicity leaching procedure (TCLP) and the synthetic precipitation leaching procedure (SPLP) tests. This suggests that As is immobilized in the soil.

# Chapter 1

# INTRODUCTION

## 1.1 Chromium

### 1.1.1 Occurrence, Sources & Toxicity

Chromium is a transition metal, in the sixth group of the periodic table. Chromium(0) has an electronic configuration of $4s^1\ 3d^5$, due to the lower energy of the high spin configuration. This element exhibits different oxidation states, from (I) to (VI). Trivalent chromium is the most stable form, and it is the principal oxidation state of chromium found in the environment (Wikipedia.com). Many countries in the world mine chromium, mostly as chromite ($FeCr_2O_4$). Nowadays, the three biggest exploiters of natural chromium in the world are South Africa, Kazakhstan, and India. Other countries producing chromite include Finland, Brazil, Turkey, Russia, Iran, and China. Although the United States has an estimated natural reserve of chromium ore of 7 million metric tons that could be used in the future, most of the chrome currently used by the industry comes from imports (Crescenzi, 2005). The big American Cr ore companies that used to be the largest producers of chromium in the world during the $19^{th}$ century, mines that are located for example in the Soldiers Delight and the Bare Hills district of Baltimore City, are no longer active. In 2007, only one chromium mining company remained in the USA.

Trivalent chromium is not very mobile in soils since it is insoluble at most environmental conditions. Its ionic form in solution is positively charged (sometimes

neutral too), which promotes its retention on negatively charged soil fractions. Also, tetravalent chromium is an essential nutrient that helps the human body utilize sugar, protein, and fat. However, Cr(VI), the second most stable form of chromium, is much more mobile in the environment, because of its high saturation index and negative ionic form. Additionally, contrary to Cr(III), Cr(VI) is rarely found in nature. Its presence in environmental systems is mainly due to anthropogenic sources, mostly from industrial activities (Kimbrough *et al.*, 1999). Chromate is considered to be more toxic than Cr(III) in the environment, due to its mobility and its strong oxidizing capacity. Although Cr(VI) is reduced to Cr(III) under most biological conditions, this element can induce DNA deletions in bacteria and animals (Kirpnick-Sobol, 2006), and it is known to be carcinogenic for humans (De Flora, 2000). De Flora (2000) compared Cr(VI) as a "Trojan Horse" in the human body: hexavalent chromium can reach the cells of the lower respiratory tracks after inhalation via a nonspecific anion channel, and easily cross the cell membranes, after which Cr(VI) is reduced. According to De Flora (2000), Cr(VI) is reduced in specific cell compartments, the cytosol being a greater reduction site than in the endoplasmic reticulum, in the mitochondria, or in the nucleus. The products of Cr(VI) reduction in cells are the short-lived reactive intermediates Cr(V) and Cr(IV), as well as Cr(III), which is the most stable form of chromium and cannot be removed from the cell wall. Once Cr(III) is produced in the cell, it can bind to DNA, forming monofunctional and bifunctional DNA adducts to the bases and phosphodiester backbone (Komanov, 2007). After Cr(VI) is reduced, Cr(III), Cr(IV), and Cr(V) can be involved in subsequent reactions that produce hydroxyl radicals and hydrogen peroxide, which can damage the DNA sequence (Komanov, 2007).

Chromium has many chemical properties that make this metal unique among the transition metals. Firstly, it can form at high temperatures a dense and thin layer with oxygen in a spinel structure, protecting underlying metals such as nickel or iron from electrochemical corrosion. This chromium passivation is a well-known industrial process to produce resistant materials, like for instance a stainless steel material, which is, by definition, a steel alloy containing a minimum of 11.5 wt% chromium. This type of alloy does not stain, corrode, or rust as easily as ordinary steel, although it is not entirely stain-proof. This chromium property has been known for centuries, and was used for instance by the Chinese during the 3$^{rd}$ century BC of the Qin Dynasty to coat weapons with bronze (Wikipedia.com). Chromium has many other applications. For example, it has been also used as dyes and paints for centuries. As a matter of fact, the name of this element has been derived from the Greek word chroma, which means color, in reference to the fact that Cr is known to cause a number of colors in a variety of materials. During the 1800s, chromium was primarily used as a component of paints and in tanning salts. Nowadays, metal alloys account for 85% of the use of chromium. It is also used by industry as a catalyst, as a chemical reagent, as a mordant (i.e, fixing agent), as a gasoline additive, as a high electrical conductor, etc... (Wikipedia.com). Inevitably, these industrial uses have repercussions in the environment. Although Cr(VI) can come from natural sources -for example, it can be produced when Cr(III)-bearing minerals dissolve and react with manganese oxide (Oze *et al.*, 2007)-, its presence in environmental systems is mainly due to anthropogenic activities. Generally speaking, chromium anthropogenic sources can be divided in two categories, direct and indirect. The direct sources come from chromium industrial activities, which include chromite ore refining, ferrochromium production,

refractory production, chromium chemical production, chromium plating, steel production, and leather tanning. Indirect sources include emissions from a given industrial activity using a process requiring feedstock or fuel where chromium is present as an impurity. These include coal and oil combustion, cement production, municipal refuse and sewage sludge incineration, cooling towers, asbestos mining and milling, and coke ovens (Kimbrough *et al.*, 1999).

The east coast of the United States was particularly affected by chromium pollution until very recently. Most of the national production of Cr(VI)-based chemicals obtained from the processing of Cr(III)-bearing ore was carried out by three companies located in Hudson County of New Jersey, from 1905 to 1975 (Burke *et al.*, 1991; Felter and Douson, 1996, http://www.state.nj.us/dep/srp/siteinfo/chrome /bkgrnd.htm). These three companies were PPG Industries, Inc. (PPG), whose former chromium chemical production facility was located at Garfield Avenue in Jersey City; Allied Signal, Inc. (Allied) previously located on Route 440 in Jersey City; and Occidental Chemical Corp., Maxus Energy Corp. and Chemical Land Holding Inc., previously located on Belleville Turnpike in Kearny. Although these three companies in 2008 are no longer active or have stopped processing chromium ores, a significant quantity of anthropogenic chromium still persists in the Hudson County area. The industrial residues from the chromium ore process, which contain significant amounts of chromium (between 2% and 7% -mostly Cr(III), but also with a small amount of Cr(VI)-), were deposited in the environment in various ways, such as fill material in the development of residential, commercial, and industrial sites. The New Jersey Department of Environmental Protection (NJDEP) estimated that the three companies produced and then deposited in the environment over two million tons of chromium

over 70 years during their activity in the 20th century. A few years ago, the department identified over 160 sites in the Hudson County area contaminated with chromium residues. Since many of these sites were located in urban residential areas -at least 130 sites in 1991- (Burke *et al.*, 1991), the NJDEP launched a chromium-cleaning program in 2005, and by February 2007, most contaminated sites in residential areas were remediated. At the present time, the NJDEP is still coping with the cleaning up of the remaining contaminated sites, using legal actions for reimbursements from the three companies mentioned above who are responsible for the pollution, or from their predecessors. In 2005, the JJDEP notably sued Honeywell, which is the direct predecessor of Allied Chemical.

Other countries have faced the same kind of environmental complications from improper storage and depositing industrial chromium ore residues, like England or Japan (Burke *et al.*, 1991). Consequently, many industries in the world have changed the way chromium ore is being processed. The use of a "no-lime" technique has been found to reduce the solid waste versus product ratio from three to one, and also to change the character of hazardous solid waste into inert waste (Kimbrough *et al.*, 1999).

### 1.1.2 Chemical Properties of Chromium

#### 1.1.2.1 Redox Reactions

The two stable forms of chromium are Cr(III) and Cr(VI). Chromium can be oxidized or reduced from one form to the other in the environment, depending upon concentrations of the reactants, pH of the media, temperature, light intensity, and other entities involved in the reaction (surfaces/sorbents, complexing agents, bacteria,

oxidizers/reducers, etc...). Manganese oxides are the main natural soil component that can convert Cr(III) to Cr(VI), while $V^{2+}$, $Fe^{2+}$, $S^{2-}$, $HNO_2$, $HSO_3^-$, and some organic species can reduce Cr(VI) to Cr(III) (Kimbrough *et al.*, 1999). Since water is one of the reactants involved in many chromium oxidation reactions, along with Cr(III) and the oxidizing agent, the conversion from Cr(III) to Cr(VI) rarely takes place in dry systems. Cr(III) is an octahedral hydrolysable molecule, which is usually positively charged in most environmental settings. It has a chromium atom surrounded by six other molecules that can be either water molecules or hydroxides, depending upon the pH of the medium (Figure 1.1).

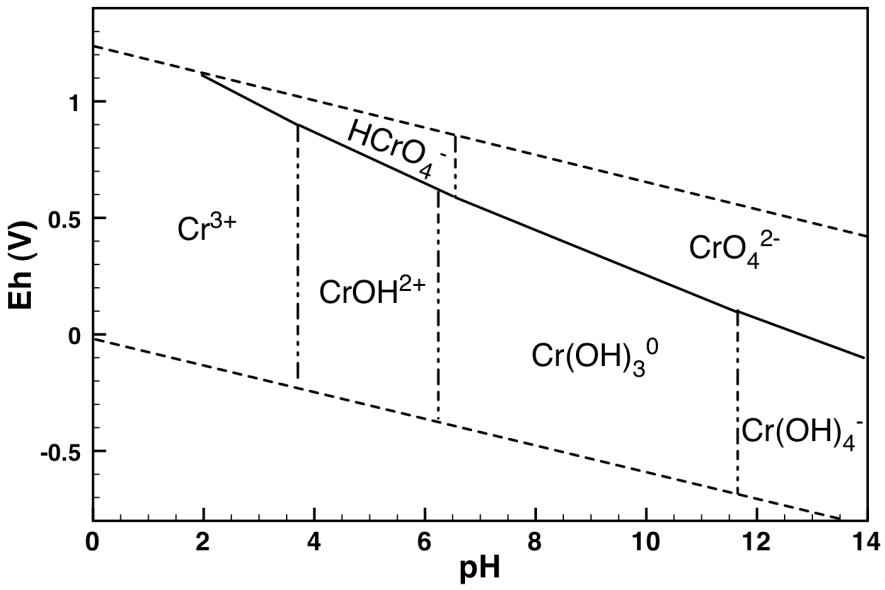


**Figure 1.1** Eh versus pH diagram for chromium (adapted from Rai *et al.*, 1989)

Inorganic or organic ligands can also be bound to Cr(III) and substitute for water or hydroxide molecules. Tetrahedral Cr(VI) does not hydrolyze, and it is always surrounded by four oxygen atoms at relatively low concentrations. Chromate $CrO_4^{2-}$ becomes hydrogen chromate $HCrO_4^{2-}$ and chromic acid $H_2CrO_4$ at lower pHs. Cr(VI) can also dimerize at high concentrations to become dichromate species ($HCr_2O_7^-$ and $H_2Cr_2O_7$).

#### 1.1.2.2 Precipitation/Dissolution Reactions

Trivalent chromium species have a low solubility index and are not soluble at most environmental conditions. Aqueous Cr(III) can form different hydroxide precipitates depending upon the concentration and the pH of the medium. The chemical properties and thermodynamic aspects of these chromium hydroxide precipitates have been reviewed in Rai *et al.* (1986).

Heavy metals can have their solubility lowered near surfaces. In that case, the precipitates formed are called "surface precipitates", and the equilibrium constant is lower than the K of the same precipitate in bulk solution. Three phenomena can be responsible for the decrease in solubility of an element close to a surface: 1) The solid surface may lower the energy of nucleation by providing sterically similar sites (McBride, 1991); 2) The activity of the surface precipitate is <1 (Sposito, 1986); and 3) The solubility of the surface precipitate is lowered because the dielectric constant of the solution near the surface is less than that of the bulk solution (O'Day *et al.*, 1994).

Although Cr(VI) is soluble at most environmental conditions, it can form salts with divalent cations, such as $Sr^{2+}$, $Zn^{2+}$, $Pb^{2+}$, and $Cu^{2+}$. Therefore, these Cr(VI) precipitates can provide a continual source of chromate ions in the environment (Kimbrough *et al.*, 1999).

#### 1.1.2.3 Sorptions/Desorption Reactions

Like other heavy metals, Cr tends to tightly sorb on soil components. For example, Cr(III) binds as an inner sphere complex with goethite and hydrous ferric oxide (Charlet and Manceau, 1992), silica (Fendorf *et al.*, 1994), and birnessite (Fendorf, 1992). Similarly, Cr(VI) is bound to goethite as an inner sphere complex (Fendorf *et al.* 1997).

## 1.2 Manganese oxides

### 1.2.1 Structures

Manganese is the 10th most abundant element in the earth's crust. It is present in the environment in three main oxidation states, Mn(II), Mn(III), and Mn(IV). Manganese(III) and Mn(IV) fall into the insoluble oxides and hydroxides category in the solubility classification of elements, due to their intermediate ionic potential, defined as z/r (where z is the ionic charge, and r is the radius). Therefore, strong bonds form between oxygen and Mn(IV) or Mn(III). Some manganese oxides mostly contain Mn(IV) (birnessite, for example), Mn(III) (manganite, for instance), or a mix of these two oxidation states. Additionally, although Mn(II) is considered to be a soluble cation due to its lower ionic potential, many manganese oxides also contain some Mn(II), like for example hollandite (made of both Mn(IV) and Mn(II)), or hausmannite (made of both Mn(III) and Mn(II)). The type of $MnO_2$ that forms in the environment depends on many different chemical and physical soil parameters, like manganese and oxygen contents, temperature, and bacteria. There are more than thirty varieties of manganese oxides in the environment (Post, 1999). These manganese oxides can be found either in coarse aggregates or fine-grained. Manganese nodules are ubiquitously found on the Earth's surface, both on continents and in the ocean. For

example, it is believed that manganese aggregates cover between 10% and 30% of the deep floor of the Pacific Ocean (Post, 1999). Like aluminum oxides, iron oxides, or organic matter, the fine-grained manganese oxides can coat soil components, including clay minerals. Even when they are present in soils in small quantity, manganese oxides can be involved in many different chemical reactions, due to their high surface areas, high sorption capacity, and strong oxidation capacity. Inorganic and organic ionic species can sorb on manganese oxide surfaces by electrostatic interactions. Cations sorb on manganese oxides that have low Point of Zero Charge (PZC) and negatively charged surfaces under most environmental conditions (for instance vernadite, which has a PZC of 2.7). Similarly, anions sorb on high PZC manganese oxides with a positively charged surface (for instance the surface of pyrolusite, which has a PZC of 7.3), since the average pH of many soils is below pH 7 (Sparks, 2003). In addition to their important sorption capacities, manganese oxides can be involved in redox reactions. For example, some manganese oxides, like birnessite, can oxidize Se(IV) to Se (VI) (Scott and Morgan, 1996), Cr(III) to Cr(VI) (Fendorf, 1992), and As (III) to As(V) (Nesbitt *et al.*, 1998).

All the types of manganese oxides share the same octahedral unit cell, made of one atom of manganese surrounded by six oxygen atoms. The spatial organization of that unit cell defines the type of manganese oxide. Although there are a lot of different varieties of manganese oxides, one could divide them in two main categories, the tunnel-structured oxides (including for example pyrolusite, todorokite, & MnOOH oxides) with square or rectangular cross sections, and the sheet-structured oxides (including chalcophanite, lithiophorite, & buserite) (Post, 1999).

### 1.2.2 Three Poorly Crystalline Manganese Oxides: Random Stacked Birnessite (RSB), Acid Birnessite (AB), and Vernadite/∂$MnO_2$/Hydrous Manganese Oxide (HMO)

Manganese oxides have many different structures and degrees of crystallinity. However, the most common forms found in the environment are fine-grained particles and have usually poorly crystalline structures, making their identification hard to determine with XRD (Post, 1999). Therefore, the generic name "manganese oxide" is usually used to refer to any kind of Mn oxides/hydroxides minerals found in soils. Two previous studies have compared the Cr(III) oxidation capacities of some manganese oxides that were drastically different in nature (Kim *et al.*, 2002; Weaver and Hochella, 2003). The chemical formulas and structure types of these manganese oxides are summarized in Table 1.1, as well as three different poorly crystalline manganese oxides: random stack birnessite (RSB), acid birnessite (AB), and vernadite/∂$MnO_2$/hydrous manganese oxide (HMO). The differences in manganese oxide-Cr(III) oxidation capacities observed in these two previous studies were quite predictable since tunnel structure minerals and sheet structure minerals were compared to each other. One gap in the literature is that no study has compared the Cr(III) oxidation capacities of manganese oxides that have similar poorly crystalline structures, like for example RSB, AB, and HMO. These three minerals could be compared to the fine-grained manganese oxides ubiquitously found in nature, including biogenic manganese oxides, which usually have an amorphous birnessite-like structure. The difference between HMO, AB, and RSB lies in the spatial

**Table 1.1** Formula and type of RSB, AB, HMO, and the manganese oxides used in two previous studies

| Name | Formula & Structure | Kim *et al.*, 2002 | Weaver & Hochella, 2003 | This study |
|---|---|---|---|---|
| random stack birnessite | $MnO_2$ , sheet structure | | | |
| verdanite | $MnO_2$ x n $H_2O$, sheet structure | | | |
| acid birnessite | $MnO_2$, sheet structure | | | |
| todorokite | (Ca, Na, K)(Mn(IV) ,$Mn(III))_6O_{12}$ $3.5H_2O$, tunnel structure | √ | | |
| manganite | MnOOH, 1x1 tunnel structure | | √ | |
| hausmannite | Mn(II) $Mn(III)_2O_4$, spinnel structure | | √ | |
| lithiophorite | $LiAl_2(Mn(IV)_2Mn(III))O_6(OH)_6$ , sheet structure | √ | √ | |
| birnessite | $(Na,Ca)Mn_7O_{14}$ $2.8H_2O$ , sheet structure | √ | √ | |
| romanechite | $Ba(Mn(IV),Mn(III))_5O_{20}$. $34H_2O$, 2x3 tunnel structure | | √ | √ |
| cryptomelane | $K(Mn(IV),Mn(III))_8O_{16}$ , 2x2 tunnel structure | | √ | √ |
| pyrolusite | Mn[III, IV] $O_2$ , 1x1 tunnel structure | √ | √ | √ |

orientation and area of their layers, as well as the space between layers (Villalobos *et al.*, 2003). Consequently, these three minerals have different degrees of crystallinity, HMO being the most defect rich, and RSB the most crystalline, which also implies different surface areas and sorption site availabilities. This is supported by the x-ray diffraction (XRD) data of these three minerals, shown in Figure 1.2, which suggest that these minerals have different degrees of crystallinity. Additionally, the SEM results shown in Figure 1.2 suggest that the minerals are physically different to each other. Since RSB, HMO and AB may also exhibit different Mn oxidation states, it is likely that each of them has a specific capacity to oxidize Cr(III).

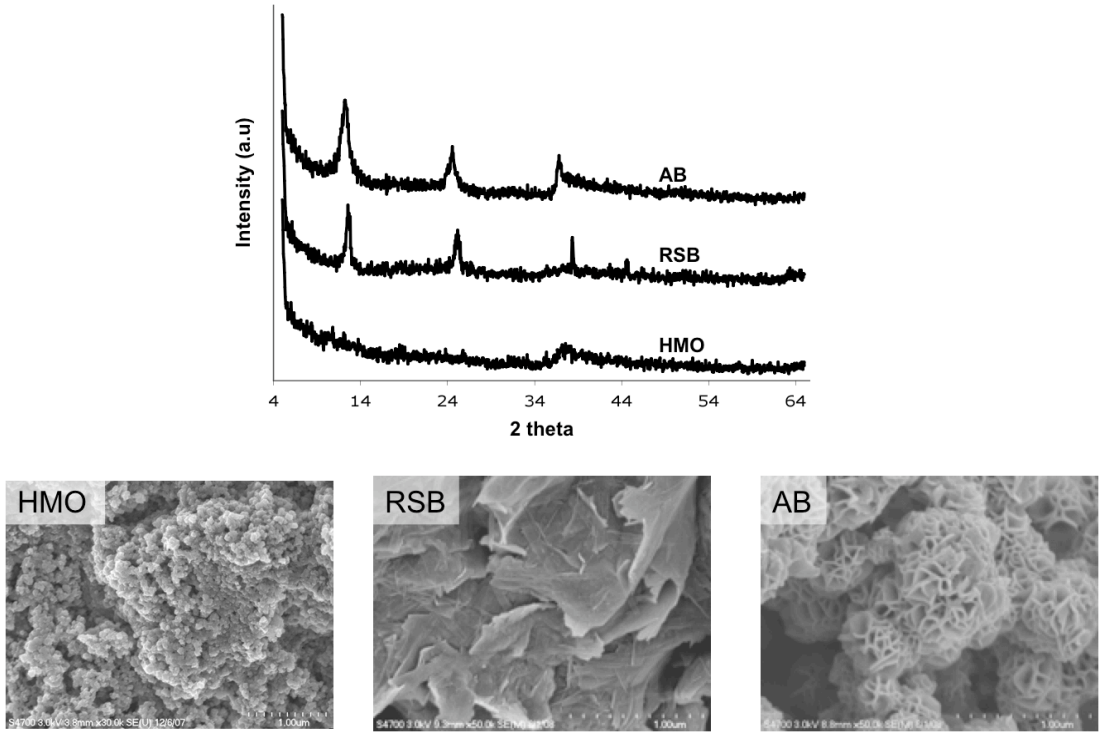


**Figure 1.2** XRD spectra (top) and SEM data (bottom) of AB, RSB, & HMO

### 1.2.3 Mn(II) Oxidation and Mn(IV) Reduction Quantum Mechanisms

The electron transfers and orbital rearrangements occurring during Mn(II) oxidation by $O_2$ were described in Luther (2005). The oxidation of Mn(II) to Mn(IV) occurs via single electron transfer and inner sphere bonding, due to orbital symmetry constraints between Mn(II) HOMO and $O_2$ LUMO. The Mn(II) electronic configuration is [Ar] $4s^1$ $3d^5$, with a high spin configuration. The $d^5$ level is split in two sub energy levels due to the crystal field; the bonding $t_{2g}$ ($\pi$) level, which contains

3 electrons, and the anti bonding HOMO $e_g$ ($\sigma$) sub level, which contains 2 electrons. Since the LUMO of $O_2$ is a $\pi$ orbital, Mn(II) and $O_2$ must be linked via an inner sphere complex during electron transfer, since the outer sphere complex is symmetry forbidden for two dissimilar orbitals like ($\pi$) of $O_2$ and ($\sigma$) of Mn(II). Also, the transfer most likely proceeds via a one-electron transfer step. That is to say, Mn(II) does not lose two electrons right away to become Mn(IV), it actually loses one electron to become Mn(III), a reaction intermediate. Then, Mn(III) can lose or gain an electron, to become either Mn(IV) or Mn(II). A single electron transfer is expected since the electron density of the $dz^2$ orbital in the $e_g$ level is spread in the three Cartesian coordinate axes, while the electron density of the $dx^2$-$y^2$ orbital in $e_g$ level is only spread in the xy plane.

Although a one electron transfer mechanism is most likely for both the oxidation of Mn(II) and the reduction of Mn(IV) due to orbital symmetry constraints, a two-electron transfer is also theoretically possible during Mn(IV) reduction. In that case, two electrons as a lone pair can fill up the two spin states of one $e_g^*$ orbital of Mn(II), before one electron transfers to the second $e_g^*$ orbital. The two electrons cannot directly fill the two orbitals of the $e_g^*$ level of Mn(II), because that case would require a reductant with two orbitals that can donate one electron each.

### 1.3 Manganese Oxide & Cr(III) Reactions

Cr(III) is oxidized to Cr(VI) by $MnO_2$ in soils (Fendorf 1992). This is the main reaction to naturally produce Cr(VI) in the environment, as opposed to Cr(VI) production from industrial activities. The amount of Cr(VI) produced from this natural reaction notably depends upon the pH of the medium, the nature of the manganese oxides (surface area, degree of crystallinity, sorption site availability,

etc...), and the concentration of both chromium and manganese oxides. However, in addition to oxidation, another reaction can occur during Cr(III) sorption on the manganese oxide surface. Trivalent chromium can precipitate on the manganese oxide surface in a chromium hydroxide surface precipitate. The kinetics and mechanisms of Cr(III) oxidation are discussed in 1.3.1, while the kinetics and structures of Cr(III) surface precipitation are discussed in 1.3.2

### 1.3.1 Cr(III) Oxidation by $MnO_2$: Kinetics and Mechanisms

#### 1.3.1.1 $MnO_2$ Physical & Chemical Property Dependence

Two studies, Kim *et al.* (2002), and Weaver and Hochella (2003), compared the capability of different manganese oxides to oxidize Cr(III) to Cr(VI). The structures of the manganese oxides used in those studies were previously detailed in section 1.2.2. Both studies used a batch experiment approach to measure the kinetics of Cr(III) oxidation over time. Their respective experimental conditions are summarized in Table 1.2. Weaver and Hochella (2003) found the following hierarchy in Cr(III)-oxidizing ability: birnessite> hausmannite>> romanechite> cryptomelane>> manganite = pyrolusite>> lithiophorite. Kim *et al.* (2002) found birnessite>> todorokite> lithiophorite> pyrolusite. These results suggest that the differences in reactivity are related to the structure of the manganese oxides, and more specifically to the degree of amorphous character. The most reactive mineral in both studies was birnessite, which is, as a matter of fact, the least crystalline mineral of the manganese oxides studied in both studies. Birnessite converted ≈80% of the initial Cr(III) concentration after 100 hours of reaction in Weaver and Hochella (2003), while 64%

**Table 1.2** Kinetics of Cr(III) by $MnO_2$: experimental conditions used in two batch studies

| Parameter | Kim & Moon, 1998 | Weaver & Hochella, 2003 |
|---|---|---|
| Ionic Strength | 0.01M KCl | 0.01M NaNO3 |
| Suspension Density | 0.4 & 0.8 g/L | 0.5g/L |
| pH | 3 & 6 | 4.4 |
| Cr(III) concentration | 200 μM | 100 μM |
| Reaction Time | 12 hours | 100 hours |

of Cr(III) was converted to Cr(VI) with the birnessite used by Kim *et al.* (2002). Additionally, another study (Kim and Moon, 1998) showed up to a 20% increase in Cr(VI) production by a less crystalline birnessite, which confirms that the degree of crystallization of manganese oxides influences the mineral's capability to oxidize Cr(III). Also, the surface area, which is related to the degree of crystallinity, can be also taken into account to predict Cr(VI) kinetics & extent of production. The hierarchy in surface area for the seven manganese oxides studied by Weaver and Hochella (2003), is birnessite> romanechite> cryptomelane> hausmannite> manganite ≈ pyrolusite ≈ lithiophorite. Therefore, this classification follows quite similarly the reactivity hierarchy discussed above, with the exception of manganite, which has a smaller surface area than romanechite and cryptomelane. The capability of manganese oxides to oxidize Cr(III) also depends on the manganese oxidation state on the mineral surface. XPS results from Kim *et al.* (2002) also suggest that the higher the Mn(IV)/Mn(III) content in $MnO_2$, the more Cr(III) is oxidized. This is due to the fact that Cr(III) can supply more electrons to Mn(IV) (up to two electrons) than to Mn(III)

(just one electron). Consequently, the extent of chromium (III) oxidation also depends on the mineral's manganese oxidation state, and a higher Mn(IV) content over Mn(III) content in the chemical structure of $MnO_2$ implies a higher Cr(VI) production.

#### 1.3.1.2 Cr(III) Oxidation Mechanisms

Cr(III) oxidation to Cr(VI) on the surface of the manganese oxide proceeds in successive step reactions. Three general steps successively occur: i) Cr(III) sorbs on the mineral surface, ii) electron transfer between chromium and manganese as well as oxygen ligand rearrangements, and iii) desorption of reactions products. The kinetics and mechanisms of these three steps are still not completely understood, and were previously discussed by Manceau and Charlet (1992), Johnson and Xyla (1991), Fendorf (1992), Silvester *et al.* (1995), Banerjee and Nesbitt (1999), and Nico and Zasoski (2000).

##### 1.3.1.2.1 Cr(III) Sorption Mechanisms

The binding mechanism of Cr(III) sorption on manganese oxides –outer-sphere versus inner-sphere complex- is still not known (Nico and Zasoski, 2000). Previous studies suggested that Cr(III) sorbs on birnessite as an inner-sphere complex, both experimentally by EXAFS fitting (Manceau and Charlet, 1991) and theoretically using a Molecular Orbital Theory (MOT) approach (Fendorf, 1992). According to MOT, a symmetry allowed reaction must follow these criteria: 1) the molecular orbitals must align for a good overlap, 2) the lowest unoccupied molecular orbital (LUMO) of the oxidant should be lower than that of the highest occupied molecular orbital (HOMO) of the reductant or within 6 eV, and 3) the bond breaking/forming products must be in agreement with expected products (Luther, 1990).

Fendorf (1992) showed with MOT that it is impossible to obtain a significant orbital overlap necessary for an outer-sphere electron transfer from Cr(III) directly to Mn(IV), since the HOMO of Cr(III) is a $d_{xz}$ $\pi$ orbital and the LUMO of Mn (IV) is a $d_z^2$ $\sigma^*$ orbital (Figure 1.3). Fendorf (1992) showed that electron transfer from Cr(III) to manganese(IV) is possible when an oxygen atom is bound between manganese and chromium. The filled p orbital of the oxygen acts as a bridge that facilitates the electron transfer (indirect symmetry allowed outer-sphere mechanism in Figure 1.3). The electron from the chromium $d_{xy}$ orbital can transfer to the $p_x$ orbital of oxygen, and, after intra atomic e- transfer from the $p_x$ orbital to the $p_z$ orbital of oxygen, the electron can finally be transferred to the manganese. Although Fendorf (1992) called this mechanism an inner-sphere mechanism, it does not necessarily require a chemical bond between Cr(III) and oxygen for the electron to be transferred. Therefore, this looks like an indirect symmetry allowed outer sphere mechanism case (with oxygen not bound to either Cr(III) or Mn), instead of an inner sphere mechanism as was discussed in Fendorf (1992). For inner sphere complexes (Cr(III) directly binds to oxygen) electrons can transfer through aligned orbitals, similarly to a symmetry allowed outer sphere complex, but also directly through the chemical bond (sigma bond or the pi bond) between Cr(III) and oxygen.

Silvester *et al.* (1995) concluded, from experimental observations, that the sorption between Cr(III) and Na-buserite occurred via an outer-sphere mechanism. Their overall mechanism considered both the sorption of Cr(III) on the mineral surface and the first electron transfer from Cr(III) to Mn(IV) as one, first single reaction.

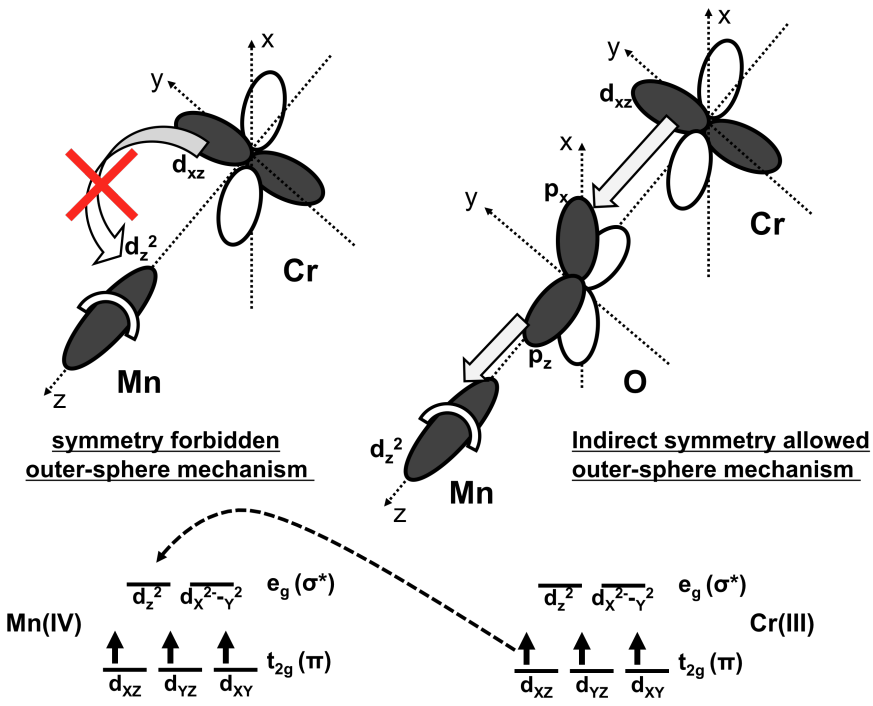


**Figure 1.3** Outer-sphere complex and indirect symmetry allowed outer-sphere complex between Cr(III) and Mn(IV), according to MOT (adapted from Fendorf, 1992)

Therefore, the first step of their overall Cr(III) oxidation mechanism was:

$$Cr(III)_{aq} + MnO_2 \Rightarrow Cr(IV) + e- \qquad (1.1)$$

Silvester *et al.* (1995) assumed that reaction (1.1) was the limiting step of their overall mechanism since Cr(III) has much lower electron transfer rates and ligand exchange rates than Cr(IV), and Cr(V), based on crystal field theory. Indeed, Cr(III) is a $d^3$ ion; its three electrons that fill each of the three $d_{xy}$, $d_{xz}$, and $d_{yz}$ bonding orbitals produce a crystal field more stable than the crystal field of Cr(IV) $d^2$, and Cr(V) $d^1$. Silvester *et*

*al.* (1995) measured the rate constant k of the Cr(III) oxidation at different pH values to infer the sorption mechanism of Cr(III) on manganese oxide. They found that all k values were very similar to each other, regardless of the change in pH. They concluded that since pH didn't have any effect on the rate constant of the reaction (i.e, the rate limiting step (1)), Cr(III) sorption rates were not affected by changes in pH, and thus no ligand exchange mechanisms (i.e, inner sphere complex, which is pH dependent) occurred during reaction 1. Therefore, they concluded that the sorption mechanism was an outer sphere complex.

Their conclusion is valid only if one does not consider reaction (1) as two separate steps that have different kinetics: a Cr(III) sorption step, followed by an electron transfer step. If the two steps occur successively -which is likely to be the case- the limiting step would be either Cr(III) sorption on the manganese oxide -step (a)-, or electron transfer -step (b)-. With two separate steps, the overall rate constant k being not pH dependent would not necessarily mean that the sorption mechanism is outer sphere. Indeed, the chromium ligand exchange rate is pH dependent and gets lower as pH increases (for example, $Cr(OH)^{2+}$ will sorb 75 times faster than $Cr^{3+}$ ) while Cr(III) does not readily oxidize to Cr(IV) at any pH value, due to the particularly strong Cr(III) crystal field stability from the $d^3$ electronic configuration. Moreover, the standard voltages ($E^0$) also predict that the first electron withdrawal of Cr(III) will be the slowest electronic step (Nico and Zasoski, 2000). Consequently, it is possible that Silvester *et al.* (1995) didn't observe any pH dependence on the rate constant values not because the sorption mechanism was an outer sphere complex, but rather due to the fact that the first electron transfer (occuring after Cr(III) sorption) was the actual limiting step of the overall reaction. Therefore, the sorption mechanism

in their system could have been inner-sphere complexation, although the rate constant was not pH dependent. This assumption is supported by the study of Johnson and Xyla (1991). In this research, the rates of Cr(III) oxidation with manganite MnOOH were measured at different pH values, and, similarly to Silvester *et al.* (1995), the k values were found to be not pH dependent. The authors of the study suggested that the overall rate constant being pH independent probably rules out the possibility of Cr(III) sorption being the limiting step. Instead, they hypothesized that the slowest step was the first electron transfer (Cr(III) => Cr(IV)). However, they did not propose any type of sorption mechanism.

#### 1.3.1.2.2 Overall Reaction Mechanism

A detailed reaction mechanism for Cr(III) oxidation on manganese oxides was proposed in Fendorf (1992). This mechanism considered that Cr(III) sorbs primarily as a bidentate inner-sphere complex on the mineral surface, as was experimentally observed with EXAFS (Manceau and Charlet, 1991). In other words, Cr(III) is bound to two oxygen atoms, which are also bound to three manganese atoms. The oxidation state of these three manganese atoms affects Cr(III) sorption kinetics, since ligand exchange rates of Mn(IV) are slower than Mn(III) that has a $d^4$ configuration, due to the stable $d^3$ configuration of Mn(IV) (Nico and Zasoski, 2000) . In addition to the oxidation state of the three manganese atoms linked to Cr(III) via

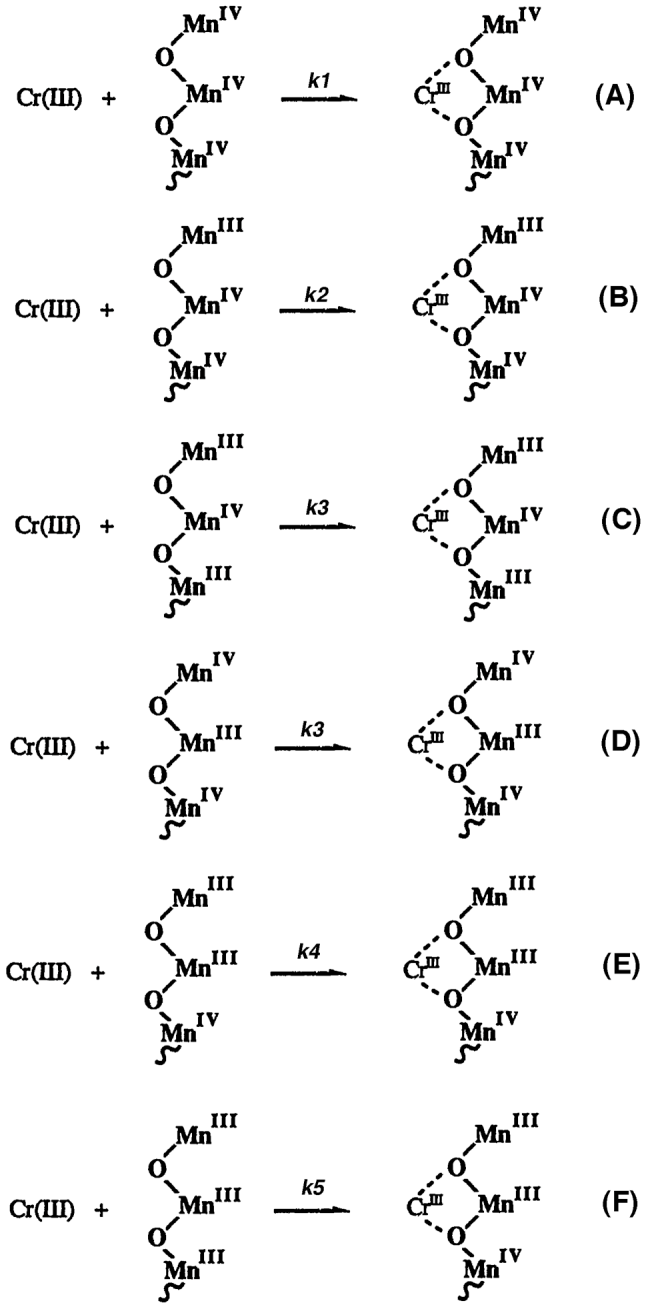


**Figure 1.4** Cr(III) sorption rate constant dependence on manganese oxidation states of $MnO_2$ surface: six possible reactions (from A to F)

two oxygen atoms, the rate of Cr(III) sorption also depends on the speciation of hydrolysable Cr(III), whose form is pH dependent: the higher the pH, the faster the ligand exchange rate of Cr(III) (Johnson and Xyla, 1991). Therefore, many factors need to be taken into account to constrain chromium sorption rates, including the chemical nature of the manganese oxide, as well as the pH of the system. Also, given the large varieties of manganese oxides existing in nature, and since each variety exhibits a different manganese oxidation state ratio (Mn(III)/ Mn(IV)), the rate of Cr(III) sorption on manganese oxides must encompass a wide range of kinetics. Therefore, the rate constant k1 for the Cr(III) sorption step in Fendorf (1992) only represents a Cr(III) bidentate inner-sphere sorption mechanism involving three Mn(IV) atoms, and one could expect another k value under other conditions. Figure 1.4 shows the Cr(III) sorption rate constant dependence on the manganese oxidation states. Six sorption reactions are possible (A to F), each of them has a specific rate constant: k1, k2, k3 -note that C and D have the same rate constant k3 since the two oxygen atoms in C and D are both linked to 2 Mn(III) and 2 Mn(IV)-, k4, and k5. From the chemical properties of Mn(III) and Mn(IV) given by the crystal field theory previously discussed, one can thus expect: $k1 < k2 < k3 < k4 < k5$. After sorption on the manganese oxide, Cr(III) oxidizes to Cr(VI) by supplying three electrons to the manganese oxide surface. Fendorf (1992) hypothesized that the electronic transfer can occur via an inner sphere mechanism in either one electron transfer step, two simultaneous electron transfer steps, or three simultaneous electron transfer steps, since the outer sphere complex mechanism is not symmetry allowed (Figure 1.3). Luther (2005) suggested that one Mn(IV) atom directly reduces to Mn(II) with two electrons at a time, which in theory is possible, but one electron is more likely, due to

the fact that a transfer to the $dx^2$-$dy^2$ and $dz^2$ of manganese would require electrons coming from two different orbitals in one ligand. Thus, it is likely that two electrons coming from the same orbital will be transferred for a short period to the $dz^2$ orbital with two opposite spin numbers, followed by one electron transfer to the $dx^2$-$dy^2$ (Luther, 2005).

Consequently, although the reaction in Fendorf (1992) shown in Figure 1.5 (A), that sketches the mechanism of three simultaneous electron transfers from

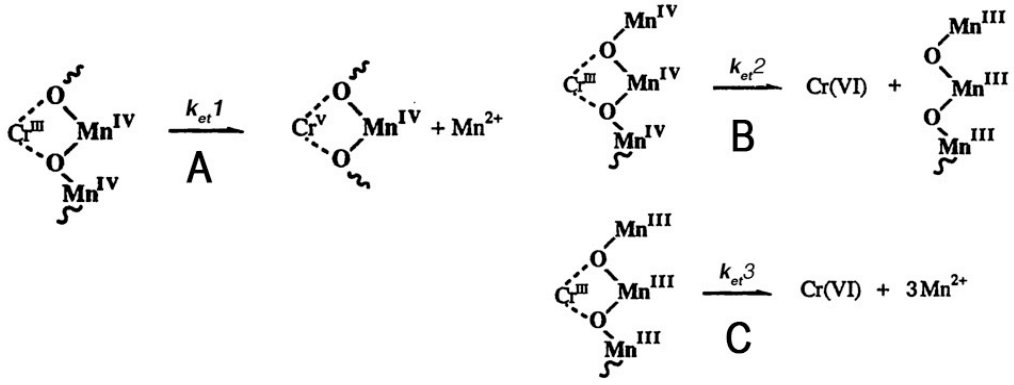


**Figure 1.5** A) Mechanism from Fendorf (1992) (adapted from Fendorf (1992)), and B & C) proposed reactions

Cr(III) to two different manganese atoms (one atom receiving two electrons) could occur, inner sphere mechanisms involving three different Mn(IV) or Mn(III) simultaneously receiving one electron is more likely to occur (Figure 1.5 (B) and Figure 1.5 (C)). The kinetics and mechanisms of the electronic transfer step(s) depend on the Mn oxidation state on the manganese oxide surface. Mn(III), which has a $d^4$ electronic configuration, can be reduced more easily than $d^3$ Mn(IV), which has a high ligand field stability due to its three $t_{2g}$ orbitals filled with one electron. Although birnessite is commonly considered to be a Mn(IV) oxide, it does contain a non-negligible amount of Mn(III) in its structure. For instance, Banerjee and Nesbitt (1999) estimated with XPS that the birnessite's surface contained 5%, 20%, and 75% of Mn(II), Mn(III), and Mn(IV), respectively. Therefore, one must take into account the presence of Mn(III) in birnessite to understand the electron transfer mechanisms during chromium oxidation. Although the electron transfer reactions proposed in Fendorf (1992) included the possible presence of Mn(III) in birnessite, only two manganese atoms -Mn(III) and/or Mn(IV)- were involved in chromium oxidation mechanisms. If one assumes a bidentate inner sphere complex for the Cr(III) sorption mechanism, one should consider three manganese atoms potentially involved in the electron transfer mechanisms. Consequently, many electron transfer pathways are possible between Cr(III) and the three manganese atoms, the kinetics of each of them depends on the oxidation number of the three manganese atoms and the number of electrons that are simultaneously lost by the chromium atom. It is likely that three electrons will be released almost at the same time by Cr(III). Indeed, Cr(III), which is a $d^3$ ion, has a very stable crystal field due to its three singly filled bonding orbitals, which makes the removal of one of these electrons difficult. Therefore, one can expect

that the first oxidation of trivalent chromium –Cr(III) to Cr(IV)- is probably the rate limiting step of the reaction. Then, due to the $d^2$ electronic configuration of Cr(IV) that makes the element reactive due to the Jahn-Teller distortion effect, a fast oxidation can occur –Cr(IV) to Cr(V)- followed by another rapid oxidation –Cr(V) to Cr(VI)- due to the $d^1$ electronic configuration of Cr(V) that also creates a Jahn-Teller distortion effect. Therefore, after the first electron has been pulled away from Cr(III), Cr(VI) forms almost instantaneously: three electrons have been released from Cr(III) almost at the same time. Therefore, considering that manganese is likely reduced with a gain of one electron at a time (Luther, 2005), and Cr(III) is releasing three electrons at a time to become Cr(VI), four electronic transfer reactions are possible (Figure 1.6).

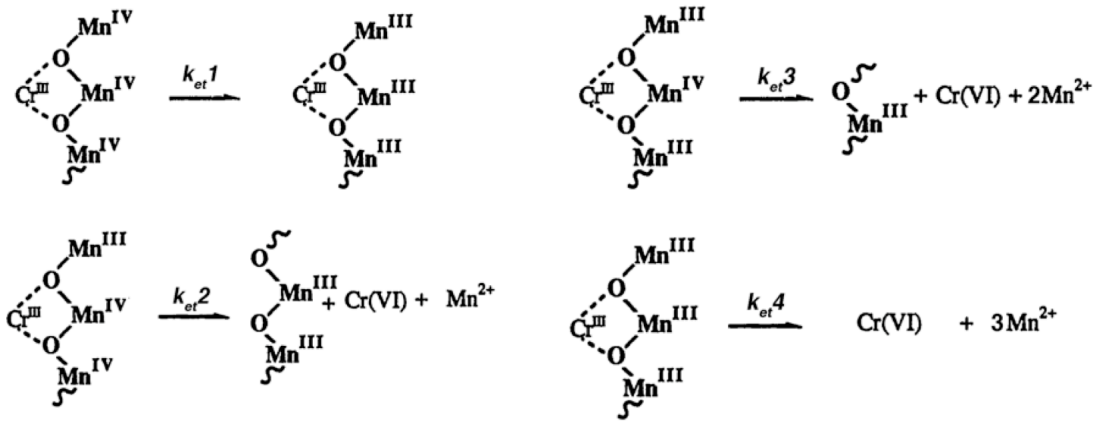


**Figure 1.6** Possible electron transfer reactions from Cr(III) to Mn(III) and/or Mn(IV)

Since the reduction of Mn(III) is faster than the reduction of Mn(IV) due to the crystal field stability of $d^3$ Mn(IV), one could expect that rate constants of the electron transfer reaction proposed in Figure 1.6 would follow the trend: $k_{et}1 < k_{et}2 < k_{et}3 < k_{et}4$.

#### 1.3.1.3 Rates Constants Reported in the Literature

The kinetics of Cr(III) oxidation by manganese oxide are typically characterized by a biphasic process in which oxidation is initially rapid followed by slow reactions. As a matter of fact, this type of kinetics is the case for many other chemical reactions occurring in soils (Kim and Moon, 1998; Fendorf and Zasoski, 1992; Nico and Zasoski, , Weaver *et al.* 2002). The first reaction period is likely due to rapid Cr(III) oxidation mechanisms with edge surface sites on the unreacted manganese oxide surface. Other phenomena can be taken into account during the second phase, including Cr(III) diffusion on/in the mineral, Cr(III) surface precipitation, dissolution of the mineral surface, inhibition of Cr(III) sorption due to Cr(III) surface precipitation that covers the $MnO_2$ surface sites, and sorption competition between Cr(III) and Mn(II).

The reactivity of Cr(III) with manganese oxides has been studied using batch techniques (Kim and Moon, 1998; Fendorf and Zasoski, 1992; Weaver *et al.* 2002). Trivalent chromium was reacted with a manganese oxide suspension, aliquots at different reaction times were filtered, and the filtrate solution was analyzed for total chromium and total manganese. Aqueous Cr(VI) was measured using the s-diphenyl carbazide (Barlett and James, 1979), while total aqueous chromium and total aqueous manganese were measured by ICP to infer the amount of Cr(III) and $Mn^{2+}$ in solution.

It is important to mention that these batch experimental techniques only enabled one to quantify Cr(VI) in solution and not the total amount of Cr(VI) produced by the oxidation of Cr(III), due to the aliquot filtering steps necessary to separate the reacting mineral suspension from the aqueous species. Even when the surface of the manganese oxide is negatively charged at experimental conditions where the pH is over the mineral's PZC, an unknown amount of negatively charged Cr(VI) can be sorbed on the manganese oxide surface -this is also the case with negatively charged arsenate sorbed to negatively charged HMO (Landrot *et al.*, in preparation). Similarly, an unknown quantity of $Mn^{2+}$, which is one of the products of Cr(III) oxidation reaction, readsorbs on the manganese oxide surface (Fendorf, 1992). Therefore, one has to measure both $Cr(VI)_{sorbed}$ and $Cr(VI)_{aqueous}$ to infer $Cr(VI)_{total}$. For instance, one could use X-Ray Photoelectron Spectroscopy (Banerjee and Nesbitt, 1999) or XANES (Peterson *et al.* 1997) to quantity $Cr(VI)_{sorbed}$ from pastes of filtered manganese oxide suspension, and then add that amount to the [Cr(VI)] measured in solution.

Rate parameter measurements of the Cr(III) oxidation using batch experimental techniques are difficult since the real concentrations of the reaction products, Cr(VI) and $Mn^{2+}$, cannot be directly quantified (not to mention the slow data acquisition time). A number of studies have reported the concentration of Cr(VI) in solution with time, which gives a good assessment of the reaction extent, the capability of the manganese oxide to oxide Cr(III), and the minimum [Cr(VI)] produced by the reaction. However, only a few studies have tried to measure the rate constant of either the intermediate steps, or the overall Cr(III) oxidation reaction. For example, Johnson and Xyla (1991) reacted Cr(III) with manganite (MnOOH), and

calculated the rate constant k and the rate order by measuring [Cr(VI)] in solution, assuming this concentration to be the total Cr(VI) produced by the reaction. They found that the reaction is first order with respect to the manganite adsorption density and also to Cr(III) concentration. Thus, their overall rate equation was second order:

$$d[Cr(VI)]/dt = k \,.\, ([Cr(III)_o] - [Cr(VI)]).\, [MnOOH] \qquad (1.2)$$

The k value was $1.08.10^{-2} \pm 0.03.10^{-2}$ L $.m^{-2}$ $s^{-1}$. Their rate equation features the concentration of manganese surface sites, instead of the total MnOOH suspension density concentration, since the inside part of many manganite particles is not exposed to the solution. However, one could also take into account that the surface is constantly consumed by the Cr(III) oxidation, which could change the assumed concentration of exchangeable sites on manganite (7.9 μmol/$m^2$) that had been measured with a fluoride adsorption experiment.

Fendorf (1992) also found an overall rate order of two when reacting Cr(III) with birnessite. To minimize the effect of readsorption or the products, a stirred flow technique was used, and the rate parameters were measured by quantifying [Cr(VI)] in solution and assuming that the concentration was the total amount of hexavalent chromium produced by the Cr(III) oxidation. Moreover, readsorption of $Mn^{2+}$ was assumed to be negligible.

#### 1.3.1.4 Concentration Effects

Cr(III) speciation in solution depends upon concentration and pH. It precipitates in bulk solution as a chromium hydroxide phase $Cr(OH)_3$ even below high concentrations and high pH values (Rai. *et al.*, 1986). Also, like many other metals in the first row of transition metals, Cr(III) can precipitate on mineral surfaces below its saturation index, as mentioned previously. Consequently, one can expect that

less Cr(III) will be oxidized to Cr(VI) on the manganese surface at high Cr(III) concentrations, since formation of Cr(III) surface precipitates occur. This has been experimentally observed; for example, Johnson and Xyla (1991) noticed that the rate of Cr(III) oxidation by manganite at pH>4.5 was lower when [Cr(III)] increased. Fendorf and Zasoski (1992) also observed that Cr(III) oxidation by birnessite was lower at high Cr(III) concentrations. The experimental conditions of both studies were such that Cr(III) could not precipitate in solution. Consequently, the variation in the extent of chromium oxidation at different Cr(III) initial concentrations was due to surface precipitation phenomena on the mineral surface.

#### 1.3.1.5 pH Effects

##### 1.3.1.5.1 pH Effects on the Total Amount of Cr(III) Oxidized at the End of the Reaction

As previously discussed, Cr(III) precipitates in bulk solution under high pH values and at relatively low concentrations (Rai. *et al.* 1986). Additionally, trivalent chromium can precipitate as a chromium hydroxide phase on the surface of manganese oxides even at concentrations under the Cr(III) saturation index. Therefore, since the amount of hydroxide ions in solution increases with increasing pH, one can expect that the probability of chromium hydroxide surface precipitation will increase with increasing pH, even at a pH range where Cr(III) is not expected to precipitate in bulk solution. Fendorf and Zasoski (1992) showed that the pH doesn't have any effect on the amount of Cr(III) oxidized by manganese oxide until pH=3.5. At higher pH values, the amount of Cr(VI) produced decreases with increasing pH. This trend was also observed in Feng *et al.* (2006): the amount of Cr(III) oxidized with birnessite was relatively the same in a pH range between pH=2 and 3.5, but decreased at pH=3.5.

The presence of chromium hydroxide surface precipitation thus decreases the amount of Cr(VI) produced, by precipitating Cr(III), and covering the surface of the manganese oxide, which impedes Cr(III) sorption and oxidation.

#### 1.3.1.5.2 pH Effects on Initial Rates

Although the total amount of Cr(VI) produced at the end of the reaction decreases with increasing pH, the initial rates of Cr(III) oxidation increases with increasing pH (Fendorf and Zazoski, 1992). Indeed, Cr(III) species are mostly positively charged over a wide [Cr(III)] and pH range, while the $MnO_2$ surface gets more negative as pH increases. Therefore, one can expect that electrostatic interactions will be high at high pH, and thus the kinetics of Cr(III) sorption will increase with increasing pH, which will also increase the initial rates of chromium oxidation.

### 1.3.1.6 Effect of Oxygen

Different species containing oxygen can oxidize Cr(III) to Cr(VI) in soils. Their respective reaction with Cr(III) as well as their $E^0$ values were summarized in Kimbrough *et al.* (1999):

A) $2Cr^{3+} + 5H_2O + 3O_3 <=> 2CrO_4^{2-} + 10H^+ + 3O_2$, $E^0$=0.87 V (1.3)

B) $2Cr^{3+} + 2H_2O + 3H_2O_2 <=> 2CrO4^{2-} + 10H^+$, $E^0$=0.58 V (1.4)

C) $3MnO_2 + 2Cr(OH)_3 <=> 3Mn^{2+} + 2CrO_4^{2-} + 2H_2O + 2OH^-$, $E^0$=1.328 V (1.5)

D) $2Cr^{3+} + 3H_2O + 2MnO_4^- <=> Cr_2O_7^{2-} + 6H^+ + 2MnO_2$, $E^0$=0.35 V (1.6)

E) $2Cr^{3+} + 7H_2O + 6Mn^{3+} <=> Cr_2O_7^{2-} + 14H^+ + 6Mn^{2+}$, $E^0$=0.18 V (1.7)

F) $2Cr^{3+} + H_2O + 3PbO_2 <=> Cr_2O_7^{2-} + 2H^+ + Pb^{2+}$, $E^0$=0.13 V (1.8)

Reaction (C), involving $Cr^{3+}$ and manganese oxide, has the highest $E^0$, which means it is the most favorable reaction from a thermodynamic standpoint. Other reactants that

can oxidize Cr(III) to Cr(VI) include ozone (A), hydrogen peroxide (B), and lead (F). The reactivity of these three species with Cr(III) depend on water chemistry, since water molecules are needed for the reaction to proceed. The most important criteria for a redox reaction to occur are favorable thermodynamic conditions (high E value for example) but also concentrations of the reactants. Therefore, although Cr(III) oxidation by ozone (A) is possible from a thermodynamic point of view, the reaction is not likely to occur in soils, since ozone levels are generally very low in the environment (Kimbrough *et al.*, 1999).

Dissolved oxygen can participate in many important redox reactions in the environment (for instance, the nitrification or the aerobic respiration). However, it has been shown that it does not interfere with the manganese oxide surface to oxidize Cr(III) to Cr(VI). For example, Eary and Rai (1987) concluded that Cr(III) reacted directly with manganese dioxide to produce Cr(VI) and not by catalyzed reactions with oxygen at the ß-$MnO_2$ surface. Their experiment consisted of reacting, in a batch vessel, Cr(III) with a manganese oxide at both aerated & unaerated conditions, and the apparent rate constant of the reaction was measured. They finally observed that only the mineral surface area to solution ratio (A/V) had an effect on the rates of Cr(III) oxidation.

#### 1.3.1.7 Sorption Competition Between Cr and Other Elements on $MnO_2$ Surfaces

The competition between Cr(III) and other ions -Al(III), Mn(II), La(III), Co(II)- on $\partial$-$Mn0_2$ surface was investigated in Fendorf (1992). In a series of experiments, each competitive ion at a concentration of 290 µM was firstly added to a suspension of $\partial$-$Mn0_2$ at 0.1 g/L in a batch vessel, followed by the addition of Cr(III).

Four sets of experiments were done at two Cr(III) concentrations, 2 μM and 15 μM, and two pH values, pH 3 and 5. Another series of batch experiments were carried out with Cr(III) and ∂-$MnO_2$, reacting at the same experimental conditions, but without addition of any competitive ions. The results of that study showed that although competitive ions were in excess compared to Cr(III), they did not affect the amount of Cr(VI) produced at the end of the reaction at pH=3. The same amount of Cr(VI) was measured in solution at this pH value, for all competitive ion experiments and for the experiment without any competitive ion. Only aluminum decreased the production of Cr(VI) at pH 5, by a significant decrease of 80% $[Cr(VI)]_{aqueous}$ produced at the end of the reaction.

The fact that $Mn^{2+}$ present in excess compared to trivalent chromium didn't change the amount of $Cr(VI)_{aqueous}$ produced was particularly noteworthy. Indeed, $Mn^{2+}$ is a product of Cr(III) oxidation, and it is known to sorb very rapidly to the manganese oxide when no other ions are present in solution, as was shown in a former study that used Electron Paramagnetic Spectroscopy to study the kinetics of $Mn^{2+}$ sorption to ∂-$MnO_2$ (Fendorf *et al.*, 1993). Consequently, it is often believed that $Mn^{2+}$ reabsorbs to the manganese oxide surface after its production from Cr(III) oxidation, sorbing on surface sites and thus preventing further Cr(III) oxidation. The competitive sorption experiments conducted in Fendorf (1992) thus suggested that trivalent chromium has much higher affinity for the manganese surface than $Mn^{2+}$ when both elements are present in solution, meaning that a $Mn^{2+}$ poisoning effect on the manganese surface during Cr(III) oxidation is finally not significant. This is also supported by Weaver and Hochella (2003) from $[Cr(VI)]_{aqueous}$ and $[Mn^{2+}]_{aqueous}$ measured in their batch experiment aliquots. The concentration of $Mn^{2+}$ only produced

by the dissolution of the mineral due to the low pH of the system ("acidic effect" $[Mn^{2+}]$, without the presence of Cr(III) in solution), as well as the concentration of $Mn^{2+}$ produced by both the dissolution of the mineral due to the low pH and the Cr(III) oxidation reaction were both measured in Weaver and Hochella (2003). They found that the ratio $[Mn^{2+}]_{aqueous}$ (with acidic dissolution substracted)/ $[Cr(VI)]_{aqueous}$ was about 1.5 for all the manganese oxides that had a Mn oxidation state about (IV), which was the case for birnessite, romanechite, cryptomelane, lithiophorite, and pyrolusite. Considering the proposed reaction between Cr(III) and $Mn(IV)O_2$ (reaction (C) on page 30) , one mole of Cr(VI) is produced for 1.5 mole of $Mn^{2+}$ produced. Therefore, $[Mn^{2+}]_{aqueous}$ (with acidic dissolution substracted)/ $[Cr(VI)]_{aqueous}$=1.5 in solution would suggest that most Cr(VI) and $Mn^{2+}$ produced on the mineral surface desorbs to solution and does not readsorb. The amount of Cr(VI) measured in solution did not change regardless of the presence of competitive ions, except with aluminum at pH=5. In that case, the amount of aqueous Cr(VI) produced at the end of the experiment decreased by 80% compared to the other experiments. At these experimental conditions, TEM showed that both Al(III) and Cr(III) formed a surface precipitate on the manganese oxide surface, most likely a metal hydroxide surface precipitate. This would suggest that the surface precipitate prevented Cr(III) from becoming oxidized by shielding the mineral surface, resulting in a decrease of $[Cr(VI)]_{aqueous}$. Therefore, these experiments showed that not only Cr(III) can precipitate on the surface of manganese oxide at high pH and below its saturation index in bulk solution, but also other elements that have similar ionic potential (ionic radius/charge of ion) to the Cr(III) ionic potential. Both $Cr^{3+}$ and $Al^{3+}$ have intermediate ionic potential values, which classify them as "insoluble oxides and

hydroxide elements". This is not the case for $Mn^{2+}$ classified as a "soluble cation" due to its lower ionic potential –thus it is less likely to precipitate on the manganese oxide surface. Consequently, the presence of these metal hydroxide precipitates can drastically decrease the amount of Cr(III) oxidized, by covering up the reactive sites on the manganese oxide surface, preventing trivalent chromium sorption and thus oxidation.

### 1.3.2 Kinetics and Structures of Chromium Surface Precipitates

#### 1.3.2.1 Kinetics of Chromium Surface Precipitate Formation

Although it has been shown that chromium hydroxide forms on manganese oxide surfaces even at pH and concentrations at which Cr(III) does not precipitate in bulk solution, the kinetics of formation of surface precipitation are still not well understood. This is mainly due to the lack of techniques that can quantify and identify mineral surface phases in real time and *in situ*. For example, although x-ray photoelectron spectroscopy (XPS) and transmission electron microscopy (TEM) are surface techniques that can quantify and identify elements on mineral surfaces, they require drying the sample before analysis, which could ultimately change the speciation of the element analyzed on the surface. X-ray absorption fine structure spectroscopy is an *in situ* technique, which is particularly useful for wet soil samples. However, rapid kinetic measurements are not possible with traditional XAFS since data collection is slow -on the order of several minutes. Fluid cell atomic force spectroscopy is an *in situ* surface technique that can measure the formation rates of surface precipitates; however, one cannot do elemental quantification with this technique.

Previous studies used XPS to investigate the kinetics of chromium hydroxide precipitate formation on manganite (Weaver *et al.*, 2002) and on birnessite (Banerjee and Nesbitt, 1999). One can use XPS to follow the formation of the surface precipitate by looking at the XPS O1s peak (Weaver *et al.*, 2002, Banerjee and Nesbitt, 1999). The XPS $Cr2p^{3/2}$ peak is challenging to interpret since it is composed of several sub-peaks that can correspond to the multiplets of Cr(III), Cr(IV), Cr(V), and the single peak of Cr(VI). All chromium oxidation states thus show up at about the same binding energy in the XPS spectrum. However, the peak of oxygen is much simpler to interpret since it contains just three sub-peaks: an oxide peak at 530.6 e V, a hydroxide peak at 532 eV, and a water peak at 533.4 eV. Since the chromium surface precipitate is a metal hydroxide phase, one can thus measure its rates of formation by looking at the growth of the hydroxide sub-peak at 532 eV in the XPS O1s peak, and comparing it with the oxide peak at 530.6 eV. Weaver et al (2002) also mentioned that the growth of the hydroxide peak correlated with the observed increase in XPS chromium peaks with reaction time, and thus concluded that $Cr(OH)_3.3H_2O$ formed at the manganite surface. The same observations were seen in the XPS results of Banerjee and Nesbitt (1999) where chromium was reacted with birnessite. The XPS hydroxide peak as well as the height ratio between the hydroxide and the oxide peaks both increased with reaction time. However, one could argue that other sources of hydroxides could contribute to the growth of the peak at 532 eV. For instance, in the case of Mn(IV) oxides (that is the case with birnessite but not with manganite, which is a Mn(III) oxide), hydroxides can be formed when $Mn(IV)O_2$ is reduced to Mn(III)OOH at low pH, before being reduced to $Mn^{2+}$. Therefore, the approach of

using the O1s XPS peak to study the formation rates of chromium hydroxide surface precipitate is limited, especially for Mn(IV) oxides.

#### 1.3.2.2 Structure of Chromium Hydroxide Surface Precipitates

Previous studies showed that the nucleation structure of Cr-hydroxide is of the γ-CrOOH type on a δ-$MnO_2$ surface, similar to that resulting from homogeneous (free) surface precipitation (Fendorf, 1992; Manceau and Charlet, 1991). Since the precipitate structure formed was not influenced by the structural parameters of the sorbent, it was proposed that the Cr(III) precipitate was not directly complexed with the δ-$MnO_2$, (Fendorf, 1992).

Metal hydroxide precipitates exhibit many different types of structures, which depend on the nature of the sorbents. For instance, Cr(III) nucleation on α-FeOOH yielded an α-CrOOH structure at the Fe-Cr interface (Charlet and Manceau, 1992) at low surface coverage after an epitaxial growth on the goethite structure. At higher surface coverage, a transition phase from α-CrOOH to γ-CrOOH occurred when the nucleation extended away from the goethite surface. Trivalent chromium nucleation on silica occurred at 20% of surface coverage (Fendorf, 1992), and resulted in a distorted γ-CrOOH growing away from the silica surface, due to mineral structural constraints that prevented epitaxial growth of Cr-hydroxide. Consequently, chromium precipitate clusters were observed on the silica surface.

Fendorf (1992) summarized the possible phenomena occurring on a mineral surface during chromium sorption, which can be correlated to other metals susceptible to precipitation as metal-hydroxide/oxide phases on mineral surfaces. First, chromium sorbs on the mineral surface in either an inner-sphere or outer-sphere complex, followed by surface nucleation of Cr(III) at low surface coverage, since the

kinetics of surface nucleation are unknown, it could occur rapidly, maybe at the same time that Cr(III) sorbs on the surface. At higher surface coverage, two phenomena can occur: 1) precipitation, for example when a γ-CrOOH phase homogenously covers a δ-$MnO_2$ surface; or 2) clustering, for example distorted γ-CrOOH growth at different sites of silica surface, forming localized clusters.

Therefore, since manganese oxides exhibit a wide variety of chemical and physical structures (Post, 1999), it is likely that Cr(III) precipitates on mineral surfaces in different ways, and the γ-CrOOH type of surface precipitate observed on δ-$MnO_2$ (Fendorf, 1992) cannot be generalized to other kinds of manganese oxides.

## 1.4 Experimental Methods to Measure Rapid Kinetic Mechanisms

The kinetics of many soil chemical processes that occur on time scales of hours, days, months, and longer time scales have been extensively studied with conventional macroscopic kinetic methods, using batch or flow techniques. Relatively slow reactions include for instance mineral crystallization and dissolution, or even some sorption and redox reactions. However, in the case of faster mechanisms occurring in soils, including for instance ion exchange or ion association processes, most of the reaction is completed before the first data point can be collected using traditional kinetic techniques.

As previously mentioned, Cr(III) oxidation by manganese oxides is a biphasic reaction where the oxidation proceeds very rapidly initially. Batch experiments or flow techniques are then not suitable to measure the initial rates of Cr(III) oxidation. Constraining the rate parameters at the early stage of the reaction is important since mass transfer phenomena are minimized during that period: the reaction rates can be directly related to chemical mechanisms occurring at the

manganese oxide surface. The knowledge of chemical rates is important; for instance, using chemical rates of Cr(III) oxidation by manganese oxide instead of apparent rates helps in developing accurate models that predict the fate and effect of chromium in soils.

Some new spectroscopic techniques that emerged over the last few decades are potentially capable of measuring the kinetics of rapid reactions occurring in soils. The description, applications, and limitations of each of these techniques are briefly discussed below.

### 1.4.1 Relaxation Techniques

Chemical relaxation methods are based on the principle that the equilibrium of a reaction mixture can be rapidly perturbed by a change in some external factor such as pressure, temperature, or electric-field strength (Amacher, 1991). After perturbing the system, one can measure the relaxation time or the time that it takes for the system to relax from the disequilibrium state to the final equilibrium. These techniques, including temperature-jump, pressure-jump, electric field pulse, and electron paramagnetic resonance (EPR)/ stopped flow can measure reaction rates on millisecond and microsecond time scales. They are thus suitable methods to measure the kinetics of many rapid soil processes including adsorption/desorption phenomena, hydrolysis of minerals, ion-exchanges processes, and complexation reactions. For example, p-jump was used to study the kinetics and mechanisms of sulfate adsorption and desorption at the goethite/water interface (Zhang and Sparks, 1990), and EPR stopped-flow was used to measure the rates of sorption/desorption of $Mn^{2+}$ on birnessite (Fendorf *et al.*, 1993). However, these techniques do not directly measure reaction rates since the kinetic parameters are

inferred from physical properties of the system. Also, although EPR has rapid data acquisition time (microseconds), it is not suitable for non-paramagnetic active species (Sparks, 1989).

### 1.4.2 Rapid Scan Attenuated Total Reflectance (ATR) Fourier Transform Infrared (FTIR)

ATR-FTIR is an established technique for studying sorption and redox processes (Parikh *et al.*, 2008), providing bonding mechanisms. It is a useful technique for biogeochemical applications as it probes the mineral/liquid interface, providing information on solid and solution phase species. Through observing shifts in IR peak location and formation of new IR peaks, sorption and/or formation of reaction products can be ascertained. For example, Parikh *et al.* (2008) used this technique to monitor chemical reaction processes for IR active compounds at the mineral/liquid interface at a temporal resolution of 2.55 seconds. Although this *in situ* technique is particularly suitable to identify species, one of its limitations is that it is difficult to quantify elements sorbed on soil surfaces. For instance, although quantifying Cr(VI) species in solution is possible, quantifying these species sorbed on the manganese surface is much harder. Indeed, since the peak shapes of $[Cr(VI)]_{sorbed}$ are different than $[Cr(VI)]_{solution}$ due to vibration mode differences, the calibration curve used to quantify chromium in solution, made from a series of aqueous chromium standards, can not be used to quantify sorbed species.

### 1.4.3 Surface Second Harmonic Generation

Surface second harmonic generation is an in situ method for probing interfaces, including solid/water interfaces in soil systems. In second harmonic generation (SHG), the light frequency is doubled, essentially converting two photons

of the original beam of energy E into a single photon of energy 2E as it interacts with noncentrosymmetric media. Surface second harmonic generation is a special case of SHG where the second beam is generated because of a break of symmetry caused by an interface. Since symmetry is only disrupted in the first (occasionally second and third) atomic or molecular layer of a system, properties of the second harmonic signal give us information about the first atomic or molecular layers only (Shen, 1989). For example, this technique was used to study the adsorption and desorption behavior of chromate at the fused quartz/water interface at pH=7 and at room temperature (Mifflin *et al.*, 2003). In this study, Cr(VI) sorbed on the surface of a fused quartz hemispherical lens was quantified and the rate constants of Cr(VI) sorption and desorption were measured. Studying Cr(III) oxidation by manganese oxides using this technique might be possible; however, it would probably necessitate having the manganese oxide coated on the surface of the SHG lens, which could be problematic since the flow inside the cell could flush away some of the coated mineral.

### 1.4.4 Quick X-Ray Absorption Spectroscopy

The main difference between QXAFS and "traditional" XAFS is the monochromator set-up. QXAFS employs an ellipsoidal driving system that moves the monochromator in a fast cyclic motion, up and down in energy (Dent, 2002). Consequently, one can successively and rapidly take several scans within a couple of seconds, which contrasts with traditional XAFS where the time of scan acquisition is on the order of minutes. The current QXAFS setup at beamline X18B at Brookhaven NY collects one scan each 0.75 second. QXAFS is an *in situ* technique that can measure rapid oxidation state changes by analyzing the X-ray adsorption near-edge structure (XANES) portion of the spectrum and rapid speciation changes by

investigating the extended X-ray adsorption fine structure (EXAFS) portion of the spectrum. For example, Mitsunobu *et al.* (2005) used this technique to study the rates of As(III) oxidation on manganese oxide, using a column approach.

## 1.5 Cr and As Speciation in Contaminated Soils

Similar to chromium, arsenic, whose presence in the environment poses a significant risk to humans, can be found at high concentrations in the soil of contaminated sites. Previous studies that investigated the speciation of Cr and As in contaminated soils found that these two elements were mainly accumulated in the Fe and Al phases (Beaulieu and Savage, 2005; Lund and Fobian, 1991; Bhattacharya *et al.*, 2002, Hopp *et al.*, 2008, Cancès *et al.*; 2008; Arčon *et al.*, 2002). Iron oxides are important As and Cr scavengers because of their abundance in the environment, surface area, and chemical affinity to As(III) and As(V) compounds (Sparks, 2003; Vodyanitskii, 2007). Additionally, Cr(III) can sorb to organic materials (Hopp *et al.* 2008), or co-precipitate with goethite to form a α-(Fe, Cr)OOH phase, due to structural similarities between the Fe(III) mineral (α-FeOOH) and the pure Cr surface precipitate phase (α-CrOOH) (Charlet and Manceau, 1992; Hansel *et al.*, 2002). Aluminum oxides can sorb As(V), and transform after a long period to a three dimensional As-Al precipitate phase (Arai and Sparks, 2002). It has been also shown that As can sorb to calcite, sulfides, kaolinite, and montmorillonite (La Force *et al.*, 2000). Lastly, manganese oxides can effectively sorb and oxidize As(III) or Cr(III), to produce As(V) or Cr(VI), the latter of which is the most toxic form of chromium (Post, 1999; Parikh and Sparks, 2008; Fendorf and Zasoski, 1992; Weaver and Hochella, 2003). Conversely, Fe oxides, sulfides, or dissolved organic substances can reduce Cr(VI) to Cr(III) (Fendorf and Guangchao, 1996).

Previous studies investigated the speciation of chromium and/or arsenic in soils from different types of sites; for example, a site located nearby a former As ore smelter (Beaulieu *et al.* 2005), a site contaminated by chromated copper arsenate, which is a very effective wood preservative (Hopp *et al.* 2008), a site impacted by mine wastes containing As (La Force, 2000), an industrial-waste site where arsenical pesticides used to be manufactured (Cancès *et al.*, 2008), a site located near a lead smelter, and contaminated with As, Pb, Cr, and Cd (Gao and Schulze, 2010), former electroplating plants contaminated with Cr (Szulczewski *et al.*, 1997), a calciner's residue dump near an arsenic smelter (Arčon *et al.*, 2005), a site near a solid waste storage area in a national laboratory (Jardine *et al.* 1999), two industrial sites contaminated by As herbicides (Yang and Donahoe, 2007), and As-contaminated mine wastes (Walker and Jamieson, 2005). Therefore, to our knowledge, no study has investigated the speciation of As and Cr in soils contaminated by former leather-tanning factories, using the current state-of-the-art molecular techniques commonly employed to probe contaminants in soils. Since the tanning process of leather employed by industrialized countries in the XIXth and the early XXth centuries used As as a dehairing agent or a colorant, like Scheele's green ($CuHAsO_3$) or Paris green ($Cu(AsO_2)_2Cu(C_2H_3O_2)_2$), and chromium as a tanning agent, these two heavy metals can be present at high concentrations in soils impacted by tannery operations. For example, the city of Wilmington, Delaware, used to be one of the nation's leading leather-tanning industries on the American East Coast in the early 1900's. In 2001, an investigation conducted by the Delaware Department of Natural Resources and Environmental Control (DNREC) identified 128 tannery footprints in the area of

Wilmington, which were subsequently clustered into 52 sites. Some of those sites were polluted with As and Cr, according to the DNREC investigation.

## 1.6 Framework of This Study

Two reactions can occur after chromium(III) is sorbed on manganese oxides, Cr(III) oxidation or Cr(III) precipitation. The first reaction results in the production of hazardous hexavalent chromium, while the second process results in the sequestration of Cr(III), which could reduce the bioavailability of this element in the environment. However, in view of the current literature, it is not known if one reaction occurs more quickly than the other, or if the two reactions occur simultaneously at an early stage of Cr(III) sorption on the manganese oxide surface. Therefore, it is important to know how rapidly these two processes occur, and to understand the relationship/dependence between the rates of Cr(VI) production and the kinetics of surface precipitation. No study has measured the chemical rates of Cr(III) oxidation by $MnO_2$, due to the lack of techniques that can follow *in situ* rapid reactions occurring in the environment. Knowing the chemical rate parameters (i.e, not apparent rates that include the effect of diffusion and/or back reactions) is needed to develop models that can accurately predict the fate of chromium in the environment. Additionally, the sorption mechanisms of Cr(III) and Cr(VI) on $MnO_2$ are unclear. The nature of the Cr surface precipitates on the $MnO_2$ surface, and their rates of formation, are not clearly understood. Although the slow rates of mineral precipitation occurring in bulk solution have been constrained using macroscopic methods, the rates of chromium hydroxide phase formation are unknown because of the difficulty in identifying and quantifying in real time and *in situ* precipitation on soil mineral surfaces. Lastly, the speciation of Cr, as well as As, another toxic metalloid potentially

toxic in the environment, found at former leather-tanning factory sites should be also investigated.

Therefore, the objectives of this study are 1) To use quick x-ray absorption spectroscopy (QXAFS) to measure the rates of Cr(III) oxidation by manganese oxides, and the kinetics of Cr surface precipitation formation on $MnO_2$; 2) To determine the mechanisms of these two simultaneous reactions occurring when Cr(III) sorbs to manganese oxides, and to understand their mutual effects and 3) To employ micro-x-ray absorption spectroscopy (μ-XAS) and bulk x-ray adsorption fine structure spectroscopy (bulk-XAFS) to study the speciation of As and Cr in a contaminated soil from a former leather-tanning site.

## 1.7 References


Amacher, M. C. (1991), Chapter 2: Methods of obtaining and analyzing kinetic data, rates of soil chemical processes, Sparks, D.L., Suarez, D.L., Eds, SSSA Spec. Publ. No. 27, 19-59, Soil Sci. Soc. Am: Madison, WI.

Banerjee, D. and Nesbitt, H. W. (1999), Oxidation of aqueous Cr(III) at birnessite surfaces: constraints on reaction mechanism, Geochemica et Cosmochimica Acta, 63, 1671-1687.

Bartlett, R. and James, B. (1979), Behavior of chromium in soils: III. Oxidation, J. Environ. Quality, 8, 31-35.

Chiswell, B. and O'Halloran, K. R. (1991), Comparison of three colorimetric methods for the determination of manganese in freshwaters, Talanta, 38, 641-648.

Daulton, T. L. and Little, B. (2006), Determination of chromium valence over the range Cr(0)-Cr(VI) by electron energy loss spectroscopy, Ultramicroscopy, 106, 561-573.

Dent, A. J. (2002), Development of time-resolved XAFS instrumentation for quick EXAFS and energy-dispersive EXAFS measurements on catalyst systems, Topics in Catalysis, 18, 27-35.

Dirilgen, N. and Dogan, F. (2002), Speciation of chromium in the presence of copper and zinc and their combined toxicity, Ecotoxicology and Environmental Safety, 53, 397-403.

Eary, E. and Rai, D. (1987), Kinetics of chromium(III) oxidation to chromium(VI) by reaction with manganese dioxide, Environmental Science & Technology, 21, 1187-1193.

Fendorf, S. E. (1995), Surface reactions of chromium in soils and waters, Geoderma, 67, 55-71.

Fendorf, S. E. and Zasoski, R. J. (1992), Chromium(III) oxidation by δ-$MnO_2$ 1. Characterization, Environmental Science & Technology, 26, 79-85.

Fendorf, S. E., Fendorf, M., and Sparks, D. L. (1992), Inhibitory mechanisms of Cr(III) oxidation by δ-$MnO_2$, Journal of Colloid and Interface Science, 153, 37-54.

Fendorf, S. E., Sparks, D. L., and Camaioni, D. M. (1993), Electron paramagnetic resonance stopped flow kinetic study of manganese(II) sorption desorption on birnessite, Soil Sci. Soc. Am. J, 57, 57-62.

Gadde, R. R. and Laitinen, H. A. (1974), Studies of heavy metal adsorption by hydrous iron and manganese oxides, Analytical Chemistry, 46, 2022-2026.

Ginder-Vogel, M., Landrot, G., Fischel, J., and Sparks, D. L. (2009), Quantification of rapid environmental redox processes using quick scanning x-ray absorption spectroscopy (Q-XAS), Proceedings of the National Academy of Sciences, 106, 16124-16128.

Gray, M. J. and Malati, M. A. (1978), The point of zero charge of manganese dioxides, J. Electroanal. Chem, 89, 135-140.

Guha, H., Saiers, J., Brooks, S., Jardine, P., and Jayachandran, K. (2001), Chromium transport, oxidation, and adsorption in manganese-coated sand, Journal of Contaminated Hydrology, 49, 311-334.

Johnson, A. C. and Xyla, A. G. (1991), The oxidation of chromium(III) to chromium(VI) on the surface of manganite (γ-MnOOH), Geochemica et Cosmochimica Acta, 55, 2861- 2866.

Kim, J. G., Dixon, J., Chusui, C. C., and Deng, Y. (2002), Oxidation of chromium(III) to (VI) by manganese oxides, Soil Sci. Soc. Am. J, 66, 306-316.

Kim, J. G. and Moon, H.S. (1998), Oxidation of chromium (III) to chromium (VI) by a series of synthesized birnessites (δ-MnO2): kinetics and oxidation capacity. Clay Science, 10, 363-374.

Kingston, S. H. M., Cain, R., Huo, D., and Rahman, M. G. M. (2005), Determination and evaluation of hexavalent chromium in power plant coal combustion by-products and cost-effective environmental remediation solutions using acid mine drainage, J. Environ. Monit, 7, 899-905.

Lin, C. J. (2002), The Chemical transformations of chromium in natural waters - A model study. Water, Air, and Soil Pollution 139, 137.

Manceau, A. and Charlet, L. (1992), X-ray adsorption spectroscopy study of the sorption of Cr(III) at the oxide-water interface. I. Molecular mechanism of Cr(III) oxidation on Mn Oxides, Journal of Colloid and Interface Science, 148, 425-442.

Mifflin, A., Gerth, K., and Geizer, F. (2003), Kinetics of chromate adsortion and desorption at fused quartz/water interfaces studied by second harmonic generation, Journal of Physical Chemistry A, 107, 9620-9627.

Mitsunobu, S., Takahashi, Y., and Uruga, T. (2005), Observation of chemical reactions at the solid-water interface by Quick XAFS combined with a column reactor, Analytical Chemistry, 78, 7040-7043.

Morgan, J. and Stumm, W. (1964), Colloid-chemical properties of manganese dioxide, Journal of Colloid Science, 19, 347-359.

Murray, J. W. (1974), The Surface chemistry of hydrous manganese dioxide, J. Colloid Interface Sci, 46, 357-371.

Murray, K. and Tebo, B. (2007), Cr(III) is indirectly oxidized by the Mn(II)-oxidizing bacterium bacillus sp. Strain SG-1, Environmental Science & Technology, 41, 528-533.

Nico, P., and Zasoski, R. (2000), Importance of Mn(III) availability on the rate of Cr(III) oxidation on $\delta$-$MnO_2$, Environmental Science & Technology, *34*, 3363–3367

Palmer, C. and Wittbrodt, P. (1991), Processes affecting the remediation of chromium-contaminated sites, Environmental Health Perspective, 92, 25-40.

Parikh, S. J., Lafferty, B. J., and Sparks, D. L. (2008), An ATR-FTIR spectroscopic approach for measuring rapid kinetics at the mineral/water interface, Journal of Colloid and Interface Science, 320, 177-185.

Peterson, M., L., Brown, G. E., Parks, G., A., and Stein, C., L. (1997), Differential redox and sorption of Cr(III/VI) on natural silicate and oxide minerals: EXAFS and XANES results, Geochemica et Cosmochimica Acta, 61, 3399-4413.

Post, J. E. (1999), Manganese oxide minerals: crytal stuctures and economic and environmental significance, Proceedings of the National Academy of Sciences, 96, 7, 3447-3454.

Rai, D., Sass, B., and Moore, D. (1987), Chromium(III) hydrolysis constants and solubility of chromium(III) hydroxide, Inorg. Chem., 26, 345-349.

Rotzinger, F., Stunzi, H., and Marty, W. (1986), Early stages of the hydrolysis of chromium(III) in aqueous solution. 3. Kinetics of dimerization of the deprotonated aqua ion, Inorg. Chem., 25, 489-495.

Sparks, D. L. (1989), Kinetics of Soil Chemical Processes, Academic Press, San Diego, CA.

Sparks, D. L. (2003), Environmental Soil Chemistry, Academic Press, San Diego, CA.

Stepniewska, Z., Bucior, K., and Bennicelli, R. P. (2004), The effects of $MnO_2$ on sorption and oxidation of Cr(III) by soils, Geoderma, 122, 291-296.

Strawn, D. G., Scheidegger, A. M., and Sparks, D. L. (1998), Kinetics and mechanisms of Pb(II) sorption and desorption at the aluminum oxide-water interface, Environ. Sci. Technol, 32, 2596-2601.

Villalobos, M., Toner, B., Bargar, J., and Sposito, G. (2003), Characterization of the manganese oxide produced by pseudonomas putida strain MnB1, Geochemica et Cosmochimica Acta, 67, 2649-2662.

Weaver, R. M. and Hochella, M. F. (2003), The reactivity of seven Mn-Oxides with $Cr^{3+}_{aq}$: a comparative analysis of a complex, environmentally important redox reaction, American Mineralogist, 88, 2016-2028.

Yang, J. W., Tang, Z. S., Guo, R. F., and Chen, S. Q. (2008), Soil surface catalysis of Cr(VI) reduction by citric acid, Environ. Progress, 27, 302-307.

# Chapter 2

# KINETICS OF CHROMIUM(III) OXIDATION BY MANGANESE(IV) OXIDES USING QUICK SCANNING X-RAY ABSORPTION FINE STRUCTURE SPECTROSCOPY (Q-XAFS)

## 2.1 Abstract

The initial kinetics of Cr(III) oxidation on mineral surfaces is poorly understood, yet a significant portion of the oxidation process occurs during the first seconds of reaction. In this study, the initial rates of Cr(III) oxidation on hydrous manganese oxide (HMO) were measured at three different pH values (pH 2.5, 3, and 3.5), using a quick X-ray absorption fine structure spectroscopy (Q-XAFS) batch method. The calculated rate constants were 0.201, 0.242, and 0.322 $M^{-1}. s^{-1}$ at pH 2.5, 3, and 3.5, respectively. These values were independent of both [Cr(III)] and [Mn(II)] and mixing speed, suggesting that the reaction was "chemically" controlled and not dependent upon diffusion at the time period the rate parameters were measured. A second-order overall rate was found at three pH values. This represents the first study to determine the chemical kinetics of Cr(III) oxidation on Mn-oxides. The results have important implications for the determination of rapid, environmentally important reactions that cannot be measured with traditional batch and flow techniques. An understanding of these reactions is critical to predicting the fate of contaminants in aquatic and terrestrial environments.

## 2.2 Introduction

Kinetics of geochemical processes range over time scales of seconds to millenia (Amacher, 1991). For example, we know that certain ion exchange, redox, and sorption processes can occur on second or faster time scales. However, some sorption processes, particularly those involving organic chemicals, may continue for periods of days and weeks before steady state is attained. Many geochemical processes are characterized by a biphasic process, a rapid reaction occurring over minutes and hours, followed by a slower reaction that continues for hours, and perhaps days. However, for ion exchange, electron transfer, and adsorption reactions, a major portion of the total reaction process often occurs on time scales of minutes with a significant part of the initial reaction having occurred before the first data point is collected using traditional batch and flow techniques. Few studies have appeared in the geochemistry literature where these rapid initial reaction rates have been measured. An electron paramagnetic resonance spectroscopy stopped-flow (EPRSF) technique was used (Fendorf *et al.*, 1993) to measure millisecond reaction rates of $Mn^{2+}$ on $MnO_2$. While this is a useful technique, it is limited to the measurement of paramagnetic elements. Chemical relaxation techniques, especially pressure-jump relaxation, have been employed to study rapid sorption processes on metal oxides. However, the kinetic rate constants are indirectly determined via linearized rate equations that are dependent on equilibrium parameters (Sparks, 1989).

The fate of chromium in soils has been extensively studied (Fendorf, 1995). Chromium is derived from both anthropogenic and natural sources, and is mainly present in two stable oxidation states, (III) or (VI). Since Cr(VI) is mobile and more toxic than Cr(III), it is of great environmental concern. Chromium can be found naturally in water at concentrations up to 10 $\mu g.L^{-1}$ (Dirilgen and Dogan, 2002).

Contaminated sites can contain chromium at much higher concentrations. For instance, at the United Chrome Products site in Corvallis, Oregon, hexavalent chromium was measured at 280 mM in groundwater and 500 mM in soil near a leaking tank used to dispose of floor drippings, washings, and product rinsates (Palmer and Wittbrodt, 1991). Another example is the old chromite ore refinement plant located in Jersey, City, NJ. This abandoned site contains about 300,000 tons of chromium wastes buried beneath the facility, according to legal and environmental experts. Manganese oxides, which are common in soils, are strong oxidizing agents and can oxidize Cr(III) to Cr(VI). A number of previous studies have investigated chromium oxidation on manganese oxides employing batch techniques (Eary and Rai, 1987; Fendorf and Zasoski, 1992; Kim and Moon, 1998; Kim and Dixon, 2002; Weaver and Hochella, 2003; Stepniewska *et al.*, 2004; Johnson and Xyla, 1991), X-ray photoelectron spectroscopy (XPS), transmission electron microscopy (TEM) (Fendorf *et al.*, 1992; Banerjee and Nesbitt, 1999), and X-ray absorption fine structure (XAFS) studies (Manceau and Charlet, 1992; Peterson *et al.*, 1997). The influence of bacteria on the oxidation rates (Murray and Tebo, 2007) and modeling approaches (Guha *et al.*, 2001; Lin, 2002) have also been studied. However, there have been no studies focusing on the "chemical" kinetics of Cr(III) oxidation on manganese oxides, i.e., the initial rates of the reaction where mass transfer phenomena are negligible. This is mainly due to the lack of experimental techniques with data acquisition fast enough to follow rapid reactions. Recent advances in the use of real-time kinetic methodologies, particularly at the molecular scale, such as Quick XAFS (Q-XAFS) (Ginder-Vogel *et al.*, 2009; Mitsunobu, 2005) and attenuated total reflectance (ATR) Fourier transform infrared (FTIR) spectroscopy (Parikh *et al.*, 2008), as well as second

harmonic generation (Mifflin *et al.*, 2003), are promising tools for measuring rapid geochemical reactions. Q-XAFS employs an ellipsoidal driving system that moves the monochromator in a fast cyclic motion, up and down in energy (Dent, 2002). Consequently, one can successively and rapidly take several scans within a couple of seconds, which contrasts with "regular" XAFS where the scan acquisition time is on the order of minutes. Our current Q-XAFS setup collects a scan each 0.75 s, which is less than the 1 minute scanning time reported in the study of 22 which is, to our knowledge, along with 21, the only application of Q-XAFS to the study of an environmental mineral/water system. With Q-XAFS, one can notably follow rapid oxidation state changes by analyzing the X-ray absorption near-edge structure (XANES) portion of the spectrum and rapid speciation changes by investigating the extended X-ray absorption fine structure (EXAFS) portion of the spectrum. In this study, the XANES region was analyzed to determine the rapid, initial oxidation of Cr(III) on hydrous manganese(IV) oxide (HMO), using Q-XAFS.

## 2.3 Materials and Methods

### 2.3.1 Chromium Solutions, Concentrations, and pH Range

All reagents and acids were ACS grade or better. Cr(III) stock solutions were prepared from chromium nitrate $Cr(NO_3)_3$ a few hours before conducting our experiments to minimize the effect of polymerization (Rotzinger *et al.*, 1986). Cr(VI) stock solutions were prepared from potassium chromate $K_2CrO_4$. Distilled deionized water (Barnstead) with a resistivity of 18.2 MΩ was used to prepare all solutions. Q-XAFS experiments and batch experiments were performed using a Cr(III) concentration range of 40-100 mM, and at three different pH values, pH 2.5, pH 3, and

pH 3.5. The synthesis and characterization of hydrous manganese oxide (HMO) are described in the Supporting Information (SI). The HMO suspension density was 20 g/L (230 mM $MnO_2$).

### 2.3.2 Hydrous Manganese Oxide (HMO)

Hydrous manganese oxide (HMO), also referred in the literature to δ-$MnO_2$, was synthesized less than a week before carrying out experiments to minimize the effect of aging. HMO is characterized by a poorly ordered layered structure, high surface area, and a point of zero charge (PZC) equal to 2.7 (Morgan and Stumm, 1964; Murray, 1974; Gray and Malati, 1978). The HMO used in this study was synthesized using the method of Gadde and Laitinen (1974). A Mn(II) nitrate solution was slowly (~30 mins) added to an alkaline permanganate solution while stirring. The molar ratio of $MnNO_3$, $KMnO_4$, and KOH was respectively 3:2:4. The oxide was repeatedly washed and centrifuged until a constant supernatant conductivity was obtained. After purging the mineral with helium, a specific surface area of 272.6 $m^2/g$ was measured via BET analysis using nitrogen as the adsorbate at 77.4K. SEM measurements of the mineral (Figure 1.2) exhibited small, disordered aggregates with an average size smaller than 0.5μm. X-ray diffraction (XRD) pattern from 5 to 65 2θ suggested a poorly ordered structure. One small, broad peak was detected at about 37 2θ, and a very small peak at 12.3 2θ, which matches the XRD pattern of δ-$MnO_2$ reported in (Villalobos *et al.*, 2003). Dissolution of HMO was studied using a stirred flow method at pH=2.5, 3, and 3.5. With this method, one could test whether Mn dissolution into solution was occurring since Mn is removed from solution. A 8mL stirred flow chamber was filled with HMO at a suspension density of 1 g/L, and a solution of 0.05M KCl at pH 2.5, 3, or 3.5 (three different experiments) was used as the

dissolution agent, at a flow rate of 0.5 mL/min. A few seconds before sealing the stirred flow chamber and beginning the flow, a small amount of 100mM HCl was quickly added to the reaction chamber to equilibrate the HMO at the correct pH (pH 2.5, 3, or 3.5). The effluent solution was collected continuously for 45 minutes, in 9 tubes (5 minute collection for each tube). Each tube contained 2.5 mL of effluent solution, which was analyzed for total manganese by ICP-Atomic Emission Spectroscopy.

### 2.3.3 pH Control

To counter the pH drop at the beginning of the reaction due to the Cr(III) stock solution acidity, an adequate quantity of 4 M KOH to attain the pH of the experiment (pH 2.5, 3, or 3.5) was manually added to the manganese oxide solution, along with Cr(III). This amount of base was less than 1% of the total volume. The $H^+$ production from the Cr(III) oxidation (eq 2.1), which resulted in a constant decrease in pH throughout the reaction, was controlled by a pH Stat (Metrohm Titrino) supplying 1 M KOH, at a maximum rate of 1 mL/min, and at a minimum rate of 25 $\mu$L/min pH was controlled within ± 0.1 pH unit over a 30 min period.

$$Cr(H_2O)_6^{3+} + 1.5\ MnO_2 \Rightarrow CrO_4^{2-} + 1.5\ Mn^{2+} + 2H_3O^+ + 3H_2O \qquad (2.1)$$

### 2.3.4 Reaction Conditions

The range of chromium concentrations used in this study (40-100 mM), while high, can occur in chromium-contaminated sites (Palmer and Wittbrodt, 1991). Our goal in this study was to measure chemical rate constants, determined from initial rate measurements using Q-XAFS, for Cr(III) oxidation by manganese oxide. Such constants are dependent only upon temperature, according to the Arrhenius equation,

and not upon concentration (Sparks, 2003). The lowest chromium concentration that could be used in this study was imposed by the Q-XAFS detection limit, which was experimentally measured at 30 ± 5 mM. This value represents the lowest concentration that can be employed to quantify the small Cr(VI) pre-edge feature appearing in the XANES spectra during the very first seconds of the Cr(III) oxidation reaction. A maximum chromium concentration of 100 mM implied to conduct our experiments below pH 3.5 to avoid Cr(III) bulk precipitation, due to the low solubility of chromium (Rai *et al.*, 1987). Consequently, all our experiments were conducted at pH 2.5, 3, and 3.5. Different hexavalent chromium remediation techniques employ synthetic reagents, for example, citric acid (Yang *et al.*, 2008) or natural reagents, e.g., acid mine drainage (Kingston *et al.*, 2005). These leaching procedures are mostly efficient when applied at very low pH. Therefore, the rate parameters of Cr(III) oxidation reported in this study could be employed to assess the fate and effect of chromium in highly Cr contaminated sites where leaching procedures are applied at very low pH values. In these cases, although Cr(VI) is remediated and reduced to Cr(III), oxidation of Cr(III) may also occur, since manganese oxides are widespread in the environment (Post, 1999). The HMO suspension densities used in the traditional batch experiment and the batch Q-XAFS experiments were chosen based on the chromium concentration range and Eq 2.1. According to Eq 2.1, the oxidation of Cr(III) implies that 1 mol of Cr(III) reacts with 1.5 mol of HMO. Therefore, knowing that the maximum Cr(III) concentration that could be employed was 100 mM, and since we wanted to ensure that oxidation was not limited by the amount of Mn oxide present, 20 g/L of HMO was chosen as the suspension density.

### 2.3.5 Batch Kinetics Studies

HMO (13.85 mL of 26 g/L) was introduced into a polypropylene tube that was used as a batch vessel. Concentrated KOH (140, 220, and 300 μL) and 2.11, 2.03, and 1.95 mL of dionized water were added to the tubes for the experiments conducted at pH 2.5, 3, and 3.5, respectively. The total volume in each tube was 16.1 mL. An overhead stirrer promoted mixing inside the batch vessel. At t = 0, 1.9 mL of 0.95 M Cr(III) stock solution was added to the tubes. Thus, the final HMO suspension density was 20 g/L, and the chromium concentration was 100 mM. During the 45 min of reaction, 500 μL aliquots were collected at different time intervals with a 1-mL syringe and filtered using a 0.22-μm nylon filter. Each experiment was conducted in duplicate. The measurements of Cr(III), Cr(VI), and Mn aqueous concentrations are described in the SI.

### 2.3.6 Elemental Measurements

All samples were diluted in a 15mM EDTA solution at pH 7, and dried in an oven for 8 hours at 45ºC before analysis. Cr(VI) and Cr(III) were then separated by chromatography, using a G3268-80001 Agilent Column in a 15 mM EDTA mobile phase at pH 7. Finally, the concentration of Cr(III), Cr(VI), and $Mn_{aqueous}$ were analyzed with an ICP-MS. The chemical equilibrium modeling system MINEQL+ (database version 4.6) revealed that at our experimental conditions, the major dissolved form of manganese was $Mn^{2+}$. This assumption was confirmed by measuring manganese both by ICP-AES (total aqueous Mn) and by colorimetry (Chiswell and O'Halloran, 1991) during one of our batch experiments. The concentration of $Cr_{aqueous}$ and $Mn_{aqueous}$ were also measured with an ICP-AES, and the results were compared with the ICP-MS data. The concentration of $Mn_{aqueous}$

measured with ICP-AES equaled the concentration of $Mn_{aqueous}$ measured with ICP-MS (almost a 0% difference), $[Cr]_{aqueous}$ measured with ICP-AES was very similar to [Cr(VI)] + [Cr(III)] measured with ICP-MS (difference less than 2%). The concentration of $Cr(VI)_{aqueous}$ was also measured by colorimetry using the s-diphenyl carbazide method (Barlett and James, 1979), and compared to [Cr(VI)] measured with ICPMS. An approximate 10% difference was found, which could be ascribed to the error range for the colorimetric method.

### 2.3.7 Q-XAFS Experiments

The Q-XAFS experiments were performed at beamline X18B, National Synchrotron Light Source, Brookhaven National Laboratory, Upton, NY. The data acquisition method collects 60,000 points/30 seconds using a Keithley current amplifier, a sixteen-channel VME analog-digital-converter (ADC), and custom programmed Linux based software. The Bragg angle of a Si(111) double crystal monochromator is controlled via an assembly containing a microstepping motor, a rotating cam, and a small brass lever arm directly attached to the monochromator tangent arm (Ginder-Vogel *et al.*, 2009; Dent, 2002). The monochromator was set at the B3 position (5900-6363 eV), to obtain the XANES portion of the Cr spectrum. The beam was detuned at 30% from its maximum $I_0$ value. A gas mixture of 20% $N_2$ and 80% He was used in $I_0$, and 100% $N_2$ was used in $I_t$ to collect transmission data for the chromium foil, and fluorescence emission was collected with a PIPS detector. The monochromator motor setup allowed us to collect a scan every 0.75 s.

### 2.3.8 Experimental Setup

The batch experiments performed at beamline X18B were carried out using experimental conditions similar to those previously described. The same concentrations/quantity of reactants and same batch vessel were used. The batch vessel used for the Q-XAFS experiments featured ~1 cm above the bottom of the vessel, i.e., above the level of the stir bar, a rectangular hole window (1-3 cm) covered with kapton tape on the tube's wall so that the beam could pass through the tube and fluorescence could be emitted and detected with a fluorescence detector, and a stirrer was used to minimize mass transfer phenomena. One end of the tubing, containing the Cr(III) stock solution, was connected to the top inlet of the batch vessel with the other end of the tubing attached to a syringe placed outside the hutch. When the tube containing the manganese oxide solution, the fluorescence detector, the Cr(III) tubing, and the electrode of the pH stat were finally set at their respective positions, the hutch was closed and quick scanning was initiated. After one minute of data collection, the Cr(III) stock solution was remotely injected inside the batch vessel via the syringe outside the hutch. Although both Cr(VI) and Cr(III) possess a pre-edge feature in their respective XAFS spectrum, the Cr(VI) pre-edge feature at 5993.5 eV is prominent, and it is directly related to the proportion of Cr(VI) in the system. Therefore, one just has to measure the height of the pre-edge feature and compare it to a set of Cr(III)/Cr(VI) mixtures to determine the quantity of Cr(VI) present in the system within a 1-5% error margin (Peterson *et al.,* 1997). Before conducting the kinetic experiments, XANES spectra for standard solution mixtures of 100 mM $[\text{chromium}]_{\text{total Cr(III)+Cr(VI)}}$ were collected and are shown in Figure 2.1.

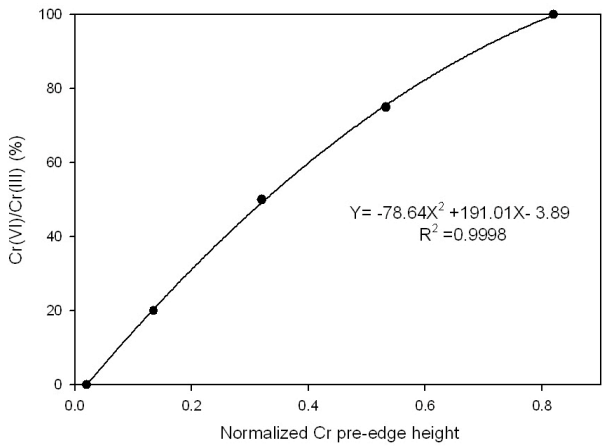


**Figure 2.1** Chromium pre-edge height calibration curve. Height of Cr(VI) pre-edge was measured from XANES spectra of standard solution mixtures of 100 mM [chromium]$_{\text{total Cr(III) + Cr(VI)}}$. The mixtures are respectively 0 % Cr(III)- 100 % Cr(VI), 25 % Cr(III)- 75 % Cr(VI), 50 % Cr(III)- 50 % Cr(VI), 80 % Cr(III)- 20 % Cr(VI), and 100 %Cr(III)- 0 % Cr(VI)

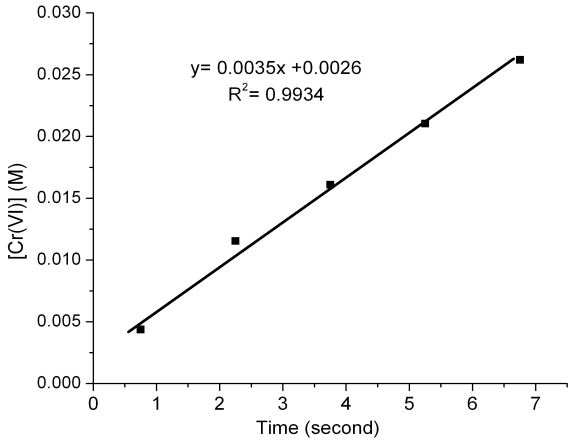


**Figure 2.2** Initial rate measurement for an experiment at pH 2.5, where [Cr(III)]=80 mM, and [HMO]=20 g/L

### 2.3.9 Calculation of Initials Rates and Rate Constants

The reaction expression for Cr(III) oxidation by HMO is an equilibrium reaction (see Eq. 2.1). The overall rate equation contains both forward and backward reactions. However, if one measures the reaction kinetics at an early stage, only the forward reaction needs to be considered (Sparks, 1989). In this case, the rate equation is reduced to:

$$\frac{d[Cr(VI)]}{dt} = k[Cr(III)]^{\alpha}[MnO_2]^{\beta} \qquad (2.2)$$

where *k* is the rate constant in $M^{-1}$ $sec^{-1}$, and α and ß are the partial rate coefficients. Another simplification can be made by successively applying a large excess of one of the reactants and varying the concentration of the other reactant (isolation method). One thus would end up getting an even more simplified rate equation, since the reactant in large excess would be considered constant throughout the reaction and thus would not appear in the rate equation expression. An overall reaction order would then be assumed, and the integrated rate law equation would be applied with the [Cr(VI)] experimental values. If a linear trend resulted, the assumed rate order would be validated. However, the isolation method could not be applied in this study because of the inability to have a large excess of one of the reactants. With our particular system, the Cr(III) concentration could not be increased to more than 100 mM due to solubility factors, and could not be decreased below 30 mM because of the Q-XAFS detection limit. Similarly, increasing the HMO suspension density above 30 g/L would have resulted in a high suspension viscosity, which would have complicated the stirred batch experiments. Decreasing the HMO concentration to a much lower value was also not possible, since a small amount of HMO would have resulted in a small amount of Cr(VI) produced, and thus the quantification of Cr(VI) at early stages of the

reaction would have been compromised. Consequently, the initial rate method was applied to determine the rate parameters for the oxidation reaction rather than the isolation method. With this approach, one of the reactants is fixed at a constant value (but not necessarily in excess) in a set of experiments, while the concentration of the other reactant is successively varied. Therefore, both of the reactants must be considered in the overall rate equation. During the early stage of the reaction, a linear relationship relates [Cr(VI)] and time. The slope of this linear trend is the initial rate i, which is defined as:

$$\frac{d[Cr(VI)]}{dt} = k[Cr(III)]_0^{\alpha}[MnO_2]_0^{\beta} = i \tag{2.3}$$

where k, $\alpha$ and ß were defined earlier, 0 represents the initial concentrations, and i is the initial rate of the reaction. To measure the partial rate coefficient of chromium R at a given pH value for the experiments where [$MnO_2$] was fixed and [Cr(III)] was varied, Eq. 2.6 was used, which is a simplified expression of Eq. 2.4:

$$\frac{i_{exp1} = k\left[Cr(III)_{exp1}\right]^{\alpha}\left[MnO_{2\,fixed}\right]^{\beta}}{i_{exp2} = k\left[Cr(III)_{exp2}\right]^{\alpha}\left[MnO_{2\,fixed}\right]^{\beta}} \tag{2.4}$$

where exp= experiment

Hence:

$$\frac{i_{exp1}}{i_{exp2}} = \left(\frac{\left[Cr(III)_{exp1}\right]}{\left[Cr(III)_{exp2}\right]}\right)^{\alpha} \tag{2.5}$$

Therefore:

$$\alpha = \frac{\mathrm{Log}\left(\frac{i_{\exp 1}}{i_{\exp 2}}\right)}{Log\left(\frac{\left[\mathrm{Cr(III)}_{\exp 1}\right]}{\left[\mathrm{Cr(III)}_{\exp 2}\right]}\right)} \tag{2.6}$$

To measure the partial rate coefficient of manganese β at a given pH value for the experiments where [Cr(III)] was fixed and $[MnO_2]$ was varied, Eq. 2.9 was used, which is a simplification of Eq. 2.7:

$$\frac{i_{\exp 3} = \mathrm{k}\left[\mathrm{Cr(III)}_{\mathrm{fixed}}\right]^{\alpha}\left[\mathrm{MnO}_{2\ \exp 3}\right]^{\beta}}{i_{\exp 4} = \mathrm{k}\left[\mathrm{Cr(III)}_{\mathrm{fixed}}\right]^{\alpha}\left[\mathrm{MnO}_{2\ \exp 4}\right]^{\beta}} \tag{2.7}$$

Thus:

$$\frac{i_{\exp 3}}{i_{\exp 4}} = \left(\frac{\left[\mathrm{MnO}_{2\ \exp 3}\right]}{\left[\mathrm{MnO}_{2\ \exp 4}\right]}\right)^{\beta} \tag{2.8}$$

Therefore:

$$\beta = \frac{\mathrm{Log}\left(\frac{i_{\exp 3}}{i_{\exp 4}}\right)}{Log\left(\frac{\left[\mathrm{MnO}_{2\ \exp 3}\right]}{\left[\mathrm{MnO}_{2\ \exp 4}\right]}\right)} \tag{2.9}$$

The rate constant k was calculated for each experiment using the i values experimentally measured, and the β and α calculated for each pH values, using Eq. 2.10, which is a rearrangement of Eq. 2.3:

$$k = \frac{i}{\left[\mathrm{Cr(III)}\right]^{\alpha}\left[\mathrm{MnO}_2\right]^{\beta}} \tag{2.10}$$

Although initial rate methods are more difficult to perform than isolation methods since *i* must be measured in a very short time period, the Q-XAFS technique was able

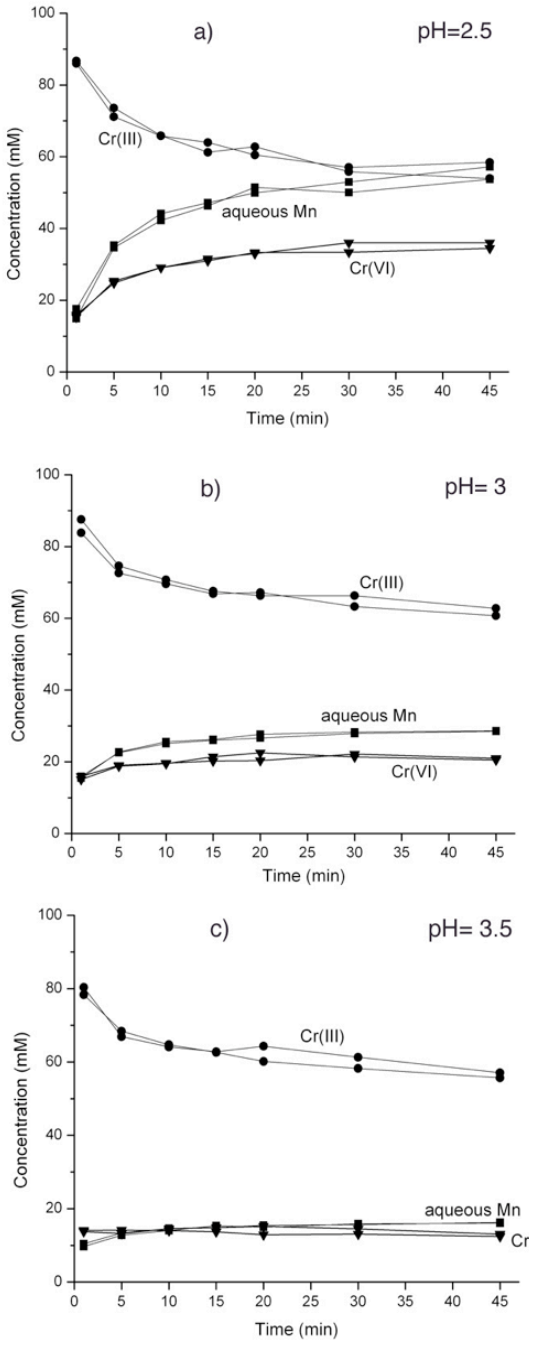


**Figure 2.3** Kinetics of Cr(III) oxidation on HMO at a) pH 2.5, b) pH 3, and c) pH 3.5, using a batch technique and reaction conditions of 100 mM Cr(III) and 20 g/L HMO

to collect enough data points at the beginning of the reaction to determine initial rates (Figure 2.2).

## 2.4 Results and Discussion

### 2.4.1 Traditional Batch Kinetic Experiments

The results of the batch experiments conducted at pH 2.5, 3, and 3.5, are depicted in Figure 2.3 a, b, and c, respectively. The lower the pH, the more the reaction (Eq. 2.1) is shifted toward the products, i.e, more Cr(VI) and aqueous Mn are present in solution at pH 2.5 than at pH 3.5 (Figure 2.3). Stirred flow experiments, to test if the manganese oxide dissolves in acidic medium, showed no manganese dissolution from the HMO, for the three different pH values (data not shown). Consequently, the high manganese production obtained during our batch experiments and depicted in Figure 2.3 is derived from the oxidation of chromium on the manganese oxide surface, rather than HMO dissolution due to the acidic medium. The sum of aqueous Cr(III) and Cr(VI) for each aliquot, at each pH value, is lower than 100 mM, meaning that chromium is sorbed on HMO. This amount increases with reaction time and pH value. At pH 3.5, about 12 mM of Cr(VI) is present in solution after 45 min, whereas about ~18 mM is present in solution at pH 3 after 45 min, and ~35 mM is present at pH 2.5. Lower values of dissolved $Cr(VI)_{aqueous}$ at pH 3.5 compared to lower pH values is not due to more chromate anions being retained on HMO, since the mineral surface is negatively charged at pH 3.5 (PZC 2.7 for HMO). Consequently, lower $Cr(VI)_{aqueous}$ concentration with increasing pH suggests lower Cr(III) oxidation rates. The formation of a chromium hydroxide precipitate on the surface of the manganese oxide may be responsible for the low Cr(III) oxidation rates

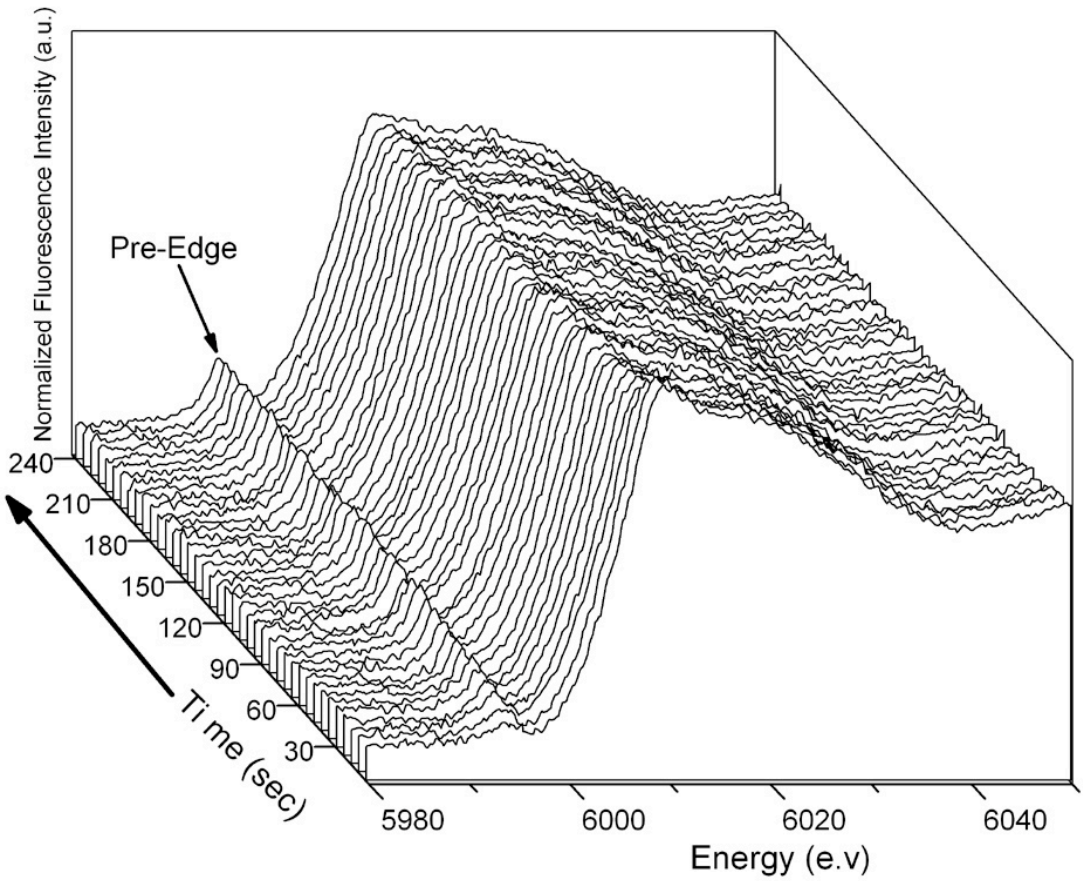


**Figure 2.4** Cr(III) oxidation kinetics using a QXAFS technique, at pH 2.5, [Cr(III)]=100mM, [HMO]=20g/L and 0-240 seconds. Each XANES spectrum shown represents 3 seconds of the reaction (average of four 0.75s spectra).

at pH 3.5 and the higher amount of chromium sorbed at this pH compared to lower pH values, since Cr(III) starts to precipitate close to pH 3.5 at the chromium concentration used in the experiment (Rai *et al.*, 1987). This precipitate could both reduce the

amount of available Cr(III) to react with the HMO, and shield the mineral surface, preventing further Cr(III) sorption, and thus, oxidation (Fendorf *et al.*, 1992). The formation of a chromium hydroxide surface precipitate was reported on the surface of birnessite, which belongs to the hexagonal birnessite family, like HMO (Villalobos *et al.*, 2003).

### 2.4.2 Q-XAFS Experiments

Data collected from a typical Q-XAFS batch experiment conducted at pH 2.5 is depicted in Figure 2.4. The growth of the XANES pre-edge feature at 5993.5 eV demonstrates that Cr(VI) is produced in the batch vessel as time proceeds. Cr(III) oxidation is particularly rapid during the first 120 s of the reaction, when about 35 mM of chromate is produced, followed by a slower rate. This biphasic trend taking place within the first 4 minutes was not only observed for the experiment shown in Figure 2.4, but also for all experiments carried out in this study to measure the rates of Cr(III) oxidation.

After 240 s (4 min) of the experiment shown in Figure 2.4, 30 mM of Cr(VI) were produced (Figure 2.5), which represents 30% of [Cr(III)] initially introduced. At the same experimental conditions, about 25 mM was measured with the traditional batch method. The latter experimental approach only measures aqueous Cr(VI), and not the total amount of Cr(VI), i.e., aqueous Cr(VI) and chromate sorbed on the manganese oxide, while the Q-XAFS experiment measures both aqueous and sorbed chromate. The higher Cr(VI) concentration measured with batch Q-XAFS compared to the traditional batch kinetic method at the same reaction times suggests that some chromate is sorbed on the surface of HMO at pH 2.5. To obtain further evidence that Cr(VI) is present on the manganese oxide surface, traditional batch

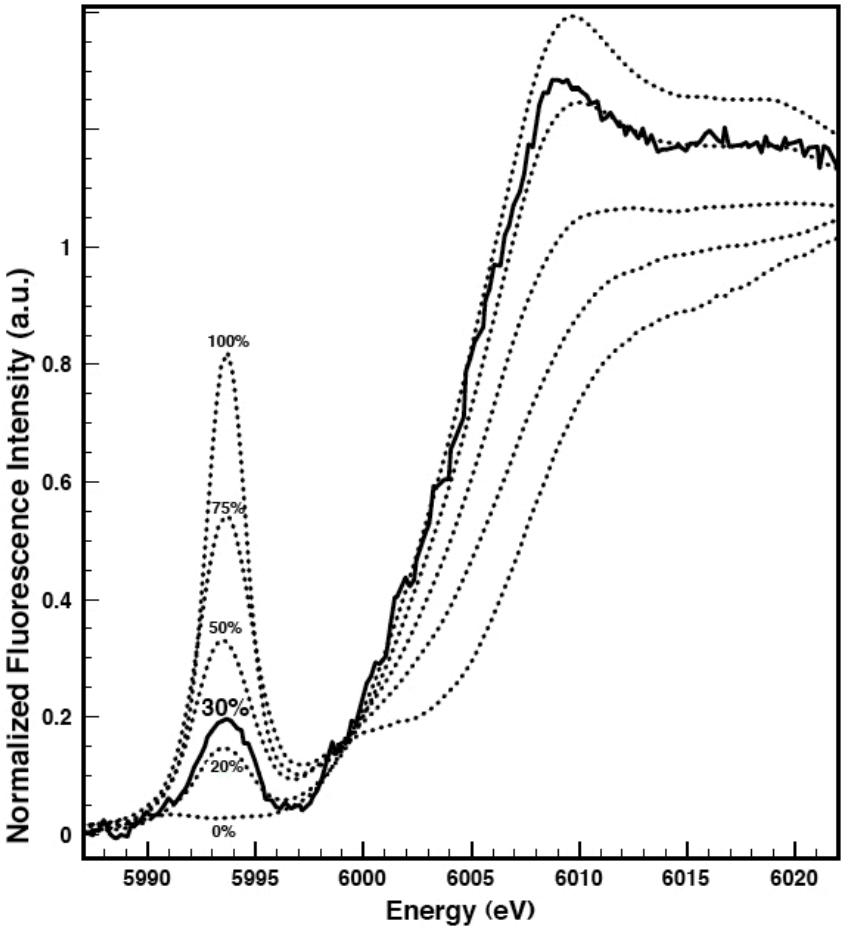


**Figure 2.5** Percentage of Cr(VI) produced in 4 minutes. Bold line: spectrum of Cr(III) oxidation kinetics at 240 second reaction time (average of two 0.75s Q-XAFS spectra), at pH 2.5, [Cr(III) ]$_0$=100 mM, [HMO]=20 g/L. Dashed lines: XANES spectra for standard solution mixtures of 100 mM [chromium]total Cr(III) + Cr(VI) : 100 % Cr(VI), 75 % Cr(VI), 50 % Cr(VI), 20 % Cr(VI), and 0 % Cr(VI)

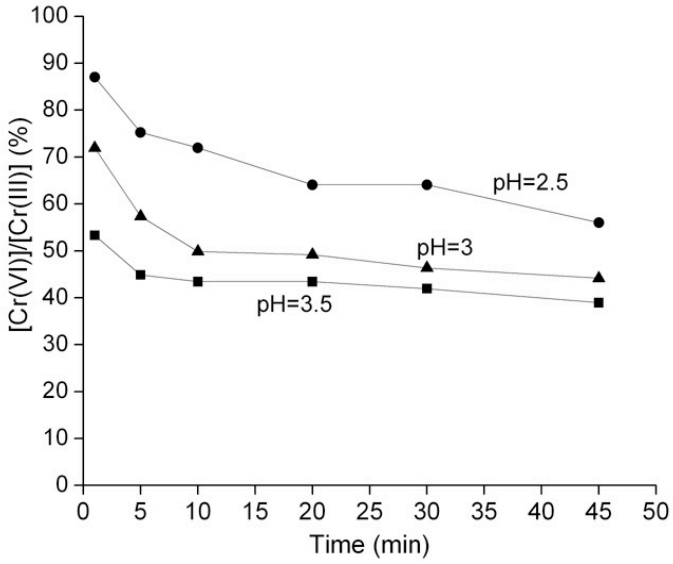


**Figure 2.6** Percentage of Cr(VI)/Cr(III) in the HMO pastes based on the pre-edge feature at 5993.5 eV, at pH 2.5, 3, and 3.5

experiments with the same experimental conditions were carried out near beamline X18B in a laboratory at the NSLS. Aliquots were taken out at different time intervals (1, 5, 10, 15, 20, 30, and 45 min) and filtered with a 0.22-μm filter. Manganese oxide pastes were analyzed immediately with bulk X-ray absorption spectroscopy to measure the ratio of Cr(VI) to Cr(III) in the pastes (Figure 2.6), by calculating the height of the pre-edge feature at 5993.5 eV. Figure 2.6 shows that at pH 2.5 and a 1 min reaction time, 87% of the chromium was Cr(VI), suggesting that chromate is sorbed on the manganese oxide. This proves that using a Q-XAFS batch method to measure the rates for Cr(III) oxidation with HMO at these experimental conditions is

**Table 2.1** Initial conditions, measured initial rates, and rate parameters The partial rate coefficients α, β at pH 2.5, pH 3, and pH 3.5 shown in this table are averaged values from α and β calculated using Eqs. 2.6 and 2.9 and by combining the initial rates measured at different experimental conditions. The rate constant for each experiment was measured with Eq. 2.10. Since all experiments were duplicated, the initial rates and rate parameters are reported with two values separated with "/". The standard error (95% confidence interval) for each initial rate is italicized. Averages of duplicate values are highlighted in bold.

| | | initial rates (mol/L/sec) | | | $k\ (M^{-1}\ s^{-1})$ | | |
|---|---|---|---|---|---|---|---|
| [Cr(III)] (mM) | [HMO] (g/L) | pH = 2.5 | pH = 3 | pH = 3.5 | pH = 2.5 | pH = 3 | pH = 3.5 |
| 100 | 20 | 0.0045/0.0052 | 0.0045/0.0045 | 0.0045/0.0047 | 0.204/0.228 | 0.277/0.202 | 0.295/0.364 |
| | | *(0.00036/0.00071)* | *(0.00067/0.00064)* | *(0.0004/0.0006)* | | | |
| 80 | 20 | 0.0035/0.0040 | 0.0034/0.0035 | 0.0039/0.0030 | 0.202/0.220 | 0.270/0.198 | 0.353/0.308 |
| | | *(0.00017/0.00021)* | *(0.00031/0.00066)* | *(0.00108/0.00046)* | | | |
| 60 | 20 | 0.0025/0.0029 | 0.0027/0.0028 | 0.0022/0.0022 | 0.197/0.215 | 0.303/0.208 | 0.302/0.357 |
| | | *(0.0002/0.00037)* | *(0.0004/0.00017)* | *(0.00043/0.00034)* | | | |
| 40 | 20 | 0.0017/0.0021 | 0.0015/0.0018 | 0.0012/0.0012 | 0.208/0.235 | 0.266/0.199 | 0.296/0.363 |
| | | *(0.00023/0.00003)* | *(0.00028/0.00034)* | *(0.00017/0.00017)* | | | |
| | | *Cr partial rate coefficient α* | | | | | |
| | | 1.08/1.01 | 1.13/1.05 | 1.43/1.53 | | | |
| | | **1.09** | **1.09** | **1.48** | | | |
| 100 | 20 | 0.0045/0.0052 | 0.0045/0.0045 | 0.0045/0.0047 | 0.204/0.228 | 0.277/0.202 | 0.295/0.364 |
| | | *(0.00036/0.00071)* | *(0.00067/0.00064)* | *(0.0004/0.0006)* | | | |
| 100 | 15 | 0.0035/0.0036 | 0.0035/0.0036 | 0.0037/0.0038 | 0.206/0.207 | 0.293/0.219 | 0.291/0.328 |
| | | *(0.0006/0.0005)* | *(0.00046/0.00052)* | *(0.00032/0.00054)* | | | |
| 100 | 10 | 0.002/0.002 | 0.0023/0.0020 | 0.0028/0.0029 | 0.169/0.171 | 0.287/0.244 | 0.280/0.311 |
| | | *(0.00039/0.00039)* | *(0.00001/0.00021)* | *(0.0008/0.00059)* | | | |
| 100 | 5 | 0.001/0.0012 | 0.0010/0.0014 | 0.0020/0.0022 | 0.157/0.203 | 0.257/0.316 | 0.283/0.346 |
| | | *(0.00039/0.00001)* | *(0.0001/0.0001)* | *(0.00035/0.00031)* | | | |
| | | *Mn partial rate coefficient a* | | | | | |
| | | 0.90/0.98 | 1.00/1.05 | 0.58/0.53 | | | |
| | | **0.94** | **1.02** | **0.55** | | | |
| | | | | | *k (averaged) in $M^{-1}\ s^{-1}$* | | |
| | | | | | *pH = 2.5* | *pH = 3* | *pH = 3.5* |
| | | | | | 0.192/0.211 | 0.279/0.227 | 0.300/0.340 |
| | | | | | **0.201** | **0.242** | **0.322** |

more appropriate than a traditional batch kinetic method since the entire amount of Cr(VI) produced from the chromium oxidation is measured, including the amount sorbed on the manganese oxide. A series of Q-XAFS batch experiments were carried out with different reactant concentrations and pH values to measure rate parameters for the Cr(III) oxidation by HMO (Table 2.1). The duplicate values for each experiment are very close to each other, meaning that the reproducibility of the Q-XAFS method is acceptable. To obtain the experimental initial rates, Cr(VI) was quantified from the pre-edge feature height for each experiment during a time period between time zero and the first minute of the reaction. Figure 2.7 shows examples of XANES spectra of experiments taken at different experimental conditions (pH, chromium, and manganese concentration), and the growth of the Cr(VI) pre-edge feature for each experiment. When [Cr(VI)] was plotted over the first 6 s of the reaction, a straight line resulted. The initial rate is equal to the slope (Sparks, 1989). The uncertainty in our measurements is given by the standard error of the slope, and was found to be low for most measured initial rates (Table 2.1). As an example, a plot of one initial rate measurement is depicted in Figure 2.2. For all experiments conducted at different Cr(III) concentrations (from 40 to 100 mM) and HMO suspension density (from 5 to 20 g/L), the first data point was measured at 1.5 s (average of two 0.75 scans). Data points collected after 6 ± 1.5 s resulted in a decrease of the $R^2$ (quality of the slope). Therefore, the initial rate was measured between 1.5 and 6 ± 1.5 s for all experiments, which represents 4 ± 1 data points. The $R^2$ of the slope for all experiments was ≥ 0.96. After getting the i values for each experiment, we determined the partial rate coefficients $\alpha$, $\beta$ (shown in Eq 2.2), and the rate

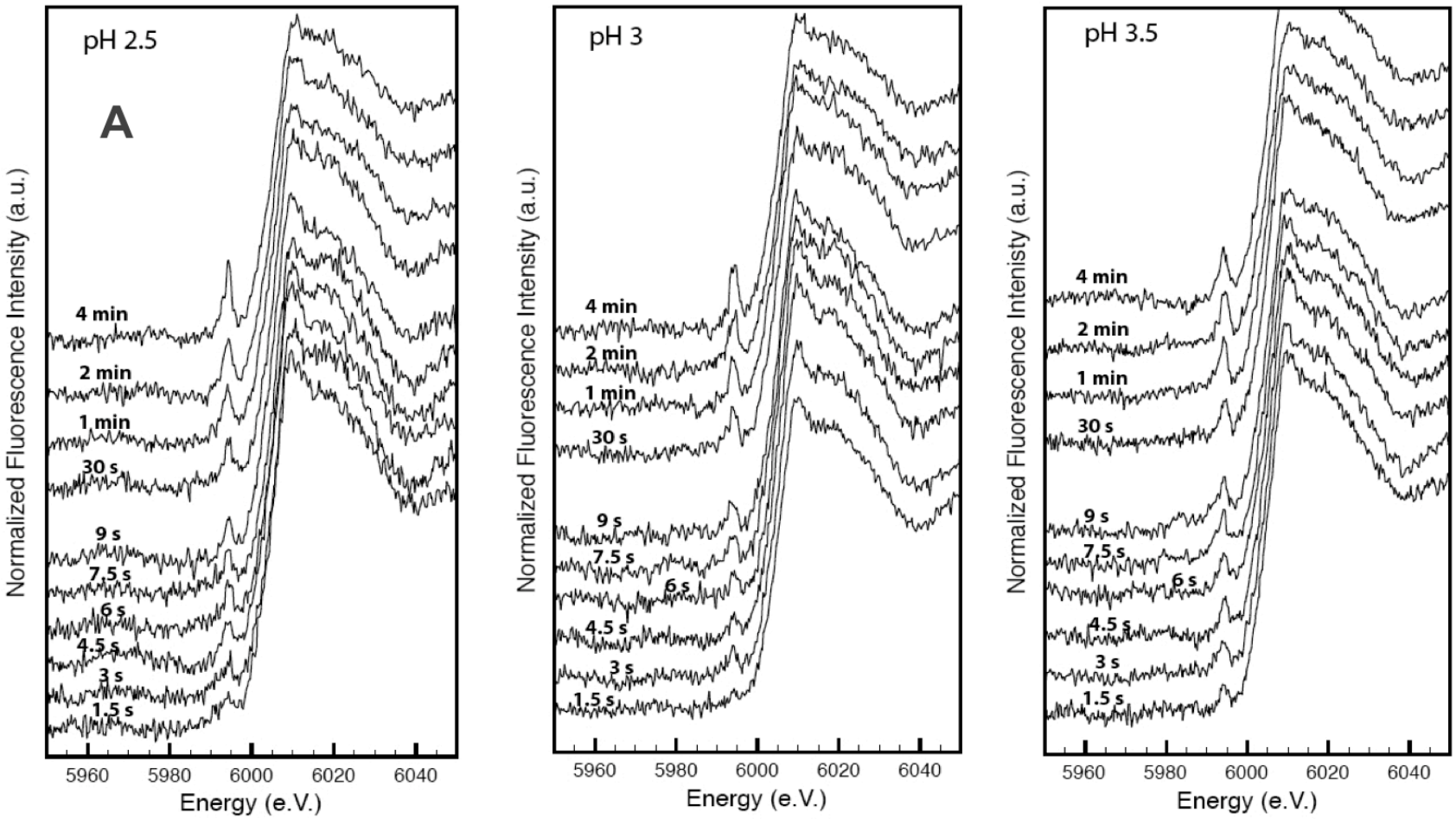
pH 2.5
A
Normalized Fluorescence Intensity (a.u.)
4 min
2 min
1 min
30 s
9 s
7.5 s
6 s
4.5 s
3 s
1.5 s
5960
5980
6000
6020
6040
Energy (e.V.)
pH 3
Normalized Fluorescence Intensity (a.u.)
4 min
2 min
1 min
30 s
9 s
7.5 s
6 s
4.5 s
3 s
1.5 s
5960
5980
6000
6020
6040
Energy (e.V.)
pH 3.5
Normalized Fluorescence Intenisty (a.u.)
4 min
2 min
1 min
30 s
9 s
7.5 s
6 s
4.5 s
3 s
1.5 s
5960
5980
6000
6020
6040
Energy (e.V.)

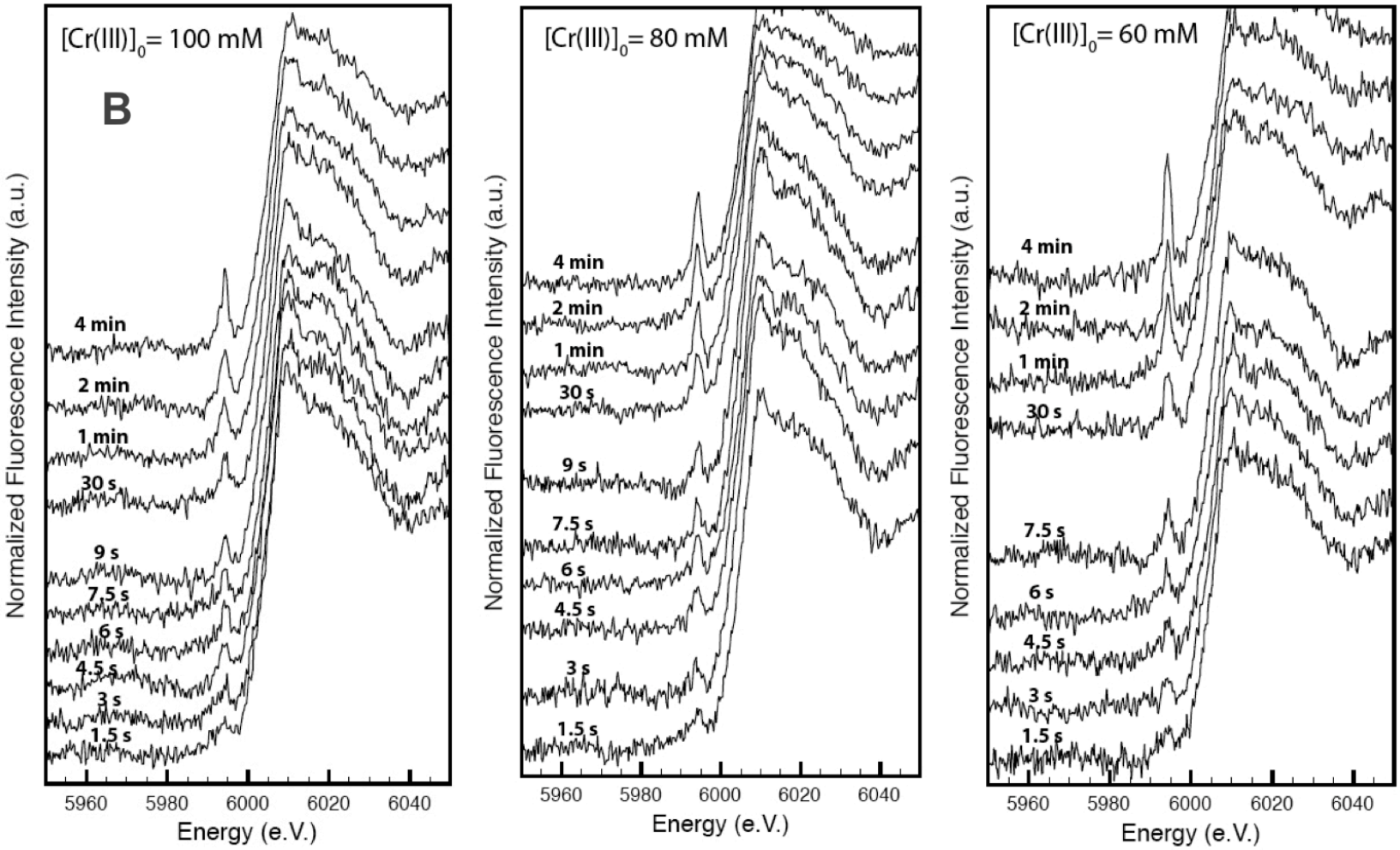
[Cr(III)]0= 100 mM
B
[Cr(III)]0= 80 mM
[Cr(III)]0= 60 mM
Normalized Fluorescence Intensity (a.u.)
Energy (e.V.)
4 min
2 min
1 min
30 s
9 s
7.5 s
6 s
4.5 s
3 s
1.5 s
5960
5980
6000
6020
6040

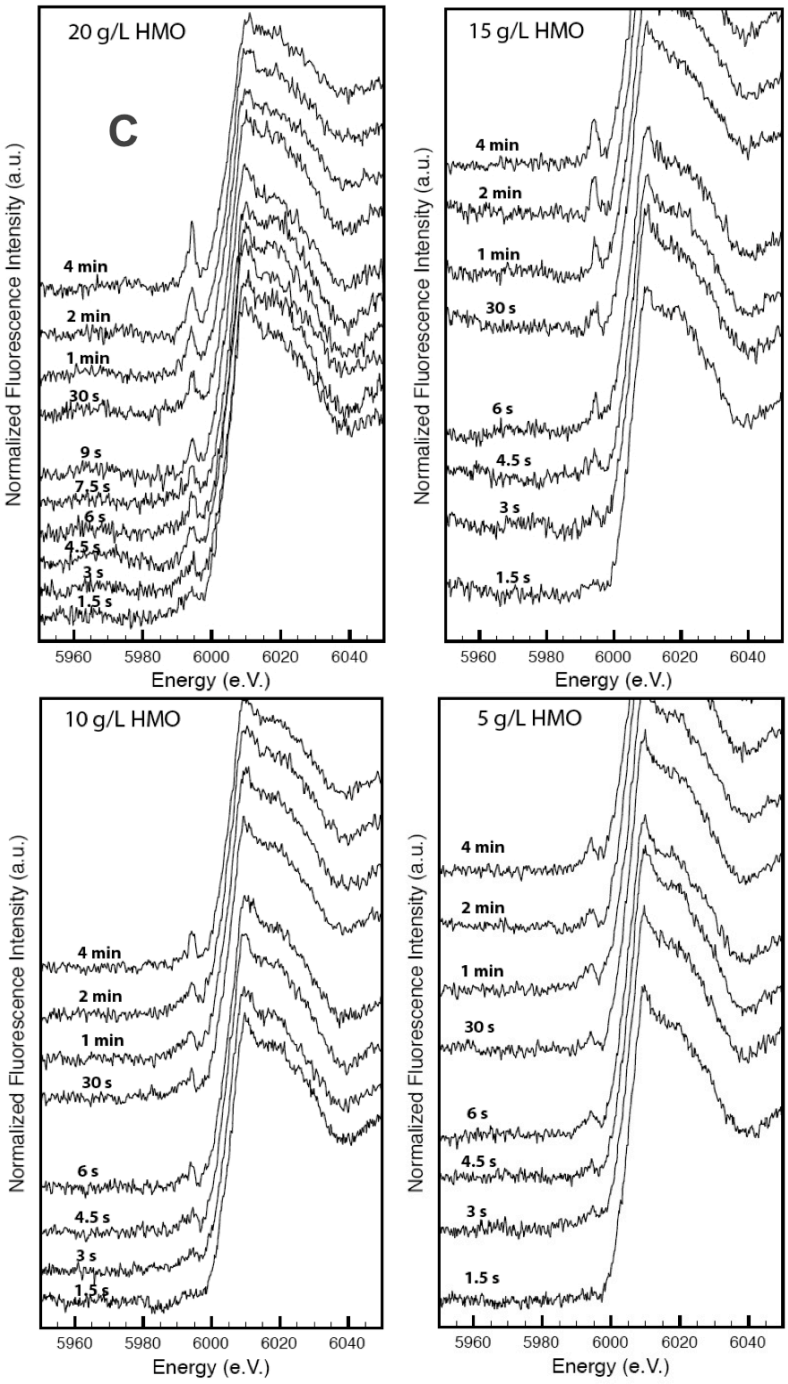


**Figure 2.7** A) Effect of pH – [Cr(III)]= 100 mM; 20 g/L HMO; pH 2.5, 3, and 3.5; B) Effect of Cr concentration – pH 2.5; 20 g/L HMO; and C) Effect of Mn concentration –pH 2.5; [Cr(III)]= 100 mM; 20, 15, 10, and 5 g/L

constants. A summary of the initial concentrations, the initial rates measured experimentally (i), and the rates parameters ($\alpha$, $\beta$, and k) for all experiments are summarized in Table 2.1. The rate parameters from Table 2.1 inserted in Eq 2.2 give these following rate equations:

$$\text{pH 2.5} \qquad \frac{dCr(VI)}{dt} = k[Cr^{3+}]^{1.04}[MnO_2]^{0.94} \qquad (2.11)$$

$$k = 0.201\ s^{-1}$$

$$\text{pH 3} \qquad \frac{dCr(VI)}{dt} = k[Cr^{3+}]^{1.08}[MnO_2]^{1.03} \qquad (2.12)$$

$$k = 0.242\ s^{-1}$$

$$\text{pH 3.5} \qquad \frac{dCr(VI)}{dt} = k[Cr^{3+}]^{1.48}[MnO_2]^{0.56} \qquad (2.13)$$

$$k = 0.322\ s^{-1}$$

The partial rate coefficients reported in Eqs 2.11, 2.12, and 2.13 show that a variation in the pH by a half unit changes the way the two reactants affect the kinetics of the reaction. These results were expected, since more Cr(III) and Mn(IV) are likely to react together when the mineral surface becomes more negatively charged at higher pH values (PZC of HMO) 2.7). The increase in the rate constant k from pH 2.5 to pH 3.5 also confirms our expectations. At the early stage of the reaction, the higher the pH, the higher the rate of Cr(III) oxidation (Fendorf and Zasoski, 1992). However, increasing the pH reduces the solubility of chromium. It may precipitate at the surface of the manganese oxide in a chromium hydroxide surface precipitate, even when the chromium concentration is below its saturation index (Manceau and Charlet, 1992).

Therefore, it has been postulated that although the initial oxidation rate is higher at high pH at the beginning of the reaction, chromium oxidation shuts down rapidly at high pH, likely due to the build up of a surface precipitate that impedes further interactions between Cr(III) and the manganese oxide surface. This surface precipitate formation was observed with birnessite for experimental conditions of pH 3.5 and a Cr(III) concentration of 770 μM (Fendorf *et al.*, 1992). These results suggest that one could divide the oxidation into two time periods: a first period during which only chromium and the HMO surface interact with each other, and a second period during which a chromium hydroxide surface precipitate forms and can influence the rates of Cr(III) oxidation. However, the kinetics of formation of the surface precipitate, as well as its exact nature, are still unknown. These particular topics will be addressed in a future study. Although a few studies have reported rates of Cr(III) oxidation on manganese oxides, comparing previous results and rate parameters to those reported in this study are difficult, because of the many differences in experimental conditions. The rate constants of trivalent chromium oxidation with $MnO_2$ notably depend on temperature, Cr(III) concentration and pH (Fendorf and Zasoski, 1992), the manganese oxide suspension density and nature (Weaver and Hochella, 2003), the kinetic equation considered (since it defines the rate constant unit), and the time scale at which the kinetic parameters are being measured (chemical rate constants versus apparent rate constants). For example, Johnson and Xyla (1991) reported *k* values for Cr(III) oxidation with manganite ($\gamma$-MnOOH). Their rate constants (in L $m^{-2}$ $s^{-1}$) were measured on several minutes (compared to a few seconds in our study), at pH between 3.5 and 9.5, and at a range of Cr(III) concentration of 0.25-5 $\mu$M (compared to 40-100 mM in our study). Therefore, it would be difficult to compare their kinetic parameters

with our results, since too many factors influence Cr(III) oxidation. Another study (Nico and Zasoski, 2000) reported rate constants for Cr(III) oxidation on acid birnessite measured over 30 min using a batch technique, at 50 $\mu$M Cr(III), 0.1 g/L of acid birnessite, and pH 3, 4, 5, and 6. The rate constant at pH 3 was equal to 0.0018 $s^{-1}$, and was 0.005 $s^{-1}$ at pH 4. Therefore, the rate constant at pH 3 reported in this previous study is much lower than the rate constant measured at pH 3 in the present study, which is probably due to the differences in experimental conditions and the time scale at which those rates were measured. The Arrhenius equation states that the chemical rate constant *k* is only dependent upon temperature, and not upon concentration or mixing speed. One sees from Table 2.1 that the *k* values are similar for all experiments carried out at a given pH and for different Cr(III) and manganese oxide concentrations. The same mixing speed value was used throughout this study: ~240 rotations per minute in the batch vessel. The experiment at pH 2.5 and 80 mM Cr(III) was repeated several times and the mixing speed was increased by a factor of 0.2, 0.5, and 1 order of magnitude. The same *k* value was obtained, regardless of the mixing speed (data not shown). Therefore, Cr(III) concentration, HMO suspension density, pH, and mixing speed did not affect the rate constants measured with quick XAFS. This further strengthens our argument that chemical reaction rates were measured in this study.

## 2.5 References

Amacher, M. C. (1991), Chapter 2: Methods of obtaining and analyzing kinetic data, rates of soil chemical processes, Sparks, D.L., Suarez, D.L., Eds, SSSA Spec. Publ. No. 27, 19-59, Soil Sci. Soc. Am: Madison, WI.

Banerjee, D. and Nesbitt, H. W. (1999), Oxidation of aqueous Cr(III) at birnessite surfaces: constraints on reaction mechanism, Geochemica et Cosmochimica Acta, 63, 1671-1687.

Bartlett, R. and James, B. (1979), Behavior of chromium in Soils: III. Oxidation, J. Environ. Quality, 8, 31-35.

Chiswell, B. and O'Halloran, K. R. (1991), Comparison of three colorimetric methods for the determination of manganese in freshwaters, Talanta, 38, 641-648.

Daulton, T. L. and Little, B. (2006), Determination of chromium valence over the range Cr(0)-Cr(VI) by electron energy loss spectroscopy, Ultramicroscopy, 106, 561-573.

Dent, A. J. (2002), Development of time-resolved XAFS instrumentation for quick EXAFS and energy-dispersive EXAFS measurements on catalyst systems, Topics in Catalysis, 18, 27-35.

Dirilgen, N. and Dogan, F. (2002), Speciation of chromium in the presence of copper and zinc and their combined toxicity, Ecotoxicology and Environmental Safety, 53, 397-403.

Eary, E. and Rai, D. (1987), Kinetics of chromium(III) oxidation to chromium(VI) by reaction with manganese dioxide, Environmental Science & Technology, 21, 1187-1193.

Fendorf, S. E. (1995), Surface reactions of chromium in soils and waters, Geoderma, 67, 55-71.

Fendorf, S. E. and Zasoski, R. J. (1992), Chromium(III) oxidation by δ-$MnO_2$ 1. Characterization, Environmental Science & Technology, 26, 79-85.

Fendorf, S. E., Fendorf, M., and Sparks, D. (1992), Inhibitory mechanisms of Cr(III) oxidation by δ-$MnO_2$, Journal of Colloid and Interface Science, 153, 37-54.

Fendorf, S. E., Sparks, D. L., and Camaioni, D. M. (1993), Electron paramagnetic resonance stopped flow kinetic study of manganese(II) sorption desorption on birnessite, Soil Sci. Soc. Am. J., 57, 57-62.

Gadde, R. R. and Laitinen, H. A. (1974), Studies of heavy metal adsorption by hydrous iron and manganese oxides, Analytical Chemistry, 46, 2022-2026.

Ginder-Vogel, M., Landrot, G., Fischel, J., and Sparks, D. L. (2009), Quantification of rapid environmental redox processes using quick scanning x-ray absorption spectroscopy (Q-XAS), Proceedings of the National Academy of Sciences, 106, 16124-16128.

Gray, M. J. and Malati, M. A. (1978), The point of zero charge of manganese dioxides, J. Electroanal. Chem., 89, 135-140.

Guha, H., Saiers, J., Brooks, S., Jardine, P., and Jayachandran, K. (2001), Chromium transport, oxidation, and adsorption in manganese-coated sand, Journal of Contaminated Hydrology, 49, 311-334.

Johnson, A. C. and Xyla, A. G. (1991), The oxidation of chromium(III) to chromium(VI) on the surface of manganite (γ-MnOOH), Geochemica et Cosmochimica Acta, 55, 2861- 2866.

Kim, J. G., Dixon, J., Chusui, C. C., and Deng, Y. (2002), Oxidation of chromium(III) to (VI) by manganese oxides, Soil Sci. Soc. Am. J., 66, 306-316.

Kim, J. G. and Moon, H. S. (1998), Oxidation of chromium (III) to chromium (VI) by a series of synthesized birnessites (δ-MnO2): kinetics and oxidation capacity, Clay Science, 10, 363-374.

Kingston, S. H. M., Cain, R., Huo, D., and Rahman, M. G. M. (2005), Determination and evaluation of hexavalent chromium in power plant coal combustion by-products and cost-effective environmental remediation solutions using acid mine drainage, J. Environ. Monit., 7, 899-905.

Lin, C. J. (2002), The Chemical transformations of chromium in natural waters - A model study, Water, Air, and Soil Pollution, 139, 137-158.

Manceau, A. and Charlet, L. (1992), X-ray adsorption spectroscopy study of the sorption of Cr(III) at the oxide-water interface. I. Molecular mechanism of Cr(III) oxidation on Mn oxides, Journal of Colloid and Interface Science, 148, 425-442.

Mifflin, A., Gerth, K., and Geizer, F. (2003), Kinetics of chromate adsortion and desorption at fused quartz/water interfaces studied by second harmonic generation, Journal of Physical Chemistry A, 107, 9620-9627.

Mitsunobu, S., Takahashi, Y., and Uruga, T. (2005), Observation of chemical reactions at the solid-water interface by Quick XAFS combined with a column reactor, Analytical Chemistry, 78, 7040-7043.

Morgan, J. and Stumm, W. (1964), Colloid-chemical properties of manganese dioxide, Journal of Colloid Science, 19, 347-359.

Murray, J. W. (1974), The Surface chemistry of hydrous manganese dioxide, J. Colloid Interface Sci., 46, 357-371.

Murray, K. and Tebo, B. (2007), Cr(III) is indirectly oxidized by the Mn(II)-oxidizing bacterium bacillus sp. Strain SG-1, Environmental Science & Technology, 41, 528-533.

Palmer, C. and Wittbrodt, P. (1991), Processes affecting the remediation of chromium-contaminated sites, Environmental Health Perspective, 92, 25-40.

Parikh, S. J., Lafferty, B. J., and Sparks, D. L. (2008), An ATR-FTIR spectroscopic approach for measuring rapid kinetics at the mineral/water interface, Journal of Colloid and Interface Science, 320, 177-185.

Peterson, M. L., Brown, G. E., Parks, G. A., and Stein, C. L. (1997), Differential redox and sorption of Cr(III/VI) on natural silicate and oxide minerals: EXAFS and XANES results, Geochemica et Cosmochimica Acta, 61, 3399-4413.

Post, J. E. (1999), Manganese oxide minerals: crytal stuctures and economic and environmental significance, Proceedings of the National Academy of Sciences, 96, 7, 3447-3454.

Rai, D., Sass, B., and Moore, D. (1987), Chromium(III) hydrolysis constants and solubility of chromium(III) hydroxide, Inorg. Chem., 26, 345-349.

Rotzinger, F., Stunzi, H., and Marty, W. (1986), Early stages of the hydrolysis of chromium(III) in aqueous solution. 3. Kinetics of dimerization of the deprotonated aqua ion, Inorg. Chem., 25, 489-495.

Sparks, D. L. (1989), Kinetics of Soil Chemical Processes, Academic Press, San Diego, CA.

Sparks, D. L. (2003), Environmental Soil Chemistry, Academic Press, San Diego, CA.

Stepniewska, Z., Bucior, K., and Bennicelli, R. P. (2004), The effects of $MnO_2$ on sorption and oxidation of Cr(III) by soils, Geoderma, 122, 291-296.

Strawn, D. G., Scheidegger, A. M., and Sparks, D. L. (1998), Kinetics and mechanisms of Pb(II) sorption and desorption at the aluminum oxide-water interface, Environ. Sci. Technol., 32, 2596-2601.

Villalobos, M., Toner, B., Bargar, J., and Sposito, G. (2003), Characterization of the manganese oxide produced by pseudonomas putida strain MnB1., Geochemica et Cosmochimica Acta, 67, 2649-2662.

Weaver, R. M. and Hochella, M. F. (2003), The reactivity of seven Mn-Oxides with $Cr^{3+}_{aq}$: a comparative analysis of a complex, environmentally important redox reaction, American Mineralogist, 88, 2016-2028.

Yang, J. W., Tang, Z. S., Guo, R. F., and Chen, S. Q. (2008), Soil surface catalysis of Cr(VI) reduction by citric acid. Environ. Progress 27, 302-307.

# Chapter 3

# KINETICS AND MECHANISMS OF CHROMIUM(III) SORPTION, SURFACE PRECIPITATION, AND OXIDATION ON HEXAGONAL MANGANESE(IV) OXIDE SURFACES

## 3.1 Abstract

This study investigated the kinetics and mechanisms of the reactions occurring during chromium(III) sorption on three hexagonal manganese(IV) oxide surfaces. Bulk Extended X-ray Absorption Fine Structure spectroscopy (EXAFS) analyses show that trivalent chromium binds to the mineral surface in an inner-sphere complex on the edges of the manganese oxide layers, and rapidly oxidizes to Cr(VI), which can weakly bind to the surface in an outer sphere complex, or diffuse to solution. As more Cr(III) sorbs on Mn(IV)$O_2$, Cr(III) nucleation occurs on the mineral and simultaneously Cr(VI) oxidation rates decrease. Chromium(III) may precipitate locally on the mineral surface as a γ-CrOOH phase and extend away from the manganese oxide, if the mineral surface is saturated with ions at high ionic strength. Alternatively, Cr(III) can epitaxially nucleate in a α-CrOOH phase on the top of Mn(IV)$O_2$ layers, due to structural similarities between the surfaces of the Cr(III) precipitate and the manganese oxide. After forming, Cr(III) precipitates can desorb from the mineral surface, since more Cr(III) nucleation products are detected in solution than on the solid phase. Quick X-ray Absorption Fine Structure spectroscopy (Q-XAFS) enables us to measure *in situ* the rates of both surface precipitation

formation on manganese oxides and Cr(III) oxidation occurring in the entire batch system. The α-CrOOH phase can quickly form at high pH at the early stage of Cr(III) sorption on manganese oxides, thus competing with the rapid Cr(III) oxidation for free Cr(III) monomers in solution. Additionally, the phase can quickly reach high concentrations in the system, thus acting as a sink for Cr(III) ions. Therefore, since both Cr(III) nucleation and Cr(III) oxidation occur rapidly and potentially have opposite effects on Cr toxicity in the environment, this study, which measures for the first time the rates of Cr surface precipitation on manganese oxide surface using Q-XAFS, demonstrates the need for developing new techniques that can follow the kinetics of rapid reactions occurring in the environment.

## 3.2 Introduction

Chemical processes occurring in soils are often controlled by surfaces of soil components, such as clay minerals, oxides and (oxy)hydroxides, or organic matter (Sparks, 1989). The reactions taking place at the liquid/solid interface can transform the chemical properties of hazardous species, ultimately changing their fate and effects in the environment. For example, nickel, which is potentially carcinogenic to humans, can be sequestrated on mineral surfaces by sorbing on clay surfaces along with aluminum, which diffuses to solution from clay dissolution, to form Ni-Al LDH phases. These surface precipitates transform into a more stable mineral phase that diminishes the bioavailability of nickel in the environment (Scheinost *et al.*, 1999). Similarly, the surface of manganese oxides can drastically affect the chemical nature of chromium. Chromium(III) and (VI) can be found in soils at high concentrations, from the weathering of Cr-bearing minerals, like serpentine rocks, or from anthropogenic sources (Palmer *et al.*, 1991; Oze *et al.*, 2007). Previous studies showed

that trivalent chromium sorption on $MnO_2$ surfaces can result in two reaction pathways that have opposite effects on chromium toxicity in the environment. Chromium(III) can either oxidize on the manganese oxide surface, to become Cr(VI) (Fendorf and Zasoski, 1992; Weaver and Hochella, 2002), which is mobile and more toxic than Cr(III), or precipitate on the $MnO_2$ surface to form a Cr(III) oxyhydroxide phase, which can prevent further Cr(III) oxidation (Manceau and Charlet, 1992; Fendorf *et al.*, 1992). Precipitation on soil surfaces can form locally, at sub-monolayer surface coverage, and at a sorbent concentration below the saturation index at which the element starts to precipitate in bulk solution. Surface precipitation occurs since the surface provides sterically similar sites, which decreases the energy of nucleation of the sorbate (McBride, 1991) –the surface then works as a template that helps form molecular structures; also, the activity of the precipitate is lower than one nearby the surface (Sposito, 1986). Lastly, surface precipitation can occur since the solubility of the precipitate is lowered because the dielectric constant of the surface is less than that of the bulk solution (O'Day *et al.*, 1994). A few studies found an intimate relationship between the mineral surface structure and the nature of the precipitate phase. For example, chromium(III) precipitating on α-FeOOH results in a α-CrOOH structure bound to the mineral in an inner sphere complex, which grows in an unstrained epitaxial fashion on the mineral surface (Charlet and Manceau, 1992). As the precipitate keeps on accumulating progressively away from α-FeOOH, the effect of the surface on nucleation diminishes; chromium then starts to precipitate in a γ-CrOOH phase. Conversely, chromium(III) sorption on silica surfaces results in a non-epitaxial γ-CrOOH precipitate phase that locally extends away from the surface, due to

structural incompatibilities between the mineral and chromium nucleation products (Fendorf, 1994).

Chromium surface precipitates in a γ-CrOOH structure (similar to lepidocrocite) have been detected on a variety of manganese oxides (Manceau and Charlet, 1992; Fendorf *et al.*, 1992). This is also the phase that forms when Cr(III) precipitates in bulk solution. The phase was identified by bulk XAFS spectroscopy (Manceau and Charlet, 1992), using the Cr-reacted $MnO_2$ solid fraction of filtered aliquots taken from a batch system, and by Electron Diffraction (ED) TEM (Fendorf *et al.*, 1992). In the latter study, $MnO_2$ was coated on a grid and dipped into a Cr(III) solution before TEM analysis. Therefore, both studies did not measure the formation of the surface precipitate *in situ*. Their respective experimental approaches could have introduced some artifacts, like for example some structural modifications occurring on the mineral surface between the time of the sampling and the time of the measurements, or during the rinsing of the reacted mineral, which could have desorbed some species weakly sorbed on the mineral surface. One study followed the formation *in situ* of a chromium surface precipitate on a Mn(III) oxyhydroxide using a fluid cell TMAFM (Weaver *et al.*, 2002). Although the nucleation phase was subsequently identified with XPS as a chromium hydroxide phase, its crystal structure was not specified. Therefore, the kinetics of chromium surface precipitate formation on manganese oxides are still unclear, and the nature of these phases are still not well understood. Nevertheless, it has been postulated that chromium surface precipitation could play an important environmental role during Cr(III) sorption on manganese oxides. It could inhibit Cr(III) from oxidizing to Cr(VI) by decreasing the amount of Cr(III) in solution and/or shielding the manganese surface (Fendorf *et al.*, 1992).

The goal of this study is to measure *in situ* the kinetics of the two reaction pathways that can occur during chromium(III) sorption on manganese oxides, i.e. an oxidation reaction and surface precipitation, using Quick X-ray Absorption Fine Structure Spectroscopy (Q-XAFS). This technique was recently employed to measure the "chemical" rates of chromium(III) oxidation by hydrous manganese oxide (HMO) (also called δ-$MnO_2$), the synthetic analogue of vernadite (Villalobos *et al.*, 2003) during the first few seconds of the reaction (Landrot *et al.*, 2010). In the present study, the "apparent" rates of chromium oxidation by HMO and two other similar hexagonal Mn(IV) oxides, i.e. random stack birnessite (RSB), and acid birnessite (AB), are measured with Q-XAFS on a time scale of dozens of minutes, to compare with the kinetics of Cr(III) surface precipitation. The objective is to assess the temporal relationship between these two Cr(III) reaction pathways that potentially have opposite effects on chromium toxicity in the environment. Also, the mechanisms of Cr(III) oxidation and precipitation are constrained based on the kinetics data in this study. The choice of hydrous manganese oxide as the reactant is based on the fact that it is a strong oxidizer, capable of reacting with chromium(III) and other elements, including arsenic(III) (Parikh and Sparks, 2008; Ginder-Vogel *et al.*, 2009; Landrot *et al.*, 2010). This manganese oxide is also a very poorly crystalline mineral, similar to the biogenic manganese oxides naturally found in the environment (Villalobos *et al.*, 2003). The two other manganese oxides chosen in this study, AB and RSB, are similar to HMO in nature, since these three manganese oxides have layered structures, made of unit cells each featuring a manganese atom octahedrally coordinated with six oxygen atoms (Post, 1999). The difference between HMO, AB, and RSB lies in the spatial orientation and area of their layers, as well as the space between layers.

Additionally, these three minerals have different degrees of crystallinity, HMO having the least crystalline perfection and smallest crystal size, and RSB having the highest degree of crystallinity. Their capacity to react with Cr(III) are compared in this study, to assess the importance of the mineral structure on the time-dependent reactions involving Cr(III) and $MnO_2$.

## 3.3 Material and Methods

### 3.3.1 Experimental Approach

#### 3.3.1.1 Reactant and standard syntheses

All solutions were prepared with distilled dionized water, produced from a Barnstead system. Random Stack Birnessite (RSB) was synthesized by slowly mixing two reactants, KOH at a concentration of 8 M, and $Mn(II)Cl_2$ at 0.4 M. After bubbling both solutions with $N_2$ for several hours, the Mn(II) solution was slowly titrated with KOH solution. The mixture was cooled down to approximately 5°C for about one hour. Then, $O_2$ was vigorously bubbled in the vessel for three hours. Acid birnessite (AB) was prepared by boiling a solution of 0.4 M $KMnO_4$, which was titrated with a solution of 12N HCl, with a 1/10 volumetric ratio of the acid over the permanganate solution (McKenzy 1971). Hydrous manganese oxide (HMO) was synthesized by slowly adding a manganese(II) nitrate solution to an alkaline permanganate solution. The amounts of manganese(II) nitrate, potassium permanganate, and sodium hydroxide were mixed in the mole ratio 3:2:4. (Gadde and Laitinen, 1974). All synthesized minerals were washed via centrifugation until a constant conductivity was reached in the supernatant, and then stored before conducting the experiments. The manganese oxides were synthesized no longer than a week before starting the

experiments. The surface areas of the three minerals measured by BET, using nitrogen as the adsorbate at 77.4K, were 78 $m^2/g$ , 84 $m^2/g$, and 272 $m^2/g$ for RSB, AB, and HMO, respectively. The XRD patterns of the three minerals and SEM analysis confirmed that the three minerals were successfully synthesized.

The γ-CrOOH standard was synthesized by adjusting the pH of a 20 mM $CrCl_3$ solution to pH 6. This pH was maintained for 24 hours (Hansel *et al.*, 2003). The α-CrOOH standard was synthesized hydrothermally with a 0.3 M $Cr(NO_3)_3.9H_2O$ solution at 2.3 MPa and 200 °C (Sileo *et al.*, 2004). Both minerals were washed via centrifugation until a constant conductivity was reached in the supernatant, and were analyzed by XRD to confirm the two phases.

#### 3.3.1.2 Batch Experiments

In a 400 mL vessel containing a manganese oxide solution (AB, RSB, or HMO) at a suspension density of 20 g/L and 50 mM KCl, 20 mL of 1 M Cr(III) was introduced at t=0 to obtain a final concentration of 50 mM. The experiments were conducted at pH=2.5, pH=3, and pH=3.5. Chromium is not expected to precipitate in bulk solution at these three pH values, since the pH limit at which Cr(III) starts to precipitate is ≈ 3.6 at Cr(III)= 50 mM, according to equation (1) (Rai *et al.*, 1987, Banerjee and Nesbitt, 1999).

$$\log K = 5.78 = \log [Cr(OH)_2^+] - 2\log[H^+] \qquad (3.1)$$

Since the addition of the concentrated chromium stock solution to the system resulted in an instantaneous variation in pH, a quantity of 4M KOH or 2N HCl (volumes in Appendix A) was manually added to the system at the beginning of the reaction, along with Cr(III), to reach the desired pH value of the experiment (pH=2.5, pH=3, and pH=3.5) within the first 10 seconds after t=0 (t=0 being the time when

chromium is injected into the vessel). The $H^+$ production, due to Cr(III) oxidation by manganese oxides, resulting in a constant decrease in pH throughout the reaction, was controlled by a pH stat supplying 1M KOH. After chromium was added at t=0, 20 mL aliquots were taken from the vessel at different time intervals (1 min, 5 min, 10 min, 20 min, 30 min, 1 hour, and 6 hours) and filtered. Each aliquot was used for different purposes. Firstly, 10 mL of the aliquot was rapidly put in 15 mL tubes and centrifuged for 4 minutes at 9000 rpm to quench the reactions between Cr and the manganese oxide. The solid phase was then used to conduct replenishment experiments, and the concentrations of Cr(III), Cr(VI), and $Mn_{aqueous}$ in the supernatant were measured with Inductively coupled Plasma-Mass Spectroscopy (ICP-MS) after chromatographic separation, using a G3268-80001 Agilent Column, in a 15 mM EDTA mobile phase at pH=7. Additionally, 10 mL of the aliquot was put in 15 mL tubes and centrifuged for 4 minutes at 9000 rpm. After removing the supernatant, the waste paste of $MnO_2$ was mounted on sample holder for bulk XAFS analysis.

#### 3.3.1.3 Replenishment experiments

Three desorption agent solutions were used to conduct replenishment experiments: a DI water solution, a 50 mM $Al^{3+}$ solution made from $Al(NO_3)_3$ salt dissolved in DI water, and a solution of 50 mM $PO_4^{3-}$ prepared from potassium dihydrogen phosphate 98 % dissolved in DI water. The three solutions contained KCl at 50 mM. The pH of the three solutions was adjusted with $HNO_3$ to pH 2.5, 3, or 3.5. Each desorption agent solution was reacted for 24 hours in 15 mL tubes under vigorous shaking with the solid phase of the 10 mL centrifuged batch experiment aliquots, which represents ~200 mg of Cr-reacted $MnO_2$. The tubes were cyclically centrifuged every 24 hours, for a total of 6 replenishments. After each centrifugation,

the concentrations of Cr(III), Cr(VI), and $Mn_{aqueous}$ in the supernatant were measured using the same protocol described earlier, while the Cr-reacted $MnO_2$ solid phase was again reacted for 24 hours by shaking with 10 mL of a fresh desorption agent solution.

#### 3.3.1.4 Stirred Flow Experiments

At the end of the batch experiments, a 24 mL aliquot was taken from the batch vessel after Cr(III) reacted with $MnO_2$ for 6 hours, to conduct three stirred-flow experiments. Firstly, 8 mL of the aliquot was put in a 8 mL stirred-flow reactor chamber. The 50 mM $Al^{3+}$ desorption agent solution used for the replenishment experiments was used as the influent solution, flowing through the stirred-flow chamber with stirring, via a peristaltic pump at a flow rate of 1 mL/min. A 0.22 μm-pore size filter prevented the solid phase from leaving the stirred-flow chamber and passing to the effluent solution. Another 8 mL of the aliquot taken from the batch kinetic vessel was used to perform stirred flow experiment similar to the one previously described, but using the $PO_4^{3-}$ solution as the influent solution. Lastly, an experiment was conducted with the remaining 8 mL of the aliquot, which was put in the stirred-flow chamber, using the desorption agent solution that only contains KCl at 50 mM as the influent solution. The effluent solution was collected by a fraction collector (Isco's Foxy Junior) every 4 mL for 1 hour in 15 tubes, which were labeled from 1 to 15. The concentration of Cr(III), Cr(VI), and $Mn_{aqueous}$ were measured in tubes 1, 3, 6, 9, 11, 13, and 15, using the same protocol described earlier.

Stirred-flow, batch kinetic, and replenishment experiments were performed in duplicate.

### 3.3.2 Solid Phase Analysis

#### 3.3.2.1 Bulk XAFS Analysis

$MnO_2$ pastes and Cr standards were mounted on Teflon sample holders, sealed with Kapton tape, and analyzed at the Cr K-edge (5989 eV) by bulk x-ray absorption fine structure spectroscopy (XAFS), at beamline X11 A, National Synchrotron Light Source (NSLS), Brookhaven National Laboratory, Upton, NY. The 300 mA synchrotron beam was detuned from a Si(111) monochromator in $I_0$ by 30% to reject higher harmonics. The gas mixture in $I_o$ was 70% helium, 30% nitrogen, and the fluorescence signal was collected with a Lytle cell detector at room temperature. A Vanadium filter was used to remove elastic radiation from the fluorescence emissions. The sample holder was oriented at 45° to the incident beam. Three spectra were collected per sample, and averaged for data analysis. Spectra were calibrated at the chromium pre-edge feature at 5993.5 eV. Data were analyzed with the SIXPACK/IFEFFIT program. The concentration of Cr(VI) in the samples was measured from the pre-edge feature at 5993.5 eV from the normalized XANES spectra, using a set of normalized XANES spectra of mixed Cr(III)/Cr(VI) standards (Peterson *et al.*, 1997; Landrot *et al.*, 2010). Fourier transformed extended x-ray absorption fine structure (EXAFS) spectra that were $k^3$ weighted were used for shell-by-shell fitting of the data. Model compounds used in FEFF6l calculations were Eskolaite ($Cr_2O_3$) for the Cr(III)-O path, and Tarapacite ($K_2CrO_4$) for the Cr(VI)-O path. Eskolaite was also used to generate the first Cr-metal shell path, knowing that an imaginary Eskolaite mineral with manganese atoms substituted for chromium gave the same fitting results, but with a slightly higher $\chi^2$ value. The coordination number of Cr(III)-O in our models was constrained based on the coordination number of Cr(VI)-

O, and was defined as $CN_{Cr(III)-O} = (1-(CN_{Cr(VI)-O}/4)) \times 6$. The contribution of the triangular multiple scattering Cr-O-O-Cr in the $Cr(VI)O_4$ tetrahedron was also considered in our fits (Peterson *et al.*, 1996): all the fitting parameters, i.e. multiple scattering coordination number for ($CN_{m.s}$), the multiple scattering Debye-Waller factor ($\sigma^2_{m\text{-}s}$), and the multiple scattering radial distance ($R_{m.s}$) were constrained based on Cr(VI)-O fitting parameters, and respectively defined in our models as $CN_{m.s.} = 3 \times CN_{CrVI\text{-}O}$, $\sigma^2_{m\text{-}s.} = 2*\sigma^2 Cr_{(VI)\text{-}O}$, and $R_{m.s.} = (Rreff_{m.s} / Rreff_{Cr(VI)\text{-}O}) * R_{Cr(VI)\text{-}O} = (2.98/1.64) * R_{Cr(VI)\text{-}O.}$

#### 3.3.2.2 TEM Analysis

A few milligrams of dried manganese oxides reacted with Cr(III) for 1 hour were dispersed in deionized water and briefly ultrasonified. A small amount of the solution was deposited on a 200-mesh Cu grid and dried. The samples were analyzed with a Philips CM300 FEG microscope equipped with an Oxford light element energy dispersive X-ray spectroscopy (EDS) detector and a Gatan GIF 200 CCD imaging system. Data analysis was carried out with Gatan Digital Micropraph 1.8 software for the image processing, and the EDS data were analyzed with the software package ES Vision4. Selected Area Electron Diffraction (SAED) data were processed with DiffTools scripts developed by David Mitchell (Mitchell, 2008).

### 3.3.3 Real time, *In Situ* Experiments

Q-XAFS experiments were conducted at beamline X18 B, at the NSLS. The batch experimental set-up was identical to the one used in a former study where the chemical rates of chromium(III) oxidation were measured (Landrot *et al.*, 2010). In this present study, the batch vessel contained a suspension of $MnO_2$ at 20 g/L and

50 mM KCl, and a Cr(III) stock solution was injected at the beginning of the reaction to obtain a concentration of 50 mM in the vessel. The reaction was carried out at pH 2.5, 3, and 3.5. The experiments were conducted at the Cr K edge (5989 eV), and duplicated at the Mn K edge (6539 eV). For all experiments, the gas mixture in $I_0$ was 70% He and 30% $N_2$, and the detuning was 30%. The data acquisition method collected 600,000 points/5 minutes using a Keithley current amplifier, a sixteen-channel VME analog-digital-converter (ADC), and custom programmed Linux based software. A five-minute QXAFS scan collected about 226 single XAFS spectra (1.3 s per spectrum), which were subsequently cropped into individual files. The Q-XAFS data acquisition started one minute before Cr(III) injection in the batch vessel via a syringe outside the beamline hutch (Landrot *et al.*, 2010), and continued for four more minutes. After the first 5 minute scan was finished, another scan automatically started; this cycle repeated throughout the kinetic experiment, which lasted 72 minutes. Finally, a total of nine 5 minute Q-XAFS scans were collected per kinetic experiment, since the Q-XAFS scanning system reset for a dead time of 179 seconds (3 minutes) between each 5 minute scan. After cropping each scan to 226 single XAFS spectra, 116 single spectra collected around t=0 and t=4 minutes were averaged together to one XAFS spectrum, representing t=2 minutes of the reaction, since it is an average of spectra collected during the first four minutes. The same number of single XAFS spectra was averaged to get merged spectra representing t= 10 minutes, t= 30 minutes, and t= 60 minutes. The data were processed similarly for the duplicate experiments conducted at the Mn K edge. Additionally, single Q-XAFS spectra collected during the first minute of the Q-XAFS data collection (i.e. before chromium was injected in

the batch vessel) were averaged together to get one XAFS spectrum representing the unreacted $MnO_2$.

Data were analyzed with the SIXPACK/IFEFFIT program. Chi spectra of the samples and Cr standards, which were $k^2$ weighted, were used for least square fitting of the data within a k-range of 2-10.

## 3.4 Results and Discussion

### 3.4.1 Identification of Chromium Sorption Products on Hexagonal Birnessites

#### 3.4.1.1 Identification at the Molecular Level

A previous study employed bulk XAFS to identify chromium nucleation products forming on the surface of a variety of manganese oxides (Manceau and Charlet, 1992). Chromium precipitated as a γ-CrOOH phase on the surface of all the manganese oxides studied, which were reacted with chromium for less than two minutes. The Fourier transformed EXAFS of the reacted $MnO_2$ all featured chromium atom distances at 3.00 to 3.05 and 3.94 to 4.03 Å, which are characteristic features of a γ-CrOOH phase. Another study showed, using electron diffraction (ED) TEM, that γ-CrOOH formed on the surface of acid birnessite (Fendorf, 1992). The authors hypothesized that the precipitate was not directly complexed on the surface, but weakly sorbed in the interfacial region of the mineral. Otherwise, in case of direct bonding with manganese oxide, Cr(III) would oxidize to Cr(VI). The precipitate forms since an electrostatic term incorporated in the algebraic expression of the free energies of formation, due to the effect of the charged $MnO_2$ surface, decreases the solubility constant of the Cr(III) precipitation reaction. Consequently, the Cr(III) precipitate would form and spread over the mineral surface, which in turn would inhibit Cr(III)

oxidation by impeding electron transfer between Cr(III) and Mn(IV)/Mn(III), and decrease the amount of Cr(III) present in solution. However, if a γ-CrOOH phase is indeed forming during Cr(III) sorption on the surface of manganese oxide, one should compare the structure of $MnO_2$ and the surface precipitate together to predict how the precipitate will be distributed on the mineral. The chromium(III) nucleation product could either spread over the mineral surface in an unstrained fashion, in case of structural similarities between the precipitate and the surface, or continue to grow away from the mineral in case of structural incompatibilities. This intimate relationship between the structures of sorbent and nucleation product, that influences the spatial distribution of the surface precipitate, was observed in the case of Cr(III) sorbing on hydrous ferric oxide (HFO), which has an α-type structure (Charlet and Manceau, 1992). Chromium complexes on the mineral surface at low surface coverage in an α-CrOOH phase. As the precipitate grows and accumulates away from the mineral, the structure of the precipitate changes from α-CrOOH to γ-CrOOH. Another study showed that Cr(III) sorbed on colloidal silica resulted in the formation of a γ-CrOOH phase, which does not complex on the mineral surface (Fendorf, 1994). In this case, the structure of the silica surface is incompatible with the γ-CrOOH structure, which prevents the precipitate from growing away from the surface. Therefore, the identification of the Cr(III) precipitate structure forming on the manganese oxide can also give insights about the way it distributes on the mineral surface, i.e. away from it or spreading on it. Constraining the distribution of the surface precipitate is important for understanding the Cr(III) nucleation effect on Cr(III) oxidation by manganese oxide.

The percentage of Cr(VI) in the solid HMO, AB, and RSB pastes reacted with Cr(III) at different times is depicted in Figure 3.1 (a). The Bulk XAFS data shown in Figure 3.1 were taken from Cr-reacted $MnO_2$ wet pastes, thus correspond to chromium sorbed on the mineral, and not chromium in solution. It appears that Cr(VI) is sorbed on the three manganese oxides throughout the entire kinetic experiment, since all XANES spectra possess a distinctive pre-edge feature at 5993.5 eV characteristic of chromium(VI) (Peterson *et al.*, 1997). Therefore, our results differ from a former study that concluded that most Cr sorbed on acid birnessite is Cr(III), based on stoichiometric calculations of Cr(VI) and Mn(II) concentrations measured in solution, and assuming that Cr(VI) binds less at higher pH values (Fendorf and Zasoski, 1992). The fact that chromium(VI) is present on the surface of the manganese oxides complicates the task of fitting the Fourier transform EXAFS spectra of the reacted minerals shown in Figure 3.1 (b), since the triangular multiple scattering Cr(VI)-O-O-Cr(VI) contributes to the EXAFS spectra (Peterson *et al.*, 1994). Fitting the EXAFS spectra also means taking into account different chromium species that can be simultaneously present on the manganese oxide surface, including Cr(III) atoms singly sorbed on the mineral, Cr(III) precipitated in one or several phases, and, according to Figure 3.1 (a), Cr(VI). Lastly, the difficulty of interpreting the EXAFS data is magnified by the fact that the EXAFS technique cannot differentiate Cr-Cr and Cr-Mn bonds, since the Mn atom only has one more proton than the Cr atom. Therefore, the first Cr-metal shell (fitting parameters are reported in Table 3.1), could be either 1) a Cr-Cr bond 2) a Cr-Mn bond or 3) averaged values of a mixture of Cr-Cr and Cr-Mn bonds.

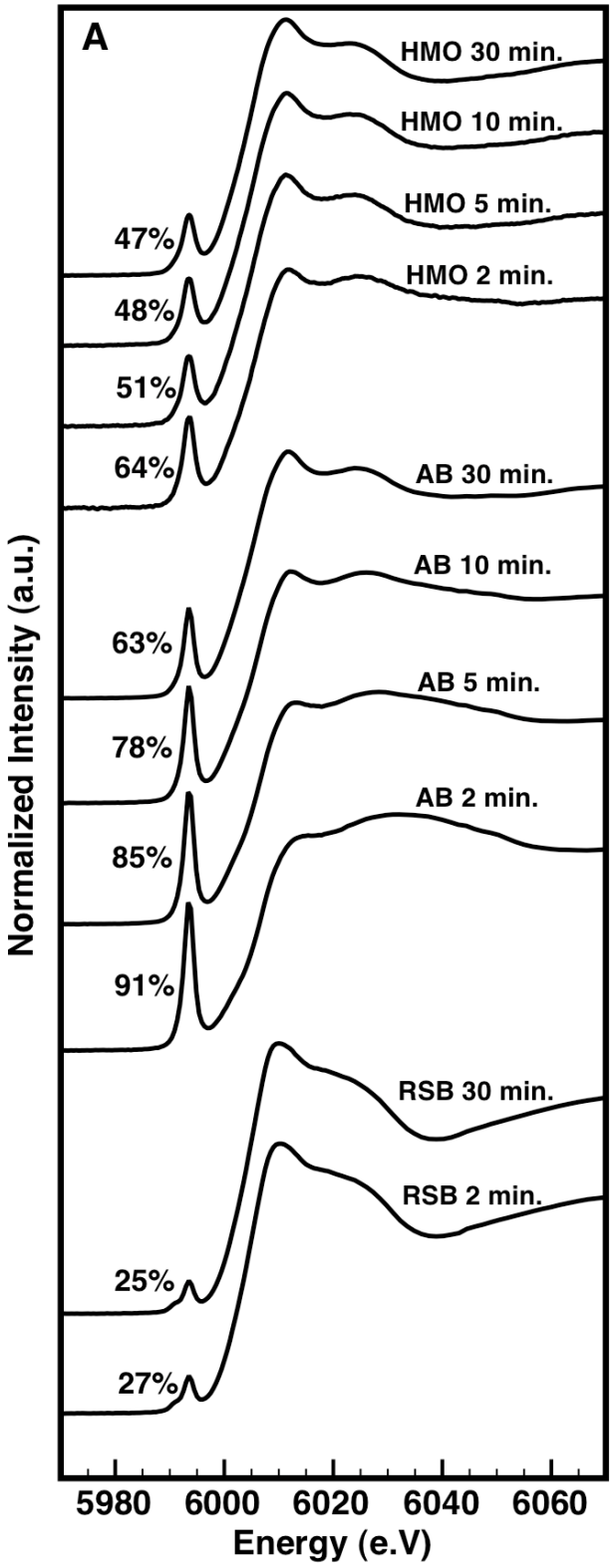
A
HMO 30 min.
HMO 10 min.
HMO 5 min.
HMO 2 min.
47%
48%
51%
64%
AB 30 min.
AB 10 min.
AB 5 min.
AB 2 min.
63%
78%
85%
91%
RSB 30 min.
RSB 2 min.
25%
27%
Normalized Intensity (a.u.)
5980
6000
6020
6040
6060
Energy (e.V)

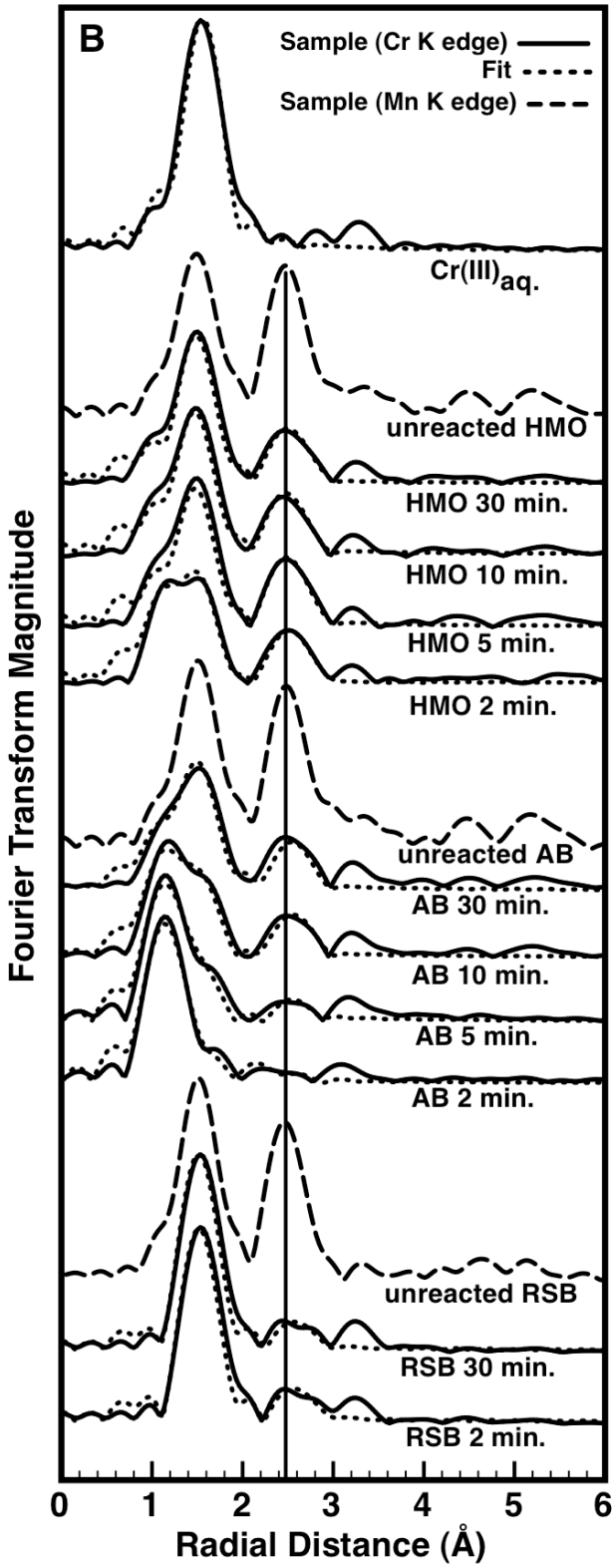
B
Sample (Cr K edge)
Fit
Sample (Mn K edge)
Cr(III)aq.
unreacted HMO
HMO 30 min.
HMO 10 min.
HMO 5 min.
HMO 2 min.
unreacted AB
AB 30 min.
AB 10 min.
AB 5 min.
AB 2 min.
unreacted RSB
RSB 30 min.
RSB 2 min.
Fourier Transform Magnitude
0
1
2
3
4
5
6
Radial Distance (Å)

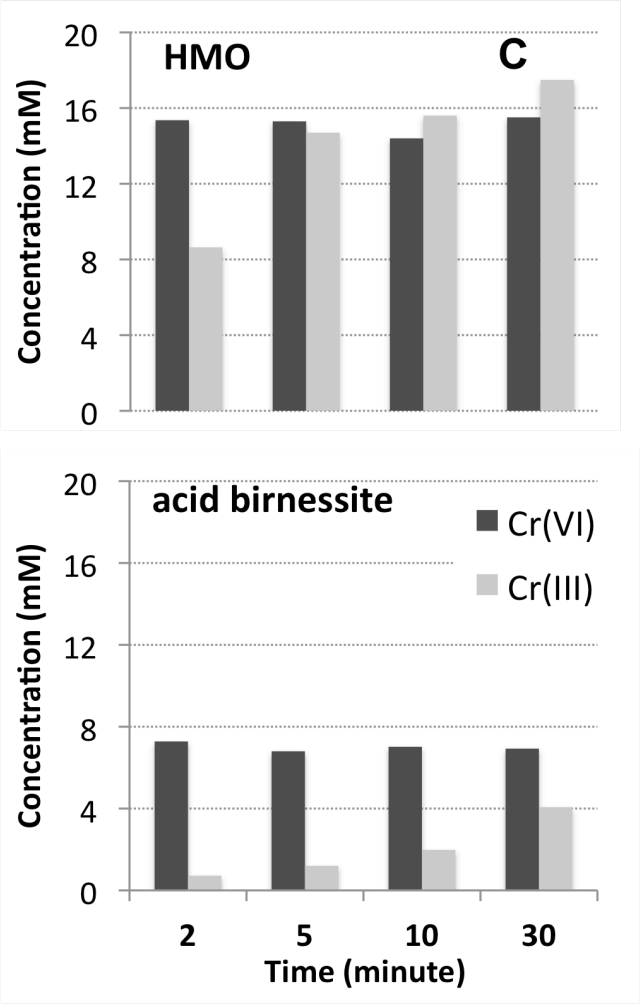


**Figure 3.1** (a) Quantity of Cr(VI) in % inferred from normalized XANES spectra of AB, HMO, and RSB at different reaction times (b) Fourier transforms of AB, HMO, and RSB at different reaction times and (c) Amount of Cr(III) and Cr(VI) sorbed on HMO and AB over time at pH 3. The quantities were measured from the percentage of Cr(III) and Cr(VI) sorbed on the surface of AB and HMO at 2, 5, 10, and 30 minutes (Figure 3.1 (a)) and the total amount of chromium sorbed on AB and HMO at pH 3 and at 2, 5, 10, and 30 minutes (Figure 3.2).

Most of chromium sorbed on AB at the beginning of the reaction (2 minutes) is chromium(VI) (Figure 3.1 a). Since more than 90% of the chromium is Cr(VI) for this sample, it is possible to consider that the Fourier transformed EXAFS spectrum of AB at t= 2 minutes depicted in Figure 3.1 (b) is only representative of chromate sorbed on AB. This seems reasonable since there is only one Cr(VI)-O shell at 1.61 Å in the Fourier transform; no other-shells are present at longer radial distances. Therefore, Cr(VI) is likely bound to the mineral surface in an outer sphere complex. As the reaction proceeds on the surface of AB, the increase in Cr(III) sorbed relative to Cr(VI) sorbed on the mineral is observed from the progressive shift of the first shell Cr-O from ~1.6 Å to ~2.0 Å.

The same trend can be seen on HMO, although the increase in Cr(III) over Cr(VI) content seems to be more rapid than AB (Figure 3.1 (b)). RSB reacted with Cr(III) does not seem to contain Cr(VI) as the two other manganese oxides during the time period of these experiments. The amount of chromate sorbed on RSB at 2 minutes is also similar to that at 30 minutes (Figure 3.1 (a)), and the Fourier transformed EXAFS spectra of RSB reacted at 2 minutes and 30 minutes appear to be identical (Figure 3.1 (b)).

The analysis of Cr(III), Cr(VI), and $Mn_{aqueous}$ concentrations in solution for the experiments conducted with HMO and AB (Figure 3.2), shows that 6 mM and 15 mM of Cr(VI) were present in solution when Cr(III) reacted for 30 minutes with AB, and HMO, respectively. In comparison, less than 2 mM of Cr(VI) is present in solution after 30 minutes of Cr(III) reacting with RSB (not shown). Therefore, RSB does not oxidize Cr(III) as much as HMO and AB. The highest amount of chromate

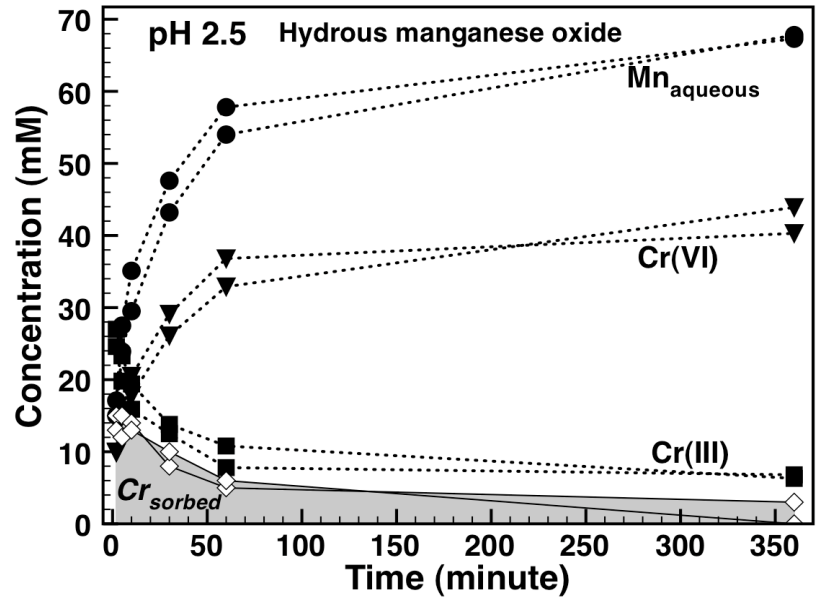
pH 2.5 Hydrous manganese oxide
Mn aqueous
Cr(VI)
Cr(III)
Cr sorbed
Concentration (mM)
Time (minute)
0
10
20
30
40
50
60
70
0
50
100
150
200
250
300
350

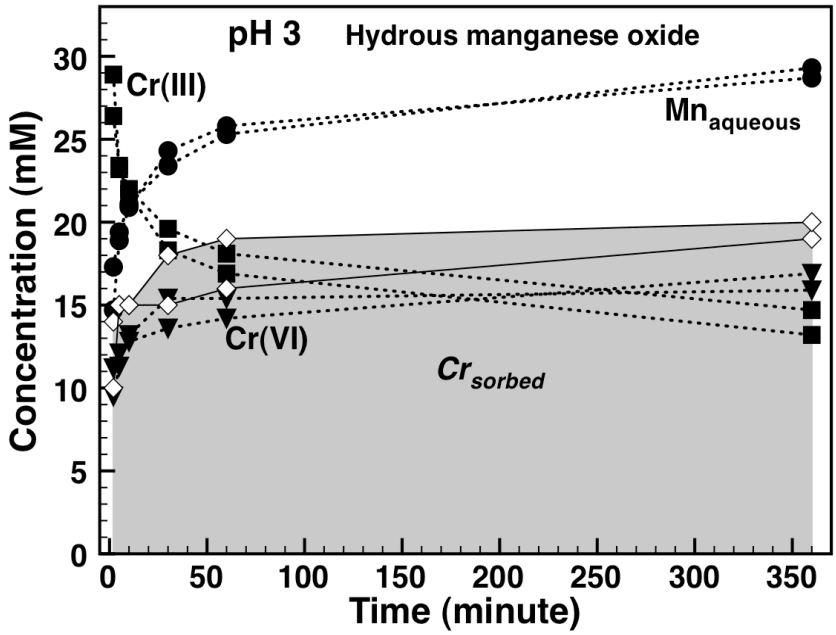
pH 3 Hydrous manganese oxide
Cr(III)
Mn aqueous
Cr(VI)
Cr sorbed
Concentration (mM)
Time (minute)
0
5
10
15
20
25
30
0
50
100
150
200
250
300
350

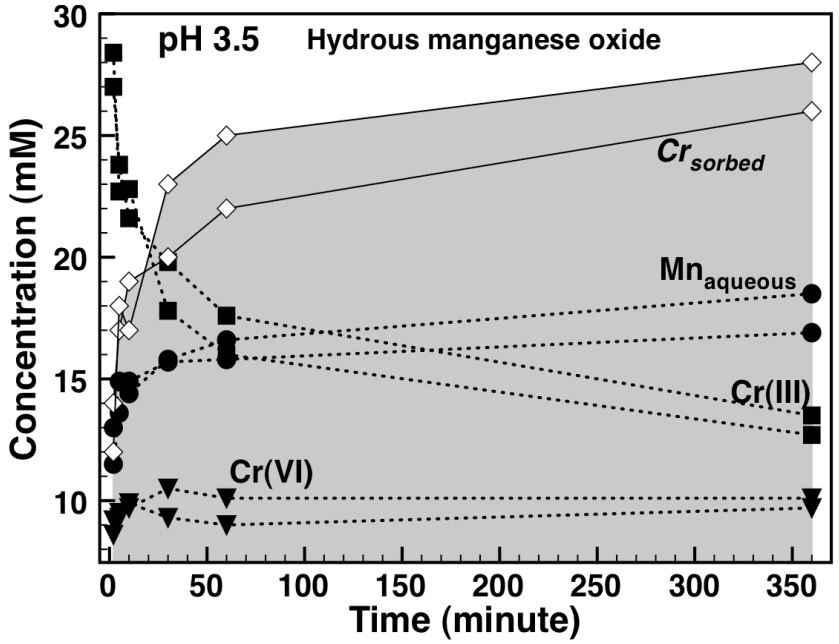
pH 3.5
Hydrous manganese oxide
Concentration (mM)
Time (minute)
Cr sorbed
Mn aqueous
Cr(III)
Cr(VI)

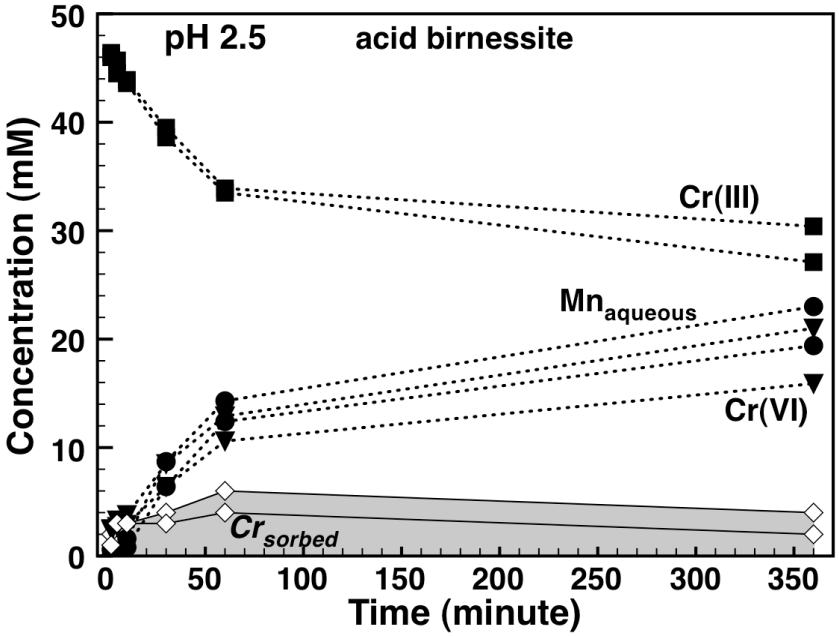
pH 2.5
acid birnessite
Concentration (mM)
Time (minute)
Cr(III)
Mn aqueous
Cr(VI)
Cr sorbed

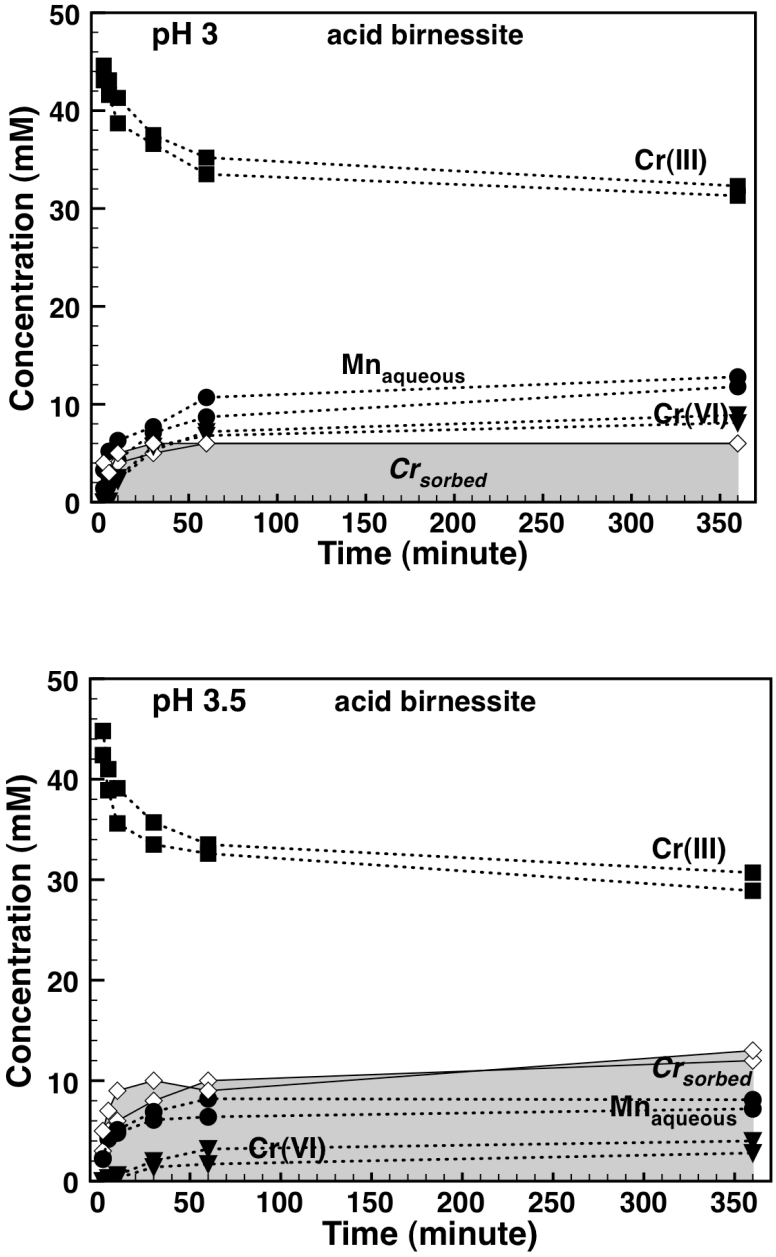


**Figure 3.2** Kinetics of Cr(III) oxidation on HMO and AB at (a) pH 2.5, (b) pH 3, and (c) pH 3.5, using a batch technique and reaction conditions of 50 mM Cr(III) and 20 g/L HMO and AB. The grey area represents the amount of Cr sorbed on $Mn(IV)O_2$, which was measured by subtracting the amount of Cr(III) and Cr(VI) measured in solution at 2, 5, 10, 30, 60, and 360 minutes from the amount of Cr(III) introduced at t=0 in the batch vessel (50 mM).

was produced with HMO, and the effect of pH on Cr(III) oxidation was significant: after Cr(III) reacted with HMO for 6 hours, 43 mM, 16 mM, and 10 mM of Cr(VI) was measured in solution at pH 2.5, 3 and 3.5, respectively. The amount of Cr(VI) sorbed on HMO was also higher compared to AB (Figure 3.1 (c)). Less chromate was sorbed on RSB compared to AB and HMO, since less than 5 mM of chromium was sorbed on RSB at pH 2.5, 3, and 3.5 (not shown). HMO sorbed more chromium (grey area in Figure 3.2) than AB, and the amount of chromium sorbed increased with pH. Therefore, HMO is the most reactive manganese oxide towards Cr sorption and Cr(III) oxidation. Previous studies have shown a wide variation in the Cr(III) oxidizing capacity of several manganese oxides that had different oxidation states (Mn(III) and/or Mn(IV)), and structure types (tunnel structure versus layer structure) (Weaver *et al.*, 2003; Kim *et al.*, 1998; Kim *et al.*, 2002). Our results suggest that the capacity of $MnO_2$ to oxidize Cr(III) can also vary between minerals having similar structure and oxidation states. Among the three manganese oxides studied, HMO is not only the strongest Cr(III) oxidizer, but apparently also the most poorly crystalline mineral, based on XRD and SEM data (XRD patterns of HMO, AB, and RSB in Figure 1.2), and has the highest surface area. The least powerful oxidizer is RSB, which has the lowest surface area and is the most crystalline mineral, based on XRD patterns. Therefore, the variation in Cr(III) capacity among the three manganese oxides in this study is related to the degree of crystallinity of the minerals and the number of available surface sites. Since our goal is to measure the kinetics of surface precipitation occurring on the manganese oxides and compare them with the rates of Cr(III) oxidation simultaneously occurring on the mineral surface, we conducted our

Q-XAFS in situ experiments only with AB and HMO (section 3.2), since no Cr(III) oxidation occurs with RSB between 2 minutes and 30 minutes.

Although the Fourier transformed EXAFS of AB reacted with Cr(III) for 2 minutes features only a Cr-O shell because Cr(VI) is sorbed on AB in an outer sphere complex mechanism, a second peak appears at t=5 minutes at about 2.87 ±0.04 Å, whose amplitude grows with time (Figure 3.1 (b)). One study similarly found a radial distance at 2.90 Å for the second shell of chromium sorbed on sodium birnessite (Charlet and Manceau, 1992). This second coordination sphere was assigned to a Cr-Mn(IV) shell for three reasons. Firstly, a Cr-Cr(III) shell would have resulted in a greater radial distance, at about 3.00 Å. Also, although Cr-Cr(VI) would result in a smaller radial distance than Cr-Cr(III), no significant amount of Cr(VI) was present in the sample. Finally, the radial distance of the first Mn-Mn shell of the unreacted sodium birnessite was also measured at 2.90 Å, which suggested similarities in local structure around Mn and Cr in the mineral. Similarly in our study, the second shell of the Fourier transformed EXAFS of AB reacted with Cr(III) for 5 minutes depicted in Figure 3.1 (b) can be assigned to a Cr-Mn(IV) shell. Indeed, although Cr(VI) is 85% of the chromium sorbed on AB at t=5 minutes, Cr(VI) should not contribute to the second shell, assuming that the Cr(VI) sorption mechanism does not change between t=2 minutes and the rest of the reaction. Additionally, the radial distance of the first Mn-Mn shell of unreacted AB is 2.90 Å, which suggests that Cr is sorbed on the mineral in an inner-sphere complex mechanism, and both Mn and Cr share the same structural environment. Lastly, the low coordination number of the Cr-Mn(IV) shell of AB at t=5 min suggests that Cr is sorbed on the edge sites of AB

**Table 3.1** Fitting parameters of Fourier transforms depicted in Figure 3.1 (b) and Figure 3.3 (b)

| | | | | Cr(VI)-O | | | Cr(III)-O | | | Cr(VI)-O M.S. | | | Cr-Cr/Cr-Mn | | |
|---|---|---|---|---|---|---|---|---|---|---|---|---|---|---|---|
| pH | $MnO_2$ | time | $\Delta E_0$ | CN | R(Å) | $\sigma^2$ | $CN^{(A)}$ | R(Å) | $\sigma^2$ | $CN^{(B)}$ | $R(Å)^{(C)}$ | $\sigma^{2(D)}$ | CN | R(Å) | $\sigma^2$ |
| 2.5 | HMO | 2 m | -6.2 ±3.1 | 2.9 ±0.2 | 1.60 ±0.01 | 0.002 ±0.001 | 1.6 | 1.98 ±0.02 | 0.006 ±0.005 | 8.8 | 2.92 | 0.004 | | | |
| 2.5 | HMO | 5 m | -4.4 ±4.5 | 2.2 ±0.4 | 1.62 ±0.01 | 0.002 ±0.001 | 2.7 | 1.96 ±0.02 | 0.003 ±0.003 | 6.6 | 2.94 | 0.003 | 1.0 ±0.6 | 2.89 ±0.03 | 0.003 ±0.004 |
| 2.5 | HMO | 10 m | 0.7 ±6.9 | 2.0 ±0.1 | 1.63 ±0.02 | 0.003 ±0.003 | 2.9 | 1.98 ±0.03 | 0.003 ±0.003 | 6.1 | 2.95 | 0.005 | 1.6 ±1.4 | 2.92 ±0.03 | 0.004 ±0.004 |
| 2.5 | HMO | 30 m | 0.8 ±4.1 | 1.8 ±0.3 | 1.63 ±0.01 | 0.002 ±0.002 | 3.3 | 1.98 ±0.02 | 0.004 ±0.003 | 5.3 | 2.96 | 0.004 | 1.4 ±0.8 | 2.93 ±0.03 | 0.003 ±0.004 |
| 3 | HMO | 2 m | -1.2 ±5.1 | 2.0 ±0.4 | 1.62 ±0.01 | 0.002 ±0.002 | 3.0 | 1.97 ±0.02 | 0.005 ±0.004 | 6.0 | 2.94 | 0.004 | 1.2 ±0.7 | 2.92 ±0.03 | 0.003 ±0.004 |
| 3 | HMO | 5 m | -1.2 ±2.5 | 1.7 ±0.3 | 1.63 ±0.01 | 0.003 ±0.002 | 3.4 | 1.97 ± 0.01 | 0.002 ±0.002 | 5.2 | 2.97 | 0.006 | 1.2 ±0.5 | 2.92 ±0.02 | 0.002 ±0.002 |
| 3 | HMO | 10 m | -0.2 ±3.3 | 1.6 ±0.3 | 1.62 ±0.01 | 0.003 ±0.003 | 3.7 | 1.97 ±0.02 | 0.003 ±0.002 | 4.7 | 2.95 | 0.005 | 1.5 ±0.8 | 2.92 ±0.02 | 0.003 ±0.003 |
| 3 | HMO | 30 m | 0.7 ±2.5 | 1.4 ±0.3 | 1.62 ±0.01 | 0.003 ±0.003 | 3.9 | 1.98 ± 0.01 | 0.003 ±0.001 | 4.2 | 2.95 | 0.006 | 1.4 ±0.7 | 2.94 ± 0.02 | 0.004 ±0.004 |
| 3.5 | HMO | 2 m | 0.4 ±2.6 | 1.6 ±0.3 | 1.63 ±0.01 | 0.003 ±0.002 | 3.6 | 1.98 ±0.01 | 0.003 ±0.002 | 4.7 | 2.95 | 0.005 | 1.5 ±0.6 | 2.93 ±0.02 | 0.003 ±0.003 |
| 3.5 | HMO | 5 m | 0.4 ±2.1 | 1.4 ±0.3 | 1.63 ±0.01 | 0.004 ±0.003 | 4.1 | 1.98 ± 0.01 | 0.002 ±0.001 | 4.1 | 2.96 | 0.008 | 1.3 ±0.6 | 2.93 ±0.01 | 0.003 ±0.003 |
| 3.5 | HMO | 10 m | 0.5 ±2.6 | 1.3 ±0.3 | 1.62 ±0.01 | 0.004 ±0.004 | 4.1 | 1.98 ± 0.01 | 0.003 ±0.001 | 3.8 | 2.95 | 0.008 | 1.5 ± 0.8 | 2.93 ± 0.02 | 0.004 ±0.004 |
| 3.5 | HMO | 30 m | 0.3 ±2.0 | 1.3 ±0.3 | 1.64 ± 0.01 | 0.006 ±0.004 | 4.0 | 1.98 ± 0.01 | 0.002 ±0.002 | 3.9 | 2.97 | 0.012 | 1.2 ± 0.6 | 2.94 ± 0.01 | 0.003 ±0.003 |
| 3 | AB | 2 m | -5.8 ±3.0 | 3.3 ±0.3 | 1.61 ±0.01 | 0.003 ±0.001 | 1.1 | 2.01 ±0.04 | 0.007 ±0.007 | 9.8 | 2.92 | 0.006 | | | |
| 3 | AB | 5 m | -7.2 ±5.1 | 2.8 ±0.4 | 1.60 ±0.01 | 0.002 ±0.001 | 1.9 | 1.97 ±0.02 | 0.006 ±0.006 | 8.3 | 2.90 | 0.005 | 0.5 ±0.2 | 2.87 ±0.04 | 0.003 ±0.005 |
| 3 | AB | 10 m | -4.5 ±5.6 | 2.3 ±0.5 | 1.61 ±0.01 | 0.002 ±0.002 | 2.5 | 1.96 ±0.02 | 0.005 ±0.006 | 6.9 | 2.93 | 0.004 | 1.0 ±0.9 | 2.89 ±0.04 | 0.003 ±0.006 |
| 3 | AB | 30 m | -1.3 ±5.2 | 1.7 ±0.4 | 1.62 ± 0.01 | 0.002 ±0.002 | 3.5 | 1.97 ±0.02 | 0.004 ±0.003 | 5.0 | 2.95 | 0.004 | 1.4 ±1.0 | 2.92 ±0.04 | 0.004 ±0.005 |
| 3 | RSB | 2 m | 1.7 ±2.5 | 1.0 ±0.3 | 1.62 ±0.03 | 0.008 ±0.007 | 4.6 | 1.98 ± 0.01 | 0.002 ±0.001 | 2.9 | 2.94 | 0.016 | 1.3 ±1.0 | 2.98 ±0.03 | 0.008 ±0.009 |
| 3 | RSB | 30 m | 2.5 ±2.3 | 0.9 ±0.3 | 1.60 ±0.03 | 0.007 ±0.006 | 4.7 | 1.99 ± 0.01 | 0.002 ±0.001 | 2.7 | 2.90 | 0.014 | 0.8 ±0.8 | 2.97 ±0.03 | 0.005 ±0.007 |

*(A)* $CN_{CrIII-O}$ defined as $CN_{CrIII-O} = (1-(CN_{CrVI-O}/4)) \times 6$

*(B)* $CN_{multiple\ scattering}$ defined as $CN_{m.s.} = 3 \times CN_{CrVI-O}$

*(C)* $R_{multiple\ scattering}$ defined as $R_{m.s.} = 1.822 * R_{CrVI-O}$ *(see text)*

*(D)* $\sigma^2_{multiple\ scattering}$ defined as $\sigma^2_{m.s.} = 2 * \sigma^2_{CrVI-O}$

rather than on the vacancy sites, since the latter case would imply that chromium is surrounded by six manganese atoms.

Similarities in percentage of Cr(VI) on the surface, Fourier transformed EXAFS, and fitting parameters (Table 3.1) are illustrated for the experiments involving AB at pH 3 (Figure 3.1) and HMO at pH 2.5 (Figure 3.3). Therefore, the same conclusions are made: the Fourier transformed EXAFS of reacted HMO at pH 2.5 and t=2 minutes is mostly representative of Cr(VI) sorbed on the mineral in an outer-sphere complex; at time t=5 minutes, Cr(III) sorbs on HMO in an inner-sphere mechanism and shares the same structural environment than Mn atoms in HMO, since both reacted and unreacted HMO possess a first metal-metal shell at ≈2.90 Å. The low coordination number of the Cr-Mn(IV) shell also suggests that Cr is sorbed on the edge sites of HMO rather than on the vacancy sites. The peak at 2.90 Å increases in amplitude and slightly in radial distance with reaction time. Also, experiments performed at higher pH resulted in slightly higher radial distance for the Cr-metal shell. Values higher than 2.90 Å could mean that the shell is not purely Cr-Mn(IV), but a mixture of Cr-Mn and Cr-Cr shells. Since the amount of Cr(III) sorbed on the surface increases with time (Figure 3.1 (c)), the increase is more significant at higher pH values (Figure 3.3 (c)), and the radial distance of the Cr-metal shell increases and gets closer to the radial distance of two chromium atoms found in Cr(III) nucleation products at about 2.98- 3.01 Å, as chromium(III) progressively nucleates on AB and HMO. The increase in the radial distance of the shell is not due to the presence of Mn(III) in the mineral due to Cr(III) oxidation, otherwise, R distance and amplitude of the Cr-metal shell would have grown faster at lower pH values when Cr(III) oxidizes

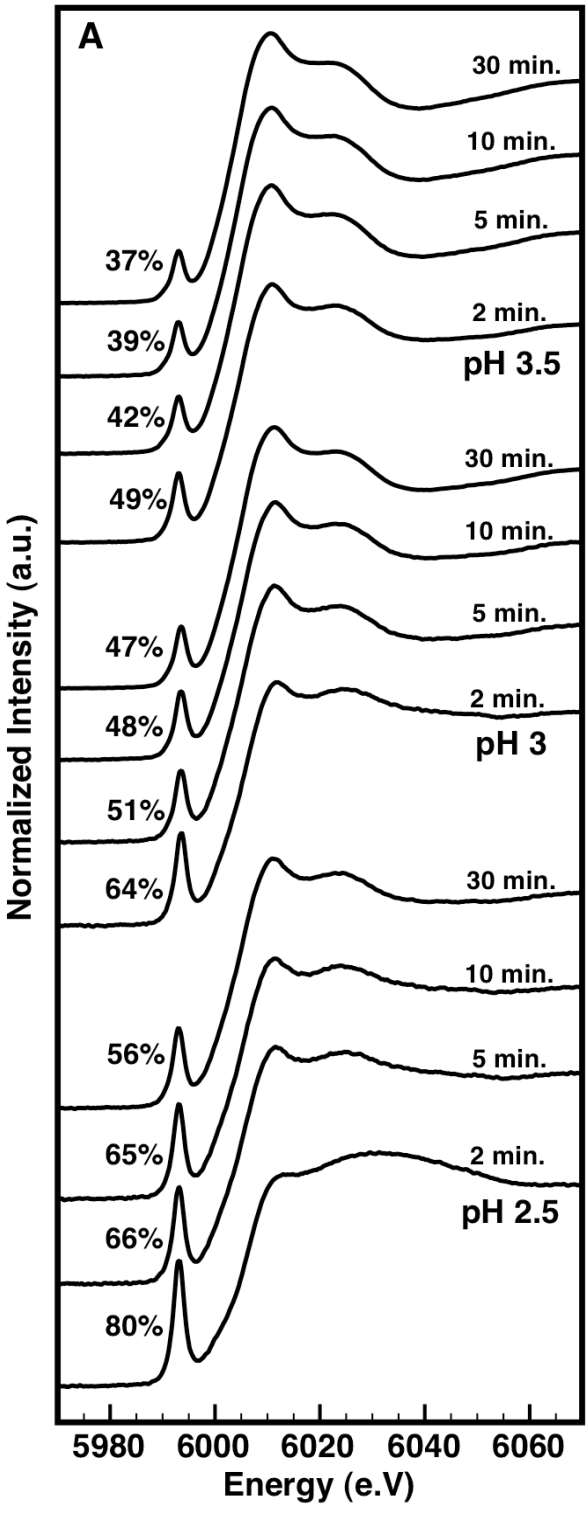
A
30 min.
10 min.
5 min.
37%
2 min.
39%
pH 3.5
42%
30 min.
49%
10 min.
5 min.
47%
2 min.
48%
pH 3
51%
64%
30 min.
10 min.
56%
5 min.
65%
2 min.
pH 2.5
66%
80%
Normalized Intensity (a.u.)
5980
6000
6020
6040
6060
Energy (e.V)

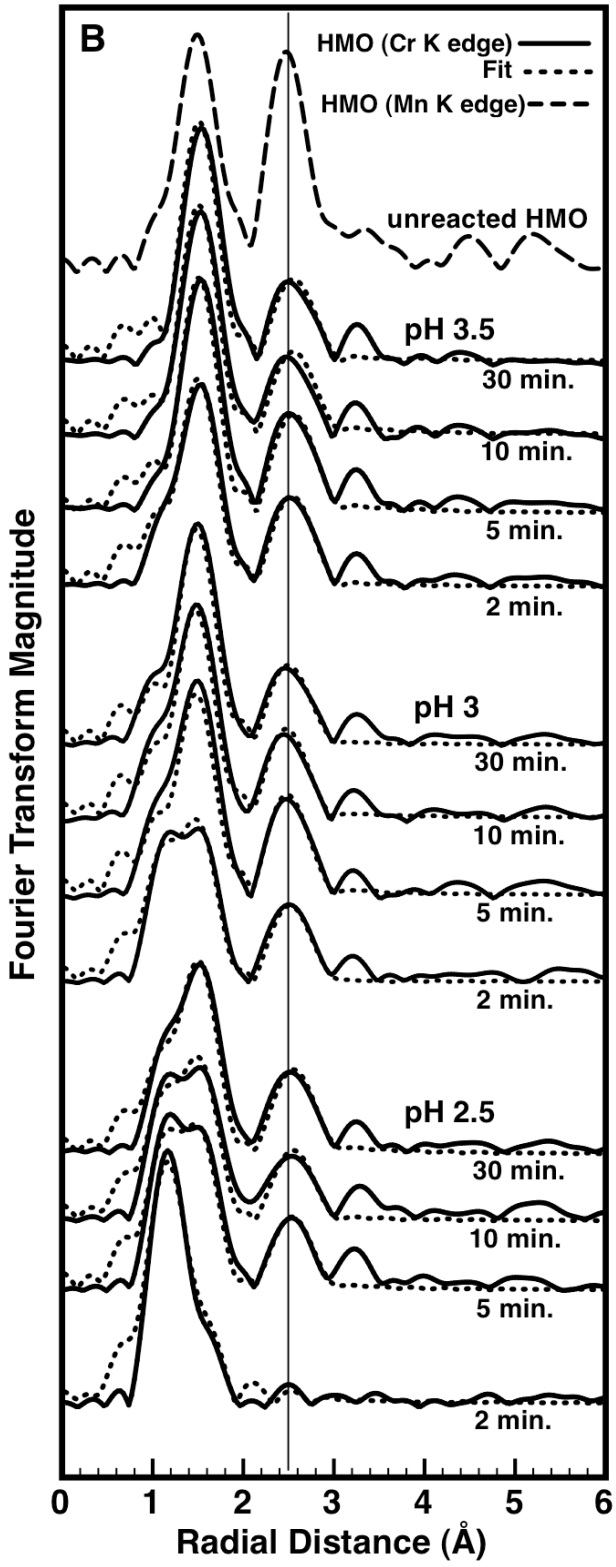
B
HMO (Cr K edge)
Fit
HMO (Mn K edge)
unreacted HMO
pH 3.5
30 min.
10 min.
5 min.
2 min.
pH 3
30 min.
10 min.
5 min.
2 min.
pH 2.5
30 min.
10 min.
5 min.
2 min.
Fourier Transform Magnitude
0
1
2
3
4
5
6
Radial Distance (Å)

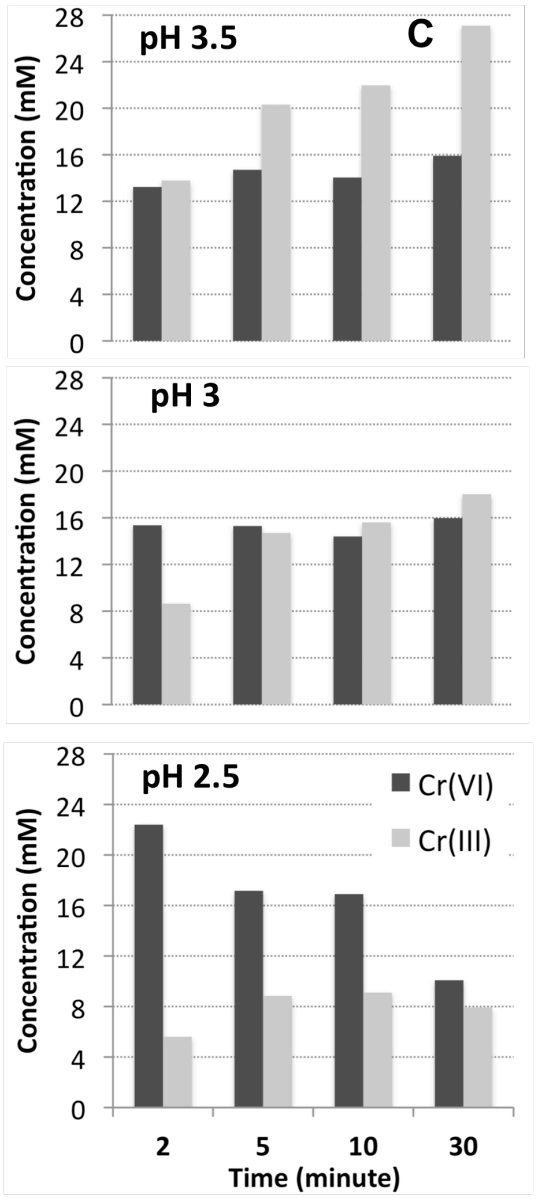


**Figure 3.3** (a) Quantity of Cr(VI) in % inferred from normalized XANES spectra of HMO at different reaction times and at pH 2.5, 3, and 3.5 (b) Fourier transforms of HMO at different reaction times and at pH 2.5, 3, and 3.5 and (c) Amount of Cr(III) and Cr(VI) sorbed on HMO over time and at pH 2.5, 3, and 3.5. The quantities were measured from the percentage of Cr(III) and Cr(VI) sorbed on the surface of HMO at 2, 5, 10, and 30 minutes (Figure 3.3 (a)) and the total amount of chromium sorbed on HMO at pH 2.5, 3, 3.5, and at 2, 5, 10, and 30 minutes (Figure 3.2).

the most. (the opposite trend is seen in our results). Additionally, the radial distance of the Cr-metal shell for RSB is around 3.0 Å throughout the experiment (Figure 3.1 (b), and Table 3.1), although not much Cr(III) oxidation occurred in the system, which suggests that Cr(III) nucleation might have formed on the mineral surface at the early stage of the experiment. It has been reported that Cr(III) precipitates in a γ-CrOOH phase on the surface of several manganese oxides (Manceau and Charlet, 1992, Fendorf *et al.*, 1992). This precipitate is characterized by two Cr-Cr shells at 3.00 to 3.05 and 3.94 to 4.03 Å, and is similar to the phase forming when Cr precipitates in bulk solution. Grimaldiite, also called α-CrOOH, can form on iron oxides (Charlet and Manceau 1992; Hansel *et al.*, 2002) but has never been detected on manganese oxides this far. This Cr(III) precipitate is characterized by two Cr-Cr shells at 3.00 to 3.05 and 3.40 to 3.45 Å. Therefore, if a γ-CrOOH had formed on the surface of AB, HMO, and RSB, one would see a peak at around 4 Å in the Fourier transformed EXAFS depicted in Figure 3.1 (b) and Figure 3.3 (b). None of the data features a peak at such radial distance. However, one peak is present in all spectra at ≈3.55 Å, and the amplitude does not seem to vary significantly during the kinetic experiments performed with RSB, AB, and HMO. This peak was not considered in our fits since it is also present in the Fourier transformed EXAFS of the aqueous Cr(III) standard (Figure 3.1 (b)), and could be attributed to either Cr(III) polymers present in solution that sorbed on the minerals (Rotzinger, 1986) or Cr(III) linear multiple scatterings. Therefore, our results depicted in Figure 3.1 (b) and 3.3 (b) suggest that no γ-CrOOH is present on the surface of HMO, AB, and RSB at any reaction time, because of the lack of a peak around 4.00 Å. The presence of an α-CrOOH is questionable since no peak clearly

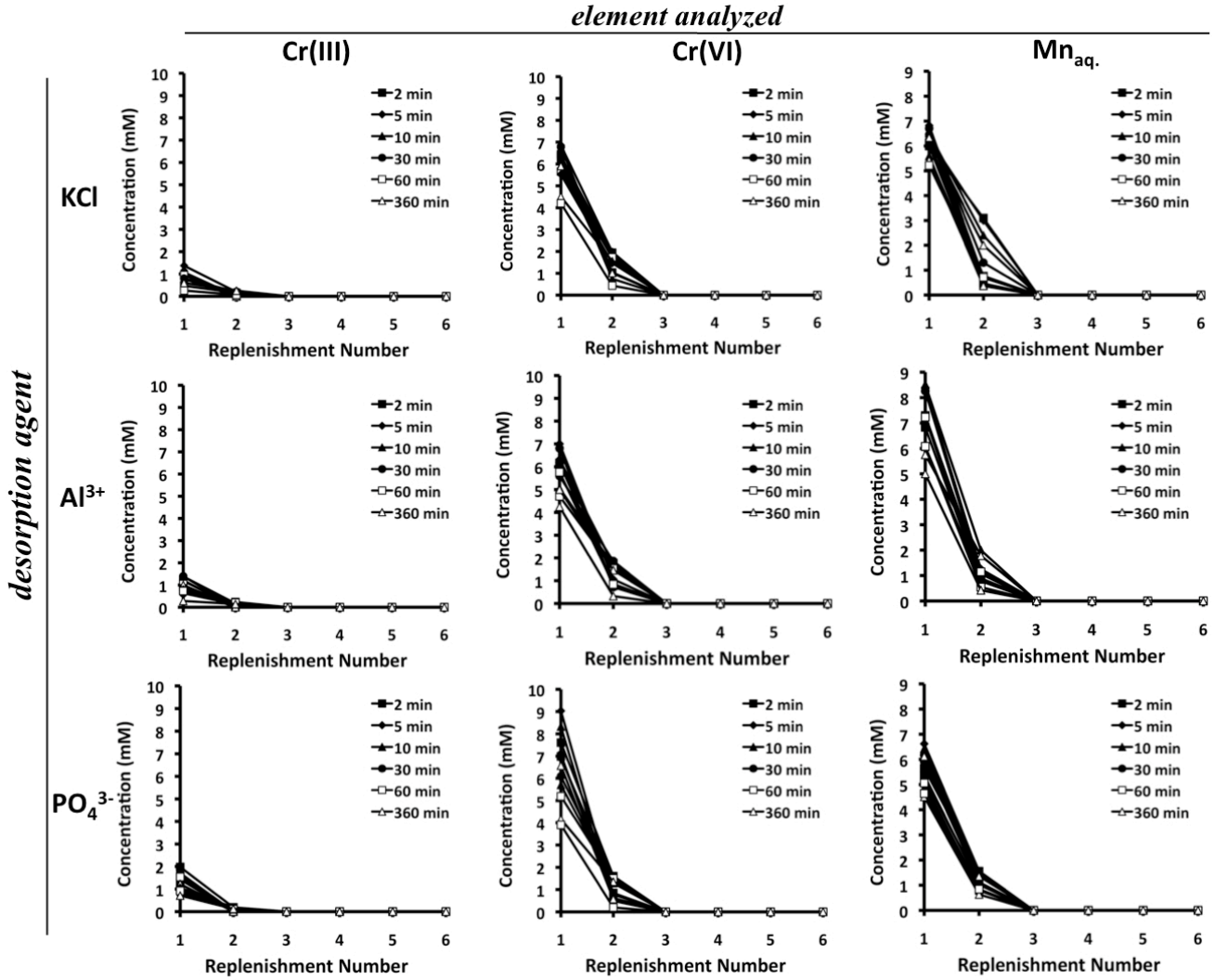


**Hydrous Manganese Oxide, pH 2.5**

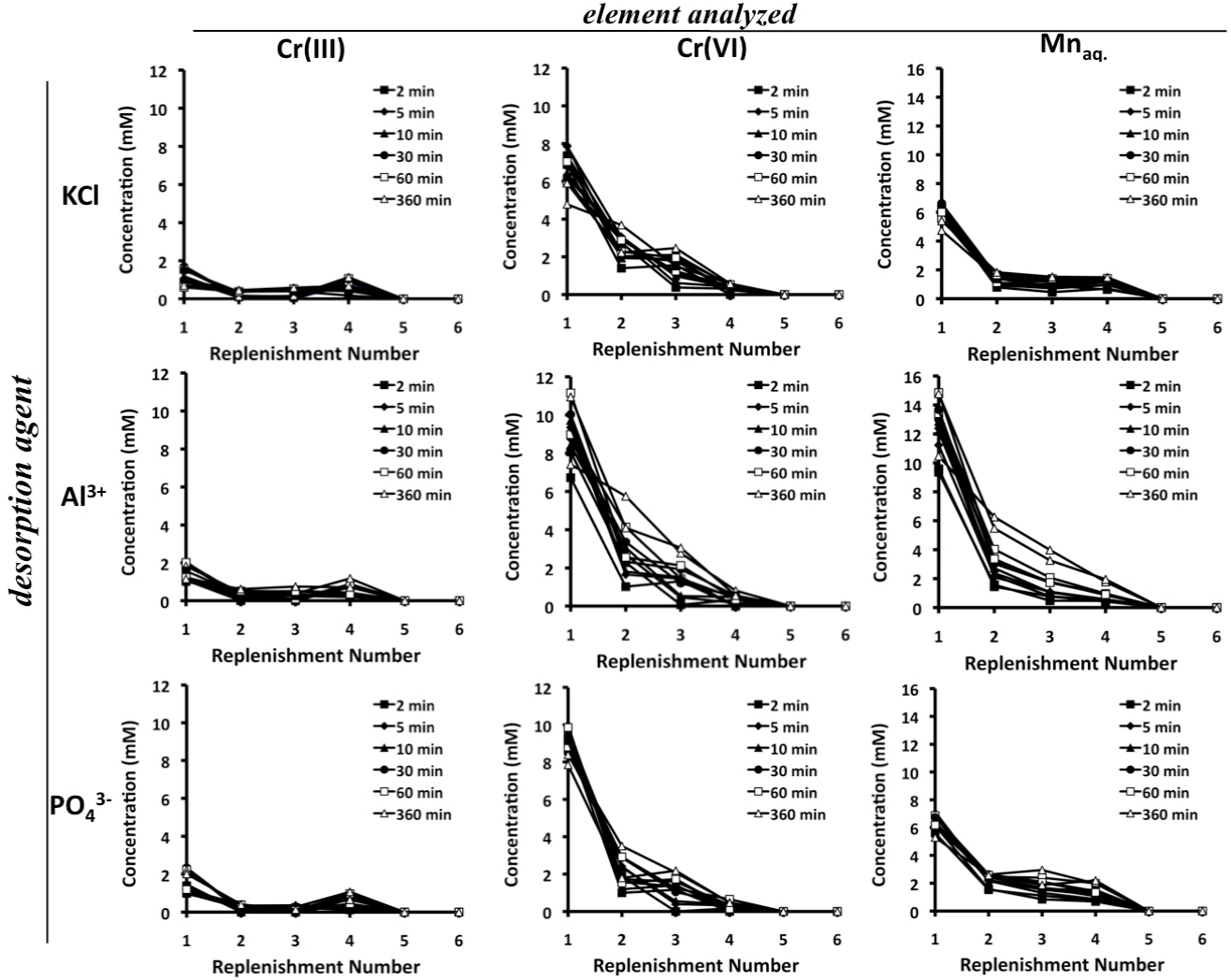
element analyzed
Cr(III)
Cr(VI)
Mn$_{aq.}$
desorption agent
KCl
Al$^{3+}$
PO$_4^{3-}$
Concentration (mM)
Replenishment Number
2 min
5 min
10 min
30 min
60 min
360 min
Hydrous Manganese Oxide, pH 3

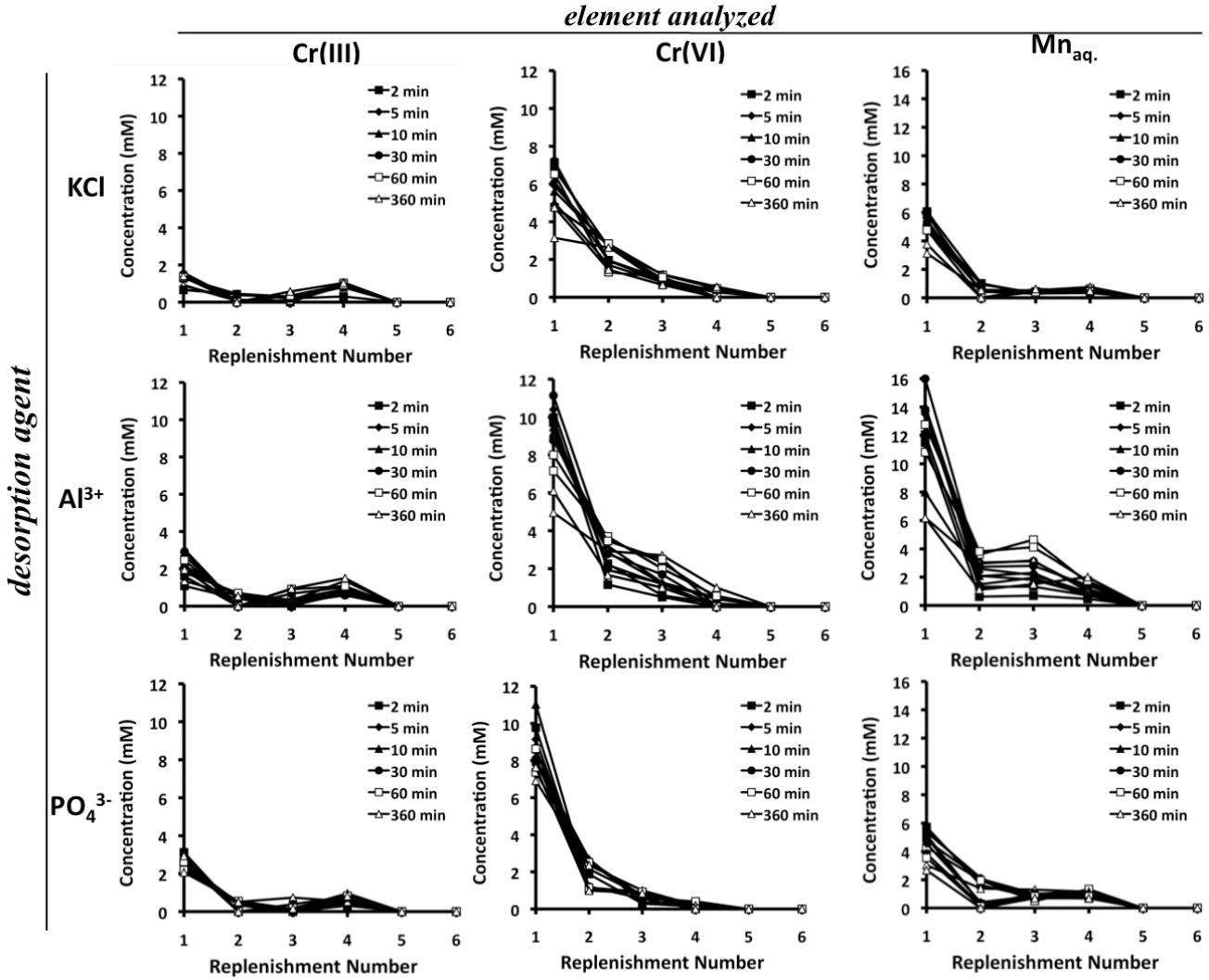
element analyzed
Cr(III)
Cr(VI)
Mn$_{aq.}$
desorption agent
KCl
Al$^{3+}$
PO$_4^{3-}$
Concentration (mM)
Replenishment Number
2 min
5 min
10 min
30 min
60 min
360 min
Hydrous Manganese Oxide, pH 3.5

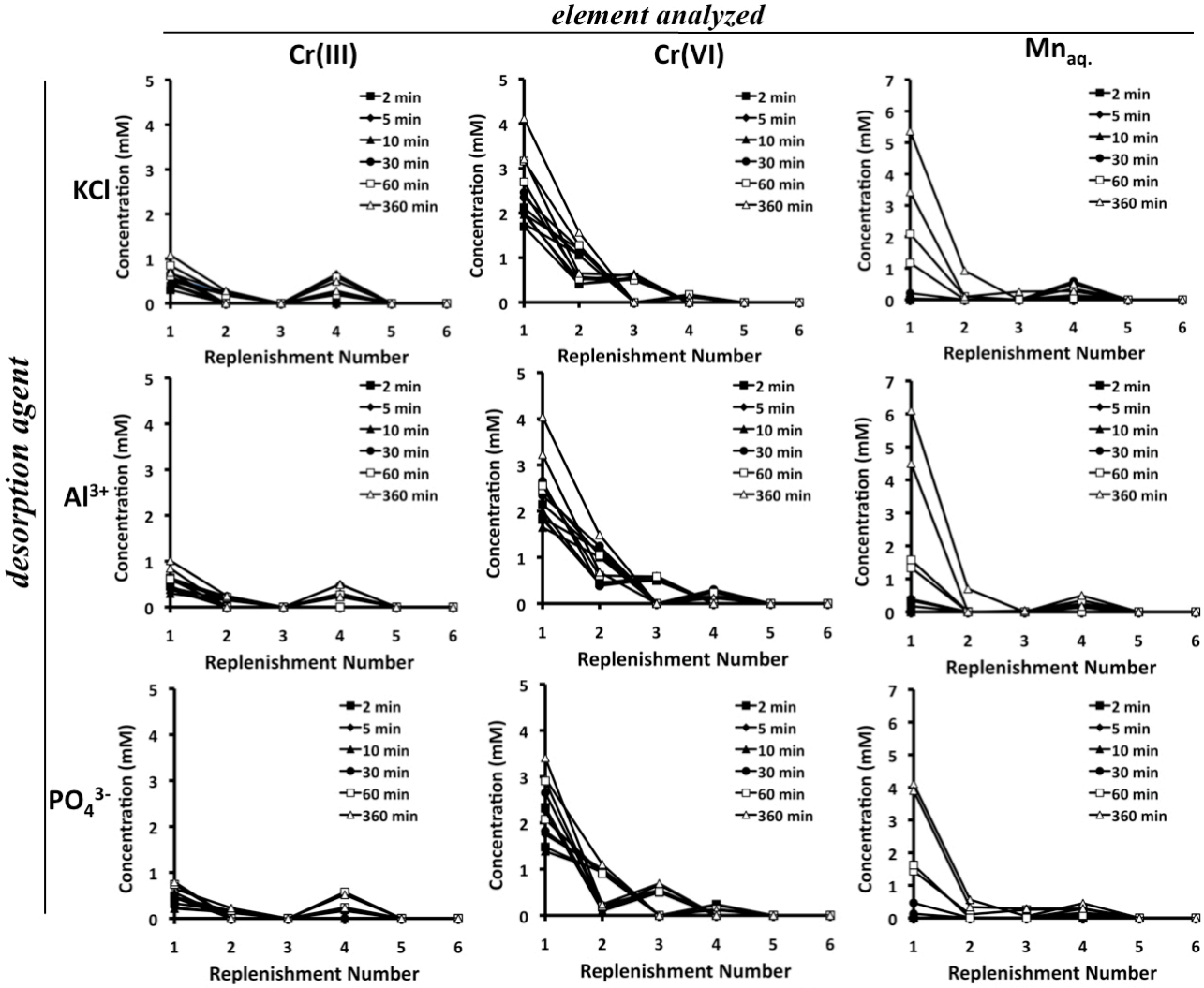
element analyzed
Cr(III)
Cr(VI)
Mn$_{aq.}$
desorption agent
KCl
Al$^{3+}$
PO$_4^{3-}$
Concentration (mM)
Replenishment Number
2 min
5 min
10 min
30 min
60 min
360 min
Acid Birnessite, pH 2.5

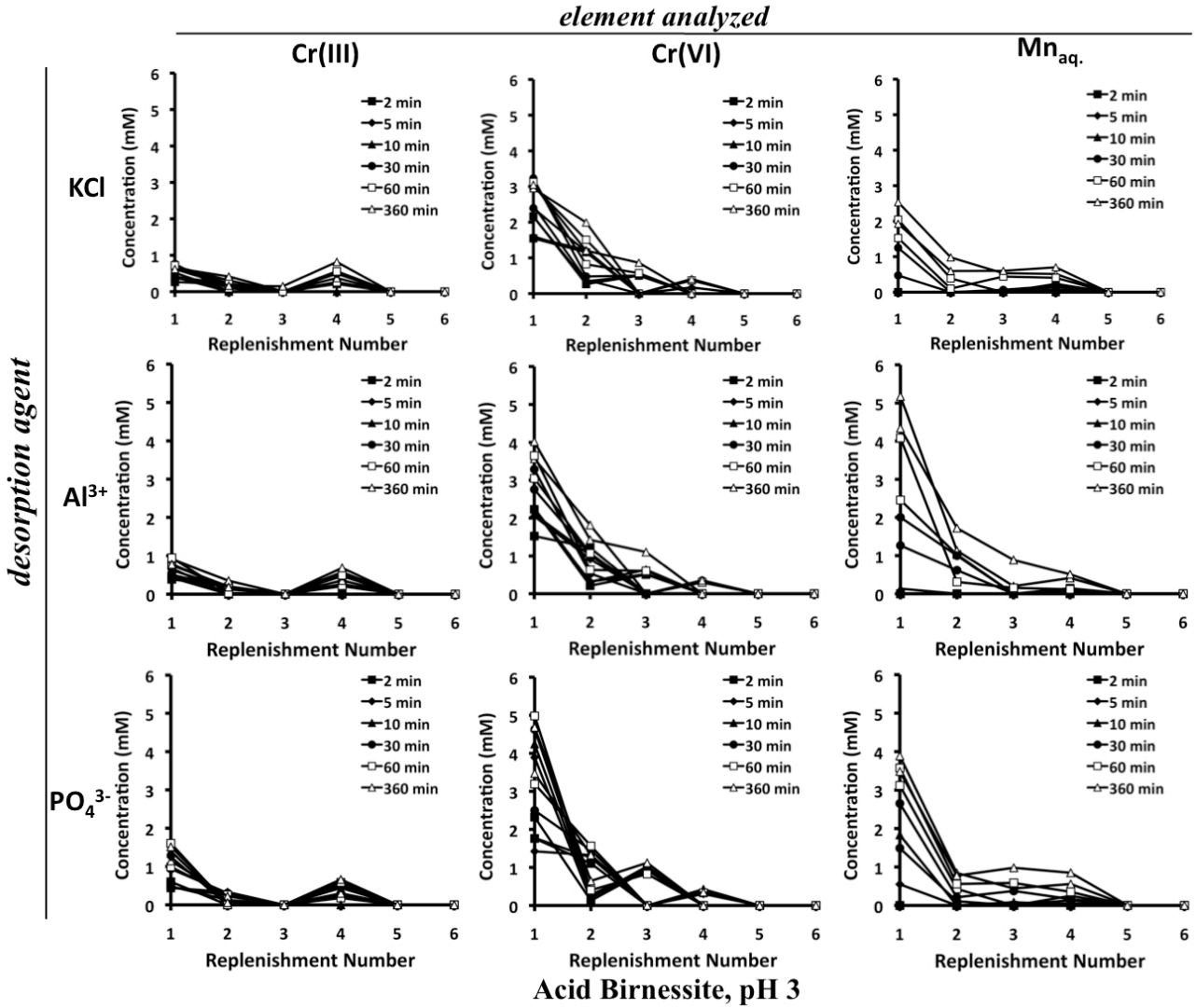
element analyzed
Cr(III)
Cr(VI)
Mn aq.
desorption agent
KCl
Al3+
PO4 3-
Concentration (mM)
Replenishment Number
2 min
5 min
10 min
30 min
60 min
360 min
Acid Birnessite, pH 3

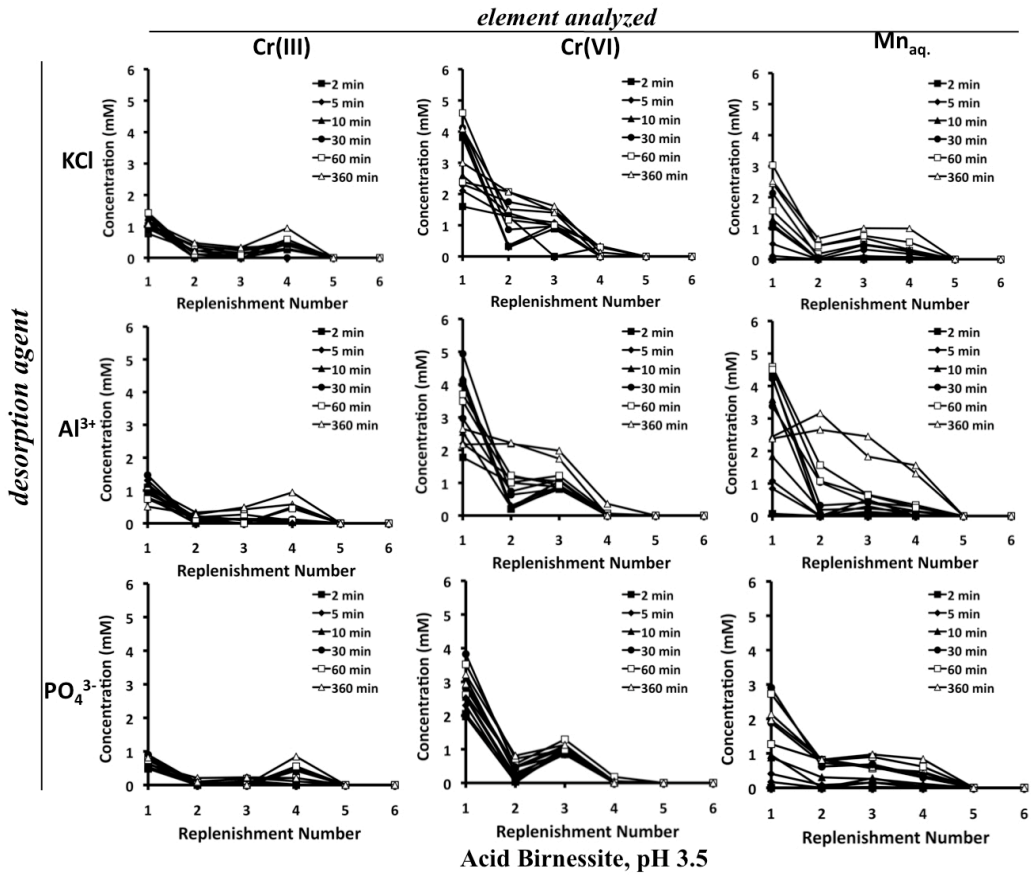


**Figure 3.4** Amount of Cr(III), Cr(VI), and Mn(II) desorbed by replenishments after Cr(III) was reacted with HMO and AB for 2, 5, 10, 30, 60, and 360 minutes, with 50m M of KCl, $Al^{3+}$ , and $PO_4^{3-}$ as the desorption agent, at pH 2.5, 3, and 3.5

appears around 3.40 to 3.45 Å in all Fourier transformed EXAFS spectra. However, one could hypothesize that the distinct peak at 3.55 Å masks the amplitude of the peak at 3.45 Å, in case α-CrOOH precipitation was occurring.

Replenishment experiments were conducted to complement our bulk XAFS results, which suggest that Cr(VI) is sorbed on AB and HMO in a outer-sphere complex at least during the first two minutes of the reaction. The results for the experiments with HMO and AB reacted with Cr(III) for 2, 5, 10, 30, 60, and 360 minutes, and using KCl, $Al^{3+}$, or $PO_4^{3-}$ as the desorption agent, are depicted in Figure 3.4. The choice of aluminum as the desorption agent was based on the fact that this element can compete with Cr(III) for sorption sites on $Mn(IV)O_2$. Indeed, it has been shown that $Al^{3+}$ can significantly sorb on $Mn(IV)O_2$ when Cr(III) is also present in solution, decreasing the amount of Cr(VI) produced, which is not the case for other metals like La(III), Co(II), or Mn(II) that do not compete with Cr(III) for $Mn(IV)O_2$ sorption sites (Fendorf, 1992). Figure 3.4 shows that Cr(VI) desorbs similarly from HMO and AB reacted with Cr(III) for different time periods at pH 2.5, 3, and 3.5, when $Al^{3+}$ is used as the desorption agent, suggesting that the sorption mechanisms of Cr(VI) do not change throughout the reaction between Cr(III) and $Mn(IV)O_2$. The same results were observed for the experiments performed with other desorption agents, i.e. 50 mM of KCl (the electrolyte solution) or 50 mM of $PO_4^{3-}$, which can desorb some metals via a ligand exchange mechanism (Masue *et al.,* 2007). Therefore, Cr(VI) seems to be weakly bound to the mineral throughout the reaction between Cr(III) and $Mn(IV)O_2$.

To summarize, our results show that a major part of Cr(III) oxidation takes place at the beginning of the reaction for HMO and AB, based on the amount of

Cr(VI) in solution (Figure 3.2) and the percentage of Cr(VI) on the minerals at t= 2 minutes (Figure 3.1 (a) and 3.3 (a)). Trivalent chromium sorbs in an inner-sphere complex mechanism on the edges of $Mn(IV)O_2$, in either a bidentate binuclear complex on the edge sides of the mineral, or in a bidentate mononuclear complex on the edge side corners (Figure 3.5). While Cr(VI) is sorbed on the manganese oxide in an outer-sphere complex, the amount of Cr(III) sorbed on AB and HMO increases with time (Figure 3.1 (c) and 3.3 (c)), which means that Cr(III) is accumulating on the mineral surface, and the Cr(III) uptake is more pronounced at higher pH. Larger radial distances of the first Cr-metal shell in the Fourier transformed EXAFS for all samples indicates that Cr(III) nucleates on the mineral surface. However, the presence of a γ-CrOOH phase is not observed on AB, HMO, and RSB, which differs from previous studies that showed that this precipitate forms on many manganese oxides (Manceau and Charlet, 1992; Fendorf *et al.*, 1992). The reason is not due to differences in experimental conditions, since according to equation (1), 50 mM of Cr(III) at pH 3.5 is closer to the pH limit at which Cr(III) starts to precipitate in solution ($pH_{limit}$ 3.54) than 1 mM of Cr(III) at pH 4 ($pH_{limit}$ 4.39) (Fendorf *et al.*, 1992), and 1.88 mM of Cr(III) at pH 4 ($pH_{limit}$ 4.25) (Manceau and Charlet, 1992). The ratio between Cr(III) concentration and manganese oxide suspension density was also the highest in this study. The lack of surface precipitation evidence in the Fourier transformed EXAFS of our reacted manganese oxides could be due to the concentration of Cr(III) nucleation product being too low compared to Cr(III) monomers sorbed on the manganese oxide. However, the formation of an α-CrOOH phase, although never reported to form on $MnO_2$, might explain why the radial distance of the first Cr-metal shell of the Fourier

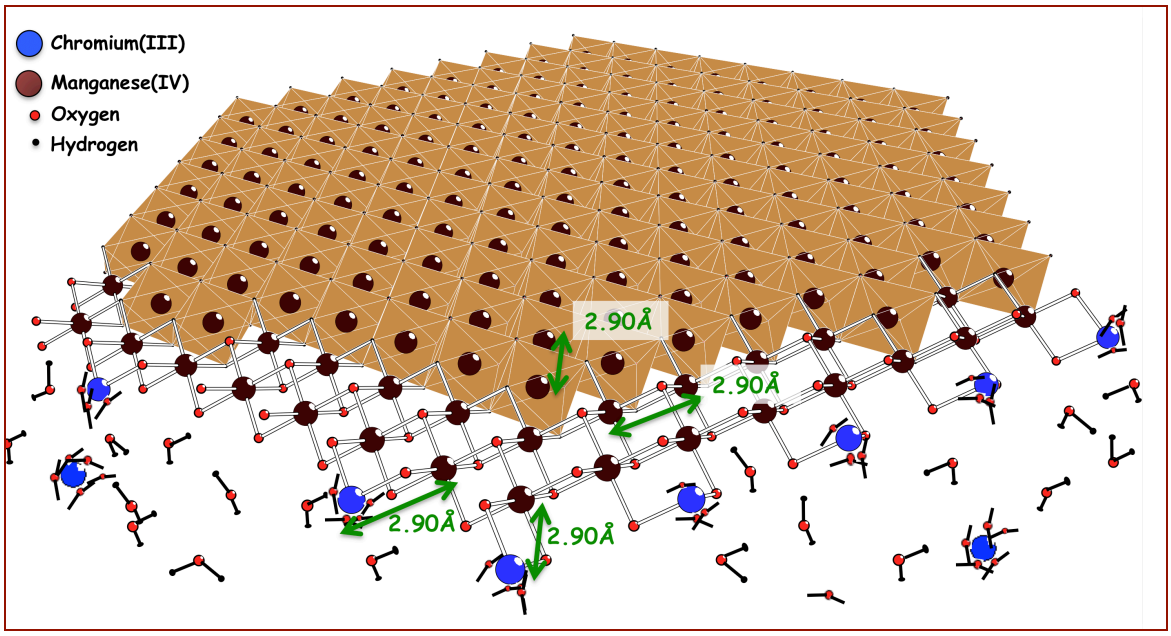


**Figure 3.5** Chromium(III) sorption mechanism on $Mn(IV)O_2$: Cr(III) binds in a bidentate binuclear complex on the edge sides and a bidentate mononuclear complex on the edge corners.

transformed EXAFS increases with time, assuming that surrounding peaks with greater amplitudes in the spectra would mask its peak at 3.45 Å.

### 3.4.1.2 Macroscopic Identification

No major change in morphology or sign of precipitate formation is seen in high resolution TEM (HRTEM) images of Cr(III)-reacted AB and HMO compared to the unreacted AB and HMO (Figure 3.6). The analysis of reacted and unreacted HMO HRTEM are more difficult to interpret than AB since the images reveal a very

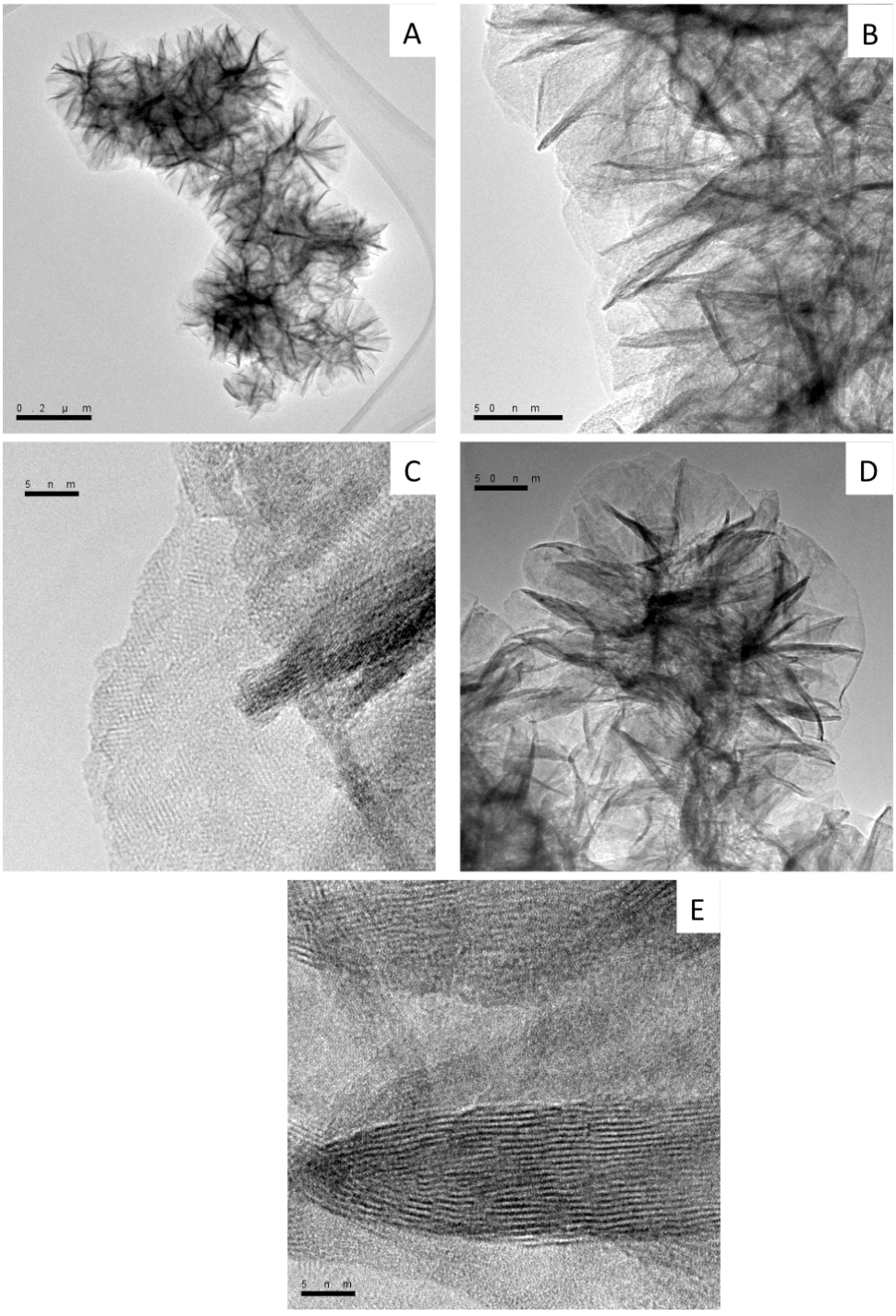


**Figure 3.6** Images A, B, C: HRTEM of AB reacted for 1 hour with 50 mM of Cr(III) at pH 3.5. Images D and E: HRTEM of unreacted AB**.**

heterogeneous mineral structure, mostly amorphous, which also features some crystalline regions locally distributed (HRTEM images of HMO not shown in Figure 3.6). Also, EELS and EDS measurements on HMO are difficult since the mineral is rapidly damaged at the spot exposed to the electron beam.

Chromium seems to be more partitioned towards the edge of AB agglomerates, according to EDS data taken at various locations in the Cr(III)-reacted mineral. Figure 3.7 depicts the EDS patterns taken in the middle of a AB flake randomly chosen (pattern A) and in the rim of the same flake (pattern B), and shows chromium accumulates on the edge three times more than in the center of the flake, according to height of the Cr peak.

Manganese(IV) is detected by EELS in various regions of the reacted acid birnessite. Additionally, Mn(III) is measured locally at some spots close to the edges of AB agglomerates (Figure 3.8 (b)). The data obtained with Q-XAFS, a technique which probes chromium both in solution and sorbed to the mineral, only shows Mn(IV) or Mn(II) present in the system throughout the reaction (section 3.2). This also support that the formation of Mn(III) occurs locally on $MnO_2$, probably only on the surface of the mineral exposed to the solution. The main oxidation state of chromium is (III), according to EELS measurements and peak positions of several chromium oxidation states reported in a previous study (Daulton and Little, 2006). Figure 3.8 (a) shows that the SAED pattern of HMO reacted with Cr(III) is similar to the SAED pattern of the unreacted phase, which is probably due to both reacted and unreacted HMO being very poorly crystalline. Likewise, the SAED pattern of AB reacted with Cr(III) is similar to the SAED pattern of the unreacted phase. The two chromium

phases γ-CrOOH and α-CrOOH are not detected in the Cr-reacted AB, using SAED. Consequently, in case one of these Cr phases did form during Cr(III) sorption on manganese oxides, it could have desorbed to solution after formation on the mineral surface, or perhaps the precipitate is too diffuse on the $MnO_2$ surface to be detected by SAED.

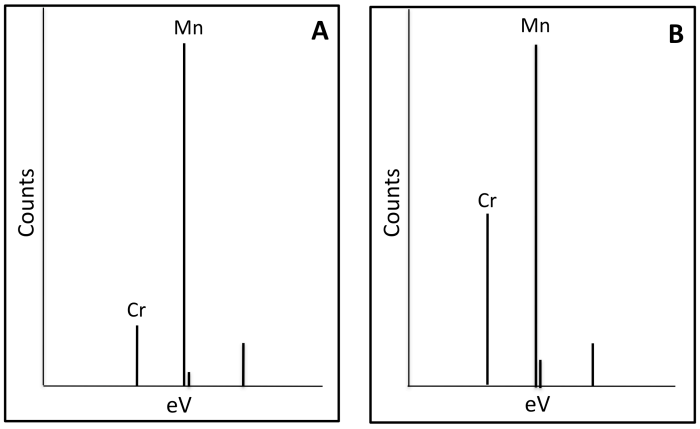


**Figure 3.7** EDS patterns taken in the middle (pattern A) and on the rim (pattern B) of an acid birnessite flake.

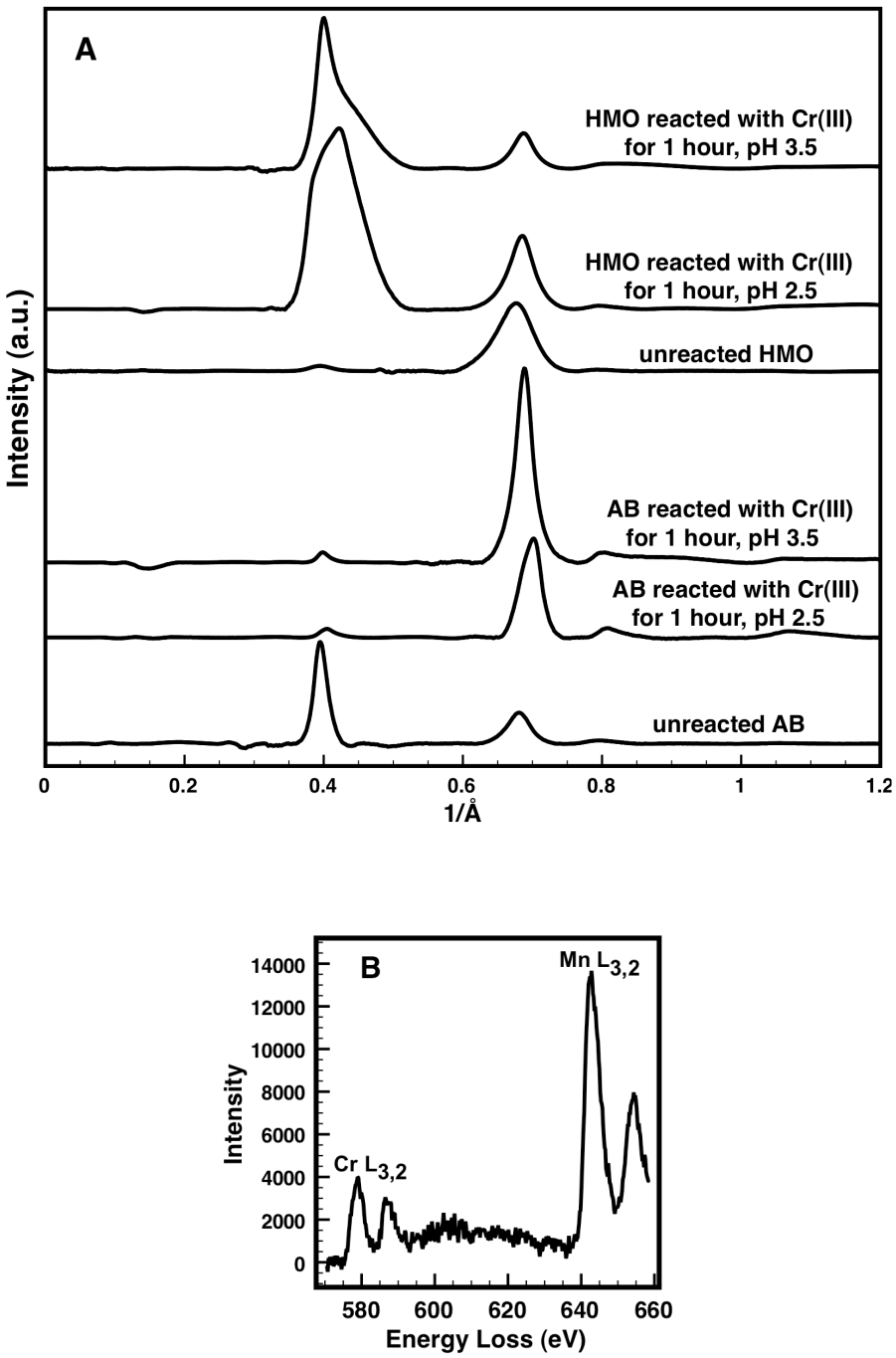


**Figure 3.8** (a) SAED patterns of unreacted HMO and AB, and 1 hour Cr(III)-reacted AB and HMO, at pH 2.5 and 3.5, and (b) EELS pattern of 1 hour Cr(III)-reacted AB.

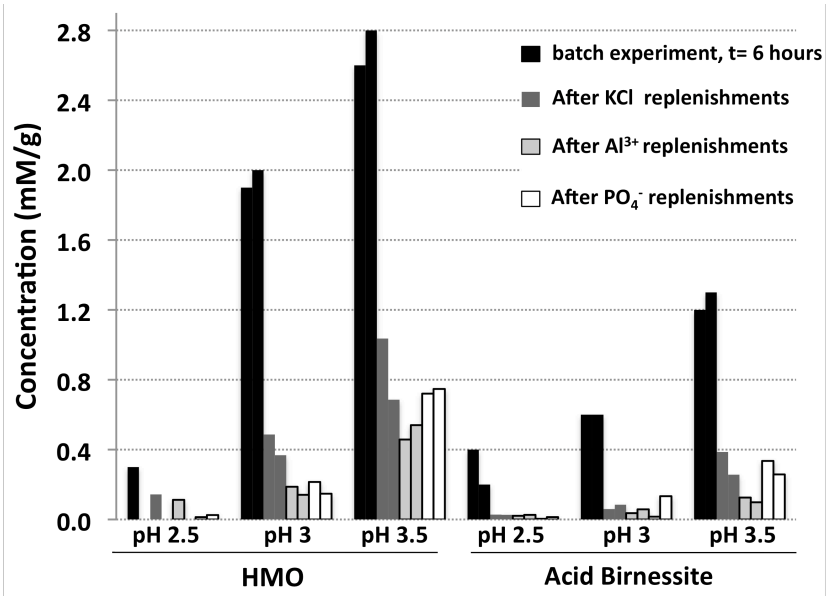


**Figure 3.9** In black color: amount of chromium sorbed on $Mn(IV)O_2$ measured from Figure 3.2 in mM/g, when 50 mM of Cr(III) reacted for 6 hours with 20 g/L of HMO or AB at pH 2.5, 3 and 3.5; in grey and white colors: amount of chromium in HMO or AB measured when the $Mn(IV)O_2$ solid phase, after replenishment experiments conducted at pH 2.5, 3, and 3.5, were digested with 8N HCl.

Trivalent chromium did not significantly desorb from HMO and AB during the replenishment experiments (Figure 3.4), although it is present on the mineral surface (Figure 3.1 (c) and Figure 3.3 (c)). Therefore, the samples of AB and HMO that underwent desorption experiments were centrifuged at the end of the replenishment cycles, and the $Mn(IV)O_2$ solid fractions were digested with 8N HCl, to measure the total amount of chromium that remains on the mineral (Figure 3.9) after conducting the desorption experiments. Although no Cr(III) and Cr(VI) seemed to

desorb from AB and HMO during the last replenishment cycle (Figure 3.4), the digestion of the manganese oxides suggests that some chromium still remains sorbed on $Mn(IV)O_2$ after the desorption experiments. Since Cr(VI) is bound to $Mn(IV)O_2$ in an outer sphere mechanism, chromate is likely to have been entirely desorbed during the replenishment experiments. Therefore, the amount of chromium remaining on the mineral after the desorption experiments is likely Cr(III). The fact that this amount of chromium did not desorb from the mineral, although strong desorption agents were applied (especially $PO_4^{3-}$), suggests that chromium is tightly bound to $Mn(IV)O_2$, which supports the TEM data that suggests that Cr(III) is sorbed on the mineral surface.

The suspensions of HMO and AB that were reacted with Cr(III) for 6 hours during the batch experiments shown in Figure 3.2 were used to conduct stirred flow experiments, and the same desorption agents used in the replenishment experiments were applied in the flow experiments. Although Cr(III) is consumed by the oxidation reaction during the batch experiments (Figure 3.2), it is likely to be present in the system at t=6 hours since a significant amount of Cr(III) progressively sorbed on the surface throughout the first hour (Figure 3.1 (c) and 3.3 (c)), and probably kept on sorbing on the surface until t=6 hours. Therefore, the low concentration of Cr(III) measured in the effluent solution during the stirred-flow experiments conducted with the Cr-reacted HMO and AB suspensions (Figure 3.10), suggests that some Cr(III) present in the manganese oxide suspension was strongly sorbed to $Mn(IV)O_2$, and could not be removed by the desorption agents used in the stirred-flow Experiments. The results obtained with

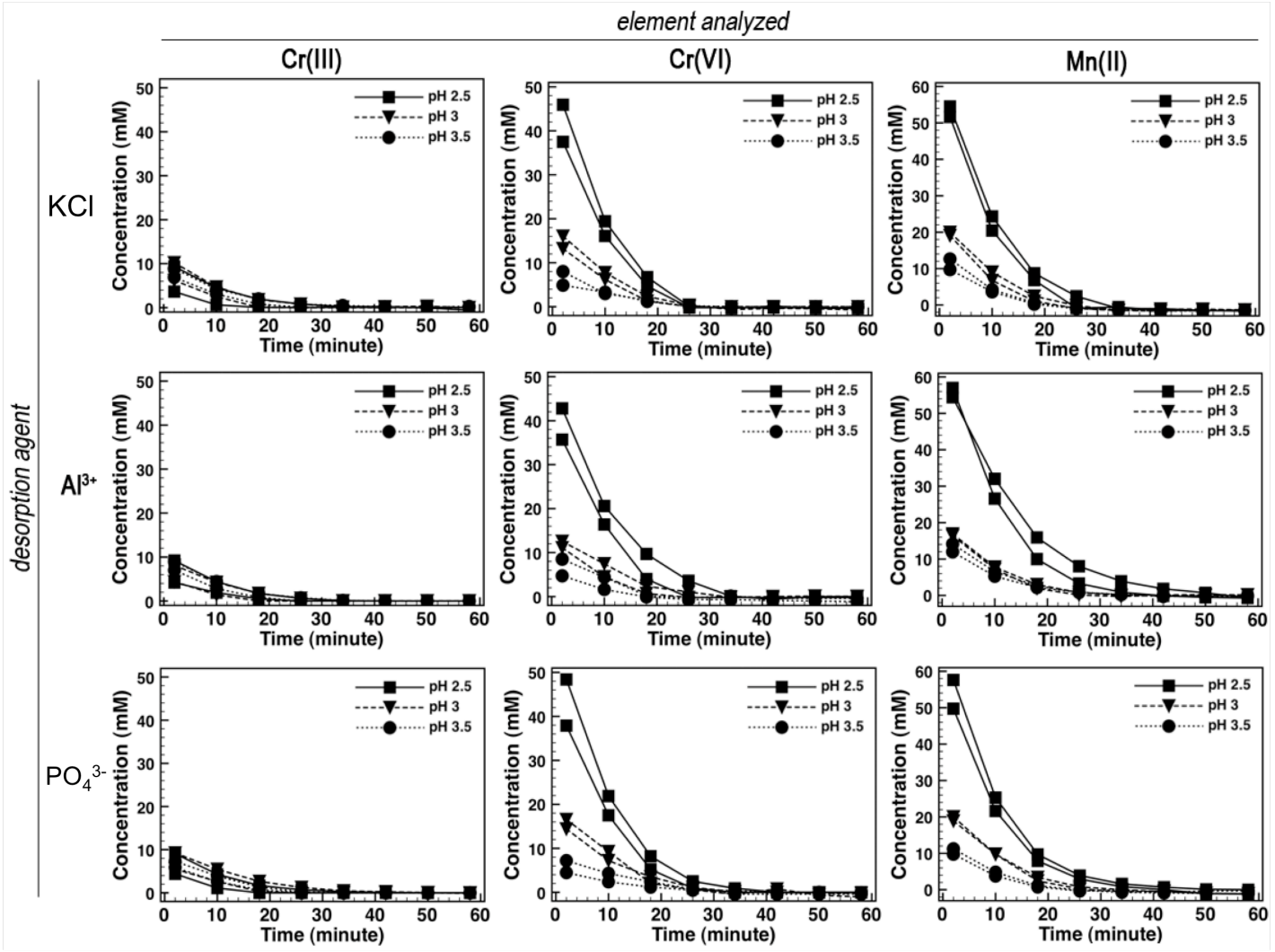


**Hydrous Manganese Oxide**

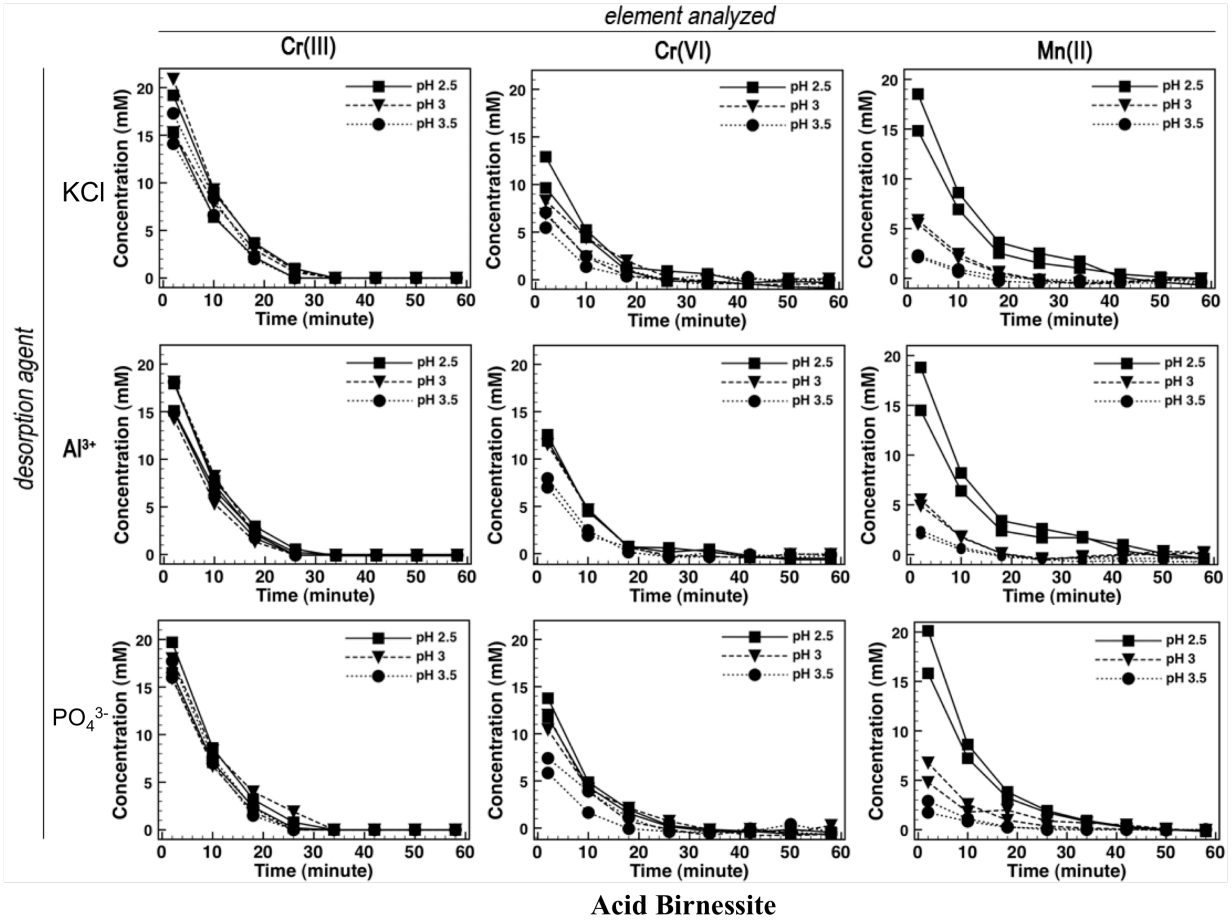


**Figure 3.10** Concentrations of Cr(III), Cr(VI), and Mn(II) measured by stirred flow experiments, with a suspension of HMO and AB reacted with 50 mM Cr(III) for 6 hours in the stirred flow chamber, and using as the flow solution a 50 mM KCl solution, 50 mM $Al^{3+}$ solution, and 50 mM $PO_4^{3-}$ solution, at pH 2.5, 3, and 3.5

stirred-flow experiments thus support the data obtained with the replenishment experiments, which suggest that Cr(III) is strongly bound to $Mn(IV)O_2$.

### 3.4.2 Real-Time Kinetics of Chromium Precipitation and Oxidation

#### 3.4.2.1 Chromium Surface Precipitation Kinetics

Q-XAFS experiments were conducted to measure in-situ the rates of chromium surface precipitation on manganese oxides. Compared to the bulk XAFS data for Cr-reacted $Mn(IV)O_2$ wet pastes shown in section 3.1, that represent Cr sorbed on the mineral, the Q-XAFS batch experimental method employed in this study probes chromium in the entire system, i.e. not only Cr sorbed, but also Cr in solution (Landrot *et al.*, 2010).

Chromium can precipitate on various mineral surfaces to form γ-CrOOH and α-CrOOH phases (Manceau and Charlet, 1992; Fendorf *et al.* 1992; Hansel *et al.* 1992). Therefore, two standards of these minerals were used to perform linear combinations, in addition to Cr(III) and Cr(VI) aqueous standards, on Q-XAFS spectra of Cr(III) reacted with HMO for 2, 10, 30, and 60 minutes at pH 2.5, 3 and 3.5. The results depicted in Figure 3.11 show that good fits were obtained for all spectra. Both γ-CrOOH and α-CrOOH standards contribute significantly to the fits, but their respective contribution depends on pH. At pH 2.5, the formation of a γ-CrOOH precipitate is relatively slow during the first ten minutes of the reaction, representing less than 10% of the total Cr amount in the system, and reaches ≈ 25% of the total amount of Cr in the system at t=60 minutes. At pH 3, the formation of this phase is less pronounced. Additionally, α-CrOOH is present in the system at this pH value, and its formation rates are faster than those for γ-CrOOH. Both precipitates represent at

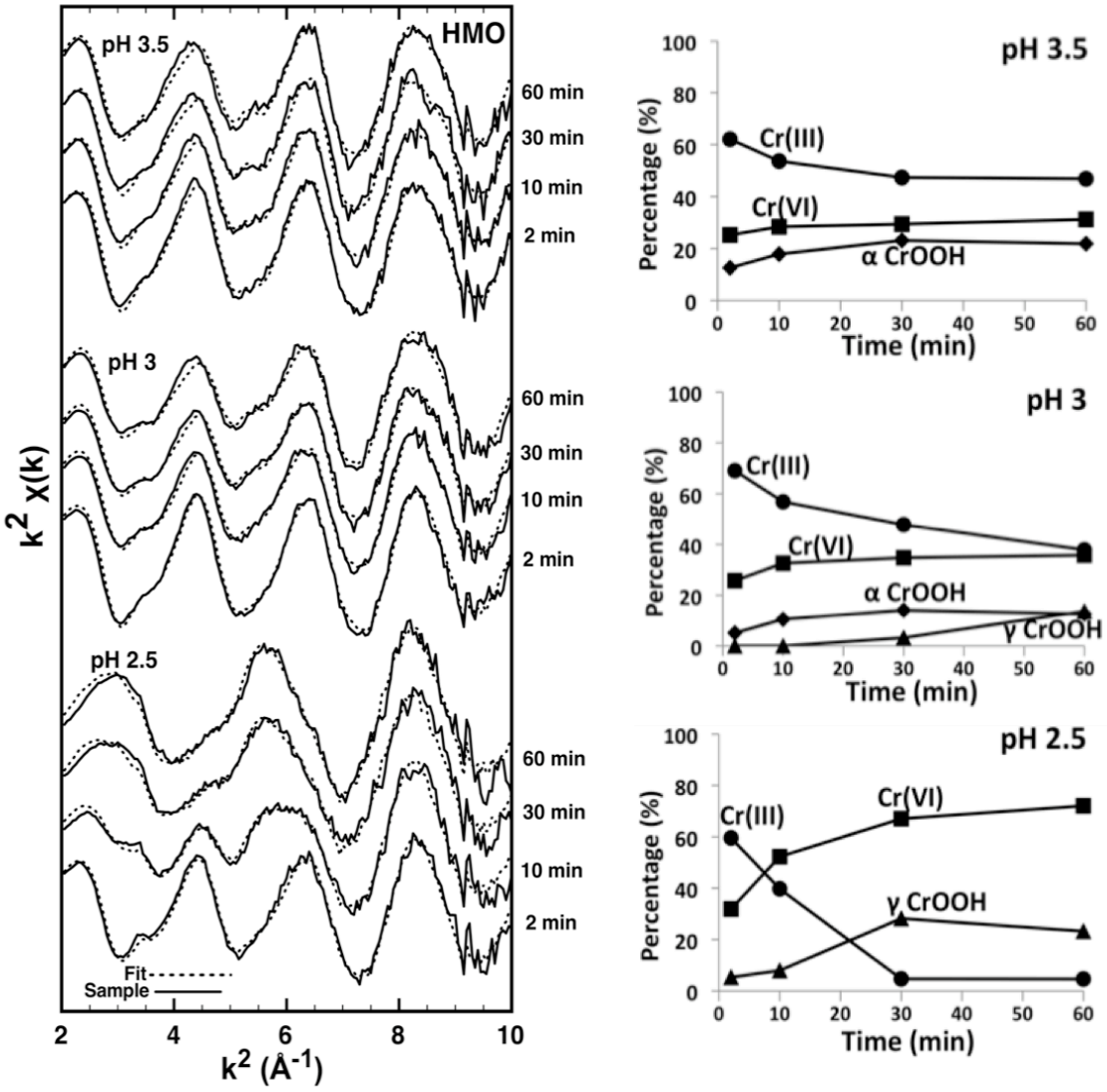


**Figure 3.11** Linear combination of Q-XAFS chi spectra of HMO reacted for 2, 10, 30, and 60 minutes with Cr(III) at 50 mM and pH 2.5, 3, and 3.5 and corresponding percentages of Cr(III), Cr(VI), α-CrOOH, and γ-CrOOH precipitate phases.

t= 60 minutes about 10% of the total amount of Cr in the system. Finally at pH 3.5, only α-CrOOH forms, and accounts for more than 20% of the total amount of Cr after 30 minutes of the reaction. Therefore, the extent of α-CrOOH formation on HMO increases with pH. The same trend is observed for the experiments performed with AB (Figure 3.12), although in this case, γ-CrOOH does not contribute to the linear combination fit at the three pH values. Also, α-CrOOH is not present in the system at pH 2.5, and its rates of formation at pH 3 and 3.5 are slow. The presence of this precipitate does not seem to significantly influence the rate of Cr(III) oxidation during the HMO experiments, since more than 50% of both reactions reached apparent equilibrium within the first two minutes of the reaction at pH 3 and 3.5. The γ-CrOOH phase standard contributes significantly to the linear combination fit at pH 2.5 for the HMO experiment at pH= 2.5, less at pH 3, and not at all at pH 3.5. One could have expected the opposite trend since more γ-CrOOH should form on the mineral surface when the pH gets closer to the limit at which chromium(III) starts to precipitate in bulk solution. The formation on the surface of HMO of the α-CrOOH phase, whose amount increases as the pH increases, and the formation of a γ-CrOOH phase, whose amount decreases as the pH increases, could be explained by comparing their respective structures with the surface of HMO on which theses two Cr phases are believed to originally form, since the pH values of our experiments preclude Cr precipitation in bulk solution. The structure of $Mn(IV)O_2$, which is made up of a layer of manganese atoms each octahedrally coordinated by six oxygen atoms, and the structure of α-CrOOH share similar geometries at their respective top faces (Figure 3.13), although two Cr atoms are separated by 2.96 Å across octahedral edges in the α-CrOOH phase, which is slightly higher than the distance between two Mn atoms

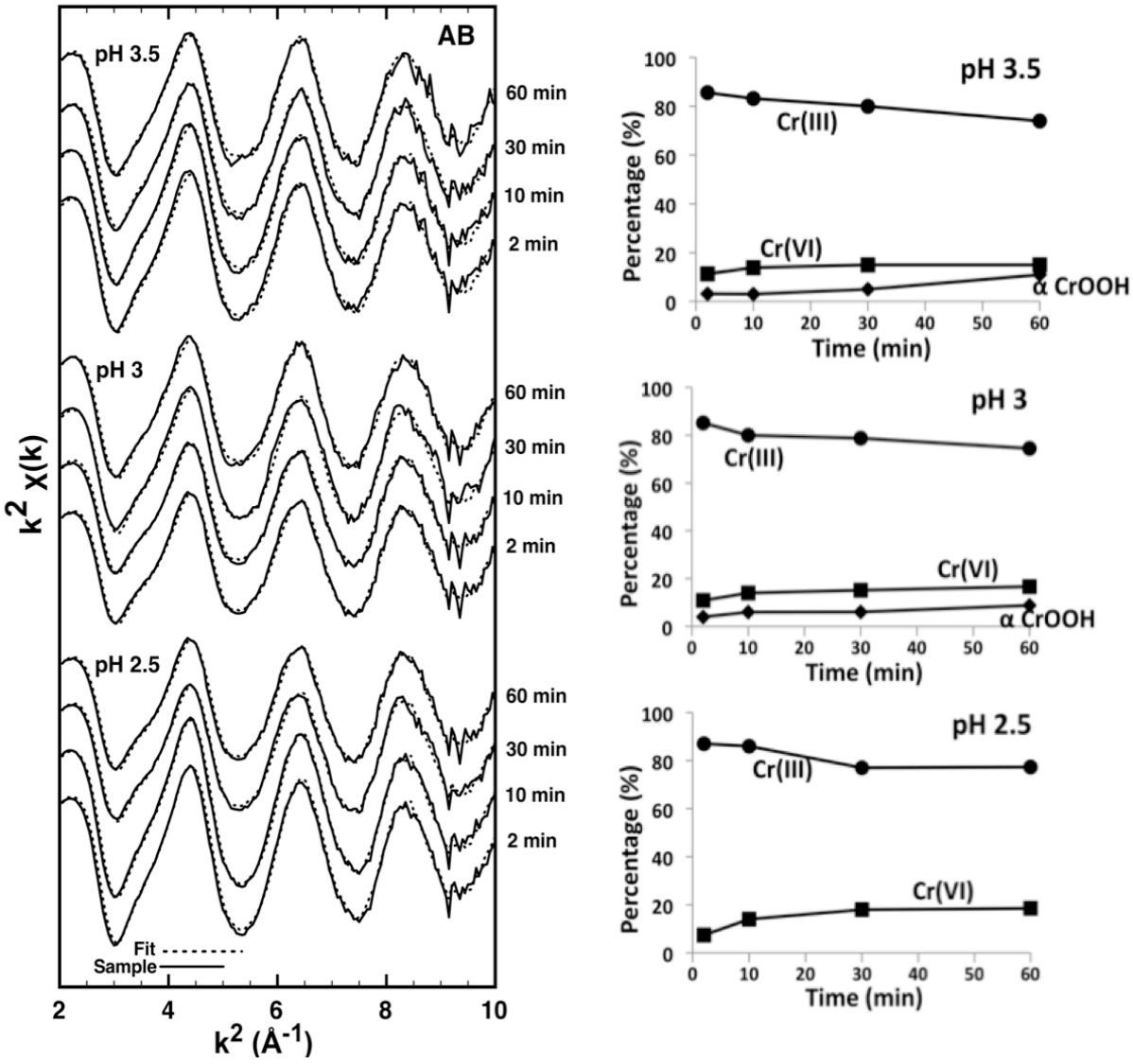


**Figure 3.12** Linear combination of Q-XAFS chi spectra of AB reacted for 2, 10, 30, and 60 minutes with Cr(III) at 50mM and pH 2.5, 3, and 3.5, and corresponding percentages of Cr(III), Cr(VI), and α-CrOOH precipitate phase.

across octahedral edges in the $Mn(IV)O_2$ (2.90 Å). One could predict that α-CrOOH would form on top of $Mn(IV)O_2$, and the oxygen atoms of the top face of the chromium phase would be linked to the oxygen atoms of the manganese oxide's top face by water molecules via hydrogen bonding. The surface of $Mn(IV)O_2$ would decrease the energy of nucleation of the surface precipitate by providing sterically similar sites (McBride, 1991), enabling it to form and spread on the top surface of the $Mn(IV)O_2$. The surface precipitate should not directly complex on the $Mn(IV)O_2$ surface, otherwise, Cr(III) would react with the mineral to oxidize to Cr(VI), instead of nucleating (Fendorf, 1992). Lastly, the amount of α-CrOOH formed in the system should increase with pH, since more OH ligands bound to Cr(III) at higher pH implies a higher sorption rate of Cr(III) on the surface. This is indeed supported by our results depicted in Figures 3.11 and 3.12. However, from a structural standpoint, it is less likely that γ-CrOOH will growth epitaxially on the top face of the manganese oxide than α-CrOOH. Firstly, the distance between two chromium atoms of 2.98 Å across the octahedral edges is slightly larger than those found in α-CrOOH, which would thus imply more straining if the precipitate was epitaxially forming on the $Mn(IV)O_2$. Additionally, less hydrogen bonds between the two minerals could form if the γ-CrOOH was growing on top of the manganese oxide (Figure 3.13) since the octahedra are orientated differently. Therefore, if the γ-CrOOH was forming on $Mn(IV)O_2$, it would more likely form locally on the surface and then expand away from the manganese oxide. The presence of γ-CrOOH during the experiment conducted with HMO at pH 2.5, its smaller amount in the system at pH 3, and its non-

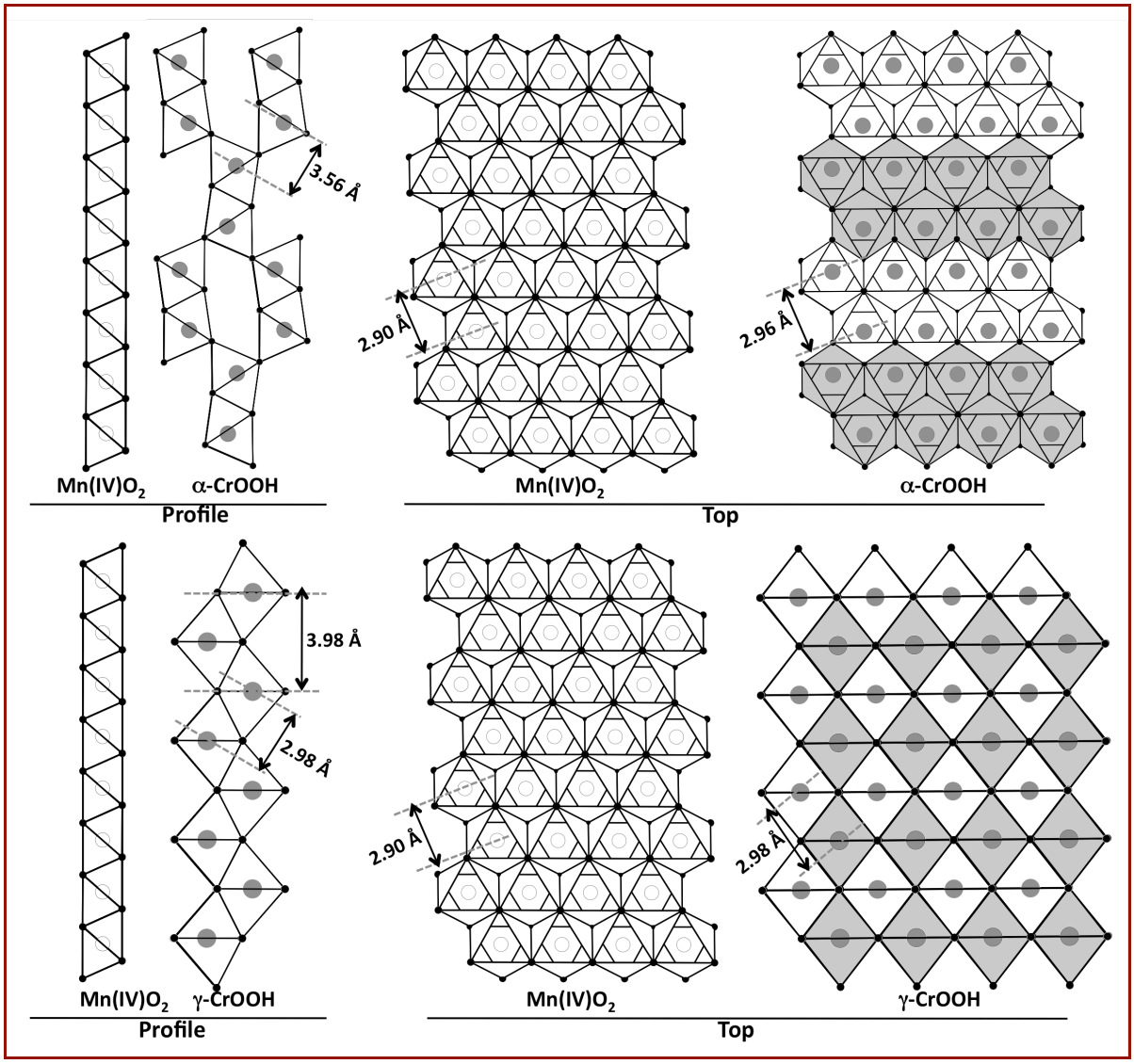


**Figure 3.13** Structure of $Mn(IV)O_2$ compared to γ-CrOOH structure and α-CrOOH structure (profile and top views).

existence at pH 3.5, could be explained in two ways. Firstly, the experiment where Cr(III) reacts with HMO at pH 2.5 results in the highest production of Cr(VI) in the system as compared to other experimental conditions, and also has the highest production of Mn(II) by far (section 3.2.2). Therefore, the surface consumption of $Mn(IV)O_2$ is particularly advanced at pH 2.5 due to Cr(III) oxidation, which implies less surface area on the mineral surface for α-CrOOH to epitaxially grow. The Cr precipitate would rather form locally on the manganese oxide surface and expand away from it in a γ-CrOOH phase. Additionally, since Cr(VI) can sorb on the mineral in an outer-sphere complex and Mn(II) also has a strong affinity for the $Mn(IV)O_2$ surface (Fendorf *et al.*, 1993), the amount of charged species bound to HMO should be particularly high at pH 2.5. This would physically impede α-CrOOH from growing on the surface, and instead promote γ-CrOOH formation and expansion away from the mineral. This hypothesis would also explain why previous studies systematically reported the presence of γ-CrOOH on various manganese oxides (Manceau and Charlet, 1992; Fendorf *et al.*, 1992). The ionic strength used in their experiments were higher than in our study, and the mineral suspension densities were lower: 555 mM of NaCl in 1.5-9.6 g/L of different manganese oxides (Manceau and Charlet, 1992), and 100 mM $NaNO_3$ in 0.02 g/L of AB (Fendorf *et al.*, 1992), compared to 50mM of KCl in 20 g/L of AB or HMO in our studies. Therefore, the manganese oxide interlayers and edges in their experiments were more saturated than in our study -inhibiting the formation of α-CrOOH at the vicinity of the manganese oxide surface. However, since the dielectric constant on the mineral surface was still lower than the dielectric constant in solution, a γ-CrOOH precipitate was forming around the mineral surface.

Both α-CrOOH and γ-CrOOH phases are not detected in the manganese oxide wet pastes but are present in the entire system, according to Q-XAFS data. Therefore, these surface precipitates could diffuse to solution after forming on the mineral surface, since the latter is being consumed by the Cr(III) oxidation at least during the first 30 minutes of our experiments. Additionally, the α-CrOOH could form and epitaxially grow on the manganese oxide surface, until desorbing into solution at a point where the weak hydrogen bounds linking the Cr phase and the mineral surface could no longer overcome the increasing straining in the α-CrOOH structure.

#### 3.4.2.2 Chromium Oxidation Kinetics

The amount of Cr(VI) produced when Cr(III) reacts with HMO or AB for 2, 10, 30, and 60 minutes and at pH 2.5, 3, and 3.5, is depicted in Figure 3.14 (a). Collection of Q-XAFS spectra in the XANES region enables one to measure the total amount of Cr(VI) in the system, i.e. both in solution and that sorbed to the manganese oxide (Landrot, *et al.*, 2010). Measuring the height of the Cr(VI) pre-edge feature in the XANES region is believed to be the most accurate method to quantify Cr(VI) in the system (Peterson *et al.*, 1997). The quantities of Cr(VI) in percentages showed in Figure 3.14 (a) were compared to the percentages of Cr(VI) measured in the system with the linear combination results (Figures 3.11 and 3.12), and an averaged difference of ~5% was seen between the two methods. The amount of Cr(VI) in the system increases with time in all experiments (Figure 3.14 (a)), and the extent of Cr(III) oxidation is higher at low pH. Additionally, the amount of Cr(VI) produced within two minutes at pH 3.5 by HMO is more than the amount of Cr(VI) produced in 1 hour

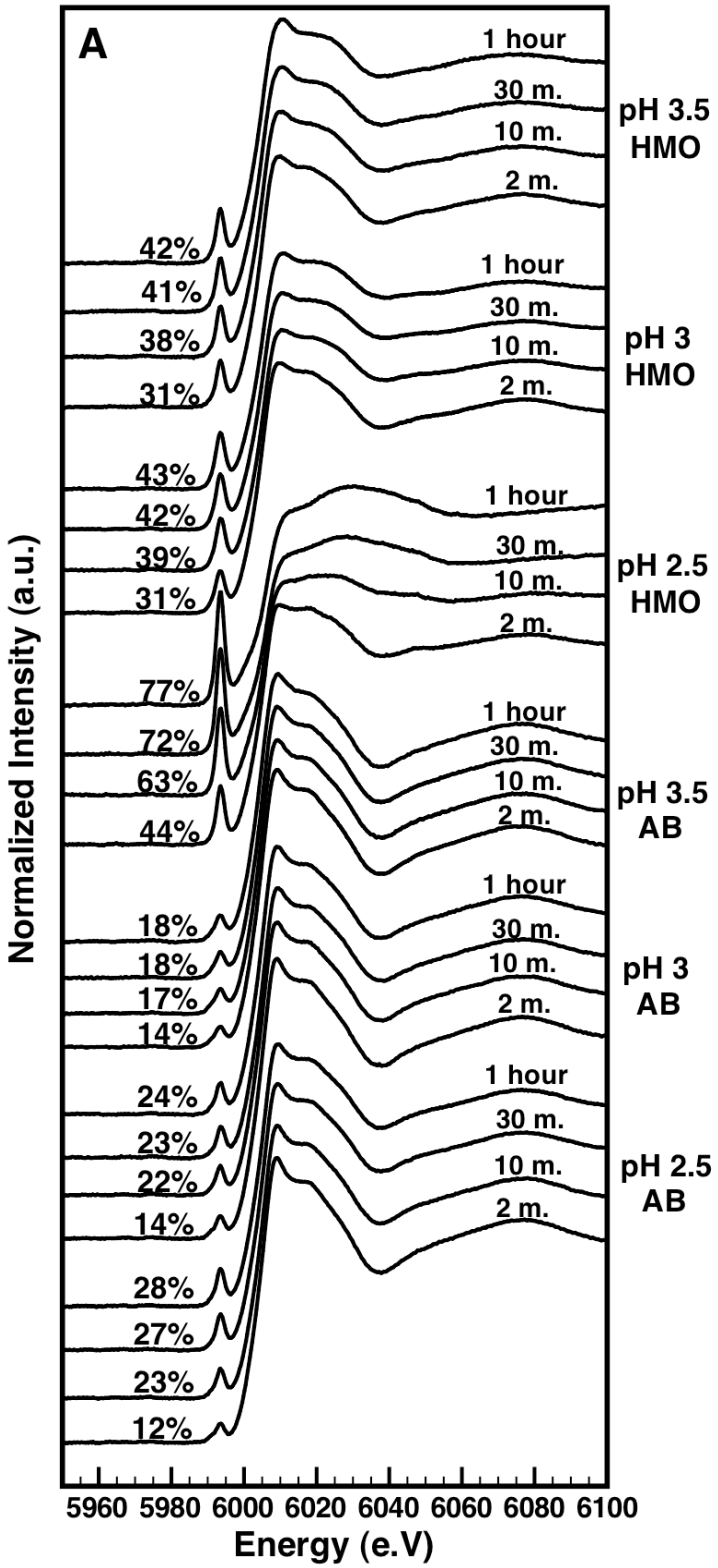
A
1 hour
30 m.
10 m.
2 m.
pH 3.5
HMO
42%
41%
38%
31%
1 hour
30 m.
10 m.
2 m.
pH 3
HMO
43%
42%
39%
31%
1 hour
30 m.
10 m.
2 m.
pH 2.5
HMO
77%
72%
63%
44%
1 hour
30 m.
10 m.
2 m.
pH 3.5
AB
18%
18%
17%
14%
1 hour
30 m.
10 m.
2 m.
pH 3
AB
24%
23%
22%
14%
1 hour
30 m.
10 m.
2 m.
pH 2.5
AB
28%
27%
23%
12%
Normalized Intensity (a.u.)
5960 5980 6000 6020 6040 6060 6080 6100
Energy (e.V)

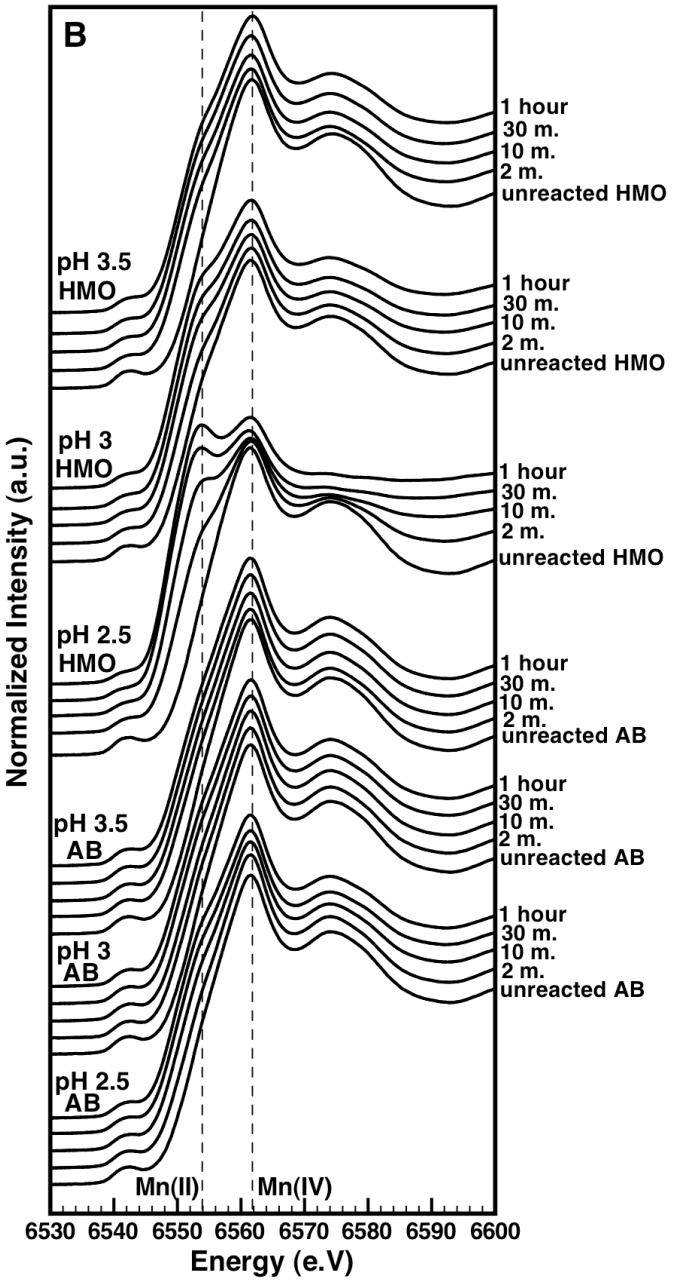


**Figure 3.14** (a) Percentage of Cr(VI) produced from normalized Q-XAFS XANES spectra at the Cr K-edge. (b) Normalized Q-XAFS XANES spectra at the Mn K-edge. The dashed lines represent the position in eV of the white line of a Mn(II) standard ($MnCl_2$) at 6554 eV and a Mn(IV) standard (Vernadite) at 6562 eV.

at pH 2.5 by AB. Therefore, although HMO and AB share the same type of structure, HMO is by far more reactive than AB. The large difference in Cr(VI) produced is related to the number of surface sites of each mineral, since normalizing the amount of Cr(VI) in the system by the surface area of each mineral gives the same order of values, with, in fact, AB oxidizing slightly more Cr(III) than HMO.

The normalized XANES spectra of the same set of experiments taken at the Mn K-edge are depicted in Figure 3.14 (b). These spectra show the variation in Mn oxidation state in the entire system as the kinetic experiments proceed. Both unreacted AB and HMO are essentially $Mn(IV)O_2$, based on the position of their white lines at 6562 e.V. When the manganese oxides react with Cr(III), a hump in the spectra at 6554 e.V grows with time, which suggests that Mn(II) is produced in the system. The rates of the hump growth increases at lower pH, and HMO produces more Mn(II) than AB at the same pH values, because of their respective capacity to oxidize Cr(III). The possible presence of Mn(III) was investigated in the experiment that shows the most variation in the XANES white line (Figure 3.14 (b)), i.e., the experiment carried out with HMO at pH 2.5. Three isosbestic points are seen when stacking the XANES spectra representing t= 2, 10, 30, and 60 minutes of this experiment (Figure 3.15), suggesting that only two oxidation states, Mn(II) and Mn(IV), are present in the system. Additionally, PCA analysis showed that the $k^3$ weighted chi spectra representing t= 2, 10, 30, and 60 minutes of the experiment carried out with HMO at pH 2.5 could be described by only two components. Both $k^3$ weighted chi spectra of the Mn(IV) standard (vernadite) and Mn(II) standard were target transformed and gave "excellent" SPOIL values of 1.4 and 1.2, respectively (Seiter *et al.*, 2008). The variation in Mn oxidation states for all other experiments compared to the experiment

performed with HMO at pH 2.5 looks similar, based on the shape of the XANES spectra (Figure 3.14 (b)), but suggests lower rates. Therefore, Mn(III) is not detected in all Q-XAFS experiments.

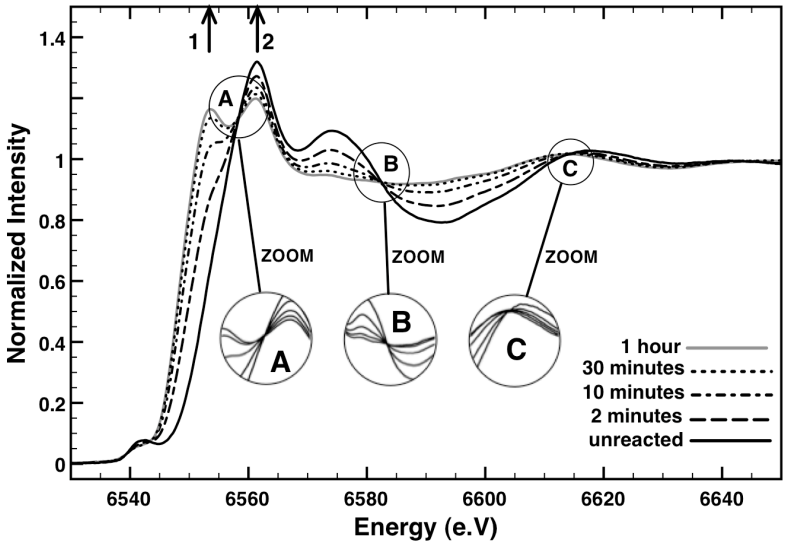


**Figure 3.15** Isosbestic points of normalized Q-XAFS XANES spectra at the Mn K-edge of the experiment conducted with 50mM Cr(III) + 20 g/L HMO at pH 2.5. Arrow 1 and 2 represent the position in eV of the white line of a Mn(II) standard ($MnCl_2$) at 6554 eV and a Mn(IV) standard (vernadite) at 6562 eV, respectively.

### 3.4.2.3 Continuum of Cr(III) Oxidation and Surface Precipitation

Chromium(III) sorption on hexagonal $Mn(IV)O_2$ at high Cr concentration results in either Cr(III) oxidation to Cr(VI), or surface precipitation. Oxidation can occur when chromium sorbs in an inner-sphere complex on the edge sites of the minerals, in bidentate binuclear and bidentate mononuclear mechanisms, respectively on the top sides of the manganese oxides, or on the layer corners. Simultaneously, precipitation of Cr(III) in an α-CrOOH phase on $Mn(IV)O_2$ top surface layers and γ-CrOOH formation around the mineral can occur, without direct contact with the mineral surface. When Cr(III) reacts with HMO at pH 3.5, Cr(III) oxidation and Cr(III) surface precipitation in a α-CrOOH phase occur rapidly, and a major portion of both reactions is completed within two minutes (Figure 3.11). Using similar conditions to our experiments, a previous study using Q-XAFS spectroscopy showed that the chemical rates for Cr(III) oxidation increased with pH (Landrot *et al.*, 2010), which supported the hypothesis that the rate limiting step for Cr(III) oxidation is the complexation of Cr(III) with $MnO_2$ (Fendorf *et al.*, 1992), and not electron transfer (Manceau and Charlet, 1992). The slow ligand exchange rate of Cr(III), due to its stable $d^3$ orbital configuration, increases with pH since more OH ligands are bound to Cr(III), which facilitates Cr(III) adsorption on $MnO_2$. Also, Cr(III) sorption is faster due to the increased negative charge of the mineral surface. Therefore, both oxidation and surface precipitation rates increase at higher pH at the early stage of Cr(III) sorption. However, contrary to Cr(III) nucleation, the extent of Cr(III) oxidation decreases at higher pH (Figure 3.14 (a)). It has been postulated that Cr(III) surface precipitation progressively affects Cr(III) oxidation by masking the reactive site on the manganese oxide and decreasing the amount of Cr(III) in solution (Fendorf *et al.* 1992). The continuous accumulation of Cr(III) on the manganese oxide surface

(Figure 3.1 (a)), whose rates increase at higher pH (Figure 3.3 (a)), and progressive decrease in Cr(VI) production, which levels off more rapidly at higher pH (Figure 3.14 (a)), indeed suggest that Cr(III) oxidation is inhibited by Cr(III) nucleation on the manganese oxide surface. Chromium nucleation products can account for almost the total amount of Cr present on the $MnO_2$ surface, e.g. when Cr(III) reacts with RSB at pH 3 for 2 minutes (Table 3.1), since the radial distance of the first Cr-metal shell in the Fourier transform EXAFS of this sample is similar to the radial distance of a Cr(III)-Cr(III) shell in a pure Cr(III) nucleation product (~3.0 Å) (Manceau and Charlet, 1992). Afterwards, no Cr(III) oxidation occurs from t=2 minutes to t=60 minutes during the experiment, suggesting that Cr(III) nucleation products blocked Cr(III) oxidation. However, although Cr(III) accumulation on the surface affects Cr(VI) production, one cannot conclude that Cr(III) surface precipitation is entirely responsible for the Cr oxidation inhibition. Indeed, although α-CrOOH and/or γ-CrOOH seem to be the main Cr(III) precipitates forming in the entire system, the nature of the Cr(III) nucleation products on the surface of HMO, AB, and RSB have not been clearly constrained. The data from EELS analyses suggest that Mn(III) is locally present in AB reacted with Cr(III). Similarly, the presence of Mn(III) on the surface of Cr(III)-reacted manganese oxides was detected in previous studies by XPS, a technique which enables one to measure oxidation states of species present on the top 1 to 10 nm of the material being analyzed (Banerjee and Nesbitt, 1999; Weaver and Hochella, 2002). Therefore, a possible scenario could be that the surface locally transforms into another phase at the location where Cr(III) oxidizes to Cr(VI), and the newly formed phase could not oxidize Cr(III) as much as $Mn(IV)O_2$, thus inhibiting Cr(III) oxidation in the system. Since this new phase forms locally on the edge of the

mineral, it cannot be identified by SAED, which analyzes the Cr-reacted mineral in a circular surface of about 1 μm diameter. Surface precipitation, occurring either locally on the $MnO_2$ surface and expanding away from the mineral (γ-CrOOH phase), or epitaxially on the layer top faces (α-CrOOH phase) would not directly hinder Cr(III) from oxidizing on the edge sites of the mineral layers. Therefore, Cr(III) surface precipitates do inhibit Cr(III) oxidation by decreasing the amount of Cr(III) atoms in solution that could potentially oxidize on $Mn(IV)O_2$, but do not necessarily mask the edge sites of the mineral surface where Cr(VI) forms.

### 3.5 Conclusions

Sorption of Cr(III) on manganese oxides results in multiple reactions occurring at the mineral/water interface. The kinetics and mechanisms of these reactions were measured in this study using a multi-technique approach. Bulk XAFS was useful in assessing the rates of Cr(III) accumulation on the mineral surface as well as the pH dependence of the process. It also constrained the mechanisms of Cr(III) and Cr(VI) sorption on $Mn(IV)O_2$. Manganese oxides could locally transform into a new phase on the edge of the mineral between $Mn(IV)O_2$ and the solution. This phase, containing Mn(III), and perhaps Cr(III) in its structure, could diminish the amount of sites available on $Mn(IV)O_2$ for Cr(III) oxidation, and thus be responsible for the decrease in the rates of Cr(VI) production measured in the system with Q-XAFS. The hypothetical presence of a new phase containing Cr(III) is supported by the results obtained from the replenishment and stirred-flow experiments, which showed that a significant amount of Cr(III) sorbed to the manganese oxide is immobilized in the mineral. Surface precipitation does not directly impede Cr(III) from sorbing on the mineral surface, but significantly decreases the amount of Cr(III) in solution, acting as

a sink for Cr(III). The nature of the surface precipitate forming on $Mn(IV)O_2$ depends on pH, the structure of the mineral surface, and probably the ionic strength. Our results show that Cr(III) nucleation rates at high pH can be rapid, and the amount of precipitate formed on a large mineral surface can be high. Therefore, surface precipitation is beneficial for the environment, since it can reduce the amount of Cr(VI) produced when Cr(III) sorbs on manganese oxides.

## 3.6 References


Banerjee, D. and Nesbitt, H. W. (1999), Oxidation of aqueous Cr(III) at birnessite surfaces: constraints on reaction mechanism, Geochemica et Cosmochimica Acta, 63, 1671-1687.

Charlet, L. and Manceau, A. (1992), X-ray adsorption spectroscopy study of the sorption of Cr(III) at the oxide-water Interface. II. Adsorption, Coprecipitation, and surface precipitation on hydrous ferric interface, Journal of Colloid and Interface Science, 148, 443-468.

Daulton, T. L. and Little, B. (2006), Determination of chromium valence over the range Cr(0)-Cr(VI) by electron energy loss spectroscopy, Ultramicroscopy, 106, 561-573.

Fendorf, S. E. (1992), Oxidation and sorption mechanisms of hydrolysable metal ions on oxides surfaces, PhD Dissertation, University of Delaware, Newark, DE.

Fendorf, S. E. and Zasoski, R. J. (1992), Chromium(III) oxidation by δ-$MnO_2$ 1. Characterization, Environmental Science & Technology, 26, 79-85.

Fendorf, S. E., Fendorf, M., and Sparks, D.L. (1992), Inhibitory mechanisms of Cr(III) oxidation by δ-$MnO_2$, Journal of Colloid and Interface Science, 153, 37-54.

Fendorf, S. E., Lamble, G. M., Stapleton, G. M., Kelley, G. M., and Sparks, D. L. (1994), Mechanisms of chromium(III) sorption on silica. 1. Cr(III) surface structure derived by extended x-ray adsorption fine structure spectroscopy, Environmental Science & Technology, 28, 284-289.

Fendorf, S. E., Sparks, D. L., and Camaioni, D. M. (1993), Electron paramagnetic resonance stopped flow kinetic study of manganese(II) sorption desorption on birnessite, Soil Sci. Soc. Am. J., 57, 57-62.

Gadde, R. R. and Laitinen, H. A. (1974), Studies of heavy metal adsorption by hydrous iron and manganese oxides, Analytical Chemistry, 46, 2022-2026.

Ginder-Vogel, M., Fischel, J., Landrot, G., and Sparks, D. L. (2009), Quantification of rapid environmental redox processes using quick scanning x-ray absorption spectroscopy (Q-XAS), Proceedings of the National Academy of Sciences, 106, 16124-16128.

Hansel, C. M., Wielinga, B. W., and Fendorf, S., E. (2002), Stuctural and compositional evolution of Cr/Fe solids after indirect chromate reduction by dissimilatory iron-reducing bacteria, Geochemica et Cosmochimica Acta, 2002, 401-412.

Kim, J. G., Dixon, J., Chusui, C. C., and Deng, Y. (2002), Oxidation of chromium(III) to (VI) by manganese oxides, Soil Sci. Soc. Am. J., 66, 306-316.

Kim, J. G. and Moon, H. S. (1998), Oxidation of chromium (III) to chromium (VI) by a series of synthesized birnessites (δ-MnO2): kinetics and oxidation capacity, Clay Science, 10, 363-374.

Landrot, G., Ginder-Vogel, M., and Sparks, D. L. (2010), Kinetics of chromium(III) oxidation by manganese(IV) oxides using quick scanning x-ray absorption fine structure spectroscopy (Q-XAFS), Environmental Science & Technology, 44, 143-149.

Manceau, A. and Charlet, L. (1992), X-ray adsorption spectroscopy study of the sorption of Cr(III) at the oxide-water interface. I. Molecular mechanism of Cr(III) oxidation on Mn Oxides, Journal of Colloid and Interface Science, 148, 425-442.

Masue, Y., Loeppert, R., and Kramer, T. (2007), Arsenate and arsenite adsorption and desorption behavior on coprecipitated aluminum: iron hydroxides, Environmental Science & Technology, 41, 837-842.

McBride, M. B. (1991), Processes of heavy and transition metal sorption by soil minerals, Interactions at the soil colloid-soil solution interface, Kluwer Academic Publisher, Dordrecht.

McKenzie, R. M. (1971), The synthesis of birnessite, cryptomelane, and some other oxides and hydroxides of manganese, Mineral. Mag., 38, 493-502.

Mitchell, D. R. G. (2008), DiffTools: sofware tools for electron diffraction in DigitalMicrograph, Microscopy Research and Technique, 71, 588-593

O'Day, P. A., Brown, G. E., and Parks, G. A. (1994), X-ray adsorption spectroscopy of cobalt(II) multinuclear surface complexes and surface precipitates on kaolinite, Journal of Colloid and Interface Science, 165, 269-289.

Oze, C., Bird, D., K. , and Fendorf, S., E. (2007), Genesis of hexavalent chromium from natural sources in soil and groundwater, Proceedings of the National Academy of Sciences, 104, 6544-6549.

Palmer, C. and Wittbrodt, P. (1991), Processes affecting the remediation of chromium-contaminated sites, Environmental Health Perspective, 92, 25-40.

Parikh, S. J., Lafferty, B. J., and Sparks, D. L. (2008), An ATR-FTIR spectroscopic approach for measuring rapid kinetics at the mineral/water interface, Journal of Colloid and Interface Science, 320, 177-185.

Peterson, M. L., Brown, G. E., and Parks, G. A. (1996), Direct XAFS evidence for heterogeneous redox reaction at the aqueous chromium/magnetite interface, Colloids and Surfaces, 107, 77-88.

Peterson, M. L., Brown, G. E., Parks, G. A., and Stein, C. L. (1997), Differential redox and sorption of Cr(III/VI) on natural silicate and oxide minerals: EXAFS and XANES results, Geochemica et Cosmochimica Acta, 61, 3399-4413.

Post, J. E. (1999), Manganese oxide minerals: crytal stuctures and economic and environmental significance Proceedings of the National Academy of Sciences, 96, 7, 3447-3454.

Rai, D., Sass, B., and Moore, D. (1987), Chromium(III) hydrolysis constants and solubility of chromium(III) hydroxide, Inorg. Chem., 26, 345-349.

Rotzinger, F., Stunzi, H., and Marty, W. (1986), Early stages of the hydrolysis of chromium(III) in aqueous solution. 3. Kinetics of dimerization of the deprotonated aqua ion., Inorg. Chem., 25, 489-495.

Scheinost, A. C., Ford, R., and Sparks, D. (1999), The role of Al in the Formation of secondary Ni precipitates on pyrophyllite, gibbsite, talc, and amorphous silica: a DRS study, Geochemica et Cosmochimica Acta, 63, 3193-3203.

Seiter, J., Staats-Borda, K., Ginder-Vogel, M., and Sparks, D. L. (2008), XANES spectroscopic analysis of phosphorus speciation in alum-amended poultry litter, Waste Management, 37, 477-485.

Sileo, E. E., Ramos, A. Y., Magaz, G. E., and Blesa, M. A. (2004), Long-range vs. short-range ordering in synthetic Cr-substitued goethites, Geochemica et Cosmochimica Acta, 68, 3053-3063.

Sparks, D. L. (1989), Kinetics of Soil Chemical Processes, Academic Press, San Diego, CA.

Sposito, G. (1986), Distinguishing adsorption from surface precipitation. In: Hayes, J. A. D. a. K. F. (Ed.), Geochemical proceses at mineral surfaces, Am. Chem. Soc., Washington, DC.

Villalobos, M., Toner, B., Bargar, J., and Sposito, G. (2003), Characterization of the manganese oxide produced by pseudonomas putida strain MnB1, Geochemica et Cosmochimica Acta, 67, 2649-2662.

Weaver, R. M. and Hochella, M. F. (2003), The reactivity of seven Mn-Oxides with $Cr^{3+}_{aq}$: a comparative analysis of a complex, environmentally important redox reaction, American Mineralogist, 88, 2016-2028.

Weaver, R. M., Hochella, M. F. , and Ilton, E. S. (2002), Dynamic processes occuring at the $CrIII_{aq}$ -manganite (γ-MnOOH) interface: Simultaneous adsorption, microprecipitation, oxidation/reduction, and dissolution, Geochemica et Cosmochimica Acta, 66, 4119-4132.

# Chapter 4

# ARSENIC AND CHROMIUM SPECIATION IN AN URBAN CONTAMINATED SOIL

## 4.1 Abstract

The speciation of As and Cr in a contaminated soil was studied by micro x-ray fluorescence spectroscopy (μ-XRF), and bulk x-ray absorption spectroscopy (bulk XAFS). The soil was taken from a park in Wilmington, DE, which had been an important center for the leather tanning industry along the Atlantic seaboard of the United States, until the early 20th century. The concentrations of As, Cr, and Pb measured at different locations in the park were often far above the background levels of these heavy metals in the State of Delaware. Results from micro x-ray absorption near-edge structure spectroscopy (μ-XANES) and bulk XAFS analyses show that Cr(III) and As(V) are mainly present in the soil, with insignificant amounts of Cr(VI) and As(III). The apparent absence of chromate may be notably due to the association between Cr and Fe in different regions of the soil. Micro x-ray fluorescence spectroscopy (μ-XRF) maps show that these two elements are distributed together in regions where their concentrations are diffuse, and at local spots where their concentrations are high. Iron oxides, which can reduce Cr(VI) to Cr(III), are present at some of these hot spots where Cr and Fe are highly concentrated, based on the results obtained by micro x-ray diffraction spectroscopy (μ-XRD) analyses. Results from bulk extended x-ray absorption fine structure spectroscopy (EXAFS) analyses suggest that

As is mainly associated with Al in the soil, and to a minor extent with Fe, which is supported by μ-XRF and μ-XRD results. Arsenate may be sorbed to aluminum oxides, which might have transformed after a long period of time into an As-Al precipitate phase, having a structure and chemical composition similar to mansfieldite. The latter hypothesis is supported by the fact that only a small amount of As present in the soil was desorbed using the characteristic toxicity leaching procedure (TCLP) and the synthetic precipitation leaching procedure (SPLP) tests. This suggests that As is immobilized in the soil.

## 4.2 Introduction

The city of Wilmington, in New Castle County, Delaware, was one of the capitals of the leather tanning industry on the American East Coast, from the late 1800's to the early 1900's. In 2001, an investigation by the Delaware Department of Natural Resources and Environmental Control (DNREC) identified 128 tannery sites in Wilmington area, which were subsequently clustered into 52 sites (http://www.dnrec.state.de.us/dnrec2000/Divisions/AWM/sirb/docs/pdfs/misc/asburyPark.pdf). Although many of these sites, which are covered by buildings and parking lots, have been cleaned up after the DNREC investigation, due to their close proximity to residential areas, some of them still remain untreated. Since arsenic compounds were used at various stages of the tanning process, this element is often found at high concentrations in soils at former tanning factories, especially the "beam houses", where hides were de-haired in large vats of arsenic solution, using realgar (AsS). The tanning process also employed arsenic-based coloring agents such as Scheele's green ($CuHAsO_3$) and Paris green ($Cu(AsO_2)_2Cu(C_2H_3O_2)_2$), as well as sodium arsenate leather preservatives. Additionally, the waste generated at the tanning factories often

contained chromium, since the chrome-tanned leather technique was one of the leather tanning methods used in the second part of the 19th century, which employed chromium salts, including Cr(III) sulfate (Wikipedia.com). The latter chemical was often synthesized at the tanning factories, by reducing sodium dichromate with sulfur dioxide.

The goal of this study is to determine the concentrations, distributions, and potential toxicity of Cr and As present in the soil of Christiana Park, located on Church Street, adjacent to the Christiana River, in Wilmington, using synchrotron-based techniques. According to a report issued by DNREC (http://www.awm.delaware .gov/SIRB/Lists/SIRB%20Plans%20%20Proposed%20and%20Final/Attachments/61/ Christina%20Park%20Proposed%20Plan.pdf), this park, about 6.6 acres in size, was created in the early 20th century, by landfill operations. Miscellaneous materials, including soil, brick, glass, garbage, coal ash, and slag, were used to cover up a native marsh and alluvial deposits from Christiana River. Several industrial and commercial sites, including tanneries, surrounded the park until the early 20th century. According to DNREC, the 52 tannery sites identified in the Wilmington area were located for the most part along Walnut, Tatnall, and Monroe Streets, near the Christiana River. Five of these sites are less than two blocks away from Christiana Park. Therefore, it is likely that some of the fill materials used to create the park were wastes generated from the surrounding tanning factories.

Previous studies have reported that As and Cr in contaminated soils are mainly associated with Fe and Al phases (Beaulieu and Savage, 2005; Lund and Fobian, 1991; Bhattacharya *et al*., 2002, Hopp *et al*., 2008, Cancès *et al*.; 2008; Arčon *et al*.**,** 2002). Iron oxides are important As and Cr scavengers because of their

abundance in the environment, surface area, and chemical affinity for As(III) and As(V) compounds (Sparks, 2003; Vodyanitskii, 2007). Additionally, Cr(III) can sorb to organic materials (Hopp *et al*. 2008), or co-precipitate with goethite to form a α-(Fe, Cr)OOH phase, due to structural similarities between the Fe(III) mineral (α-FeOOH) and the pure Cr surface precipitate phase (α-CrOOH) (Charlet and Manceau, 1992; Hansel *et al*., 2002). Aluminum oxides can sorb As(V), and transform after a long period to a three dimensional As-Al precipitate phase (Arai and Sparks, 2002). It has been also shown that As can sorb to calcite, sulfides, kaolinite, and montmorillonite (La Force *et al*., 2000). Lastly, manganese oxides can effectively sorb and oxidize As(III) or Cr(III), to produce As(V) or Cr(VI), the latter being the most toxic form of chromium (Post, 1999; Parikh and Sparks, 2008, Fendorf and Zasoski, 1992, Weaver and Hochella, 2003). Conversely, Fe oxides, sulfides, or dissolved organic substances can reduce Cr(VI) to Cr(III) (Fendorf and Guangchao, 1996). Therefore, to assess the potential toxicity of chromium and arsenic in the soil of Christiana Park, one not only has to determine the oxidation states of these two species, but also their compartmentalization in the soil and their association with soil components that can potentially change their chemical properties. This can be achieved using μ-XAS and μ-XRF analyses. Accordingly, the co-localization of Cr/Mn, and Cr/Fe, and the distribution of Cr oxidation states are determined in this study with μ-XRF and μ-XANES. Additionally, since Fe and Mn can have opposing effects on Cr oxidation states, and also due to the drastic variability in mineral oxidation capacity among the different types of manganese oxides, the nature of the Mn and Fe mineral phases at hot spots featuring Cr, Fe, and Mn, in the fluorescence maps can be determined with μ-XRD. Lastly, the oxidation states of As and its local

environment at the molecular scale are determined by bulk-XAFS. The information provided in this study about Cr and As speciation in the soil of Christiana Park could be useful in deciding on the best remedial action strategy for other As and Cr contaminated sites.

## 4.3 Material and Methods

### 4.3.1 Sample Collection and Soil Analysis

Soil samples were collected at eight locations randomly chosen in the park. Samples were taken at two depths per location, between 0 and 8 inches, and 8 to 16 inches. Soil samples were digested with an aqua regia mixture, and elemental concentrations were measured with ICP-AES. Soil samples from two locations, labeled "Soil 1" and "Soil 2", with the highest arsenic and chromium concentrations were selected for macroscopic and synchrotron-based analyses. The pH and Eh of each sample was determined by mixing ~0.5 g soil with ~10 mL DDI water, settling for 20 minutes, and measuring using a combination electrode. The Synthetic Precipitation Leaching Procedure (SPLP) and the Toxicity Characteristic Procedure (TCLP) for arsenic were applied to Soil 1 and 2, according to EPA methods 1311 and 1312. The samples were then centrifuged and analyzed by GF-AAS for total As concentration in solution. Soil samples 1 & 2 were also sieved to 25 μm for bulk x-ray absorption fine structure (bulk XAFS) and micro-XAS analysis.

### 4.3.2 Bulk X-Ray Absorption Fine Structure (Bulk XAFS) Analyses

Soil samples were analyzed at the As K-edge by bulk x-ray absorption fine structure spectroscopy (XAFS), at beamline 11-2 at the Stanford Synchrotron Radiation Laboratory (SSRL), Stanford University, CA. The beamline features a

Si(220) monochromator crystal, which was detuned by 30% for harmonic rejection, and a 30-element Ge solid state detector, with 25 operating channels. The monochromator was calibrated by assigning an energy value of 11874 eV at the inflection point of the first derivative in the XANES region of a As(V) powder standard. The soil samples, sieved to ≤ 25 μm, were mounted on sample holders and sealed with kapton tape, and oriented at 45° to both the unfocused incident beam and the Ge detector. Three XAFS spectra per sample were collected and averaged together. Data was processed using the SIXPACK/IFEFFIT and ATHENA/IFEFFIT software analysis packages. Fourier transformed extended x-ray absorption fine structure (EXAFS) spectra, which were $k^3$ weighted, were used for shell-by-shell fitting of the data. Mansfieldite was used in FEFF6l calculations as a model compound for the Al-O path and Al-Al path.

### 4.3.3 Micro XAS Analyses

Soil 1 & 2 were analyzed with μ-XRF, μ-XANES, and μ-XRD, at beamline 2.3, SSRL, and at beamline X27A, National Synchrotron Light Source (NSLS), Brookhaven, Upton, NY. At beamline X27A, the monochromator was calibrated at the Ni(0) K-edge (8333 eV), using a nickel foil, and the μ-XANES data were collected at the Cr edge and at the As edge. At beamline 2.3, a potassium chromate standard was used to calibrate the monochromator at 5993.5 eV, i.e. the energy of the XANES pre-edge feature of Cr(VI) (Peterson *et al.*, 1997), and the μ-XANES data were collected only at the Cr K-edge. Micro-XRF analyses were conducted at beamlines 2.3 with the monochromator set at 12000 eV, a 2.5x2.5 μm beam, a 200 ms dwell time per pixel, and a step size of 10 μm. The peak intensities for Ni, S, Fe, As, Cr, Mn, Ti, Ca, K, and Zn were collected at each pixel of μ-XRF maps,

which were 1x1.2 mm in size. For each sample, a small amount of ≤ 25 μm soil fraction was deposited on scotch tape. Flipping over the sample holder and gently shaking it removed most of the deposit. Only a very thin layer of soil remained on the scotch tape, which was then analyzed by μ-XRF. The monochromator was set at 12000 eV to collect μ-XRF maps at beamline X27A. The beam was 10x15 μm, the dwell time per pixel was 6 seconds, and the step size was 20 μm. The peak intensities for Cu, Fe, As, Cr, Mn, Ti, Ca, K, and Zn were collected at each pixel in the μ-XRF maps, which were 2x2 mm in size. Unfortunately, it is not possible to collect μ-XRF of aluminum on any hard x-ray microprobe like the ones at beamlines X27A and 2.3 because Al K-alpha fluorescence (1.487 keV) is so low in energy that the entire signal is absorbed by the air path between the sample and detector. For all analysis conducted at X27A, (μ-XRF, μ-XANES, and μ-XRD), the samples were mounted on a SupraSil (trace element free) quartz slide, with Cyanoacrylate-based adhesive and Scotchcast electrical resin as the embedding material (Spectrum Petrographics). Micro-XRD data were taken with the monochromator set at 17479 eV and an $Al_2O_3$ standard was used to calibrate the diffraction patterns.

## 4.4 Results and Discussion

### 4.4.1 Soil Composition

The soil samples taken at eight random locations in the park contained in average 33 ppm Cr, 40 ppm As, and 67 ppm Pb at a depth of 0 to 8” below the surface, and 56 ppm Cr, 153 ppm As, and 296 ppm Pb at a depth of 8 to 16” below the surface (Appendix B). According to a document released by the DNREC (http:// www.dnrec. state.de.us/DNREC2000/Divisions/AWM/sirb/DOCS/PDFS/Misc/RemStnd.pdf),

typical Cr, As, and Pb concentrations in Delaware soils range respectively from 5 to 30, 1 to 10, and 30 to 100 ppm. Therefore, the concentrations of these three elements measured in the Christiana Park soils were all above the State average. Since the federal regulatory definition of a "soil lead hazard" is a Pb concentration of 400 ppm or greater in a composite sample of bare soil in a play area, two soil samples, with lead concentrations of 1156 and 572 ppm, fell in this range. Among the eight locations chosen in the park, soil samples from two locations were selected for macroscopic and synchrotron-based analyses, based on their arsenic and chromium concentrations. The first location, whose soil was labeled "Soil 1" in Figure 4.1, was chosen due to the high concentration of arsenic at depth a 8-16" (985 ppm). It had the highest As content found in the park. Another location, labeled "Soil 2", was chosen since As concentrations in the soil were lower than in Soil 1, but are still above the background As concentration in Delaware soils. A report issued by the DNREC in 2002 reported the concentrations of As and Cr measured at two former tannery sites in Wilmington, which were located a few blocks away from Christiana Park, were on average 7 ppm As, and 22 ppm Cr, and the soil at the second site contained an average of 6 ppm As and 23 ppm Cr. Therefore, the average concentrations of arsenic and chromium in the soil at eight locations in Christiana Park are significantly higher than the As and Cr concentrations measured in the DNREC study at the two former tannery sites. This is likely due to the location of the park near the Christiana River, which was probably polluted by wastes from surrounding tanneries, and the fact that the park was constructed using landfill materials that could have included some industrial waste materials. Like arsenic, the concentration of manganese in soil 1 increases from 0-8" to 8-16" (359 and 981 ppm, respectively). The concentrations of iron and aluminum

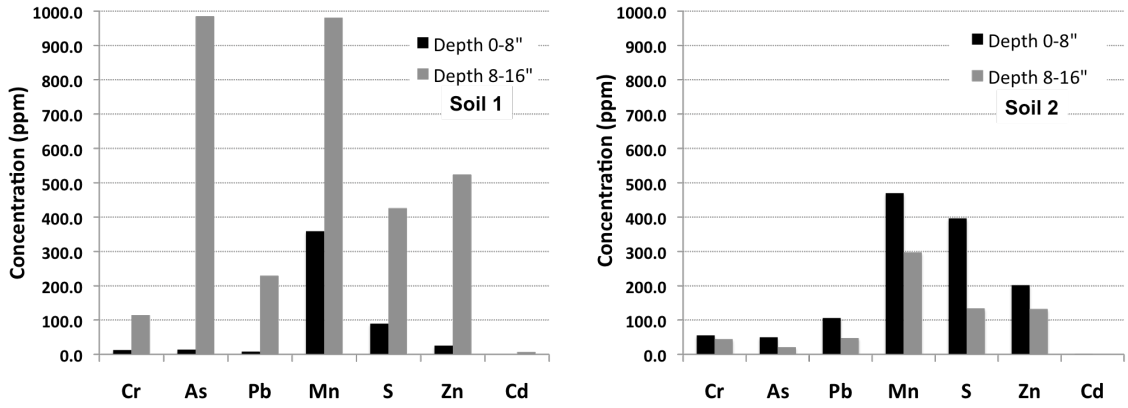


**Figure 4.1** Concentrations, in ppm, of several elements in Soil 1 and 2

are high at both locations (Appendix B). The concentration of aluminum also increases with depth in soil 1, from 6284 ppm at 0-8", to 24890 ppm at 8-16". Although quartz was the most prominent element, based on XRD in soil 1 and 2 (data not shown), dolomite was prominent in soil 1 at a depth of 0-8". Since this mineral can be used as building stone, refractory brick for furnace linings, or ornamental stone, it was probably added to the soil as a landfill material.

### 4.4.2 Elemental Distribution

Arsenic desorption from Soil 1 & 2 was conducted based on the EPA's Synthetic Precipitation Leaching Procedure (SPLP) and Toxicity Characteristic Procedure (TCLP). Both desorbed only a very small amount (less than 3%) of arsenic from soil 1 & 2 at each depth (0-8" to 8-16"), which suggests that arsenic is strongly

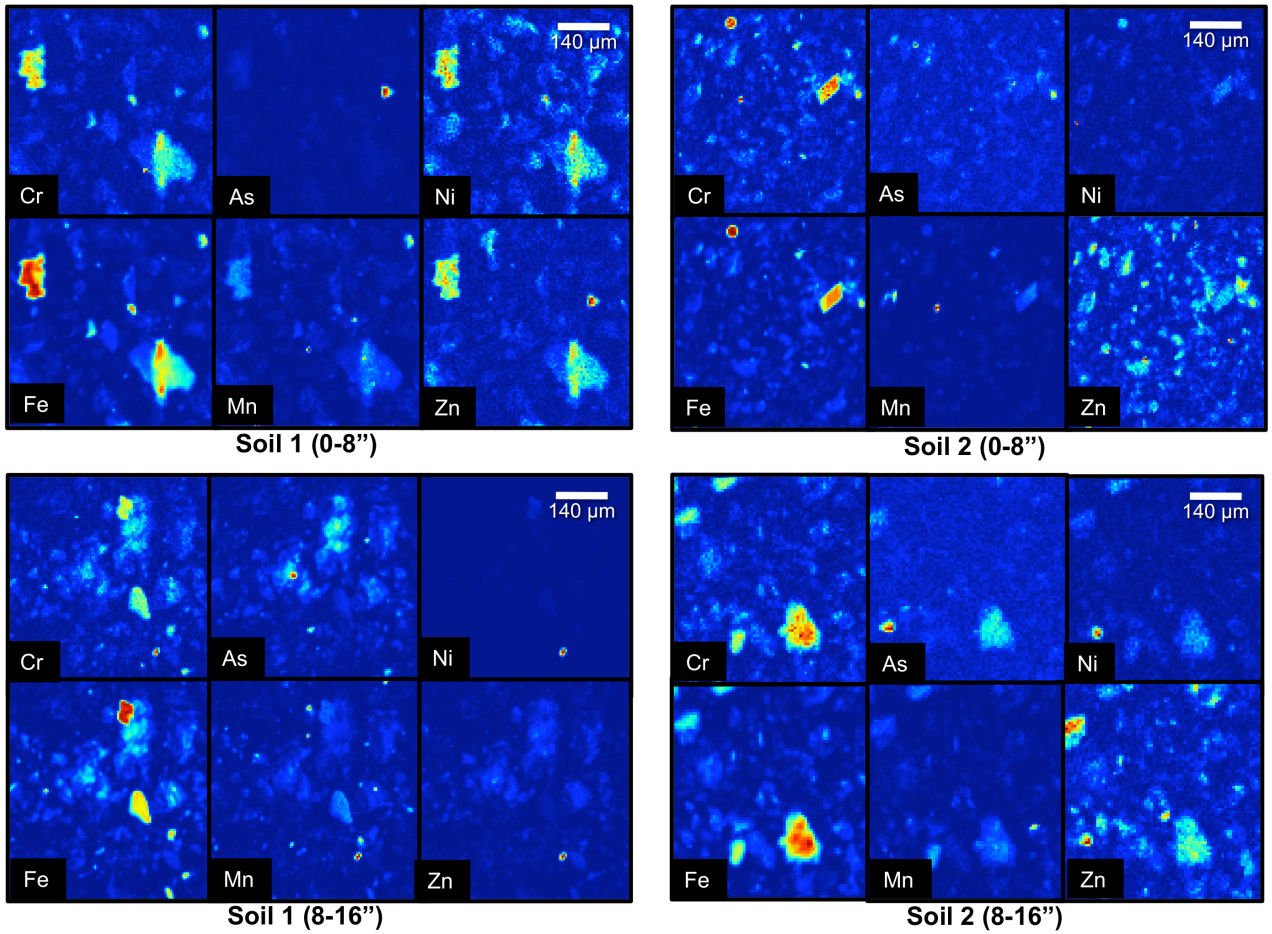


**Figure 4.2** Spatial distribution of Cr, As, Fe, Mn, Zn, and Ni in Soil 1 & 2 at depths of 0-8" and 8-16" below the surface. The colors represent elemental concentrations, with blue< yellow<red.

sorbed to the soil. Chemical extraction procedures have been extensively employed to determine elemental distribution of arsenic and chromium in contaminated solid (Cancès *et al.*, 2008; Hopp *et al.*, 2008; Yang and Donahoe, 2007; La Force *et al.* 2000). However, the accuracy of these techniques is limited, since re-adsorption and redistribution of the target element can occur during the extraction procedures. Therefore, the concentration of the target element can be over or under estimated (Ostergren *et al.*, 1999; Van Herreweghe *et al.*, 2003). Nevertheless, previous studies that employed extraction procedures consistently reported similar As and Cr distribution in soils. Arsenic is often sorbed to Al oxides (Beaulieu *et al.*, 2005; Hopp *et al.* 2008; Vodyanitskii, 2009; Arčon *et al.*, 2005; Szulczewski *et al*., 1997) and/or Fe oxides (La Force *et al*., 2000; Cancès *et al*., 2008; Gao and Schulze, 2010; Vodyanitskii, 2009; Walker *et al*., 2005). Both elements tend to distribute more at superficial depths in contaminated soils (Brett *et al*. 2005, Hopp *et al*. 2008), and they can also sorb to organic matter (Tyrovola and Nikolaidis, 2009; Hopp *et al*. 2008). The distribution of Cr, As, Mn, Fe, Ni, and Zn in Soil 1 & 2 at depth 0-8" and 8-16" is depicted in Figure 4.2. Micro-XRF mapping images show two distinct As and Cr environments; diffused Cr and As concentrations, as well as bright, highly concentrated "hot-spots". Although the diffuse As in the soil seems to be associated with Fe, it does not seem to associate with the other elements measured by $\mu$-XRF at As hot spots, except at a few hot spots (in some $\mu$-XRF maps of Soil 1 & 2, not shown in Figure 4.2), and for zinc, as indicated by As and Zn bright hot spots in the maps of Soil 1 at 0-8" and Soil 2 at 8-16" (Figure 4.2). The association between As and Zn is well known. For instance, the two elements can sorb to the same mineral phases, e.g.,

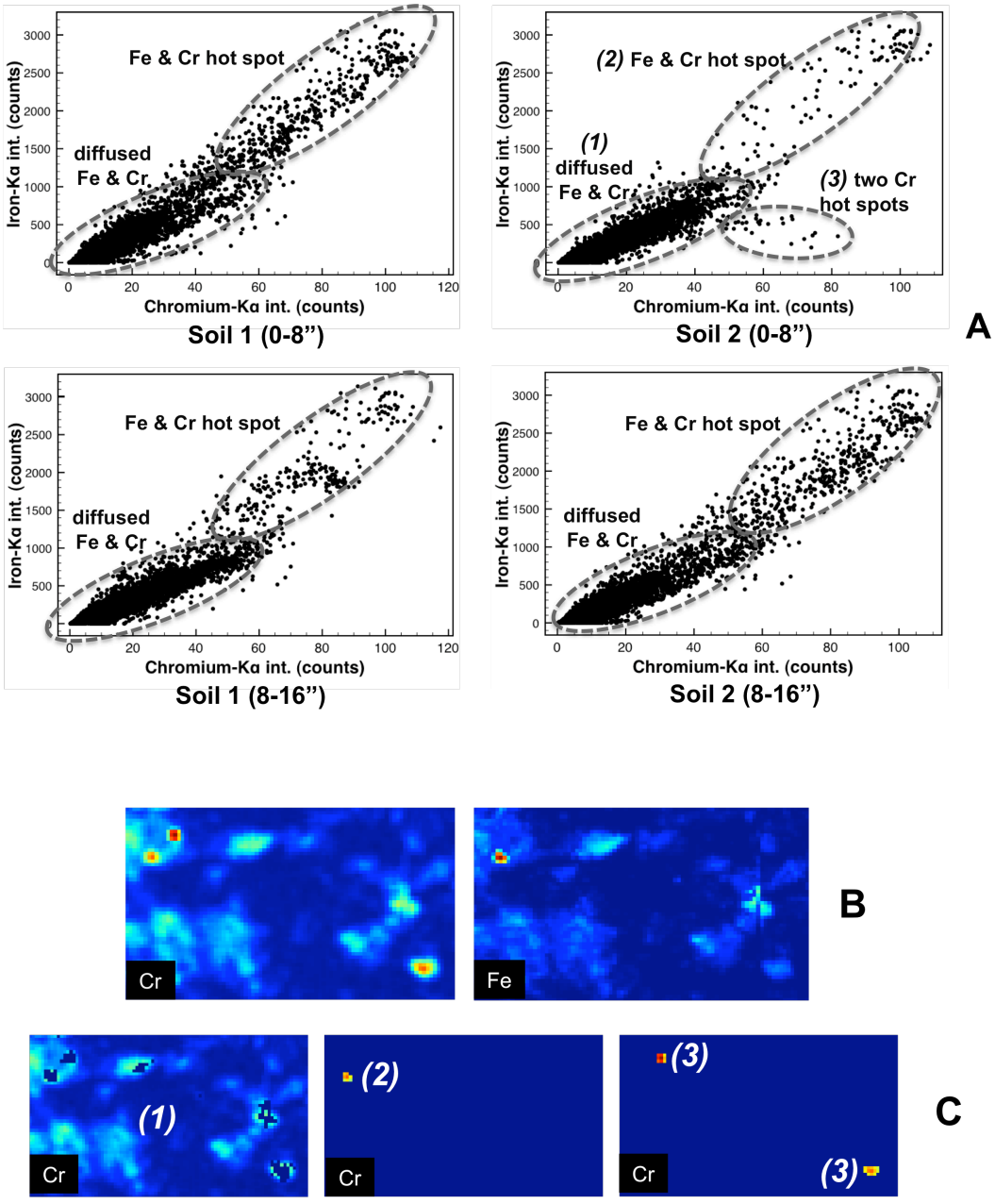


**Figure 4.3** (A) Cr and Fe correlation plots: Cr-Kα intensities over the Fe-Kα intensities per pixel in μ-XRF maps of Soil 1 & 2 at 0-8" and 8-16"; (B) Cr and Fe μ-XRF maps used to make the correlation plot of soil 2 at 0-8" depicted in (A); and (C) Reconstructed Cr μ-XRF maps after selecting with SMAK three sets of points -labeled (1), (2), and (3)- from the correlation plot of soil 2 at 0-8" depicted in (A)

gibbsite or goethite (Gräfe *et al*., 2004), or As can sorb to a Zn-bearing mineral, like hemimorphite (Mao *et al*., 2010). The distribution of Cr is correlated with the distribution of Fe in all $\mu$-XRF maps of Soil 1 & 2, for both diffuse Cr and Cr at hot spots. Figure 4.3 (A) shows the Cr-K$\alpha$ intensities per pixel in each $\mu$-XRF map of Soil 1 & 2 at 0-8" and 8-16", over the Fe-K$\alpha$ intensities. One command featured in Sam's Microprobe Analysis Kit (SMAK), the software written by Dr. Sam Webb to analyze data collected at beamline 2.3, enabled us to select sets of points in the correlation plots shown in Figure 4.3 (A), to reconstruct a Cr $\mu$-XRF map with each selected set of points. This command thus enables one to locate the different Cr phases in the $\mu$-XRF maps. Figure 4.3 (A) shows that two Cr phases, a diffuse Cr phase ubiquitously present in the $\mu$-XRF maps, and a Cr phase located at Cr hot spots, that also contain iron, are present in the $\mu$-XRF maps used to make the correlation plots of Soil 1 at the two depth profiles, and Soil 2 at 8-16" in Figure 4.3 (A). The $\mu$-XRF map used to make a correlation plot of Soil 2 at 0-8" in Figure 4.3 (A) features three Cr phases; a diffuse Cr phase ubiquitously distributed in the $\mu$-XRF map, and two phases that are located at Cr hot spots. One is a Cr hot spot that is also a Fe hot spot (Figure 4.3 (B)), and the second phase is located at two Cr hot spots that contain lower concentrations of Fe. Therefore, these results suggest that chromium in the soil is present in several forms, including those containing Cr and Fe. These results support those reported in previous studies that addressed the distribution of Cr in soils. These studies showed that chromium(III) can sorb to iron oxides (Hopp *et al.*, 2008; Vodyanitskii, 2009), or co-precipitate with iron (Charlet and Manceau, 1992; Hansel *et al*., 2002).

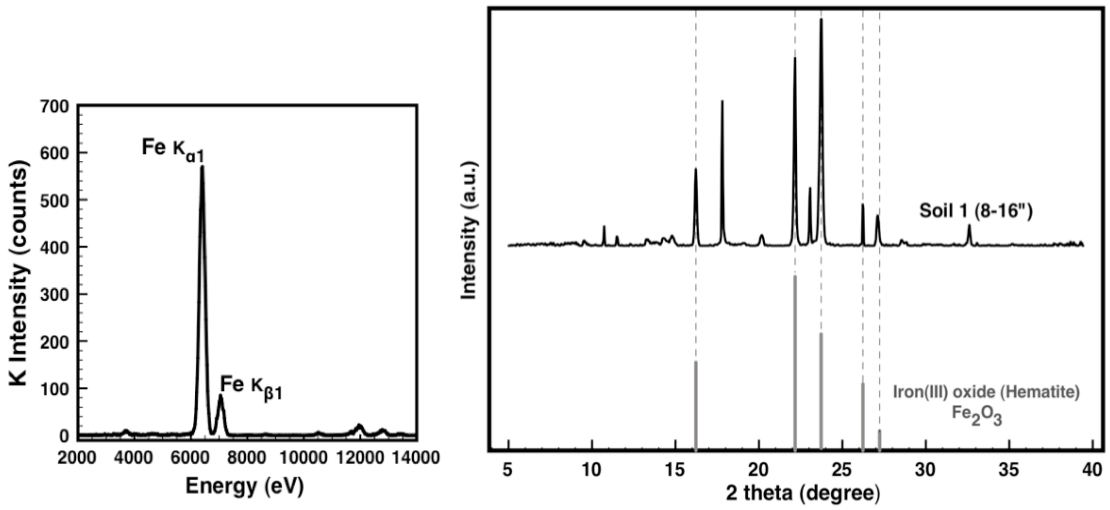


**Figure 4.4** (A) Multichannel analysis of As, Cr, Fe, Ni, S, Zn, and Ti, and (B) and μ-XRD, taken at one hot spot containing As, Cr, and Fe, in one of the μ-XRF maps of Soil 1 at 8-16".

Although arsenic is associated mainly with Zn, and to a minor extent with Fe, at hot spots in all $\mu$-XRF maps of Soil 1 & 2, As is also associated with Cr and Fe at some hot spots. The multichannel analyzer (MCA) pattern depicted in Figure 4.4 (A) and the $\mu$-XRF pattern in Figure 4.4 (B) were collected at one of these hot spots that feature As, Cr, and Fe. A high intensity of the Fe Kα1 is measured with the MCA, which collected the intensity of As, Cr, Fe, Ni, S, Zn, and Ti. The intensity of Fe Kα1 is so high in the MCA pattern that the As Kα1 is barely seen at 10,543.72 eV, and the Cr Kα1 is not detected at 5,414.72 eV. Therefore, a pure iron phase is probably present at this location. Distinct mineral phases other than quartz could not be identified from most μ-XRD patterns taken at As or Cr hot spots in all μ-XRF maps of

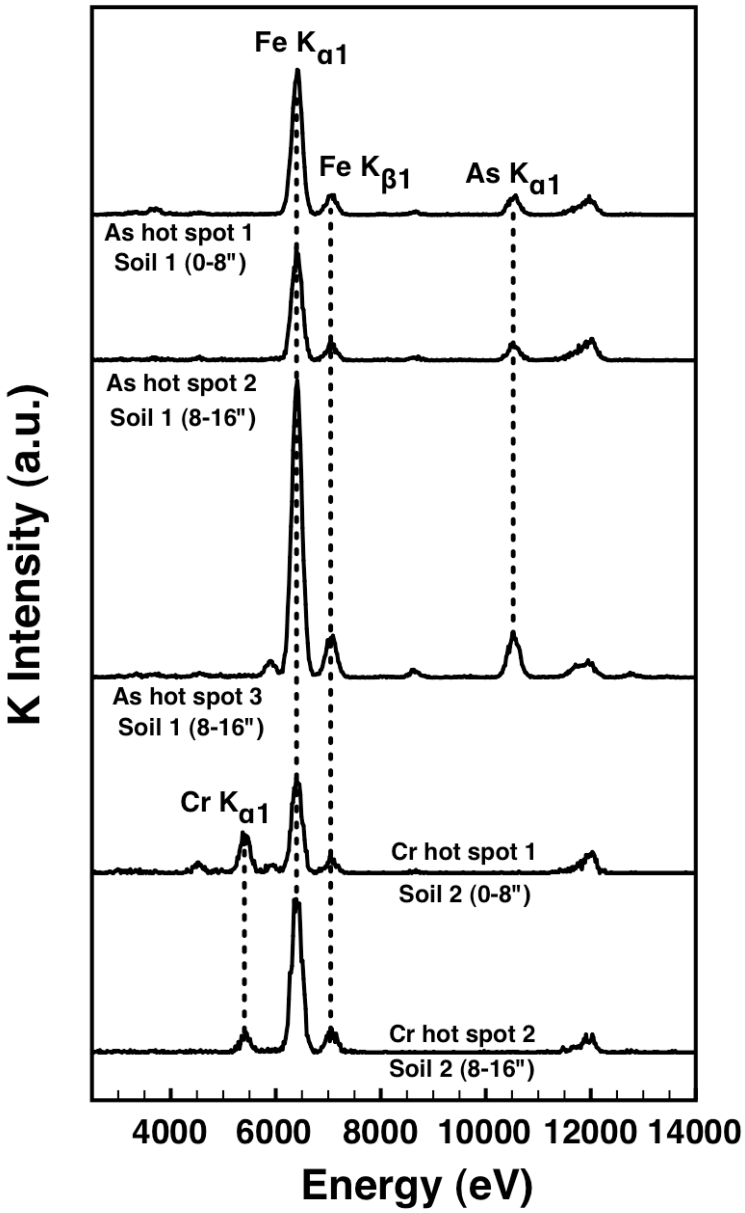


**Figure 4.5** Multichannel analyzer pattern of As, Cr, Fe, Ni, S, Zn, and Ti, taken at two Cr hot spots, and three As hot spots

Soil 1 & 2, perhaps due to the lack of crystallinity of the phases, or the concentrations were too low for μ-XRD analysis. However, the μ-XRD of the spot whose MCA pattern is depicted in Figure 4.4 (A) gave very bright diffraction peaks that were suitable for analysis. The XRD pattern matches well with the pattern of hematite ($Fe_2O_3$) (Figure 4.4 (B)). Therefore, arsenic and chromium may be sorbed to Fe(III) oxide at this location. Many MCA patterns taken at other Cr and As hot spots look similar to the one shown in Figure 4.4 (A). Although the $\mu$-XRD patterns at those hot spots did not feature distinct mineral phases other than quartz, their MCA patterns featured a high Fe Kα1 and distinct Cr Kα1 or As Kα1 peaks. Therefore, the mineral phases present at other Cr and As hot spots, like for example the two chromium hot spots and three arsenic hot spots whose MCA patterns are depicted in Figure 4.5, may feature Fe oxides. Chromium and arsenic may be present as pure amorphous phases or sorbed to these Fe phases, which are less concentrated and/or less crystalline than the hematite phase identified in Figure 4.4 (B). Different types of Cr and As sorption to Fe oxides may exist. No pure Cr phase was identified in the $\mu$-XRD pattern taken at a Cr hot spot (Figure 4.6 (B)), although a significant amount of Cr was present at this location, according to the MCA pattern depicted in Figure 4.6 (A), which shows that the Cr Kα1 peak is about a third the height of the Fe Kα1 peak. Since a Fe(III) oxy hydroxide phase was identified among the mineral phases present at this Cr hot spot (Figure 4.6 (B)), Cr may be sorbed to the surface of this mineral. Although As can sorb to the surfaces of Fe oxides, including hematite (Figure 4.4), this element can be also incorporated in the structure of Fe phases, since a iron(II, III) arsenate phase was identified in the $\mu$-XRD pattern taken at a As hot spot (Figure 4.6 (B)). However,

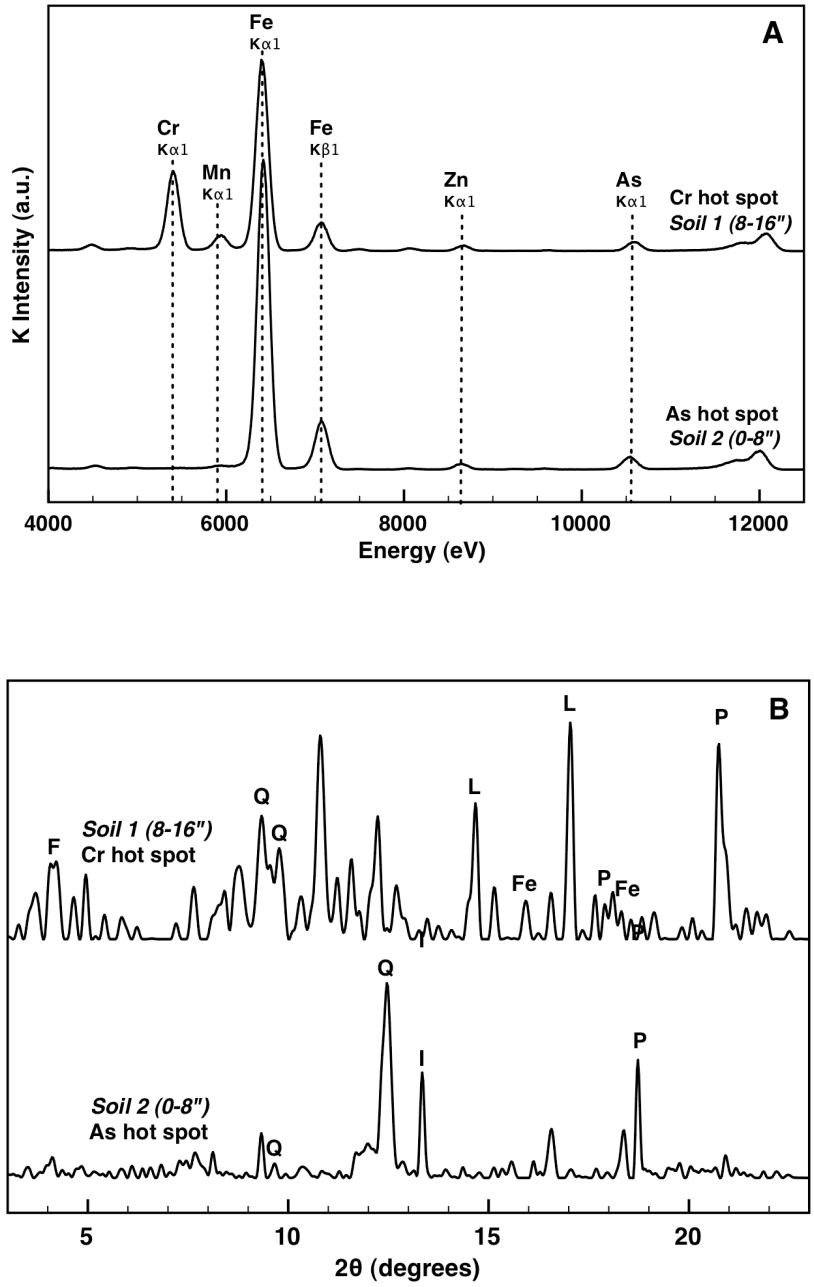


**Figure 4.6** (A) Multichannel analysis of As, Cr, Fe, Ni, Cu, and Zn; and (B) μ-XRD, taken at a Cr hot spot (Soil 1, 8-16"), and a As hot spot (Soil 2, 0-8"). Mineral phases in As hot spot: Q= quartz ($SiO_2$), P=periclase (MgO), I=Iron(II, III) arsenate ($As_6 Fe_7 O_2$); in Cr hot spot: Q= tridymite ($Si_5O_{10}$), F= felsobanyaite ($Al_4SO_{18}H_{18}$), P= periclase (MgO), L= lime (CaO), Fe= iron(III) oxide hydroxide- δ-Feroxyhyte (FeOOH)

since aluminum could not be measured by $\mu$-XRF, it is possible that Al phases also play a role in Cr and As speciation in the Christiana Park soils. The relationship between Al and the distributions of As in the soil is assessed by bulk x-ray absorption fine structure (Section 4.4.4).

Manganese associates with As and Cr only in the regions where these three elements are diffusely distributed, based on Figure 4.2 and in all $\mu$-XRF maps of Soil 1 & 2 that were collected, and does not appear to associate with As and Cr at Mn hot spots. The small amount of manganese in Soil 1 & 2, relatively compared to Al and Fe (Appendix B), suggests that Mn oxides are not present in the soil as Fe oxides. Therefore, chromium probably associates more with iron oxides than manganese oxides, which implies that Cr(VI) is not likely to form in soil, since this element can be naturally produced by manganese oxides when they react with Cr(III) (Fendorf and Zasoski, 1992; Weaver and Hochella, 2002) . Additionally, Cr(VI) in the soil is likely reduced to Cr(III), since Fe(II) oxides can reduce chromate (He and Traina, 2005).

### 4.4.3 Cr and As Oxidation States

The oxidation states of As and Cr were measured by $\mu$-XANES at several Cr and As hot spots found in the $\mu$-XRF maps of Soil 1 at 8-16" and Soil 2 at 0-8" and 8-16" below surface (Figure 4.7). No $\mu$-XANES spectrum was collected in Soil 1 at 0-8", since the concentrations of As and Cr at this depth are less than 10 ppm (Figure 4.1). Since all $\mu$-XANES shown in Figure 4.7 (A) do not feature a pre-edge feature at 5993.5 eV characteristic of Cr(VI) (Peterson *et al.*, 1992), Cr(III) is present at each hot spot analyzed. The shape of the XANES spectra can give information about the nature

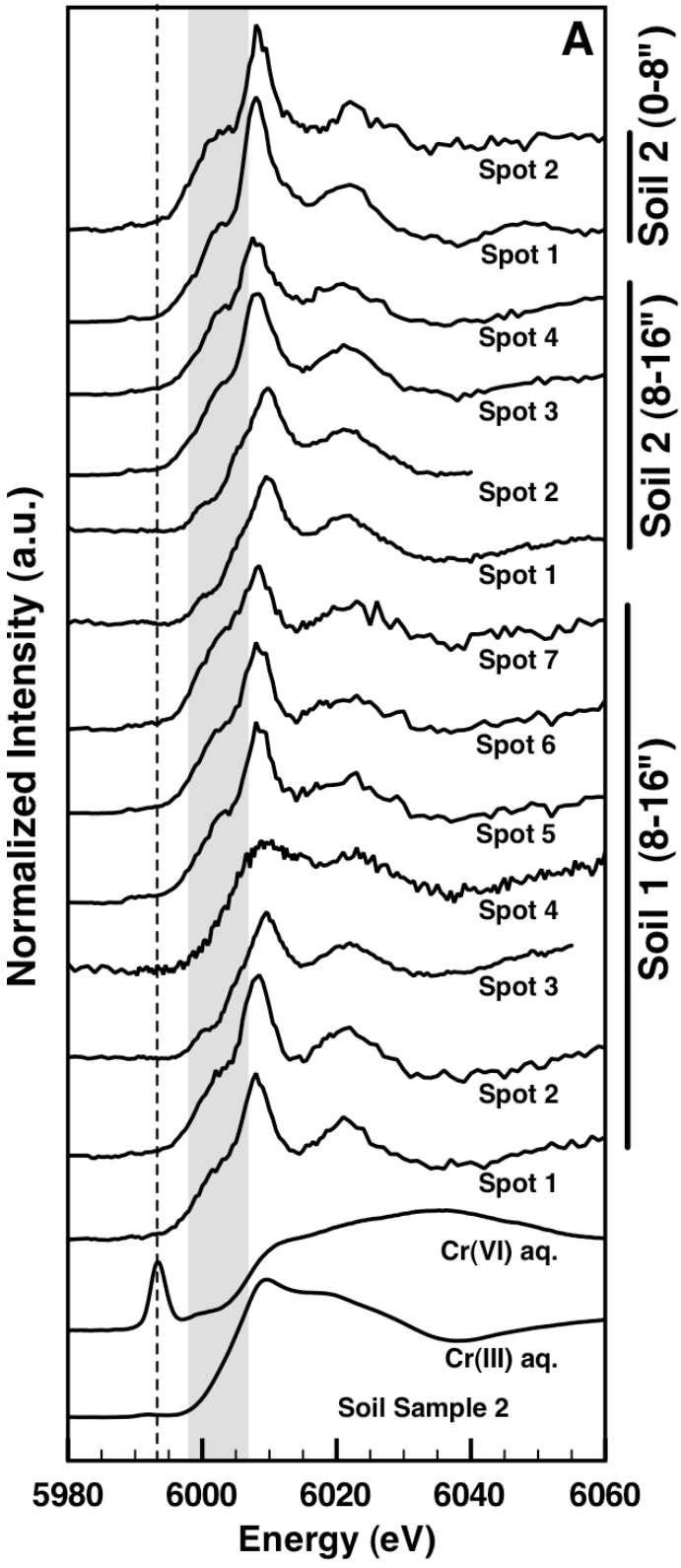
A
Spot 2
Spot 1
Spot 4
Spot 3
Spot 2
Spot 1
Spot 7
Spot 6
Spot 5
Spot 4
Spot 3
Spot 2
Spot 1
Cr(VI) aq.
Cr(III) aq.
Soil Sample 2
Soil 2 (0-8")
Soil 2 (8-16")
Soil 1 (8-16")
Normalized Intensity (a.u.)
5980
6000
6020
6040
6060
Energy (eV)

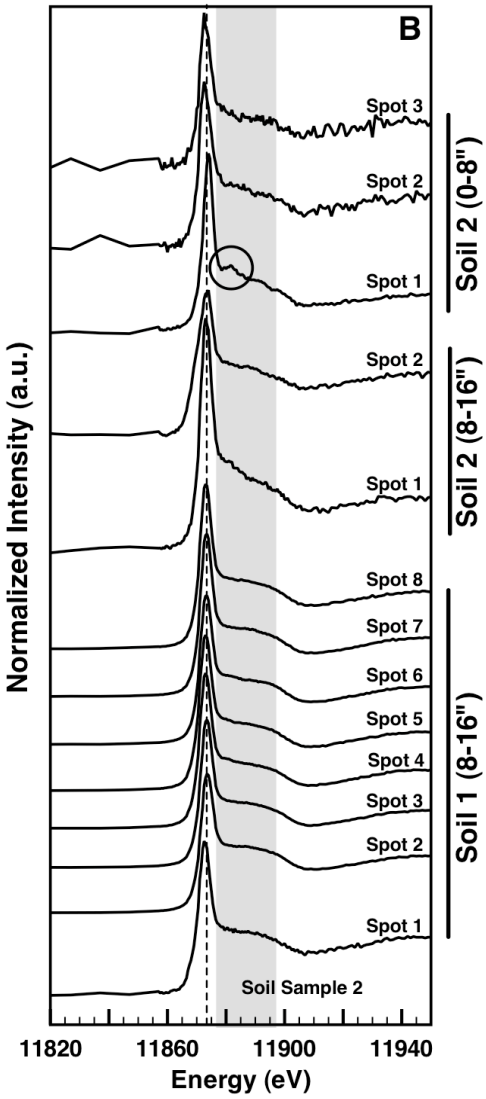


**Figure 4.7** (A) Normalized μ-XANES at the Cr K-edge taken at several Cr hot spot in Soil 1 at 8-16" below the surface and Soil 2 at 0-8"and 8-16" below the surface; and (B) Normalized μ-XANES at the As K-edge taken at several As hot spots in Soil 1 at 8-16" below the surface and Soil 2 at 0-8"and 8-16" below the surface. Grey stripe in A: highlight of the pre-white line region or the spectra; dashed line in A: position of the Cr(VI) pre-edge feature at 5993.5 eV; grey stripe in B: highlight of the post-white line region of the spectra; dashed line: position of the As(V) white line standard at 11874 eV; and circle: highlight of a post-white line feature

of the Cr(III) phase. Several $\mu$-XANES spectra shown in Figure 4.7 (A), for instance Spot 2 in Soil 2 (0-8"), feature a sharp white line, and a hump at half the height of the white line, at 6002 eV (grey stripe in Figure 4.7 (A)). These features are characteristic of a chromite ($FeCr_2O_4$) XANES standard spectrum (Werner *et al.*, 2007; Peterson *et al.*, 1997). Since chromite is a Cr ore, which can be naturally found in Delaware, Pennsylvania, and Maryland (Pearre and Heyl, 1960), the sources of Cr(III) at these hot spots may not be anthropogenic. However, some $\mu$-XANES spectra in Figure 4.7 (A) look different than the spectrum of chromite, i.e. the $\mu$-XANES spectra of spot 1 & 2 in Soil 2 at 8-16" and spot 3 in Soil 1 at 8-16", and feature a hump at about a fifth the height of the white line. Additionally, the $\mu$-XANES spectrum of spot 4 in Soil 1 at 8-16" does not feature a sharp white line like in the other spectra, and looks similar to the XANES spectrum of Cr-bearing goethite (Frommer *et al.*, 2009). Therefore, our results suggest that different mineral phases containing Cr(III) are present in the soil, and some of them may also contain Fe.

The position of the inflection point of the first derivative of each $\mu$-XANES shown in Figure 4.7 (B) is located at about 11874 eV, which means that As(V) is present at each hot spot analyzed (Ginder-Vogel *et al.*, 2009). The region located at the high-energy side of the white line (grey area in Figure 4.7 (B)) in the XANES spectra taken at the As K-edge can give insight into the mineral phase in which As is present (Cancès, *et al.*, 2005). If this region exhibits significant features, As is included in the structure of crystalline phases. Conversely, if the region does not possess any feature, As is sorbed to mineral phases or co-precipitated with other elements. The latter case corresponds to what we observe in our data since most $\mu$-XANES spectra shown in Figure 4.7 (B) do not exhibit any feature at the high-energy

side of the white line (region in the grey area in Figure 4.7 (B)). However, since the $\mu$-XANES spectrum of spot 1 in Soil 2 at 0-8" features a hump at about 11885 eV (encircled in Figure 4.7 (B)), As may be included in crystalline mineral phases at this location. Therefore, our results suggest that, similarly to Cr, As is present in the soil in various chemical environments.

### 4.4.4 Molecular Environment of As: Bulk Soil Analyses

The concentrations of Cr in all soil samples collected in Christiana Park were not high enough for bulk-XAFS analysis at beamline 11.2, which requires a few hundred of ppm of Cr, since the highest concentration found in our samples was 115 ppm. Additionally, the concentrations of As in Soil 1 at 0-8" and Soil 2 at 8-16" (14 and 21 ppm, respectively) were not high enough for bulk-XAFS analysis. Therefore, bulk-XAFS analyses were conducted only on Soil 1 at 8-16" below the surface and Soil 2 at 0-8" that had a concentration of 985 and 50 ppm, respectively. The energy positions of the XANES first derivative's inflection points of the two soil samples and the As(V) standard were similar to each other (Figure 4.8), meaning that arsenate is the main form of As in the two soil samples. To identify the As standards needed for linear combination fitting of the two soil sample EXAFS spectra, Principal Component Analysis (PCA) and target transform analysis could not be applied, since a minimum of three components (i.e. number of samples) is needed for PCA analysis. Therefore, the choice of standards used for linear combination fitting was based on a knowledge of Christiana Park's history, observations made from $\mu$-XRF maps, and the fact that these standards must contain As(V), due to the results from $\mu$-XANES and bulk-XANES analyses. The As standards considered were lead arsenate ($PbHAsO_4$), which used to be a common insecticide at many industrial facilities and farms, some

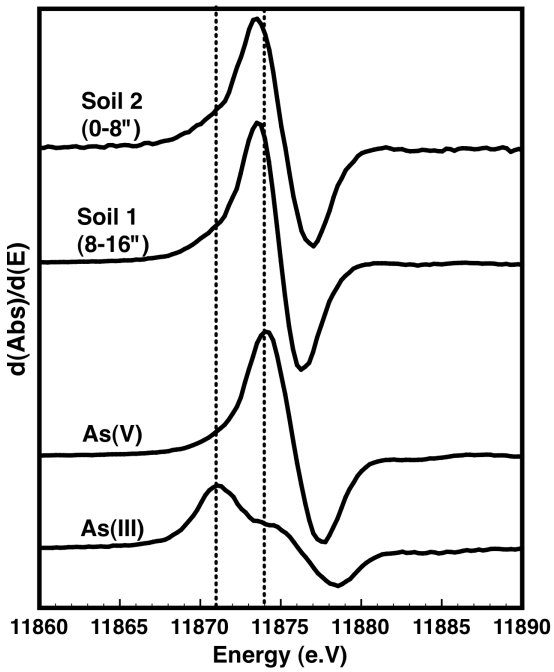


**Figure 4.8** Positions in energy of the XANES first derivative's inflection points of the two soil samples and the As(V) & As(III) standards.

As(V)-bearing minerals, including adamite ($Zn_2AsO_4OH$), chalcophyllite ($Cu_{18}Al_2(AsO_4)_3(SO_4)_3(OH)_{27}$.33H2O), scorodite ($FeAsO_4.2H_2O$), ojuelaite ($ZnFe(AsO_4)_2(OH)_2.4H_2O$), mansfieldite ($AlAsO_4.2H_2O$), alactite ($Mn_7(AsO_4)_2(OH)_8$, and calcium arsenate $Ca_3(AsO_4)_2$. Since As was associated with Zn in many hot spots in the $\mu$-XRF maps of Soil 1 & 2, three oxide standards (gibbsite, silica oxide, and goethite) reacted with 50% As(V) and 50% Zn were also selected, as well as two gibbsite and goethite standards reacted only with As(V). Arsenic(III)-bearing minerals, realgar (AsS) and arsenic trisulfide ($As_2S_3$) were also considered. Since

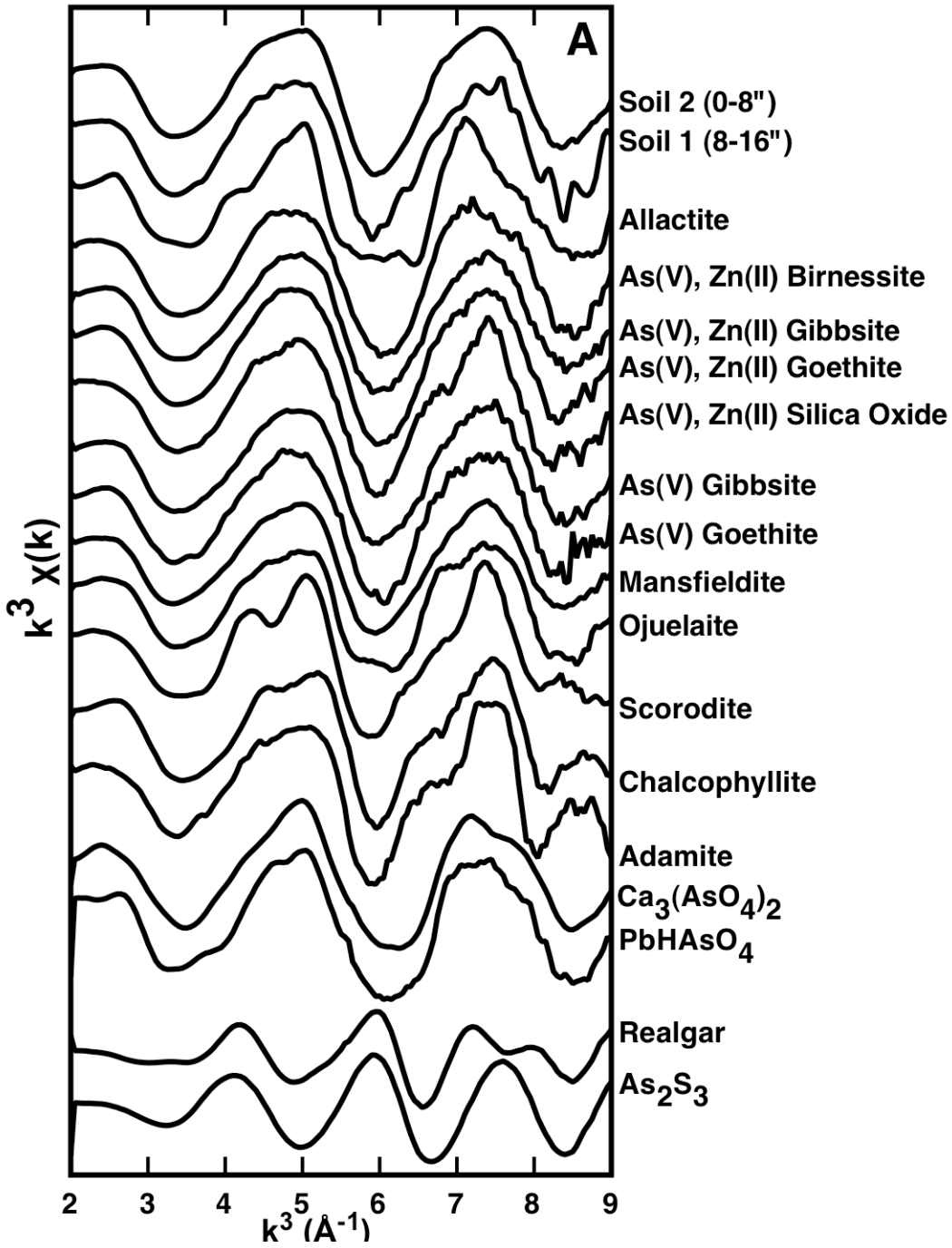
A
Soil 2 (0-8")
Soil 1 (8-16")
Allactite
As(V), Zn(II) Birnessite
As(V), Zn(II) Gibbsite
As(V), Zn(II) Goethite
As(V), Zn(II) Silica Oxide
As(V) Gibbsite
As(V) Goethite
Mansfieldite
Ojuelaite
Scorodite
Chalcophyllite
Adamite
$Ca_3(AsO_4)_2$
$PbHAsO_4$
Realgar
$As_2S_3$
$k^3\chi(k)$
2 3 4 5 6 7 8 9
$k^3$ (Å$^{-1}$)

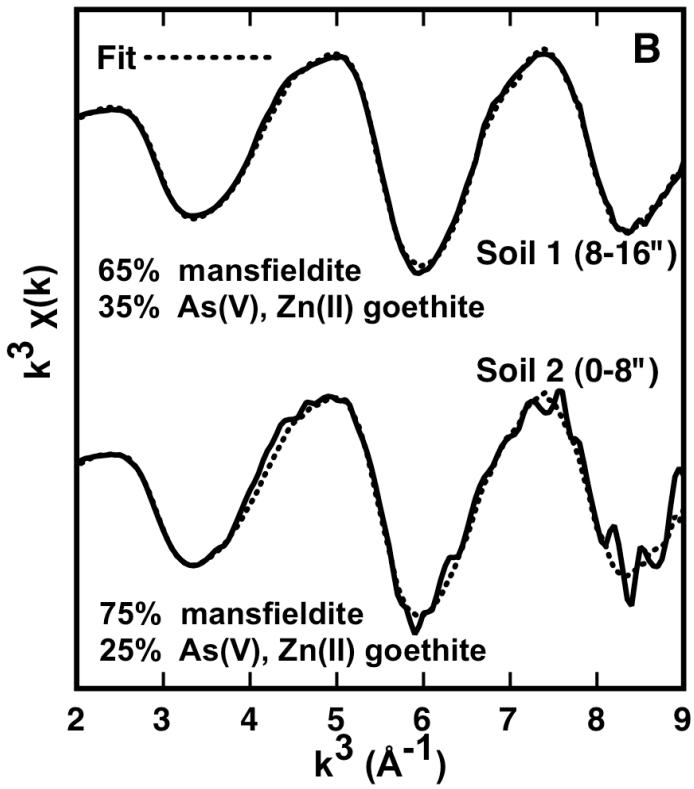


**Figure 4.9** (A) Comparison between the EXAFS spectra of As standards and EXAFS spectra of Soil 1 at 8-16" and Soil 2 at 0-8" (B) linear combination fittings of Soil 1 (8-16") & Soil 2 (0-8")

these chemicals were used during the tanning process until the early 1900's, they were found in the wastes of tanning factories, and thus could have been present in the fill materials that were used to create Christiana Park at the beginning of the 20$^{th}$ century. All these As standards were synthesized by Markus Gräfe, a former member of our laboratory.

After this preliminary selection, the EXAFS spectra of these As standards, which are shown in Figure 4.9 (A), were individually used to fit by linear combination the EXAFS spectrum of Soil 1 at 8-16", in order to find which of these standards gave the lowest linear combination's Reduced $\chi^2$, (Kelly *et al*., 2008). Three As standards gave Reduced $\chi^2$ values significantly lower than the other standards: mansfieldite (Red. $\chi^2$= 0.24), As/Zn-goethite (Red. $\chi^2$= 0.38), and As-gibbsite (Red. $\chi^2$= 0.48). Linear combination fitting on Soil 1 at 8-16" with mansfieldite & As/Zn-goethite gave a lower Reduced $\chi^2$ value (Red. $\chi^2$= 0.16), compared to when the mansfieldite standard is used individually to fit the data (Red. $\chi^2$= 0.24). This was not the case when mansfieldite & Al-gibbsite were used to fit the data (Red. $\chi^2$= 0.22). Additionally, linear combination using mansfieldite, As/Zn-goethite, and As-gibbsite did not decrease the Reduced $\chi^2$ value (Red. $\chi^2$= 0.16), compared to when the mansfieldite & As/Zn-goethite standards are used to fit the data (Red. $\chi^2$= 0.16). Therefore, the EXAFS spectra of mansfieldite & As/Zn-goethite were used to fit by linear combination the EXAFS spectrum of Soil 1 (8-16"). The same approach, based on Reduced $\chi^2$ value comparisons (Kelly *et al*., 2008), was used with Soil 2 (8-16") to determine which As standards are needed to fit by linear combination the data. Similarly to the first soil sample, the EXAFS spectra of mansfieldite & As/Zn-goethite were the best set of standards to do least squares fitting of the EXAFS spectrum of the second soil sample. The results of the linear combinations are depicted in Figure 4.9 (B). The mansfieldite standard contributes to a major part of the fits (at least 65%). The presence of this mineral, which is rarely found in nature (Allen *et al*., 1948), has never been reported in the soil of Delaware. Therefore, the mineral present in Christiana Park could be a phase that contains both As and Al, whose EXAFS

spectrum is similar to the one of mansfieldite. A former study showed that a three dimensional alumino-arsenate precipitate, whose EXAFS spectrum is also similar to the one of mansfieldite, can form when As(V) is sorbed to $\gamma$-$Al_2O_3$ for a long period of time (a few months) (Arai and Sparks, 2002). Therefore, the precipitate reported in this former study could be present in our two soil samples, since $\gamma$-$Al_2O_3$ is ubiquitously found in the environment. The contribution of the As-Zn goethite in the linear combination fits is consistent with our observations made from the $\mu$-XRF maps and the MCA analyses at As hot spots, which showed that As, Zn, and Fe can be present at the same location.

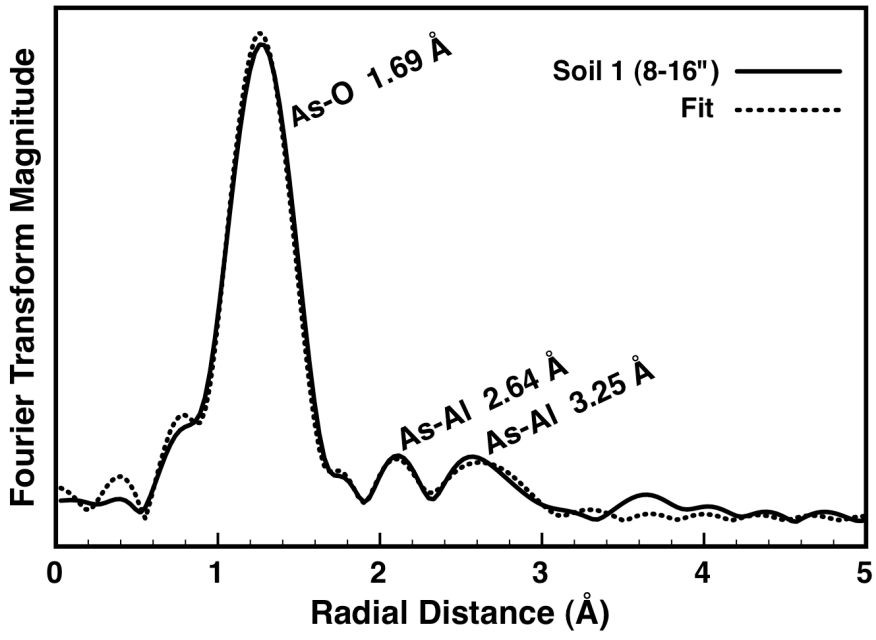


**Figure 4.10** Fourier Transform EXAFS of Soil 1 (8-16")

**Table 4.1** Shell-by-shell fitting parameters of Soil 1 (8-16”), and comparison to results from two previous studies (see text). CN= coordination number; $\sigma^2$= Debye-Waller factor; R= radial distance, in Å

| | | *shells* | | | | | | | | | | | |
|---|---|---|---|---|---|---|---|---|---|---|---|---|---|
| | ΔE0 | type | CN | $\sigma^2$ | R (Å) | type | CN | $\sigma^2$ | R (Å) | type | CN | $\sigma^2$ | R (Å) |
| Soil 1 8-16" | 7(1) | As-O | 5.1(4) | 0.003(1) | 1.69(1) | As-Al | 3.7(2.3) | 0.02(1) | 2.64(5) | As-Al | 3.2(2.7) | 0.003(3) | 3.24(6) |
| As-contaminated soil *(Arčon et al., 2001)* | -4(1) | As-O | 4.2(2) | 0.002(3) | 1.69 (1) | As-Al | 1.7(4) | 0.009(5) | 2.54(2) | Al-Fe | 1.6 (8) | 0.006(3) | 3.34(2) |
| mansfieldilte *(Arai & Sparks, 2001)* | 4(1) | As-O | 5.1(1.0) | 0.003 | 1.68(2) | | | | | As-Al | 2.95 (9) | 0.006* * *fixed* | 3.15(.13) |

Shell-by-shell fitting was only performed on Soil 1 at 8-16", due to its high As concentration (985 ppm) compared to those of Soil 1 at 0-8", and Soil 2 at 0-8" and 8-16", which were all below 51 ppm. Figure 4.10 shows the Fourier Transform EXAFS spectrum of the soil sample and the fitted spectrum, and Table 4.1 the fitting parameters, which are compared to those from two previous studies. One of the studies showed that the coordination number of the first As-O shell, in a system where As(V) is sorbed to aluminum oxides for a long period of time at pH 4.5 or 7.8, varies from 5.38 (3 days of reaction period) to 5.03 (11 months of reaction period) at pH 4.5, and from 5.47 (3 days of reaction period) to 5.10 (11 months of reaction period) at pH 7.8 (Arai and Sparks, 2002). Therefore, these values were similar to the coordination number of the first As-O shell found in our soil sample, i.e. CN= 5.1±4 (Table 4.1), the latter being higher than the coordination number of As-O ligand in the arsenate ion (CN=4). Arsenic is surrounded by a shell of aluminum atoms in our soil sample, with an As-Al radial distance of 2.64 Å. This value corresponds to the radial distances reported for a bidendate mononuclear complex observed for arsenate sorption to aluminum oxides, i.e. 2.07-2.64 Å (Arai and Sparks, 2002). Similarly, a previous study showed that As present in a contaminated soil was sorbed to Al (hydr)oxides in a bidendate mononuclear complex **(**Arčon *et al.***,** 2002). This study also found that As was surrounded by Fe atoms, with a Al-Fe distance of 3.34 Å. Although As is surrounded by a shell of atoms at 3.24 Å in Soil 1 at 8-16" (Table 4.1), which is thus similar to 3.34 Å, the best fit was obtained with an As-Al shell. Fitting the data with an As-Fe shell gave an unrealistic Debye-Waller value and coordination number for the shell. An As-Al shell with a distance of 3.24 corresponds both to the distance of As sorbed to aluminum oxide in a bidendate-binuclear complex (3.03-3.41 Å), and to the

Al-As distance in mansfieldite (3.15±13 Å) (Arai and Sparks, 2002). Therefore, although it is impossible to determine from the parameters of this shell if As is sorbed to aluminum oxides or included in a mineral that has a composition and a structure similar to mansfieldite, these results suggest that As is mainly immobilized in Al phases in Soil 1 at 8-16", which support the linear combination fitting results.

## 4.5 Conclusions

Chromium is mainly associated with iron in Soil 1 and 2, since these two elements were systematically distributed together in the regions where the concentrations of Cr and Fe were diffuse, and at hot spots where these two elements were present at high concentrations. The μ-XRD and MCA analyses performed at hot spots suggest that Cr may be naturally part of Fe-bearing minerals, or sorbed to Fe oxides in Soil 1 & 2, which is in agreement with several previous studies that showed that Fe oxides in soils are strong chromium scavengers. Therefore, if chromate, the most toxic form of chromium, is present in the soil, it is likely to undergo reduction, since Fe oxides can reduce Cr(VI) to Cr(III). Additionally, macroscopic observations from Soil 1 & 2 suggest that Cr(III), which is less toxic and mobile than Cr(VI), is not likely to be oxidized to Cr(VI) by manganese oxides, since the association between Mn and Cr was only observed in the μ-XRF maps at regions where the concentrations of these two elements were diffuse. Therefore, if tannery waste materials containing Cr(VI) were introduced in Christiana Park last century, a major part of chromate present in those wastes has been probably reduced to Cr(III) by iron oxides over the years, and perhaps also by other Cr(VI) reducers, including organic matter. This hypothesis is supported by the μ-XANES analyses taken at several Cr hot spots in Soil 1 & 2, showing that only Cr(III) is present in these locations. Therefore, the apparent

absence of Cr(VI) in the soil, the lack of high concentrations of Cr measured at different locations in Christiana Park, the distribution of Cr in the soil, and its association with other elements that can potentially affect its chemical properties, suggest that the presence of Cr in the recreation park does not pose a potential threat to the public. However, high concentrations of As were measured in the park. These concentrations exceeded by far the background level of arsenic in Delaware soils (i.e. 11 ppm). Results obtained from synchrotron-based spectroscopy suggest that arsenic is sorbed to aluminum oxides, or included in a Al-As precipitate phase similar to mansfieldite. The latter hypothesis is supported by the results from EPA's TCLP and SPLP tests, in which little As was desorbed from Soil 1 & 2. Additionally, the μ-XRD and MCA analyses conducted at hot spots suggest that As might be also sorbed to iron oxides to a minor extent, which is also supported by EXAFS linear combination fitting. Therefore, our results are in good agreement with previous studies that showed that Al and Fe phases control the distribution of As in contaminated soils. The environmental factors affecting the stability of these phases need to be determined, to better assess the potential risk to humans of As present at high concentrations in the soil. Although remedial action in Christiana Park was finally completed in 2008, which consisted of installation of a one-foot clean protective barrier on top of a geo-textile demarcation fabric across the entire site, As could still diffuse to other areas near the park, or leach to the groundwater, if the mineral phases containing this heavy metal would happen to become unstable. Additionally, the speciation and mobility of Pb, which is present in the park at high concentrations, should be also assessed.

## 4.6 References


Allen, V. T., Fahey, J. J., and Axelrod, J. M. (1948), Mansfieldite, a new arsenate, the aluminum analogue of scorodite, and the mansfieldite scorodite series, American Mineralogist, 33, 122-134.

Arai, Y. and Sparks, D. L. (2002), Residence time effects on arsenate surface speciation at the aluminum oxide-water interface, Soil Science, 167, 303-314.

Arčon, I., Van Elteren, J. T., Glass, H. J., Kodre, A., and Slejkovec, Z. (2005), EXAFS and XANES study of arsenic in contaminated soil, X-ray Spectrometry, 34, 435-438.

Beaulieu, B. T. and Savage, K. S. (2005), Arsenate adsorption structures on aluminum oxide and phyllosilicate mineral surfaces in smelter-impacted soils, Environmental Sciences and Technology, 39, 3571-3579.

Bhattacharya, P., Mukherjee, A. B., Jacks, G., and Nordqvist, S. (2002), Metal contamination at a wood preservation site: characterisation and experimental studies on remediation, Science of the Total Environment, 290, 165-180.

Cancès, B., Juillot, F., Morin, G., Laperche, V., Alvarez, L., Proux, O., Hazemann, J.-L., Brown Jr., G. E., and Calas, G. (2005), XAS evidence of As(V) association with iron oxyhydroxides in a contaminated soil at a former arsenical pesticide, processing plant, 39, 9398-9405

Cancès, B., Juillot, F., Morin, G., Laperche, V., Polya, D., Vaughan, D. J., Hazemann, J.-L., Proux, O., Brown Jr., G. E., and Calas, G. (2008), Changes in arsenic speciation through a contaminated soil profile: A XAS based study, Science of the Total Environment, 397, 178-189.

Charlet, L. and Manceau, A. (1992), X-Ray adsorption spectroscopy study of the sorption of Cr(III) at the oxide-water Interface. II. Adsorption, coprecipitation, and surface precipitation on hydrous ferric interface, Journal of Colloid and Interface Science, 148, 443-468.

Fendorf, S. E., Fendorf, M., and Sparks, D. (1992), Inhibitory mechanisms of Cr(III) oxidation by δ-$MnO_2$. Journal of Colloid and Interface Science, 153, 37-54.

Fendorf, S. and Guangchao, L. (1996), Kinetics of chromate reduction by ferrous iron, Environmental Sciences and Technology, 30, 1614-1617.

Frommer, J., Nachtegaal, M., Czekaj, I., Weng, T. C., and Kretzschmar, R. (2009), X-ray absorption and emission spectroscopy of CrIII (Hydr)Oxides: Analysis of the K-pre-Edge region, Journal of Physical Chemistry A, 113, 12171-12178.

Gao, X. and Schulze, D. G. (2010), Chemical and mineralogical characterization of arsenic, lead, chromium, and cadmium in a metal-contaminated Histosol, Geoderma, 156, 278-286.

Ginder-Vogel, M., Fischel, J., Landrot, G., and Sparks, D. L. (2009), Quantification of rapid environmental redox processes using quick scanning x-ray absorption spectroscopy (Q-XAS), Proceedings of the National Academy of Sciences, 106, 16124-16128.

Gräfe, M., Nachtegaal, M., and Sparks, D. L. (2004), Formation of metal-arsenate precipitates at the goethite-water interface, Environmental Sciences and Technology, 38, 6561-6570.

Hansel, C. M., Wielinga, B. W., and Fendorf, S., E. (2002), Stuctural and compositional evolution of Cr/Fe solids after indirect chromate reduction by dissimilatory iron-reducing bacteria, Geochemica et Cosmochimica Acta, 64, 3, 401-412.

He, T. Y. and Traina, S. J. (2005), Cr(VI) reduction and immobilization by magnetite under alkaline pH conditions: the role of passivation, Environmental Sciences and Technology, 39, 4499-4505.

Hopp, L., Nico, P. S., Marcus, M. A., and Peiffer, S. (2008), Arsenic and chromium partitioning in a Podzolic soil contaminated by chromated copper arsenate, Environmental Sciences and Technology, 42, 6481-6486.

Kelly, S. D., Hesterberg, D., and Ravel, B. (2008), Analysis of soils and minerals using X-ray absorption spectroscopy. In: A.L. Ulery and L.R. Drees, E. (Ed.), Methods of Soil Analysis, Soil Science Society of America, Madison, WI, USA.

La Force, M. J., Hansel, C. M., and Fendorf, S. (2000) Arsenic speciation, seasonal transformations, and Co-distribution with iron in a mine waste-influenced palustrine emergent wetland, Environmental Sciences and Technology, 34, 3937-3943.

Lund, U. and Fobian, A. (1991), Pollution of two soils by arsenic, chromium and copper, Denmark, Geoderma, 49, 83-103.

Mao, M., Lin, J., and Pan, Y. (2010), Hemimorphite as a natural sink for arsenic in zinc deposits and related mine tailings: Evidence from single-crystal EPR spectroscopy and hydrothermal synthesis, Geochimica et Cosmochimica Acta, 74, 2943-2956.

Ostergren, J., Brown Jr., G. E., Parks, G., and Tingle, T. (1999), Quantitative speciation of lead in selected mine tailings from Leadville, CO, Environmental Sciences and Technology, 33, 1627-1636.

Parikh, S. J., Lafferty, B. J., and Sparks, D. L. (2008), An ATR-FTIR spectroscopic approach for measuring rapid kinetics at the mineral/water interface, Journal of Colloid and Interface Science, 320, 177-185.

Pearre, N. C. and Heyl Jr, A. V. (1960), Chromite and other mineral deposits in serpentine rocks of the Piedmont Upland, Maryland, Pennsylvania and Delaware, U .S. Geol. Survey.

Peterson, M. L., Brown, G. E., Parks, G. A., and Stein, C. L. (1997), a. Differential redox and sorption of Cr(III/VI) on natural silicate and oxide minerals: EXAFS and XANES results, Geochemica et Cosmochimica Acta, 61, 3399-4413.

Peterson, M. L., White, A. F., Brown Jr., G. E., and Parks, G. A., (1997), b. Surface Passivation of Magnetite by Reaction with Aqueous Cr(VI): XAFS and TEM Results. Environmental Sciences and Technology, 31, 1573-1576.

Post, J. E. (1999), Manganese oxide minerals: crytal stuctures and economic and environmental significance, Proceedings of the National Academy of Sciences, 96, 7, 3447-3454.

Sparks, D. L. (2003), Environmental Soil Chemistry. Academic Press, San Diego, CA

Szulczewski, M. D., Helmke, P. A., and Bleam, W. F. (2009), Comparison of XANES analyses and extractions to determine chromium speciation in contaminated Soils, Environmental Sciences and Technology, 31, 2954-2959.

Tyrovola, K. and Nikolaidis, N. P. (2009), Arsenic mobility and stabilization in topsoils, Water Research, 43, 1589-1596.

Van Herreweghe, S., Swennen, R., Vandecasteele, C., and Cappuyns, V. (2003), Solid phase speciation of arsenic by sequential extraction in standard reference materials and industrially contaminated soil samples, Environmental Pollution, 122, 323-342.

Vodyanitskii, Y. N. (2009), Chromium and arsenic in contaminated soils (Review of Publications), Eurasian Soil Science, 42, 507-515.

Walker, S. R. and Jamieson, H. E. (2005), The speciation of arsenic in iron oxides in mine wastes from the giant gold mine, N.W.T.: application of synchrotron micro-XRD and micro-XANES at the grain scale, The Canadian Mineralogist, 43, 1205-1224.

Weaver, R. M. and Hochella, M. F. (2003), The reactivity of seven Mn-Oxides with $Cr^{3+}_{aq}$: a comparative analysis of a complex, environmentally important redox reaction, American Mineralogist, 88, 2016-2028.

Werner, M. L., Nico, P. S., Marcus, M. A., and Anastasio, C. (2007), Use of micro-XANES to speciate chromium in airborne fine particles in the sacramento valley, Environmental Sciences and Technology, 41, 4919-4924.

Yang, L. and Donahoe, R. (2007), The form, distribution and mobility of arsenic in soils contaminated by arsenic trioxide, at sites in southeast USA, Applied Geochemistry, 22, 320-341.

## Appendix A

## QUANTITY OF HCL OR KOH ADDED AT THE BEGINNING OF THE BATCH EXPERIMENTS, IN ML

| $Mn(IV)O_2$ | pH 2.5 | pH 3 | pH 3.5 |
|---|---|---|---|
| RSB | 3.5 HCl | 3.5 HCl | 3.5 HCl |
| AB | 0.75 HCl | 0.25 HCl | 0.25 KOH |
| HMO | 1.5 KOH | 2.5 KOH | 3.5 KOH |

## Appendix B

## PH AND CONCENTRATIONS, IN PPM, OF SEVERAL ELEMENTS IN SOIL SAMPLES TAKEN AT EIGHT LOCATIONS IN CHRISTIANA PARK, AND AT DEPTH 0-8 INCHES AND 8-16 INCHES BELOW THE SURFACE

| Sample | pH | As | Pb | Cr | Mn | Al | Fe | K | Mg | Ni | P | S | Zn | Cu |
|---|---|---|---|---|---|---|---|---|---|---|---|---|---|---|
| soil 8, 0-8" | 6.4 | 24 | 60 | 21 | 235 | 7255 | 9610 | 705 | 5549 | 8 | 373 | 177 | 111 | 25 |
| soil 8, 8-16" | 6.4 | 72 | 1156 | 43 | 517 | 14695 | 20367 | 1395 | 16848 | 19 | 716 | 322 | 243 | 66 |
| soil 7, 0-8" | 7.1 | 65 | 143 | 43 | 492 | 16807 | 21728 | 2184 | 13035 | 20 | 835 | 307 | 192 | 55 |
| soil 7, 8-16" | 8.5 | 54 | 572 | 29 | 315 | 11032 | 18227 | 1180 | 9415 | 15 | 506 | 326 | 190 | 50 |
| soil 6, 0-8" | 5.7 | 8 | 34 | 39 | 193 | 18604 | 28584 | 1835 | 3335 | 14 | 439 | 86 | 83 | 34 |
| soil 6, 8-16" | 5.7 | 23 | 121 | 58 | 436 | 17395 | 28469 | 1994 | 3717 | 20 | 737 | 387 | 210 | 60 |
| soil 5, 0-8" | 8.2 | 59 | 95 | 32 | 510 | 12601 | 19071 | 1407 | 51451 | 15 | 526 | 147 | 132 | 39 |
| soil 5, 8-16" | 5.5 | 7 | 59 | 34 | 296 | 19970 | 27622 | 1672 | 2970 | 14 | 503 | 111 | 67 | 25 |
| soil 4, 0-8" | 8.2 | 10 | 12 | 13 | 508 | 7052 | 14996 | 1055 | 83648 | 9 | 371 | 32 | 37 | 20 |
| soil 4, 8-16" | 7.9 | 55 | 154 | 76 | 747 | 21162 | 32133 | 2514 | 8924 | 23 | 852 | 272 | 291 | 84 |
| soil 3, 0-8" | 7.5 | 90 | 74 | 51 | 495 | 18425 | 25038 | 2066 | 3750 | 18 | 644 | 230 | 140 | 59 |
| soil 3, 8-16" | 5.1 | 5 | 27 | 48 | 203 | 27655 | 41507 | 2016 | 4077 | 18 | 441 | 213 | 76 | 34 |
| soil 2, 0-8" | 6.8 | 50 | 106 | 56 | 470 | 18179 | 27115 | 2249 | 5134 | 19 | 689 | 396 | 202 | 57 |
| soil 2, 8-16" | 6.7 | 21 | 48 | 45 | 297 | 21176 | 30708 | 1788 | 3952 | 17 | 469 | 134 | 132 | 39 |
| soil 1, 0-8" | 8.2 | 14 | 8 | 13 | 359 | 6284 | 13168 | 1226 | 86770 | 8 | 326 | 90 | 26 | 22 |
| soil 1, 8-16" | 7.4 | 985 | 229 | 115 | 981 | 24900 | 38660 | 3050 | 8457 | 30 | 1118 | 426 | 524 | 122 |